Chem

CellPress
OPEN ACCESS

Article

Catalytic carbon-carbon bond cleavage and carbon-element bond formation give new life for polyolefins as biodegradable surfactants

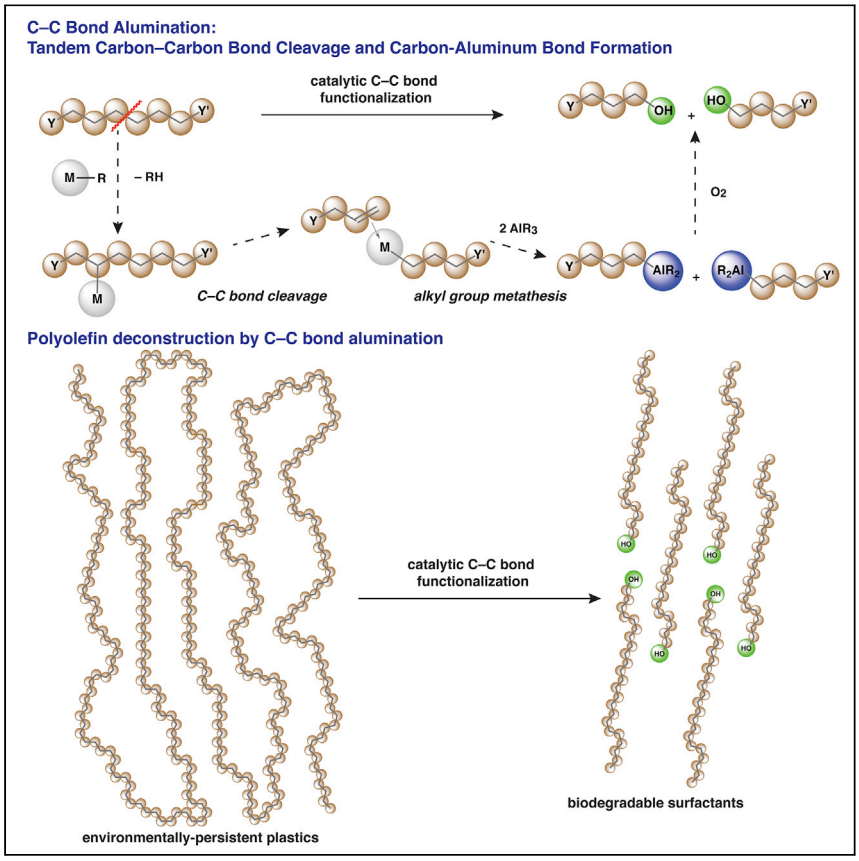

A new catalytic transformation of saturated hydrocarbons involving carbon–carbon bond cleavage and alumination is developed and investigated for the upcycling conversion of polyolefins into biodegradable fatty alcohols and fatty acids.

Uddhav Kanbur, Guiyan Zang, Alexander L. Paterson, ..., Frédéric A. Perras, Pingping Sun, Aaron D. Sadow

sadow@iastate.edu

Highlights

Catalytic C–C bond cleavage chops and functionalizes aliphatic hydrocarbons

Sustainable conversion of polyolefins into biodegradable, value-added fatty alcohols

Metalative cleavage employs earth-abundant zirconium catalysts and aluminum reagents

Kanbur et al., Chem 7, 1347–1362
May 13, 2021
https://doi.org/10.1016/j.chempr.2021.03.007

Chem

CellPress
OPEN ACCESS

Article

Catalytic carbon-carbon bond cleavage and carbon-element bond formation give new life for polyolefins as biodegradable surfactants

Uddhav Kanbur,[1,2] Guiyan Zang,[3] Alexander L. Paterson,[1] Puranjan Chatterjee,[1,2] Ryan A. Hackler,[4] Massimiliano Delferro,[4] Igor I. Slowing,[1,2] Frédéric A. Perras,[1] Pingping Sun,[3] and Aaron D. Sadow[1,2,5,*]

SUMMARY

Catalytic methods that introduce functional groups via carbon–carbon bond cleavage steps have typically been limited to moieties activated by strain or by directing groups, with few transformations engaging the bonds of only sp^3-hybridized carbon atoms in saturated hydrocarbons. Here, we report the conversion of catenated carbon chains in polyolefins, which currently represent >50% of discarded plastics, into shorter aliphatic alkylaluminum species via a sequence of zirconation via C–H bond activation, β-alkyl elimination for carbon–carbon bond cleavage, and heterobimetallic alkyl group exchange for carbon–aluminum bond formation. The versatility of aliphatic alkylaluminum species is exemplified by their subsequent conversion into high-value fatty acids or alcohols, which have applications as biodegradable surfactants and detergents. A technoeconomic analysis indicates that fatty alcohols produced from discarded polyolefins are cost competitive with conventional syntheses. Thus, this process could ameliorate economic and environmental challenges of the plastic-waste crisis.

INTRODUCTION

C–H bond metalations, in which a hydrogen atom is replaced by a metal center, have revolutionized syntheses by reducing or eliminating requirements for specific and limiting chemical functional groups.[1–3] In these metalations, the carbon-based molecular framework of the organic reactants is preserved in the functionalized products. An even wider range of starting materials could be leveraged by methods that concurrently alter the carbon-based skeleton of organic molecules and introduce new functional groups. With such transformations, for example, natural resources that contain structural components of the desired products would become available for chemical manufacturing, or framework reconstructions could increase late-stage structural diversification during multistep syntheses. C–C bond metalations, in which a metal center replaces a specific hydrocarbyl moiety, would enable these framework functionalization reactions. Current methods that install a metal center by breaking a carbon–carbon bond, however, are limited to positions activated either by thermodynamically weakened bonds or directing functional groups (Figure 1A).[4–7] On the other hand, established C–C bond cleavages involving only sp^3-hybridized carbon centers generally do not provide new carbon–heteroatom bonds. For example, alkane metathesis (Figure 1B) alters chain lengths without introducing new functional groups.[8,9] Likewise, hydrogenolysis of carbon–carbon bonds in hydrocarbons, catalyzed by heterogeneous platinum-group nanoparticles[10,11] or air-sensitive early transition metal hydrides,[12,13] provides shorter alkane products.

The bigger picture

Typical chemical synthesis constructs large, intricate products from smaller building blocks. Yet, naturally occurring resources often contain preassembled molecular components, which nonetheless are not directly suitable for conventional routes to desired products. Thus, sustainable conversions would be advanced by efficient catalytic methods that restructure the carbon-based skeletons of molecules and install functional groups.

We report the discovery of such a conversion, in which long hydrocarbon chains of polymers are broken into shorter units with the introduction of aluminum end groups. These green organoaluminum species are easily derivatized into biodegradable fatty alcohols, carboxylic acids, or halides, providing high-value, end-of-first-life applications for the catenated chains of single-use polyolefins.

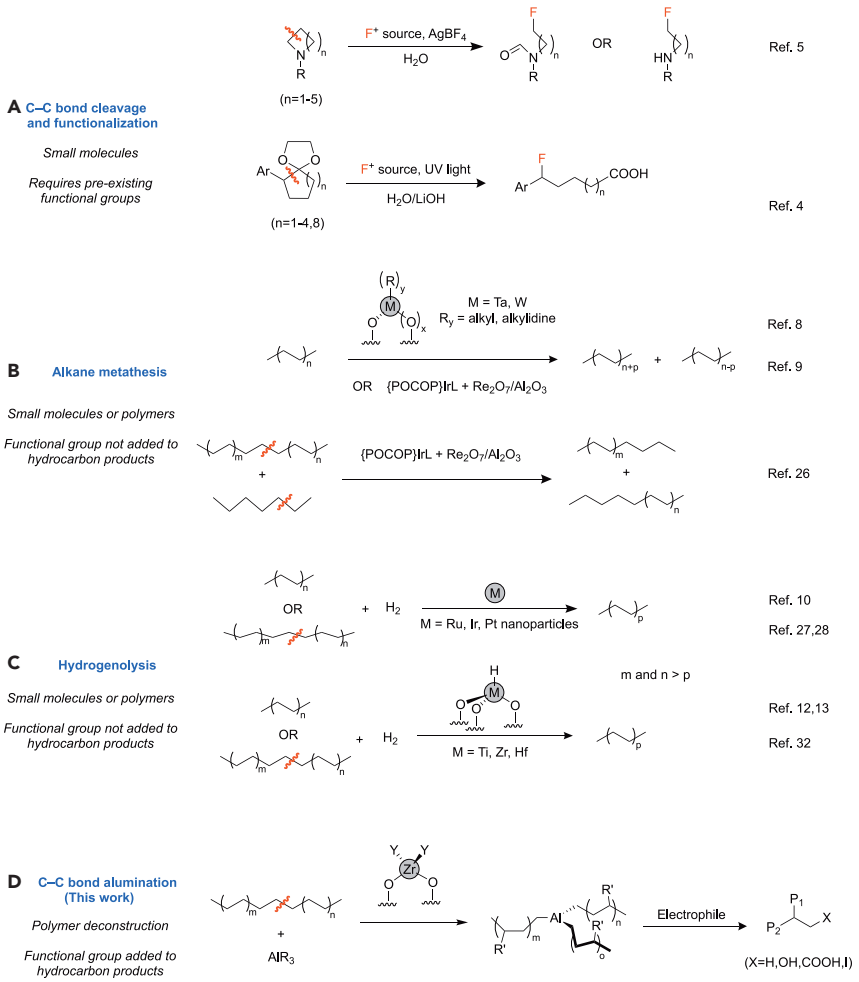

Figure 1. Catalytic methods for carbon–carbon bond cleavage

(A) Functional groups may be added at thermodynamically activated or kinetically preferred positions.

(B and C) Saturated hydrocarbons in small molecules and polymers may be shorted by alkane metathesis (B) or nanoparticle or early-metal hydride-catalyzed hydrogenolysis (C) without introduction of new functionality.

(D) Carbon–carbon bond cleavage and aluminum–carbon bond formation is catalyzed by surface-supported organozirconium species.

Molecular skeleton restructuring transformations could be useful, for instance, in the deconstruction of polymers for which there are growing environmental and socio-economic concerns.[14,15] Conventional technologies, such as mechanical recycling through melt-processing, are insufficient to fully address this global problem.[16,17] Chemical conversion of polymers have been proposed as an alternative strategy that could provide a second life for the catenated chains of used plastics.[18,19] For example, polyolefins may be transformed into liquid fuels by pyrolysis or hydrocracking,[20] polyesters may be chemically recycled via monomers,[21] plastic-to-plastic transformations can upcycle used materials into new ones,[22–25] and discarded plastics can serve as feedstocks for value-added chemical products. Alkane cross-metathesis,[26] noble-metal-nanoparticle catalyzed hydrogenolysis,[27–31] and surface-supported zirconium-hydride-catalyzed hydrogenolysis,[32] noted above, have been adapted to transform polyolefins into waxes, oils, lubricants, or alkylaromatics.

[1]US DOE Ames Laboratory, Iowa State University, Ames, IA 50011, USA

[2]Department of Chemistry, Iowa State University, Ames, IA 50011, USA

[3]Systems Assessment Center, Energy Systems Division, Argonne National Laboratory, Lemont, IL 60439, USA

[4]Chemical Sciences and Engineering Division, Argonne National Laboratory, Lemont, IL 60439, USA

[5]Lead contact

*Correspondence: sadow@iastate.edu

https://doi.org/10.1016/j.chempr.2021.03.007

Of the existing methods, only the oxidative degradation of polyolefins provides useful functionalized small molecules, such as in the conversion of high density polyethylene (HDPE) into a mixture of short α,ω-diacids (e.g., $HO_2C(CH_2)_nCO_2H$; n = 2–5), whose selectivity is governed by the rules of radical chemistry.[33] These reactions, as well as pyrolytic approaches, are currently moving toward commercial practice for the conversion of polyolefins.[18] Catalytic C–C bond metalation reactions, which provide versatile organometallic intermediates, could benefit from catalyst-controlled selectivity to enable upcycling transformations to narrow distributions of long-chain chemicals.[27,28]

Intermediate-length chain-alkylaluminum species are high among desirable targets for polymer deconstruction processes because these organometallics, conventionally synthesized using the Ziegler process, can be converted into fatty alcohols and acids through established methods.[34,35] The heteroatom-functionalized species are biodegradable and, if produced from discarded polyolefins, would provide an environmentally friendly end-of-life for some plastics. In addition, the hydrido- or organoaluminum reagents to be employed in such transformations are further advantaged because aluminum is widely available as the most abundant metal (8.2% as an oxide) in the earth's crust, and it is readily converted (or recycled) from its oxide to metal to organoaluminum species in atom-economical, optimized processes performed on a large scale.[36]

We envisioned that organotransition-metal species, generated as catalytic intermediates by cleavage of C–C bonds in saturated hydrocarbons, could undergo metathetical exchange with organo- or hydridoaluminum species, to create the new intermediate-length chain hydrocarbyl-aluminum species. Such alkyl group metathetical steps are established in carboalumination and hydroalumination of alkenes[37,38] and as chain-transfer steps in chain-shuttling block co-polymerizations of ethylene and α-olefins.[39] These processes commonly engage organozirconium catalysts. Moreover, coordinatively unsaturated zirconium sites, including surface-supported zirconium hydride in catalytic polyolefin hydrogenolysis,[32] are known to break C–C bonds by β-alkyl elimination.[40] The related β-allyl elimination and organozirconium/hydridoaluminum exchange are proposed in polybutadiene deconstruction and alumination, catalyzed by Cp_2ZrHCl (Schwartz's reagent), which attaches to the chain by hydrozirconation rather than C–H bond metalation.[41]

Here, we report the *catalytic C–C bond alumination* of sp^3-hybridized carbon in aliphatic hydrocarbons, leveraging C–H bond activation and β-alkyl elimination steps of surface organometallic zirconium chemistry.[13,42–49] Our studies have focused on identifying effective catalysts and aluminum reagents, as well as understanding their effects upon the elementary steps involved in reactions through conversions of polyethylene into fatty aliphatic alkylaluminum species.

RESULTS

Design of carbon–carbon bond alumination

The first experiments employed $Zr(CH_2CMe_3)_2$@$SiAlO_x$ (2.7 wt % Zr, 0.30 mmol Zr/g), which was prepared by grafting $Zr(CH_2CMe_3)_4$ onto partially dehydroxylated silica-alumina (0.38 mmol SiOH/g; 9.3 wt % Al; 182 m^2/g; see Figure S89) in pentane (see Supplemental experimental procedures).[47,50,51] The surface species contains an average of two neopentyl groups per zirconium center, as determined by elemental analysis using inductively coupled plasma-optical emission spectroscopy (ICP-OES) and protonolytic titration. Melted HDPE and Al*i*Bu_3 (~10:1 by weight) react in the presence of this precatalyst over 12 h at 150°C to give, after flowing

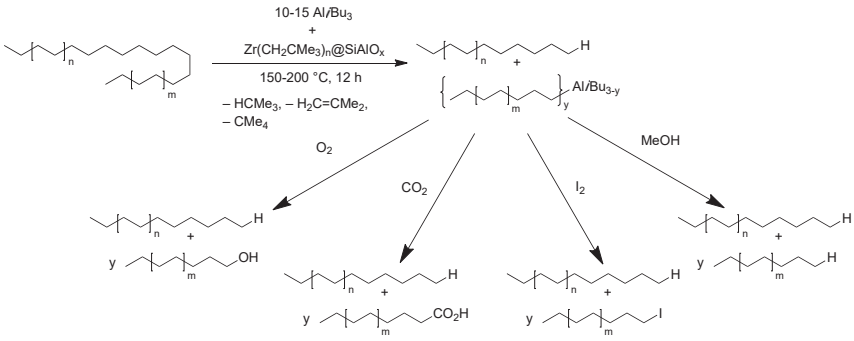

Scheme 1. C–C bond alumination followed by quenching

Routes from fatty alkylaluminum intermediates to fatty alcohols, fatty acids, alkyl halides, and hydrocarbons.

dry air through the reactor and extraction with methylene chloride, an oil containing fatty alcohols and alkanes in a nonoptimized 31% yield (based on initial HDPE mass, Scheme 1). Fatty alcohols in the product mixture corresponded to O_2-quenched organometallic species, including alkylaluminum and any active alkylzirconium intermediates, whereas hydrocarbons were present in the reaction mixture prior to quenching. Thus, the combination of $Zr(CH_2CMe_3)_2@SiAlO_x$ and Al*i*Bu_3 mediates the desired carbon–carbon bond cleavage and carbon–aluminum bond formation in aliphatic hydrocarbons.

The isolated reaction products were analyzed by infrared (IR) and 1D and 2D solution-phase nuclear magnetic resonance (NMR) spectroscopy, matrix-assisted laser desorption ionization time of flight-mass spectrometry (MALDI-TOF-MS), and gas chromatography mass spectrometry (GC-MS). The first evidence of alcohol products in the isolated oils was provided by broad signals in the IR spectrum at 3,430 and 1,090 cm^{-1} that were characteristic of ν_{O-H} and ν_{C-O} stretching bands (Figure S4). These assignments were further supported by MALDI-TOF-MS analysis, which detected functionalized monoalcohols from $C_{35}H_{71}OH$ up to $C_{64}H_{129}OH$ directly[52] and aliphatic hydrocarbons as $^{107/109}Ag^+$ adducts (see Figure S5). In addition, quantification of the components by GC-MS analysis revealed fatty alcohols from C_{12}–C_{20} and long-chain hydrocarbons C_{19}–C_{30} compose only 6% of the oil, by mass. Notably, we did not detect signals corresponding to alkenes in IR, MALDI-TOF-MS, GC-MS, or NMR spectra of the products (see below).

Analysis of 1D and 2D NMR spectra provided additional insight into the products' structural features. The ^1H NMR spectrum of the oil contained resonances at ca. 3.6 ppm, assigned to CH_2OH in alcohols (Figure S1), which correlated with the aliphatic hydrocarbon signals at 1.6 ppm in a COSY experiment (Figure S2). The 3.6 ppm resonance also correlated with ^{13}C NMR signals at 60–70 ppm in a phase-sensitive ^1H-^{13}C heteronuclear single quantum coherence (HSQC) spectroscopy experiment (Figure S3). These cross-peaks appear with the same phase as those at 30 ppm, assigned to the CH_2 signals from the polyethylene backbone, and the phase opposite to that of cross-peaks at 13 ppm assigned to methyl groups. These data indicate that the detectable alcohol groups in the oil are primary, leading to the conclusion that the direct products of C–C bond cleavage in HDPE are terminal organometallic species.

Because all molecules in the oil are either monoalcohols or alkanes (i.e., there are either one or zero OH groups per molecule), as shown by the MALDI-TOF-MS

analysis, the fraction of molecules containing functional groups (in this case, OH) is equal to the fractional number of functional groups per molecule (#FG). The #FG were calculated as the difference between the number of end groups (#EG) on a chain and the number of methyl chain ends (#CH_3). The #EG is equal to the sum of the two end groups in a linear chain and the end groups created by each of the branching points, and the number of branch points is equal to the number of methine groups (#CH), giving Equation 1 for calculating the fraction number of functional groups per molecule:

$$\#FG = \#EG - \#CH_3 = (2 + \#CH) - \#CH_3 \quad \text{(Equation 1)}$$

Using integration of the assigned ^{1}H NMR spectrum, the fact that all alcohols are terminal, and assuming that CMe_2 groups and cyclic species are insignificant, this oil is estimated to contain a 7:3 ratio of monoalcohol:alkane. The absolute yield of alcohols corresponds to ca. 50% of the total valence available from the Al*i*Bu_3 (i.e., 1.5 fatty alkyl chains per aluminum). In addition, 40% of the methyl groups present in the oil are bonded to methine carbons, and the remaining methyl groups are bonded to methylene carbons (chain or long branch ends). These MeCHRR′ moieties may be formed via 1,2-insertion of an α-olefin into a metal-alkyl, which subsequently metalates another polymer chain, or as a part of a methylalumination process (Me_3C-CH_2Al species are known to react by β-methyl elimination).[53]

At 200°C, the Zr(CH_2CMe_3)$_2$@SiAlO_x-catalyzed reaction of HDPE and 10 equiv of Al*i*Bu_3 gave a higher yield of oils (40%) (Table 1, entry 2) after 12 h. A MALDI-TOF-MS revealed shorter chains (a C_{34}-centered distribution) (Figure S10) compared with the products from the experiment at 150°C. The synthetic versatility of the alkylaluminum products was demonstrated in HDPE deconstruction reactions quenched with methanol, I_2, or CO_2 (Table 1, entries 4–6) that gave hydrocarbons, or mixtures containing alkyl iodides or fatty acids, respectively. As expected, similar C_{32}- to C_{34}-centered distributions of chains (see MALDI-TOF-MS of fatty acids in Figure 2) are obtained with protonolytic, oxidative, or electrophilic quenching agents, indicating that identical fatty alkylaluminum species are intermediates, and the quenching agent does not affect the product chain length. We also note that this catalytic system transforms postconsumer HDPE from a supermarket bag, which was otherwise untreated, as well as isotactic polypropylene (iPP) (Table 1, entries 11 and 12), which also provides functional-group-containing oils. Note that CH metalation of methyl groups in *i*PP, followed by β-alkyl elimination, readily deconstructs the polymer backbone.

Effects of aluminum reagents

On the basis of these initial results, and leveraging the analytical methods adapted to characterize the composition and structure of a distributions of functionalized chains, we investigated the effects of aluminum reagents on catalytic carbon–carbon bond cleavage and alumination in conversions of polyethylene. Essentially identical yields were obtained after 24 h of continuous heating or upon addition of a second portion of Al*i*Bu_3 after 12 h, suggesting that the zirconium catalyst was deactivated during the first portion of the reaction. Experiments with more Al*i*Bu_3 (50 equiv relative to Zr) gave only minimal amounts of oil (3%). Together, these experiments suggest that the aluminum reagent at higher quantities is involved in catalyst deactivation steps.[38] Improved conversion of HDPE was instead accomplished by adding portions of Zr(CH_2CMe_3)$_2$@SiAlO_x and Al*i*Bu_3 every 12 h. Polymer was not observed after three reaction cycles with a total oil yield of 84%.

Main-group alkyl and hydride reagents influence catalytic alkene polymerizations and could also affect these deconstruction reactions. The trend of reactivity of a

Table 1. Zr-catalyzed deconstructive functionalization of polyolefin chains

		Conditions		Yield		
Entry	Initial polymer mass (g)[a,b]	AlR_3	T (°C)	Mass (g)	% versus PO[c]	% functionalized chains
$Zr(CH_2CMe_3)_2$@$SiAlO_x$ catalyst						
1	0.63	Al*i*Bu_3	150	0.19	31	71
2	1.00	Al*i*Bu_3	200	0.4	40	68
3	1.00[d]	Al*i*Bu_3	200	0.84	84	66
4	1.00[e]	Al*i*Bu_3	200	0.38	38	N/A
5	0.54[f]	Al*i*Bu_3	200	0.23	43	68
6	0.55[g]	Al*i*Bu_3	200	0.20	36	75
7	0.51	$AlEt_3$	150	0.13	25	39
8	0.60	$AlEt_3$	200	0.15	24	54
9	0.64	$AlPh_3$	200	0.19	29	66
10	0.52	AlH_3	200	0.22	42	89
11	0.60[h]	Al*i*Bu_3	200	0.19	31	60
12	1.00[i]	Al*i*Bu_3	200	0.27	27	N/A
$Zr(OCH_2CMe_3)_2$@$SiAlO_x$ catalyst						
13	0.60	Al*i*Bu_3	200	0.21	34	51
14	0.35	AlH_3	200	0.17	49	62
15	0.85[j]	AlH_3	200	0.51	60	67
$Zr(CH_2CMe_3)_2$@SiO_2 catalyst						
16	1.00	Al*i*Bu_3	200	0.35	35	85
17	0.41	$AlEt_3$	200	0.13	33	82

PO, polyolefin; N/A, not applicable.

[a]Standard conditions: 21 kg HDPE/mol Zr, Al:Zr = 10:1, 150°C–200°C, 12 h, followed by O_2 quench to give fatty alcohols. Data in support of this table is given in Figures S1–S17.

[b]HDPE: M_n = 6.2 kDa, M_w = 38.6 kDa, Đ = 6.2.

[c]% Yield = mass of oil/mass of PO.

[d]3 portions of $Zr(CH_2CMe_3)_2$@$SiAlO_x$/Al*i*Bu_3 were added over 36 h.

[e]Quenched with MeOH to give saturated hydrocarbon products.

[f]Quenched with I_2 to provide long-chain alkyl iodides.

[g]Quenched with CO_2 to form fatty acids.

[h]Postconsumer HDPE: M_n = 5.3 kDa, M_w = 105 kDa, Đ = 19.8.

[i]*i*PP: M_n = 37.4 kDa, M_w = 117.6 kDa, Đ = 3.2. Quantitative estimation of functional group analysis of the product is not possible due to quaternary carbon centers.

[j]Performed under dynamic vacuum.

series of main-group compounds in this $Zr(CH_2CMe_3)_2$@$SiAlO_x$-catalyzed polyethylene conversion process, in terms of yields of oils, is $AlH_3 \sim AliBu_3 > AlPh_3 \sim AlEt_3 >> AlMe_3 \sim HAliBu_2$ (DIBAL-H) $\sim HAlMe_2 \sim ZnEt_2$. The Al reagents which react by hydride transfer, namely AlH_3 and Al*i*Bu_3, give higher yields of functionalized chains than reagents that only transfer organic groups such as $AlMe_3$. Several of these experiments also provide evidence for metalation and carboalumination steps that are part of the proposed reaction pathway (see below). In the absence of aluminum reagents under otherwise identical conditions, only minor amounts of light alkenes and alkanes are detected in the reaction mixture.

The most effective co-reactant for Zr-catalyzed deconstruction of HDPE was AlH_3, the reaction of which provided oil in a yield (42%) comparable with the reaction with Al*i*Bu_3 and a significantly higher proportion of alcohol chains (89%) in the oil product. Similar ranges of $C_nH_{2n+1}OH$ ($30 \leq n \leq 44$) species were observed in the MALDI-TOF-MS spectra (Figure S10 and S10.5) of oils obtained in otherwise equivalent reactions using AlH_3 and Al*i*Bu_3 at 200°C. Triethylaluminum ($AlEt_3$) was

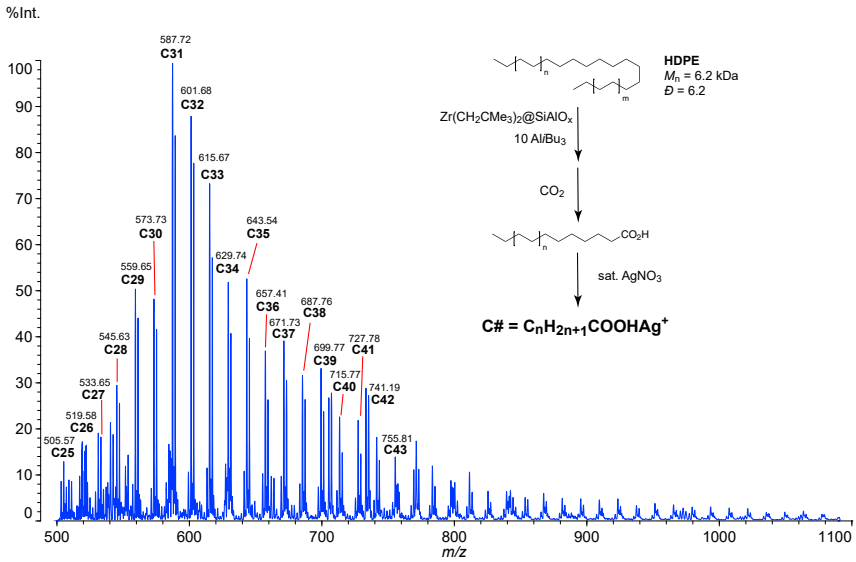

Figure 2. MALDI-TOF-MS of fatty acid distribution

The oil product obtained from the $Zr(CH_2CMe_3)_2$@$SiAlO_x$-catalyzed reaction of HDPE and Al*i*Bu$_3$ at 200°C for 12 h followed by reaction with CO_2, is analyzed as Ag^+ adducts.

less effective for carbon–carbon bond cleavage than Al*i*Bu$_3$ or AlH_3 in the presence of $Zr(CH_2CMe_3)_2$@$SiAlO_x$ as precatalyst, affording oils in 23% yield after 12 h at both 150°C and 200°C. The structure, HO-CH_2-CH(CH_2CH_3)-polymer chain, identified through a ^{1}H-^{1}H COSY experiment (Figure S34), was the dominant alcoholic species, based on the 1.53:1 ratio of integrated signals of (CH)–CH_2–CH_3 to CH_2–OH (Figure S33). The fraction of molecules containing OH, as calculated using Equation 1, was 0.39. Thus, $AlEt_3$ was less active than Al*i*Bu$_3$ and also less effective for introducing aluminum into the products, giving the highest percentage of alkanes of all reactive aluminum reagents (see Discussion). A higher yield of oil product (29% by mass after work-up with O_2) from the catalyzed reaction of HDPE and $AlPh_3$ at 200°C compared with $AlEt_3$ was partially affected by the added mass accompanied by formation of aromatic-containing species, identified by ^{1}H and ^{13}C NMR spectroscopy, and MALDI-TOF-MS (Figures S9.1–S9.6). Treatment of HDPE with either $ZnEt_2$ or $AlMe_3$, which are often effective in coordinative chain-transfer polymerization,[54,55] or aluminum hydride reagents HAl*i*Bu$_2$ and $HAlMe_2$ did not provide fatty alcohol oils after work-up.

Catalytic materials

A control experiment lacking zirconium, in which partially dehydroxylated $SiAlO_x$, Al*i*Bu$_3$, and HDPE were heated at 200°C for 12 h, returned the polymer with little change to its molecular weight (M_n = 5.8 kDa) and trace amounts (< 2%) of trimerized isobutylene from Al*i*Bu$_3$ thermolysis.[56] Although acid sites on $SiAlO_x$ (or even weaker silanols on SiO_2) mediate degradation of HDPE at 200°C,[57] Al*i*Bu$_3$ reacts to cap the few surface silanol sites[58,59] and blocks acid-promoted thermolysis to favor zirconium-catalyzed pathways. In addition, negligible amounts of oil are obtained from catalytic deconstruction/alumination experiments in which $Zr(CH_2CMe_3)_2$@$SiAlO_x$ is pretreated with H_2 to generate hydridozirconium species as the precatalyst.

We initially tested $Zr(CH_2CMe_3)_2$@$SiAlO_x$ because its surface hydrides are reported to be more active for propane metathesis and polyolefin hydrogenolysis than the

silica-supported analogs.[32,60] Our direct dynamic nuclear polarization (DNP)-enhanced[61] $^{17}O\{^{27}Al\}$ transfer of population double-resonance (TRAPDOR)[62–64] NMR experiments, however, revealed that the Zr is not in close proximity to Al centers in the precatalyst (Figure S96). More specifically, while the oxide ^{17}O sites predictably dephased following ^{27}Al irradiation, indicating the presence of O-Al linkages near the surface, the ^{17}O sites bound to Zr did not, revealing that the Zr coordinates exclusively to silanols in the precatalyst with the structure $(\equiv SiO)_2Zr(CH_2CMe_3)_2$ and not by reacting at $\equiv Si–OH–Al\equiv$ Brønsted acid sites.

We investigated a silica-supported zirconium catalyst based on this spectroscopic result. An aerosil silica-supported zirconium catalyst, $Zr(CH_2CMe_3)_2@SiO_2$, after heating with HDPE and Al*i*Bu_3 for 12 h at 200°C, provided an alcohol-containing oil in nearly equivalent yield (35%) as the silica-alumina-supported catalyst. Moreover, the oil was composed of approximately 85% alcohols and only 15% alkanes. The $Zr(CH_2CMe_3)_2@SiO_2$-catalyzed reaction with $AlEt_3$ provided the oil product in similar single-pass yield (32%) and high alcohol content (82%), as a contrast with the silica-alumina supported zirconium catalyst. These reactions afforded alcohol species with a normal, ca. C_{35}-centered distribution of monoalcohols, as detected by MALDI-TOF-MS (Figures S16.5 and S17.5, respectively). The similarly high reactivity of catalysts supported on silica and silica-alumina may be attributed to the known surface alumination and subsequent incorporation of aluminum centers into silica framework sites in reactions of excess Al*i*Bu_3 and SiO_2.[59] In fact, trace amounts of ethylsilane species were detected in GC-MS and NMR spectra of the reaction products, which was consistent with aluminum substitutions for silicon occurring in the silica support framework during the catalytic reaction. This *in situ* alumination of the silica support could influence the reactivity of the active species generated from the $Zr(CH_2CMe_3)_2@SiO_2$ precatalyst. Such an effect would not be available in alkylaluminum-free hydrogenolysis reactions catalyzed by surface-supported hydridozirconium, leading to distinct activity for zirconium supported on the two oxides.

The silica- or silica-alumina-supported neopentylzirconium, as well as the $(\equiv SiO)_3ZrH$ catalyst for polyethylene hydrogenolysis, are exceedingly sensitive to irreversible reactions with air and moisture to give deactivated materials. Thus, small amounts of protic or oxidative impurities in the polyethylene reactant could have an outsized effect upon catalytic performance. Because the alkylaluminum reactant can serve as an alkylating agent for converting alkoxyzirconium into alkylzirconium surface species, some poisoned sites could also be reactivated under catalytic conditions. In this context, we note that the polyolefin reactants used in this study, although clean and dry, were essentially used as received and did not undergo exhaustive purification prior to use. Moreover, convenient precatalysts for HDPE deconstruction should be tolerant of air and moisture. Remarkably, $Zr(CH_2CMe_3)_2@SiO_2$ exposed to O_2[65] was catalytically active for the reaction of HDPE and Al*i*Bu_3 and gave an oil in 34% yield with ca. 50% selectivity to alcohols. This air-exposed precatalytic material $Zr(OCH_2CMe_3)_2@SiAlO_x$ can also be activated by AlH_3, and the reaction with HDPE afforded a higher yield (49%) and higher selectivity alcohols (62%). Thus, alkoxyzirconium species are viable precatalysts for carbon–carbon cleavage and alumination.

Technoeconomic analysis

These polyolefin deconstruction and heterofunctionalization reactions will enable the development of incipient plastic upcycling and manufacturing efforts that are either integrated into materials recovery facilities on a small scale or centralized

over fewer, larger-scale facilities. A technoeconomic analysis (TEA) of a conceptual centralized plant (see supplemental experimental procedures; Figure S94) was carried out to process 250 metric tons (MT) of PE/day, at 90% utilization, and produce ca. 71 MT fatty alcohol sulfate/day, as well as valuable paraffinic lubricant co-products. In the design, the expenses associated with the Zr catalyst and alkylaluminum reagents are recouped by fully separating and recovering the former and by reselling the latter as $AlCl_3$ co-products (see Tables S1–S3). The estimated minimum product market price for the resultant surfactant ($C_{40}H_{81}OSO_3Na$) is US$ 3.4/kg (Figure S95), which is comparable to the US$ 1–3/kg current market price of sodium lauryl sulfate (from C_{12} alcohol).

Straightforward production of eicosanol (C_{20}) and docosanol (C_{22}), which are considerably more valuable than C_{12} alcohol (see Table S4), could further motivate collection and processing of used polyethylene. Finally, we note that the longer functionalized chains, uniquely inexpensive from this polymer deconstruction/alumination process, could find new applications for upcycled polyolefins. The fatty alcohol or fatty acid products obtained from catalytic deconstruction/alumination complement the short-chain diacids formed from oxidative polymer degradations,[33,66] unsaturated species from thermal or pyrolytic processes,[29,67] or hydrocarbons from hydrogenolysis or alkane metathesis.[26–28,32] Given the massive amounts of polyolefins that are discarded each year, this complementarity, as well as the potential new applications of long-chain fatty alcohols and acids which are inaccessible by traditional synthetic means, could benefit the implementation of this or related transformations in the incipient practice of upcycling plastics into new, value-added products.

DISCUSSION

Evidence for sequence of elementary steps

This Zr-catalyzed polyethylene deconstruction to produce long-chain alkylaluminum species likely follows the sequence of elementary steps shown in Scheme 2. First, the polymer backbone and a surface-grafted alkyl or hydridozirconium species **A** react via methylene C–H bond activation (1) to generate a midchain polymerylzirconium **B**. Then, β-alkyl elimination[40,68,69] (2) from the midchain polymerylzirconium **B** results in carbon–carbon bond cleavage to give a terminal olefin and a new oligomerylzirconium species **C**. Finally, chain transfer to aluminum[70–72] (3) occurs via heterobimetallic alkyl group metathesis of the alkylzirconium with an alkyl or hydridoaluminum species and (4) carboalumination[37] or hydroalumination[73] of the *in situ* generated olefin by AlR_3 results in a new aluminum–carbon bond.

Observations described below, made in the course of catalytic experiments, provide support for the reaction sequence shown in Scheme 2. First, evidence for metalation by alkylzirconium species in step 1 is provided by the reaction by-products. Neopentane (CMe_4) is detected in the reactor headspace within the first 15 min of experiments catalyzed by $Zr(CH_2CMe_3)_2$@$SiAlO_x$, regardless of the organoaluminum reagent used, suggesting that the polymer is metalated by a Zr-CH_2CMe_3 species. In a control experiment, CMe_4 was not detected in the reaction of HDPE with $Zr(OCH_2CMe_3)_2$@$SiAlO_x$ and Al*i*Bu_3. Thus, CMe_4 formation is associated with metalation by neopentylzirconium rather than resulting from reaction of neopentylaluminum species and/or polymer hydrogenolysis. Other organozirconium intermediates also likely react with polymer chains, via metalation, to give midchain polymerylzirconium species **B**. For example, benzene is observed in reactions involving $AlPh_3$ (prior to work-up with O_2), supporting the idea that phenylzirconium intermediates react with hydrocarbons by metalation. Oligomerylzirconium species (**C**), generated

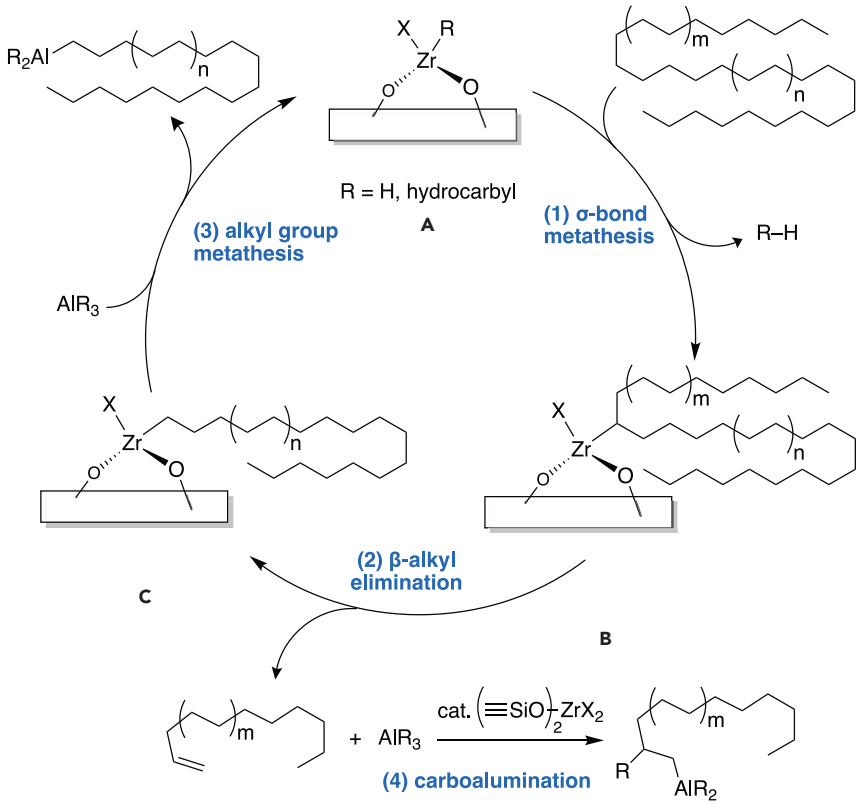

Scheme 2. Plausible sequence for polyethylene deconstruction and alumination

Possible sequence of elementary steps involved Zr-catalyzed polyethylene deconstruction into long-chain alkylaluminum species, namely (1) metalation of the polymer backbone via C–H bond activation by a grafted alkyl- or hydridozirconium species **A**, (2) β-alkyl elimination from a midchain polymerylzirconium **B**; resulting in C–C bond cleavage to give a terminal olefin and a new oligomerylzirconium species **C**; (3) alkyl group metathesis of the oligomerylzirconium with an alkyl or hydridoaluminum species; and (4) carboalumination of an *in situ* generated olefin by AlR_3 resulting in a new C–C bond.

by β-alkyl elimination of **B**, also can react with polymer chains via metalation, short circuiting the chain alumination process and leading to the observed molecular aliphatic hydrocarbon products.

Surface zirconium hydride species, formed by ligand exchange or hydride transfer reactions of alkyl zirconium and hydridoaluminum or isobutylaluminum, respectively, also likely are involved in polymer metalation of step 1. Several observations support the idea that aluminum reagents generate zirconium hydrides. First, hydridoaluminum species are formed from Al*i*Bu_3 at high temperatures.[56] Second, the reaction of $Zr(CH_2CMe_3)_2$@$SiAlO_x$ and Al*i*Bu_3 at 150°C for 4 h provided a material that contained a band in a diffuse reflectance infrared Fourier transform (DRIFT) spectrum at 1,623 cm^{-1} assigned to a ν_{Zr-H} (Figure 3) on the basis of labeling experiments and comparison to literature reports.[46,74] In particular, this signal disappeared upon treatment with D_2 (the signal for presumed ν_{Zr-D} is not resolved from Si/Al–O bands) and reappeared upon exposure to H_2 (Figure 3). The DRIFT spectrum of $SiAlO_x$ treated with Al*i*Bu_3, in contrast, was unchanged by reaction with D_2. Third, during the catalytic HDPE deconstruction and alumination reactions involving Al*i*Bu_3, isobutylene was the most abundant species in the gas phase (along with a small, but detectable amount of isobutane), which was also consistent with the generation

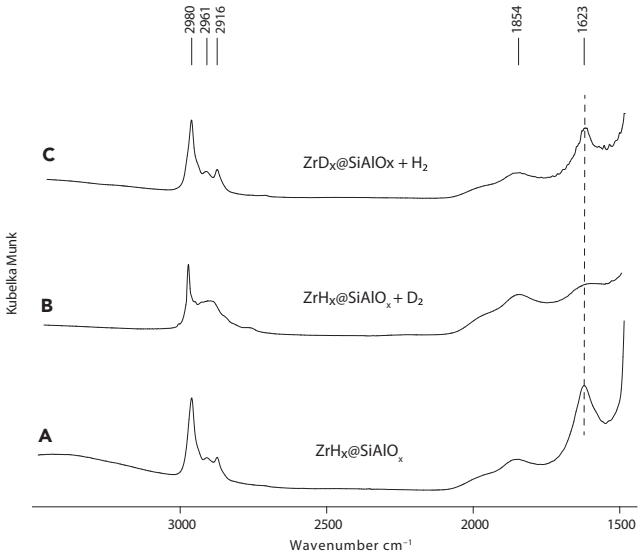

Figure 3. DRIFT spectra of ZrH@SiAlOx

(A) Room temperature DRIFT spectra of (A) $Zr(CH_2CMe_3)_2$@$SiAlO_x$ + Al*i*Bu_3 heated at 150°C for 2 h, washed with anhydrous pentane and dried *in vacuo*.

(B) D_2 gas (1 atm) passed over sample (A) at 70°C for 30 min.

(C) H_2 gas (1 atm) passed over sample (B) at 70°C for 30 min. Compare with DRIFT spectrum of $Zr(CH_2CMe_3)_2$@$SiAlO_x$ in Figure S90.

of hydridozirconium species. The reaction of $Zr(CH_2CMe_3)_2$@$SiAlO_x$ and Al*i*Bu_3 at room temperature also produced isobutylene (Figure S92), although the ν_{Zr-H} band in the DRIFT spectrum was very weak under that condition. Finally, hydride-generating aluminum reagents (AlH_3 and Al*i*Bu_3) provided higher yields of oils than reactions with alkyl ($AlEt_3$) or aryl ($AlPh_3$) transfer reagents, which may reflect increased rates of methylene C–H bond activation by hydridozirconium compared with alkyl or arylzirconium.

Midchain polymerylzirconium species **B** are cleaved via β-alkyl elimination, leading to polymer deconstruction into a shorter terminal oligomerylzirconium **C** and vinyl-terminated chain fragments in step 2. The oligomerylzirconium reacts with AlR_3 via heterobimetallic alkyl group exchange or hydride transfer to produce the oligomerylaluminum product and regenerate the alkyl- or hydridozirconium catalyst in step 3. Catalytic hydroalumination or carboalumination of the vinyl-termination polymer fragment, via insertion into alkyl- or hydridozirconium and chain transfer, affords β-branched (R_2Al-CH_2CHR–) or linear (R_2Al-CH_2CH_2-) aluminum terminated chains in step 4. These species were detected in the products of $AlEt_3$ and $AlPh_3$ and analyzed by 1D and 2D NMR spectroscopy. Thus, all functional groups terminate the chains as a consequence of the β-alkyl and chain-transfer mechanistic sequence.

We have ruled out at least one other sequence of elementary steps that could account for the observed fatty alkylaluminum products. Specifically, terminal polymerylzirconium species could also react by β-alkyl elimination to generate ethylene (Figure S93). This thermodynamically unfavorable step, the microscopic reverse of ethylene insertion during polymerization, could be coupled to an exothermic, catalytic ethylene oligomerization process that provides the medium-length chains of the alkyl aluminum or alkane products. Independent oligomerization or

polymerization experiments involving small amounts of ethylene, $Zr(CH_2CMe_3)_3$@-$SiAlO_x$, and Al*i*Bu_3 did not give fatty-alcohol-range molecular weight species. Thus, we ruled out a pathway to oils involving HDPE depolymerization to ethylene followed by Ziegler A*ufbau*-type oligomerization, although the individual elementary steps, namely ethylene formation and reinsertion, were not ruled out by this experiment.

Related side reactions, such as alkene insertion, are likely also a small part of the catalytic mechanism. In addition, the oligomerylzirconium intermediates **C** can react with small molecules, such as H_2 or benzene, through σ-bond metathesis steps to form hydrocarbons.[75] Accordingly, high alkane content was observed with the catalytic systems $Zr(CH_2CMe_3)_2$@$SiAlO_x$/$AlPh_3$ (ca. 55%) and $Zr(OCH_2CMe_3)_2$@$SiAlO_x$/Al*i*Bu_3 (ca. 50%). This influence of small molecules was further examined by removing the volatile species, in reactions of HDPE and AlH_3 in the presence of $Zr(OCH_2CMe_3)_2$@$SiAlO_x$ under continual evacuation (Table 1, entry 15). Under these conditions, a high single-pass yield (60%) was obtained, even though the mass of the reaction mixture decreased by 21%. MALDI-TOF-MS analysis of the oil formed under these conditions revealed that increased amounts of lower-molecular-weight alcohols, from $C_{20}H_{41}OH$ to $C_{38}H_{77}OH$, were formed under vacuum than in a sealed vessel. This oil contained comparable fraction of alcohol molecules (~67%) as the experiment under N_2. Clearly, the removal of small molecules from the reaction mixture slows undesired bimolecular processes relative to unimolecular chain cleavage by β-alkyl elimination. However, the relative rate of alkylaluminum formation compared with alkane production is not affected by performing the reaction under a dynamic vacuum, probably because the effective concentrations of AlR_3 and CH bonds, leading to the two kinds of products, are not significantly altered by removing volatile species.

In conclusion, the combination of β-alkyl elimination and heterobimetallic alkyl group metathetical exchange at surface-immobilized organozirconium sites provides a valuable method to install reactive groups and reconstruct the carbon skeleton of organic molecules, without the need for prior activation or directing groups. The alkylaluminum reagent can activate air-stable alkoxyzirconium species to generate highly air-sensitive hydridozirconium active sites, which are also innoculated by the alkylaluminums against poisoning. We are currently investigating the performance of commercially available, air-stable catalyst precursors to further simplify manipulations as well as sites containing robust ancillary ligands to affect the rates of β-alkyl elimination and chain-transfer steps. The relative rates of these steps affect the average carbon-chain lengths of the products, advantageously allowing catalyst-controlled mechanisms to be optimized to obtain desired products. Both Al*i*Bu_3 and AlH_3 react with alkyl and alkoxyzirconium species to generate surface zirconium hydrides. Moreover, both the catalysts and reactants are based upon earth-abundant, readily available, and nontoxic metal centers. In this regard, we have also shown that these catalytic reactions, as applied to polyolefins, are viable to compete with conventional syntheses of fatty alcohols. The current catalytic materials deconstruct polyolefins through a process that favors the cleavage of long chains.[27,29] In this scenario, the cleavage of longer chains has a more dramatic effect on the observed average molecular weight of the products than the cleavage of shorter chains. Thus, on-going efforts involve catalytic architectures, such as those that operate via processive mechanisms,[28] which lead to narrow distributions of fatty- aluminum products. This process could motivate recovery of discarded polyolefins from the environment, produce value-added chemical products, and offer an environmentally friendly end-of-life for materials currently destined for landfills.

EXPERIMENTAL PROCEDURES

Resource availability

Lead contact

Further information and requests for resources should be directed to and will be fulfilled by the lead contact, Aaron Sadow (sadow@iastate.edu).

Materials availability

This study did not generate new unique reagents.

Data and code availability

The raw NMR and IR spectra, generated during this study and shown in the supplemental information, are available at Datashare, an open-access repository at Iowa State University at https://doi.org/10.25380/iastate.13626731.

Representative procedure for catalytic alumination of polyolefins

Caution: Small organoaluminum compounds $AlMe_3$, $AlEt_3$, $Al\mathit{i}Bu_3$, $AlPh_3$ are pyrophoric and must be handled under air-free conditions. The fatty alkylaluminum products should be carefully quenched with air after full conversion of organoaluminum reagents. The HDPE reactant (1.00 g; M_n = 6.2 kDa, M_w = 38.6 kDa, Đ = 6.2), $Zr(CH_2CMe_3)_3$@$SiAlO_x$ (0.13 g, 0.039 mmol Zr; see supplemental experimental procedures for synthesis and characterization), and $Al\mathit{i}Bu_3$ (100 μL, 0.40 mmol) were loaded into a glass tube equipped with a glass-encapsulated magnetic stir bar. The tube was sealed by a stainless steel UltraTorr fitting to a closed glass tube with a sidearm containing a re-sealable Teflon-glass valve. The vessel was heated in an aluminum block at 200°C for 12 h. The volatile components of the headspace were sampled and analyzed by GC-MS, which revealed isobutylene to be the primary species. At the end of 12 h, the contents of the tube were quenched by passing dry air into the vessel for 1 h through the sidearm. The crude reaction mixture was extracted with CH_2Cl_2 (3 × 5 mL), and the volatile components were evaporated from the liquid to provide an oil (0.40 g, 40% based on starting HDPE mass) which was further analyzed by spectroscopic and analytical techniques (NMR, IR, GC-MS, MALDI-TOF-MS). MALDI-TOF-MS revealed a C_{34}-centered distribution of fatty alcohols, which was corroborated by similar distributions obtained from CO_2, I_2, and MeOH quenched experiments. The residual solid was dissolved in hot 1,2-dichlorobenzene and filtered to remove the catalyst. A solid precipitates from the filtrate upon cooling. The supernatant liquid was decanted, and the solid polymer was washed with CH_2Cl_2 (3 × 5 mL), dried under vacuum, and analyzed by IR spectroscopy.

Summary of process design

A technoeconomic analysis was conducted for a conceptual plant that processes 250 MT/day of PE. The conceptual plant, at 90% utilization, produces 70,847 kg fatty alcohol sulfate per day, co-produces 27,295 kg C_{40} lubricant product per day, 14,222 kg $AlCl_3$ salt per day, and 117,833 kg asphalt per day. The co-produced light hydrocarbons are combusted to generate electricity and steam for onsite use, and the surplus electricity of 122,777 kWh/day is exported for sale. By using market prices for feedstocks, reagents, catalysts, and other material input and co-products, the minimum market selling prices for C_{40} fatty alcohol sulfate is $3.41/kg. Given the high market value of fatty alcohols in the range of $20–60/kg (the market price of C_{40} fatty alcohol sulfate is not available but is expected to have much higher values than that of fatty alcohol precursors), the process is likely to be highly profitable.

SUPPLEMENTAL INFORMATION

Supplemental information can be found online at https://doi.org/10.1016/j.chempr.2021.03.007.

ACKNOWLEDGMENTS

This work was supported as part of the Institute for Cooperative Upcycling of Plastics (iCOUP), an Energy Frontier Research Center funded by the U.S. Department of Energy (DOE), Office of Basic Energy Sciences (BES), and Catalysis for Polymer Upcycling (CPU) funded by DOE-BES, Division of Chemical Sciences, Geosciences, and Biosciences, under contracts DE-AC-0207CH11358 (Ames Laboratory) and DE-AC-02-06CH11357 (Argonne National Laboratory).

AUTHOR CONTRIBUTIONS

Conceptualization, U.K. and A.D.S.; methodology, U.K., A.D.S., P.S., and F.A.P.; investigation, U.K., G.Z., A.L.P., and R.H.; resources, P.C. and I.I.S.; writing – original draft, U.K. and A.D.S.; writing – review & editing, U.K., A.D.S., F.A.P., P.S., and M.D.; funding acquisition, A.D.S., M.D., and F.A.P.; supervision, A.D.S., P.S., F.A.P., and M.D.

DECLARATION OF INTERESTS

The authors declare no competing interests.

Received: November 18, 2020
Revised: January 28, 2021
Accepted: March 8, 2021
Published: April 9, 2021

REFERENCES

1. Kennedy, A.R., Klett, J., Mulvey, R.E., and Wright, D.S. (2009). Synergic sedation of sensitive anions: alkali-mediated zincation of cyclic ethers and ethene. Science *326*, 706–708.
2. Chen, H., Schlecht, S., Semple, T.C., and Hartwig, J.F. (2000). Thermal, catalytic, regiospecific functionalization of alkanes. Science *287*, 1995–1997.
3. Cho, J.Y., Tse, M.K., Holmes, D., Maleczka, R.E., and Smith, M.R. (2002). Remarkably selective iridium catalysts for the elaboration of aromatic C-H bonds. Science *295*, 305–308.
4. Pitts, C.R., Bloom, M.S., Bume, D.D., Zhang, Q.A., and Lectka, T. (2015). Unstrained C–C bond activation and directed fluorination through photocatalytically-generated radical cations. Chem. Sci. *6*, 5225–5229.
5. Roque, J.B., Kuroda, Y., Göttemann, L.T., and Sarpong, R. (2018). Deconstructive fluorination of cyclic amines by carbon-carbon cleavage. Science *361*, 171–174.
6. Morcillo, S.P. (2019). Radical-promoted C−C bond cleavage: a deconstructive approach for selective functionalization. Angew. Chem. Int. Ed. *58*, 14044–14054.
7. Gozin, M., Weisman, A., Ben-David, Y., and Milstein, D. (1993). Activation of a carbon–carbon bond in solution by transition-metal insertion. Nature *364*, 699–701.
8. Basset, J.M., Copéret, C., Soulivong, D., Taoufik, M., and Cazat, J.T. (2010). Metathesis of alkanes and related reactions. Acc. Chem. Res. *43*, 323–334.
9. Haibach, M.C., Kundu, S., Brookhart, M., and Goldman, A.S. (2012). Alkane metathesis by tandem alkane-dehydrogenation–olefin-metathesis catalysis and related chemistry. Acc. Chem. Res. *45*, 947–958.
10. Flaherty, D.W., Hibbitts, D.D., and Iglesia, E. (2014). Metal-catalyzed C–C bond cleavage in alkanes: effects of methyl substitution on transition-state structures and stability. J. Am. Chem. Soc. *136*, 9664–9676.
11. Flaherty, D.W., and Iglesia, E. (2013). Transition-state enthalpy and entropy effects on reactivity and selectivity in hydrogenolysis of n-alkanes. J. Am. Chem. Soc. *135*, 18586–18599.
12. Lecuyer, C., Quignard, F., Choplin, A., Olivier, D., and Basset, J.-M. (1991). Surface organometallic chemistry on oxides: selective catalytic low-temperature hydrogenolysis of alkanes by a highly electrophilic zirconium hydride complex supported on silica. Angew. Chem. Int. Ed. Engl. *30*, 1660–1661.
13. Corker, J., Lefebvre, F., Evans, J., Lécuyer, C., Dufaud, V., Quignard, F., et al. (1996). Catalytic cleavage of the C-H and C-C bonds of alkanes by surface organometallic chemistry: an EXAFS and IR characterization of a Zr-H catalyst. Science *271*, 966–969.
14. Brahney, J., Hallerud, M., Heim, E., Hahnenberger, M., and Sukumaran, S. (2020). Plastic rain in protected areas of the United States. Science *368*, 1257–1260.
15. Jambeck, J.R., Geyer, R., Wilcox, C., Siegler, T.R., Perryman, M., Andrady, A., Narayan, R., and Law, K.L. (2015). Marine pollution. Plastic waste inputs from land into the ocean. Science *347*, 768–771.
16. Lau, W.W.Y., Shiran, Y., Bailey, R.M., Cook, E., Stuchtey, M.R., Koskella, J., Velis, C.A., Godfrey, L., Boucher, J., Murphy, M.B., et al. (2020). Evaluating scenarios toward zero plastic pollution. Science *369*, 1455–1461.
17. Borrelle, S.B., Ringma, J., Law, K.L., Monnahan, C.C., Lebreton, L., McGivern, A., Murphy, E., Jambeck, J., Leonard, G.H., Hilleary, M.A., et al. (2020). Predicted growth in plastic waste exceeds efforts to mitigate plastic pollution. Science *369*, 1515–1518.
18. Vollmer, I., Jenks, M.J.F., Roelands, M.C.P., White, R.J., van Harmelen, T., de Wild, P., van der Laan, G.P., Meirer, F., Keurentjes, J.T.F., and Weckhuysen, B.M. (2020). Beyond mechanical recycling: giving new life to plastic waste. Angew. Chem. Int. Ed. Engl. *59*, 15402–15423.

19. Rahimi, A., and García, J.M. (2017). Chemical recycling of waste plastics for new materials production. Nat. Rev. Chem. *1*, 0046.

20. Scheirs, J. (2006). Overview of commercial pyrolysis processes for waste plastics. In Feedstock Recycling and Pyrolysis of Waste Plastics, J. Scheirs, J. Scheirs, and W. Kaminsky, eds. (John Wiley & Sons), pp. 381–433.

21. George, N., and Kurian, T. (2014). Recent developments in the chemical recycling of postconsumer poly(ethylene terephthalate) waste. Ind. Eng. Chem. Res. *53*, 14185–14198.

22. Jones, G.O., Yuen, A., Wojtecki, R.J., Hedrick, J.L., and García, J.M. (2016). Computational and experimental investigations of one-step conversion of poly(carbonate)s into value-added poly(aryl ether sulfone)s. Proc. Natl. Acad. Sci. USA *113*, 7722–7726.

23. Blasco, E., Sims, M.B., Goldmann, A.S., Sumerlin, B.S., and Barner-Kowollik, C. (2017). 50th anniversary perspective: polymer functionalization. Macromolecules *50*, 5215–5252.

24. Williamson, J.B., Czaplyski, W.L., Alexanian, E.J., and Leibfarth, F.A. (2018). Regioselective C−H xanthylation as a platform for polyolefin functionalization. Angew. Chem. Int. Ed. Engl. *57*, 6261–6265.

25. Lewis, S.E., Wilhelmy, B.E., and Leibfarth, F.A. (2019). Upcycling aromatic polymers through C–H fluoroalkylation. Chem. Sci. *10*, 6270–6277.

26. Jia, X., Qin, C., Friedberger, T., Guan, Z., and Huang, Z. (2016). Efficient and selective degradation of polyethylenes into liquid fuels and waxes under mild conditions. Sci. Adv. *2*, e1501591.

27. Celik, G., Kennedy, R.M., Hackler, R.A., Ferrandon, M., Tennakoon, A., Patnaik, S., LaPointe, A.M., Ammal, S.C., Heyden, A., Perras, F.A., et al. (2019). Upcycling single-use polyethylene into high-quality liquid products. ACS Cent. Sci. *5*, 1795–1803.

28. Tennakoon, A., Wu, X., Paterson, A.L., Patnaik, S., Pei, Y., LaPointe, A.M., Ammal, S.C., Hackler, R.A., Heyden, A., Slowing, I.I., et al. (2020). Catalytic upcycling of high-density polyethylene via a processive mechanism. Nat. Catal. *3*, 893–901.

29. Zhang, F., Zeng, M., Yappert, R.D., Sun, J., Lee, Y.H., LaPointe, A.M., Peters, B., Abu-Omar, M.M., and Scott, S.L. (2020). Polyethylene upcycling to long-chain alkylaromatics by tandem hydrogenolysis/aromatization. Science *370*, 437–441.

30. Nakaji, Y., Tamura, M., Miyaoka, S., Kumagai, S., Tanji, M., Nakagawa, Y., Yoshioka, T., and Tomishige, K. (2021). Low-temperature catalytic upgrading of waste polyolefinic plastics into liquid fuels and waxes. Appl. Catal. B *285*, 119805.

31. Rorrer, J.E., Beckham, G.T., and Román-Leshkov, Y. (2021). Conversion of polyolefin waste to liquid alkanes with Ru-based catalysts under mild conditions. JACS Au *1*, 8–12.

32. Dufaud, V., and Basset, J.M. (1998). Catalytic hydrogenolysis at low temperature and pressure of polyethylene and polypropylene to diesels or lower alkanes by a zirconium hydride supported on silica-alumina: a step toward polyolefin degradation by the microscopic reverse of Ziegler–Natta polymerization. Angew. Chem. Int. Ed. Engl. *37*, 806–810.

33. Pifer, A., and Sen, A. (1998). Chemical recycling of plastics to useful organic compounds by oxidative degradation. Angew. Chem. Int. Ed. Engl. *37*, 3306–3308.

34. Ziegler, K., Krupp, F., and Zosel, K. (1960). Metallorganische verbindungen, XL Synthese von alkoholen aus organoaluminium-verbindungen. Justus Liebigs Ann. Chem. *629*, 241–250.

35. Ziegler, K., Krupp, F., Weyer, K., and Larbig, W. (1960). Metallorganische verbindungen, XLI Reaktionen der aluminiumtrialkyle mit kohlendioxyd und schwefeldioxyd. Justus Liebigs Ann. Chem. *629*, 251–256.

36. Sanders, R.E., Jr. (2012). Aluminum and aluminum alloys. In Kirk-Othmer Encyclopedia of Chemical Technology, pp. 1–64.

37. Xu, S., and Negishi, E.I. (2016). Zirconium-catalyzed asymmetric carboalumination of unactivated terminal alkenes. Acc. Chem. Res. *49*, 2158–2168.

38. Camara, J.M., Petros, R.A., and Norton, J.R. (2011). Zirconium-catalyzed carboalumination of α-olefins and chain growth of aluminum alkyls: kinetics and mechanism. J. Am. Chem. Soc. *133*, 5263–5273.

39. Arriola, D.J., Carnahan, E.M., Hustad, P.D., Kuhlman, R.L., and Wenzel, T.T. (2006). Catalytic production of olefin block copolymers via chain shuttling polymerization. Science *312*, 714–719.

40. O'Reilly, M.E., Dutta, S., and Veige, A.S. (2016). β-alkyl elimination: fundamental principles and some applications. Chem. Rev. *116*, 8105–8145.

41. Zheng, J., Lin, Y., Liu, F., Tan, H., Wang, Y., and Tang, T. (2013). Controlled chain-scission of polybutadiene by the Schwartz hydrozirconation. Chem. Eur. J. *19*, 541–548.

42. Zakharov, V.A., Dudchenko, V.K., Paukshtis, E.A., Karakchiev, L.G., and Yermakov, Y.I. (1977). Formation of zirconium hydrides in supported organozirconium catalysts and their role in ethylene polymerization. J. Mol. Catal. *2*, 421–435.

43. Yermakovt, Y.I., Ryndin, Y.A., Alekseev, O.S., Kochubey, D.I., Shmachkov, V.A., and Gergert, N.I. (1989). Hydride complexes of titanium and zirconium attached to SiO_2 as hydrogenation catalysts. J. Mol. Catal. *49*, 121–132.

44. Schwartz, J., and Ward, M.D. (1980). Silica-supported zirconium hydrides as isomerization or hydrogenation catalysts for long-chain olefins. J. Mol. Catal. *8*, 465–469.

45. Pasha, F.A., Bendjeriou-Sedjerari, A., Huang, K.-W., and Basset, J.-M. (2014). C–H and C–C activation of n-butane with zirconium hydrides supported on SBA15 containing N-donor Ligands: $[(\equiv SiNH-)(\equiv SiX-)ZrH_2]$, $[(\equiv SiNH-)(\equiv SiX-)_2ZrH]$, and $[(\equiv SiN=)(\equiv SiX-)ZrH]$ (X = −NH–, −O−). A DFT study. Organometallics *33*, 3320–3327.

46. Rataboul, F., Baudouin, A., Thieuleux, C., Veyre, L., Copéret, C., Thivolle-Cazat, J., et al. (2004). Molecular understanding of the formation of surface zirconium hydrides upon thermal treatment under hydrogen of $[(\equiv SiO)Zr(CH_2tBu)_3]$ by using advanced solid-state NMR techniques. J. Am. Chem. Soc. *126*, 12541–12550.

47. Wang, X.-X., Veyre, L., Lefebvre, F., Patarin, J., and Basset, J.-M. (2003). Preparation and characterization of zirconium containing mesoporous silicas. II. Grafting reaction of tetraneopentyl zirconium on MCM-41 and characterization of the grafted species and of the resulting materials. Micropor. Mesopor. Mater. *66*, 169–179.

48. Quignard, F., Lécuyer, C., Choplin, A., Olivier, D., and Basset, J.-M. (1992). Surface organometallic chemistry of zirconium: application to the stoichiometric activation of the CH bonds of alkanes and to the low-temperature catalytic hydrogenolysis of alkanes. J. Mol. Catal. *74*, 353–363.

49. Casty, G.L., Matturro, M.G., Myers, G.R., Reynolds, R.P., and Hall, R.B. (2001). Hydrogen/deuterium exchange kinetics by a silica-supported zirconium hydride catalyst: evidence for a σ-bond metathesis mechanism. Organometallics *20*, 2246–2249.

50. Quignard, F., Lecuyer, C., Bougault, C., Lefebvre, F., Choplin, A., Olivier, D., and Basset, J.M. (1992). Surface organometallic chemistry: synthesis and characterization of a tris(neopentyl)zirconium(IV) complex grafted to the surface of a partially dehydroxylated silica. Inorg. Chem. *31*, 928–930.

51. Tosin, G., Santini, C.C., Taoufik, M., Mallmann, A.D., and Basset, J.-M. (2006). Reactivity of Tetraneopentylhafnium, $Hf(CH_2tBu)_4$, with silica surfaces. Organometallics *25*, 3324–3335.

52. Grace, L.I., Abo-Riziq, A., and deVries, M.S. (2005). An in situ silver cationization method for hydrocarbon mass spectrometry. J. Am. Soc. Mass Spectrom. *16*, 437–440.

53. Pfohl, W. (1960). Metallorganische Verbindungen, XXXVII aluminium-tri-neopentyl. Justus Liebigs Ann. Chem. *629*, 207–209.

54. Zhang, W., and Sita, L.R. (2008). Highly efficient, living coordinative chain-transfer polymerization of propene with $ZnEt_2$: practical production of ultrahigh to very low molecular weight amorphous atactic polypropenes of extremely narrow polydispersity. J. Am. Chem. Soc. *130*, 442–443.

55. Valente, A., Mortreux, A., Visseaux, M., and Zinck, P. (2013). Coordinative chain transfer polymerization. Chem. Rev. *113*, 3836–3857.

56. Ziegler, K., Kroll, W.R., Larbig, W., and Steudel, O.W. (1960). Metallorganische Verbindungen, XXXII Zerfalls- und austauschreaktionen der aluminiumtrialkyle. Justus Liebigs Ann. Chem. *629*, 53–89.

57. Yanik, J., and Karayildirim, T. (2006). Liquefaction of municipal waste plastics over acidic and nonacidic catalysts. In Feedstock Recycling and Pyrolysis of Waste Plastics, J. Scheirs, J. Scheirs, and W. Kaminsky, eds. (John Wiley & Sons), pp. 209–224.

58. Werghi, B., Bendjeriou-Sedjerari, A., Sofack-Kreutzer, J., Jedidi, A., Abou-Hamad, E., Cavallo, L., and Basset, J.M. (2015). Well-defined silica supported aluminum hydride:

another step towards the utopian single site dream? Chem. Sci. *6*, 5456–5465.

59. Kermagoret, A., Kerber, R.N., Conley, M.P., Callens, E., Florian, P., Massiot, D., Copéret, C., Delbecq, F., Rozanska, X., and Sautet, P. (2013). Triisobutylaluminum: bulkier and yet more reactive towards silica surfaces than triethyl or trimethylaluminum. Dalton Trans *42*, 12681–12687.

60. Thieuleux, C., Maraval, A., Veyre, L., Copéret, C., Soulivong, D., Basset, J.M., and Sunley, G.J. (2007). Homologation of propane catalyzed by oxide-supported zirconium dihydride and dialkyl complexes. Angew. Chem. Int. Ed. Engl. *46*, 2288–2290.

61. Perras, F.A., Boteju, K.C., Slowing, I.I., Sadow, A.D., and Pruski, M. (2018). Direct ^{17}O dynamic nuclear polarization of single-site heterogeneous catalysts. Chem. Commun. *54*, 3472–3475.

62. Perras, F.A., Wang, Z., Kobayashi, T., Baiker, A., Huang, J., and Pruski, M. (2019). Shedding light on the atomic-scale structure of amorphous silica–alumina and its brønsted acid sites. Phys. Chem. Chem. Phys. *21*, 19529–19537.

63. Grey, C.P., and Vega, A.J. (1995). Determination of the quadrupole coupling constant of the invisible aluminum spins in zeolite HY with $^{1}H/^{27}Al$ TRAPDOR NMR. J. Am. Chem. Soc. *117*, 8232–8242.

64. Grey, C.P., and Veeman, W.S. (1992). The detection of weak heteronuclear coupling between spin 1 and spin 1/2 nuclei in MAS NMR; $^{14}N/^{13}C/^{1}H$ triple resonance experiments. Chem. Phys. Lett. *192*, 379–385.

65. Adachi, M., Nedez, C., Wang, X.X., Bayard, F., Dufaud, V., Lefebvre, F., et al. (2003). Surface organometallic chemistry of zirconium. Chemical reactivity of the $\equiv Si-O-ZrNp_3$ surface complex synthesized on dehydroxylated silica and application to the modification of mordenite. J. Mol. Cat. A: Chem. *204–205*, 443–455.

66. Bäckström, E., Odelius, K., and Hakkarainen, M. (2019). Designed from recycled: turning polyethylene waste to covalently attached polylactide plasticizers. ACS Sustainable Chem. Eng. *7*, 11004–11013.

67. Zhao, D., Wang, X., Miller, J.B., and Huber, G.W. (2020). The chemistry and kinetics of polyethylene pyrolysis: a process to produce fuels and chemicals. ChemSusChem *13*, 1764–1774.

68. Bunel, E., Burger, B.J., and Bercaw, J.E. (1988). Carbon-carbon bond activation via β-alkyl elimination. Reversible branching of 1,4-pentadienes catalyzed by scandocene hydride derivatives. J. Am. Chem. Soc. *110*, 976–978.

69. Watson, P.L., and Roe, D.C. (1982). β-alkyl transfer in a lanthanide model for chain Termination. J. Am. Chem. Soc. *104*, 6471–6473.

70. Quintanilla, E., di Lena, F., and Chen, P. (2006). Chain transfer to aluminium in MAO-activated metallocene-catalyzed polymerization reactions. Chem. Commun. (41), 4309–4311.

71. Ewart, S., Konstantinov, I., Karjala, T., Baugh, D., iii, and Munjal, S. (2020). Aluminum alkyls as highly active catalytic chain transfer agents. Macromol. React. Eng. *14*, 1900047.

72. Mogstad, A.L., and Waymouth, R.M. (1992). Chain transfer to aluminum in the homogeneous cyclopolymerization of 1,5-hexadiene. Macromolecules *25*, 2282–2284.

73. Baroni, A.C.M., Arruda, C.C.P., and Carvalho, D.B. (2017). Hydroalumination of alkenes and alkynes. In PATAI's Chemistry of Functional Groups, Z. Rappoport, ed. (John Wiley & Sons), pp. 1–24.

74. Joubert, J., Delbecq, F., Thieuleux, C., Taoufik, M., Blanc, F., Copéret, C., Thivolle-Cazat, J., Basset, J.-M., and Sautet, P. (2007). Synthesis, characterization, and catalytic properties of γ-Al_2O_3-supported zirconium hydrides through a combined use of surface organometallic chemistry and periodic calculations. Organometallics *26*, 3329–3335.

75. Waterman, R. (2013). σ-bond Metathesis: a 30-year retrospective. Organometallics *32*, 7249–7263.

Chem, Volume *7*

Supplemental information

Catalytic carbon-carbon bond cleavage and carbon-element bond formation give new life for polyolefins as biodegradable surfactants

Uddhav Kanbur, Guiyan Zang, Alexander L. Paterson, Puranjan Chatterjee, Ryan A. Hackler, Massimiliano Delferro, Igor I. Slowing, Frédéric A. Perras, Pingping Sun, and Aaron D. Sadow

Table of Contents

Supplemental Methods

Materials

General. All manipulations were carried out under inert conditions, either using Schlenk techniques or in a glovebox under a purified nitrogen atmosphere, unless stated otherwise. Dry and degassed solvents were used throughout. Pentane was sparged with nitrogen, passed through activated alumina columns, and stored under nitrogen. Benzene-d_6 was degassed via three consecutive freeze-pump-thaw cycles, dried over Na/K alloy, vacuum transferred, and stored over molecular sieves under nitrogen. Tetrakisneopentyl zirconium,[2] dimethylaluminum hydride,[3] triphenylaluminum,[4] and alane[5] were synthesized according to literature procedures. Trimethylaluminum, triethylaluminum, triisobutylaluminum, diisobutylaluminum hydride, high density polyethylene (HDPE, M_n = 6.2 kDa, M_w = 38.6 kDa, $Đ$ = 6.2), isotactic polypropylene (*i*PP, M_n = 37.4.2 kDa, M_w = 117.6 kDa, $Đ$ = 3.2), and $Al(NO_3)_3{\cdot}9H_2O$ (98%) were purchased from Sigma-Aldrich and used as received. $Na_2SiO_3{\cdot}9H_2O$ (98%), NH_4NO_3, and concentrated HCl were purchased from Fisher Scientific, and used as received. Fumed silica (Aerosil) of surface area 300 m^2/g was purchased from Evonik, calcined and partially dehydroxylated at 550° C for 12 h. Titration of the surface silanols in this material with $Mg(CH_2Ph)_2(O_2C_4H_8)_2$ revealed a surface OH loading of 0.46 ± 0.05 mmol/g.

Preparation of Silica-Alumina ($SiAlO_x$). Silica-alumina was synthesized by modification of a literature procedure.[6] In brief, sodium metasilicate nonahydrate ($Na_2SiO_3{\cdot}9H_2O$, 22.26 g, 76.8 mmol) was dissolved in H_2O (200 mL). Separately, $Al(NO_3)_3{\cdot}9H_2O$ (9.80 g, 25.6 mmol) was dissolved in H_2O (27 mL) giving a 0.95 M $Al(NO_3)_3$ solution. This $Al(NO_3)_3$ solution was then added to the Na_2SiO_3 solution in a dropwise fashion, and the mixture was stirred at 500 rpm for 5 min. The pH of the solution was adjusted to ca. 8 with HCl (0.1 M). The mixture was then stirred at 500 rpm for an additional 20 min. and spun in a centrifuge to obtain a white precipitate. The solid was sequentially washed with H_2O (2 × 35 mL), NH_4NO_3 (1.0 M, 2 × 40 mL) and H_2O (2 × 35 mL). The material was dried in an oven at 75 °C overnight and then calcined at 550 °C for 10 h to obtain ca. 12.5 g of white $SiAlO_x$ powder. ICP-OES analysis indicates that this material is 9.3±0.4 wt % Al. The BET surface area measured by N_2 sorption isotherms was 182 m^2/g (Figure S18). This material was partially dehydroxylated by heating at 700 °C under vacuum for 12 h, and then stored in the glovebox under N_2. Titration of the reactive surface hydroxyls (silanols) with $Mg(CH_2Ph)_2(O_2C_4H_8)$ revealed a surface OH loading of 0.39 ± 0.05 mmol/g.

Preparation of $Zr(CH_2CMe_3)_2$@$SiAlO_x$. This material was synthesized by a procedure adapted from reference.[7] In the glovebox, 0.30 g of $Zr(CH_2CMe_3)_4$ (0.8 mmol) was dissolved in anhydrous pentane (7 mL). This solution was added to a suspension of silica-alumina (1.00 g) in pentane (7 mL), and the resulting suspension was stirred at room temperature for 4 h. The suspension was allowed to settle, and the supernatant liquid was decanted. The residual solid was washed with pentane (3 × 5 mL) and dried overnight in vacuo to afford an off-white powder (0.92 g). This material contains 2.2 ± 0.2 CH_2CMe_3 groups per Zr center, as determined by titration of $Zr(CH_2CMe_3)_2$@$SiAlO_x$ with CH_3OH and ICP-OES (2.7 wt % Zr, 0.30 mmol Zr/g). Solid-state ^{13}C NMR spectra and infrared spectra match reported literature values (*13*). ^{13}C NMR (CP-MAS, 400 MHz): δ 94.78 (CH_2CMe_3), 32.88 (CH_2CMe_3). IR (DRIFTs, cm^{-1}): 2959, 2907, 2872, 1478, 1398, 1366, 1205, 843. Elemental analysis for $Zr(CH_2CMe_3)_2$@$SiAlO_x$: C, 3.30; H, 0.24; Zr, 2.70.

Preparation of $Zr(CH_2CMe_3)_2$@SiO_2. This material was synthesized by a procedure adapted from reference (*20*) and is compared to the reported material in references 8 and 9. In the glovebox, 0.30 g of $Zr(CH_2CMe_3)_4$ (0.8 mmol) was dissolved in anhydrous pentane (7 mL). This solution was added to a suspension of Aerosil (1.00 g) in pentane (7 mL), and the resulting mixture was stirred at room temperature for 4 h. The suspension was allowed to settle, and the supernatant liquid was decanted. The residual solid was washed with pentane (3 × 5 mL) and dried overnight in vacuo to afford an off-white powder (0.98 g).

This material contained 2.1 ± 0.2 CH_2CMe_3 groups per Zr center, as revealed by titration of $Zr(CH_2CMe_3)_2@SiO_2$ with CH_3OH and ICP-OES (3.51 wt % Zr, 0.38 mmol Zr/g). IR (DRIFTs, cm^{-1}): 2957, 2866, 1468, 1363, 1214, 1185, 1173, 1145, 823. Elemental analysis for $Zr(CH_2CMe_3)_2@SiO_2$: C, 2.32; H, 0.39; Zr, 3.51.

Materials Characterization

General. DRIFT spectra were collected using a Harrick Praying Mantis accessory and a sealed, ambient-pressure sample chamber consisting of a dome with ZnSe windows. Elemental analysis was performed using a Perkin-Elmer 2400 Series II CHN/S at the Iowa State Chemical Instrumentation Facility. Inductively Coupled Plasma-Optical Emission Spectroscopy (ICP-OES) was performed to measure the amount of zirconium present in the catalytic materials. The samples (2.0 – 4.0 mg each) were digested for 24 h in aqueous HF and aqua-regia (0.18% and 5% respectively) and analyzed in a Perkin Elmer Optima 2100 DV Inductively Coupled Plasma-Optical Emission Spectroscope. The nitrogen adsorption/desorption isotherms were measured in a Micromeritics Tristar surface area and porosity analyzer, and surface area was calculated by the Brunauer−Emmett−Teller (BET) method.

Solid-State NMR. All solid-state NMR experiments utilized a Bruker AVANCE III 400 MHz NMR spectrometer. $^{17}O\{^{27}Al\}$ transfer of populations double-resonance (TRAPDOR) experiments were performed using a triple-resonance 3.2-mm low-temperature-magic-angle-spinning (MAS) probe at a temperature of 100 K. Prior to the experiment, the sample was impregnated with a 16 mM solution of the TEKPol biradical[10] in a deuterated 1,1,2,2-tetrachloroethane solution and the magnetic field of the NMR magnet was decreased by 500 ppm from its usual position associated with the ^1H cross-effect maximum when using nitroxides. This enabled for the irradiation of the positive ^{17}O cross-effect maximum and the enhancement of the ^{17}O NMR signal via dynamic nuclear polarization (DNP). A c.a. 264 GHz gyrotron microwave source was used for the DNP experiments. In addition to DNP a hyperbolic secant pulse[11] was also applied 300 kHz away from the central transition to enhance it via population transfer from the satellite transitions. This pulse lasted 10 ms and swept over a 12.5 kHz range, corresponding to the MAS frequency used. The TRAPDOR spectra were each an accumulation of 8192 scans using a recycle delay of 3.1 s. The echo delay was set to 3.2 ms and 100 kHz ^{27}Al rf was applied during the first such delay to acquire the dephased (*S*) spectrum. All ^{17}O pulses utilized a 25 kHz effective central transition-selective rf field. An analogous spectrum was acquired in the absence of this pulse as a reference (S_0).

Catalytic Alumination of Polyolefins

General Procedure. In the glovebox, the polyolefin reactant, supported catalyst, and aluminum reagent were loaded into a glass tube equipped with a glass-encapsulated magnetic stirrer. The tube was sealed with a stainless steel UltraTorr fitting to a closed glass tube with a sidearm containing a re-sealable Teflon-glass valve. The vessel was heated in an aluminum block at the desired temperature (≥ 150 °C to ensure the polymer was above its melting point) for the required reaction time with mixing. The volatile components of the headspace were sampled and analyzed by GC-MS. After the appropriate time, the contents of the tube were quenched by passing dry air into the vessel through the sidearm for 1 h. The crude reaction mixture was extracted with CH_2Cl_2 (3 × 5 mL), and the volatile components were evaporated from the liquid to provide an oil which was further analyzed by spectroscopic and analytical techniques (NMR, IR, GC-MS, MALDI-TOF-MS). Yields of oils are given as a percentage of the starting polyolefin mass. The residual solid was dissolved in hot 1,2-dichlorobenzene and filtered to remove the catalyst. A solid crashes out from the filtrate upon cooling. The supernatant liquid was decanted, and the solid polymer was washed with CH_2Cl_2 (3 × 5 mL), dried in vacuo, and analyzed by IR spectroscopy.

Results and Analysis of Catalytic Reactions in Table 1.

1. HDPE + $Zr(CH_2CMe_3)_2$@$SiAlO_x$ + Al*i*Bu_3 (150 °C). HDPE (0.63 g), $Zr(CH_2CMe_3)_3$@$SiAlO_x$ (0.10 g, 0.030 mmol Zr) and Al*i*Bu_3 (60 µL, 0.24 mmol) were allowed to react at 150 °C for 12 h to provide an oil (0.19 g, 31%) which was characterized by NMR, IR, and MALDI as described in the main text and residual HDPE (0.44 g). MALDI-TOF-MS revealed a bimodal distribution, with maxima at $C_{39}H_{79}OH$ and $C_{54}H_{109}OH$.

2. HDPE + $Zr(CH_2CMe_3)_2$@$SiAlO_x$ + Al*i*Bu_3 (200 °C). HDPE (1.00 g), $Zr(CH_2CMe_3)_3$@$SiAlO_x$ (0.13 g, 0.039 mmol Zr) and Al*i*Bu_3 (100 µL, 0.40 mmol) were allowed to react at 200 °C for 12 h to provide an oil (0.40 g, 40%) and residual HDPE (0.50 g). Experiments with doubled initial catalyst and Al*i*Bu_3 loading with respect to polyethylene (10.5 g HDPE/mmol Zr) also gave the oil in 40% yield after 12 h at 200 °C. However, two portions of $Zr(CH_2CMe_3)_3$@$SiAlO_x$ and Al*i*Bu_3, added initially and after 12 h gave 72% total yield of oil (C_{32} ~ C_{44} alcohol distribution).

3. HDPE + $Zr(CH_2CMe_3)_2$@$SiAlO_x$ + Al*i*Bu_3 (Zr catalyst/Al*i*Bu_3 added in 3 portions). HDPE (1.00 g), $Zr(CH_2CMe_3)_3$@$SiAlO_x$ (0.11 g, 0.033 mmol Zr) and Al*i*Bu_3 (120 µL, 0.48 mmol) were allowed to react at 200 °C for 12 h. The reaction tube was cooled to room temperature and additional (same as before) portions of $Zr(CH_2CMe_3)_2$@$SiAlO_x$ and Al*i*Bu_3 were added. The mixture was heated at 200 °C for 12 h. This procedure was repeated once more (after a total of 36 h) to provide an oil (0.84 g, 84%), and no visible polyethylene was remaining.

4. HDPE + $Zr(CH_2CMe_3)_2$@$SiAlO_x$ + Al*i*Bu_3 (quenched with MeOH). HDPE (1.00 g), $Zr(CH_2CMe_3)_2$@$SiAlO_x$ (0.11 g, 0.033 mmol Zr) and Al*i*Bu_3 (100 µL, 0.40 mmol) were allowed to react at 200 °C for 12 h. The reaction tube was cooled to room temperature, and degassed MeOH (3 mL) was added. After 30 min, the solvent was removed under reduced pressure and the residue was extracted with CH_2Cl_2 (3 × 5 mL) to provide an oil (0.38 g, 38%) and residual HDPE (0.64 g).

5. HDPE + $Zr(CH_2CMe_3)_2$@$SiAlO_x$ + Al*i*Bu_3 (quenched with I_2). HDPE (0.54 g), $Zr(CH_2CMe_3)_2$@$SiAlO_x$ (0.06 g, 0.019 mmol Zr) and Al*i*Bu_3 (50 µL, 0.20 mmol) were allowed to react at 200 °C for 12 h. The reaction tube was cooled to room temperature and I_2 (0.06 g, 0.23 mmol) in anhydrous and degassed CH_2Cl_2 (5 mL) was added. After 30 min, the solvent was removed under reduced pressure, and the residue was extracted with CH_2Cl_2 (3 × 5 mL) to provide an oil (0.23 g, 43%) and residual HDPE (0.32 g). Cross-peaks in the ^{1}H-^{13}C phase sensitive HSQC spectrum of the oil (Figure S24) corresponding to proton signals at 3.1 ppm and shielded carbon signals at 10 ppm indicated the presence of -*CH*$_2$-I groups in the product.

6. HDPE + $Zr(CH_2CMe_3)_2$@$SiAlO_x$ + Al*i*Bu_3 (quenched with CO_2). HDPE (0.55 g), $Zr(CH_2CMe_3)_2$@$SiAlO_x$ (0.06 g, 0.019 mmol Zr) and Al*i*Bu_3 (50 µL, 0.20 mmol) were allowed to react at 200 °C for 12 h. The reaction tube was cooled to room temperature and evacuated. Dry CO_2 was introduced into the vessel, which was then heated to 60 °C. After 4 h, the reaction mixture was exposed to air, and the residue was extracted with CH_2Cl_2 (3 × 5 mL) to provide an oil (0.20 g, 36%) and residual HDPE (0.36 g). Cross-peaks in the ^{1}H-^{13}C HMBC spectrum of the oil (Figure S30) corresponding to carbon signals in the range of 170-180 ppm confirmed the presence of -COOH groups in the product.

7. HDPE + $Zr(CH_2CMe_3)_2$@$SiAlO_x$ + $AlEt_3$ (150 °C). HDPE (0.51 g), $Zr(CH_2CMe_3)_2$@$SiAlO_x$ (0.10 g, 0.03 mmol Zr) and $AlEt_3$ (50 µL, 0.36 mmol) were allowed to react at 150 °C for 12 h to provide an oil (0.13 g, 25%) and residual HDPE (0.41 g).

8. HDPE + $Zr(CH_2CMe_3)_2$@$SiAlO_x$ + $AlEt_3$ (200 °C). HDPE (0.60 g), $Zr(CH_2CMe_3)_2$@$SiAlO_x$ (0.10 g, 0.03 mmol Zr) and $AlEt_3$ (50 µL, 0.36 mmol) were allowed to react at 200 °C for 12 h to provide an oil (0.15 g, 24%) and residual HDPE (0.45 g).

9. HDPE + $Zr(CH_2CMe_3)_2$@$SiAlO_x$ + $AlPh_3$. HDPE (0.64 g), $Zr(CH_2CMe_3)_2$@$SiAlO_x$ (0.07 g, 0.021 mmol Zr) and $AlPh_3$ (66 mg, 0.26 mmol) were allowed to react at 200 °C for 12 h to provide an oil (0.19 g, 29%) and residual HDPE (0.49 g).

10. HDPE + $Zr(CH_2CMe_3)_2$@$SiAlO_x$ + AlH_3. HDPE (0.52 g), $Zr(CH_2CMe_3)_2$@$SiAlO_x$ (0.10 g, 0.03 mmol Zr) and AlH_3 (28 mg, 0.93 mmol) were allowed to react at 200 °C for 12 h to provide an oil (0.22 g, 42%) and residual HDPE (0.28 g).

11. HDPE Grocery Bag + $Zr(CH_2CMe_3)_2$@$SiAlO_x$ + Al*i*Bu_3. HDPE from a plastic grocery bag (0.60 g), $Zr(CH_2CMe_3)_2$@$SiAlO_x$ (0.10 g, 0.03 mmol Zr) and Al*i*Bu_3 (100 µL, 0.40 mmol) were allowed to react at 200 °C for 12 h to provide an oil (0.19 g, 31%) and a residual polymeric solid (0.41 g).

12. *i*PP + $Zr(CH_2CMe_3)_2$@$SiAlO_x$ + Al*i*Bu_3. Isotactic polypropylene (1.00 g), $Zr(CH_2CMe_3)_2$@$SiAlO_x$ (0.14 g, 0.042 mmol Zr) and Al*i*Bu_3 (120 µL, 0.48 mmol) were allowed to react at 200 °C for 12 h to provide an oil (0.27 g, 27%) and a residual polymeric solid (0.74 g).

13. HDPE + $Zr(OCH_2CMe_3)_2$@$SiAlO_x$ + Al*i*Bu_3. $Zr(CH_2CMe_3)_2$@$SiAlO_x$ (0.07 g, 0.021 mmol Zr) was exposed to dry air for 10 min at room temperature to provide $Zr(OCH_2CMe_3)_2$@$SiAlO_x$. HDPE (0.60 g), $Zr(OCH_2CMe_3)_2$@$SiAlO_x$, and Al*i*Bu_3 (100 µL, 0.40 mmol) were allowed to react at 200 °C for 12 h to provide an oil (0.21 g, 34%) and a residual polymeric solid (0.42 g).

14. HDPE + $Zr(OCH_2CMe_3)_2$@$SiAlO_x$ + AlH_3. $Zr(CH_2CMe_3)_2$@$SiAlO_x$ (0.05 g, 0.015 mmol Zr) was exposed to dry air for 10 min at room temperature to provide $Zr(OCH_2CMe_3)_2$@$SiAlO_x$. HDPE (0.35 g), $Zr(OCH_2CMe_3)_2$@$SiAlO_x$ and AlH_3 (28 mg, 0.93 mmol) were allowed to react at 200 °C for 12 h to provide an oil (0.17 g, 49%) and a residual polymeric solid (0.18 g).

15. HDPE + $Zr(OCH_2CMe_3)_2$@$SiAlO_x$ + AlH_3 (under dynamic vacuum). $Zr(CH_2CMe_3)_3$@$SiAlO_x$ (0.12 g, 0.036 mmol Zr) was exposed to dry air for 10 min at room temperature to provide $Zr(OCH_2CMe_3)_2$@$SiAlO_x$. HDPE (0.85 g), $Zr(OCH_2CMe_3)_2$@$SiAlO_x$, and AlH_3 (29 mg, 0.97 mmol) were allowed to react at 200 °C under dynamic vacuum for 12 h to provide an oil (0.51 g, 60%) and residual HDPE (0.30 g).

16. HDPE + $Zr(CH_2CMe_3)_2$@SiO_2 + Al*i*Bu_3. HDPE (1.00 g), $Zr(CH_2CMe_3)_2$@SiO_2 (0.11 g, 0.042 mmol Zr) and Al*i*Bu_3 (100 µL, 0.40 mmol) were allowed to react at 200 °C for 12 h to provide an oil (0.35 g, 35%) and a residual polymeric solid (0.54 g). Catalytic materials employing SiO_2 as the support generated small amounts of alkylsilanes at 200 °C, such as *i*Bu_2SiH_2, Et_2SiH_2 and Et_3SiH, as side products during catalysis, whereas such species were not detected in catalytic reactions of $Zr(CH_2CMe_3)_2$@$SiAlO_x$.

17. HDPE + $Zr(CH_2CMe_3)_2$@SiO_2 + $AlEt_3$. HDPE (0.41 g), $Zr(CH_2CMe_3)_2$@SiO_2 (0.05 g, 0.019 mmol Zr) and $AlEt_3$ (50 µL, 0.36 mmol) were allowed to react at 200 °C for 12 h to provide an oil (0.13 g, 33%) and a residual solid (0.29 g).

Characterization Methods for Fatty Alcohol, Acid, and Halide Products

General. 1D ^1H and $^{13}C\{^1H\}$, and 2D ^1H-^1H COSY, TOCSY and ^1H-^{13}C HSQC NMR spectra were acquired on a Brucker NEO 400 MHz spectrometer. Fourier transform infrared (FT-IR) spectra and diffuse reflectance infrared Fourier transform (DRIFT) spectra were recorded on a Bruker VERTEX 80 IR spectrometer. Samples for transmission IR were diluted with KBr and made into a pellet using a hydraulic press.

MALDI-TOF Mass Spectrometry. MALDI-TOF-MS experiments were carried out on a Shimadzu AXIMA Confidence MALDI-TOF mass spectrometer, equipped with an N_2 laser (337 nm, 25 Hz repetition rate). The mass spectra were acquired in the linear and positive ion mode. 100 laser pulses were utilized for each measurement.

Stock solutions of products were prepared in tetrahydrofuran at a 0.5 mg/mL concentration, and a stock solution of silver nitrate was prepared in a 1:1 (*v*:*v*) mixture of tetrahydrofuran and acetonitrile at a concentration of 10 mg/mL. Final sample solutions for spotting were prepared by mixing equal volumes (0.2 mL) of stock solutions of alkanes and silver nitrate. The matrix (2,5-dihydroxybenzoic acid (DHB)) solution was prepared in a 3:2 (*v*:*v*) mixture of tetrahydrofuran and methanol at a 10 mg/mL concentration. The dried-droplet method of sample deposition was employed, where 0.5 μL of the sample solution was deposited on the stainless-steel sample plate, followed by 0.5 μL of the matrix solution. The solvents were allowed to evaporate by air-drying.

DRIFT IR Experiments on Putative ZrH Surface Species

Generation of ZrH@SiAlO$_x$ and H/D exchange experiments. Zr(CH_2CMe_3)$_2$@SiAlO$_x$ (0.4 g, 0.12 mmol Zr) and excess Al*i*Bu$_3$ (0.5 mL, 1.98 mmol) were added in a glass tube in the glovebox, which was sealed with an UltraTorr fitting to a closed glass tube adapted with a sidearm containing a re-sealable Teflon-glass valve. The sealed vessel was transferred from the glovebox and attached to a Schlenk line. The reactor inserted into an aluminum block and heated at 150 °C for 2 h. The reactor was then cooled to room temperature, evacuated, taken back into the glovebox, washed with anhydrous pentane (3 × 2 mL) and dried in vacuo to provide a brown powder, which was sampled and analyzed by DRIFT IR spectroscopy (Figure 3a). The reactor was reattached to a Schlenk line and evacuated, D_2 gas was introduced at atmospheric pressure, and the reactor was sealed. The tube was heated at 70 °C for 30 min, allowed to cool, taken into the glovebox, and a sample was analyzed by DRIFT IR spectroscopy (Figure 3b). Subsequently, this material was sealed under an atmosphere of H_2, heated at 70 °C for 30 min and analyzed by DRIFT IR spectroscopy (Figure 3c).

The spectrum in Figure 3a contained a broad and prominent peak at 1622 cm^{-1}, attributed to a Zr–H stretching mode (ν_{ZrH}) based on related assignments in literature reports. This signal disappeared upon treatment of the material with D_2, indicating that the original band at 1622 cm^{-1} was indeed from a hydride species. Alternatively, the signal at 1622 cm^{-1} is reduced by exposure of the material to ambient atmosphere. To rule out adventitious air or moisture in the deuterium exchange experiment, the isotopically labeled material was treated with H_2 to regenerate the hydride signal at 1622 cm^{-1} and confirm the presence of an active hydride species in the material. Because SiAlO$_x$ and Al*i*Bu$_3$ are not catalytically competent for C–C cleavage of HDPE in the absence of surface-supported Zr species, we assign the IR signal at 1622 cm^{-1} to a catalytically active Zr-H surface species generated from the reaction of zirconium neopentyl and triisobutylaluminum. We cannot, however, rule out the presence of a bridged bimetallic species containing Zr–H–Al structures, which could also mediate metalation of polyethylene and β-alkyl elimination because the IR bands of this and Zr–H species overlap.[12]

In a second experiment, Zr(CH_2CMe_3)$_2$@SiAlO$_x$ and 3 equiv. of Al*i*Bu$_3$ were allowed to react at room temperature in benzene-d_6, and the soluble portion of the reaction mixture was analyzed by ^{1}H NMR spectroscopy (Figure S92). The analysis reveals neopentyl aluminum, isobutylene, neopentane, and isobutane are formed. Neopentyl aluminum species indicate alkyl transfer from neopentyl zirconium to aluminum, either via alkyl group exchange or by alkyl/β-hydride exchange. The former would produce isobutylzirconium species, which could undergo β-hydrogen elimination to form hydridozirconium surface sites and isobutylene, while the latter pathway would produce hydridozirconium surface sites and isobutylene directly.

Process Design and Technoeconomic Analysis

Model Description. To examine the potential process economics for the technology development of plastic conversion to fatty alcohols, a technoeconomic analysis (TEA) based on a conceptual plant with a

polymer (HDPE) processing capacity of about 250 MT/day (or output of 70,847 kg/day fatty alcohol sulfate, as a surfactant product) operating at 90% utilization, was conducted using an Aspen Plus model (Figure S94). In the conceptual plant, the HDPE feedstock is fed to a slurry reactor to react with triisobutyl aluminum, with the aid of silica-alumina supported Zr catalyst. The overall polymer conversion reaction is shown below as equation 1.

$$\begin{aligned} C_{2746}H_{5494} + 18.26\ AlC_{12}H_{27} \\ + 27.39\ O_2 + 18.23\ H_2O \end{aligned} \longrightarrow \begin{aligned} 18.23\ C_{40}H_{81}OH + 8.21\ C_{40}H_{82} + 54.78\ C_4H_8 \\ + 32.315\ C_5H_{12} + 0.132\ C_5H_{10} + 13.4\ C_6H_{14} \\ + 18.26\ Al(OH)_3 + 0.365\ C_{3961}H_{7632} \end{aligned} \quad (1)$$

HDPE reacts with triisobutyl aluminum to form $Al(OH)_3$, fatty alcohols (centered at C_{40}, with range of C_{28}-C_{55}), long chain paraffins (centered at C_{40}, with range of C_{20}-C_{45}), C_5-C_6 linear paraffins, C_4 olefins, and some heavy gummy residuals (represented by $C_{3961}H_{7632}$) under relative mild condition of 200 °C and 1.2 bar (followed by air quenching in Cooler 1 in Figure S94). The fatty alcohols are expected to be high quality feedstock for surfactant production,[13] long chain paraffins are expected to present high quality lubricant.[14] The light hydrocarbons can be sold as diluent. In the present study, the light carbons are combusted to self-sustain the system. The heavy residual can be sold as asphalt or combusted for energy supply. Both scenarios are feasible, and the present study chose the scenario to combust light hydrocarbons and sell asphalt, as an example, given the absence of asphalt heating values.

As the light hydrocarbons (C_4-C_6) flows to Boiler for combustion to provide electricity and steam for plant usage, the slurry stream (a liquid solid mixture containing all the products and catalyst) is separated in the Solid filter at 120 °C (Figure S94). The long chain paraffins and fatty alcohols are in liquid state and are separated from the solid mixture via filtration. The separation of long chain paraffins and fatty alcohols is rather complex, requiring a series of solvent extraction and distillation processes, as the fatty alcohol is not soluble in water given its the long paraffinic chain feature dominates its property. By considering the feedstock value of fatty alcohol for surfactant production, we determine that relative to the complex and thus costly separation of fatty alcohol and long chain paraffins, it would be more economical to extend the facility boundary to include surfactant production process that not only produces more valuable final products but also separates long chain paraffins, using the reaction shown below as equation 2.

$$C_{40}H_{81}OH + SO_3 \longrightarrow C_{40}H_{81}OSO_3H \xrightarrow{NaOH} C_{40}H_{81}OSO_3Na + H_2O \quad (2)$$

SO_3 is fed into Reactor 1 at elevated temperature (45 °C) and pressure (27.4 bar) to react with the fatty alcohol while long chain paraffins are unreactive. The resulting alcohol sulfate $C_{40}H_{81}OSO_3H$ and long chain paraffin will flow to Reactor 2, where aqueous NaOH is introduced to convert $C_{40}H_{81}OSO_3H$ to sodium fatty alcohol sulfate $C_{40}H_{81}OSO_3Na$, which dissolves in aqueous phase. By using a separator, the aqueous $C_{40}H_{81}OSO_3Na$ is separated, dried and sold as a final product. Meanwhile, the long chain paraffins in the oil phase can be further distilled to remove light compounds and sold as a lubricant product. The light compounds are diverted to Boiler for combustion for energy supply.

The solid phase from the solid filter includes asphalt, $Al(OH)_3$, and solid $ZrX/SiAlO_x$ catalyst. Asphalt can be separated from the rest at elevated temperature by transforming to liquid phase, filtered by liquid-solid filtration, then sold as a final asphalt product after proper cooling. Meanwhile, $Al(OH)_3$ and solid $ZrX/SiAlO_x$

catalyst could be separated via reacting with aqueous HCl in Reactor 3. The solid $Al(OH)_3$ will react with HCl to form $AlCl_3$ (equation 3) that dissolves in aqueous phase while $ZrX/SiAlO_x$ is unreacted. By using the solid liquid filter, the $ZrX/SiAlO_x$ catalyst can be recovered and recycled to the Slurry reactor for reuse, and the aqueous $AlCl_3$ is dried and sold as a final product.

$$Al(OH)_3 + 3\ HCl \longrightarrow AlCl_3 + 3\ H_2O \quad (3)$$

A waste-water treatment plant is not included in the design, as we assume the relatively small plant will discharge to municipal waste water treatment plant for treatment.

The product has a minimum C_{40} fatty alcohol sulfate market selling price, or breakeven price of $3.41/kg. Currently, the market price of C_{40} sodium fatty alcohol sulfate is not available, thus the price of C_{12} fatty alcohol sulfate (sodium lauryl sulfate) is used as an approximate estimate. C_{12} fatty alcohol sulfate has a price range of $1-3/kg, based on various purities. For the present study, the resulting C_{40} fatty alcohol sulfate is expected to have much higher market price than the sodium lauryl sulfate, making the process profitable. Examples of retail prices for long carbon chain fatty alcohols are listed in Table S4.

Table S1. Flow rate and cost of materials input, energy inputs and products.

Material consumptions	Flow rate (kg/hr)	Production (kg/day)	Price ($/kg)	References
HDPE	10416.67	250,000	0.274	https://resource-recycling.com/plastics/2019/07/17/modest-changes-in-scrap-plastics-pricing/
H_2O	8613.45	206,723	Footnote *a*	
$Al(C_4H_9)_3$	979.33	23,504	3.0	https://www.lookchem.com/casno100-99-2.html
Zr Catalyst	1354.17	32,500	2000	https://www.sigmaaldrich.com/catalog/product/aldrich/221880?lang=en&region=US, https://www.sigmaaldrich.com/catalog/product/aldrich/278327?lang=en&region=US, https://www.sigmaaldrich.com/catalog/product/aldrich/274496?lang=en&region=US
Air	1018.75	24,450		
SO_3	393.64	9,447	20.0	https://dir.indiamart.com/impcat/sulphur-trioxide.html
NaOH	196.65	4,720	0.52448	2018 NREL report,[1] see footnote for 2016 dollars
HCl	540.79	12,979	0.15	https://www.icis.com/explore/resources/news/2019/01/03/10300671/outlook-19-us-hcl-market-expects-stronger-demand-firming-prices/
Cooling water	1508337.87	36,200,109	Footnote *a*	
Products	**Flow rate (kg/hr)**		**Price ($/kg)**	
$C_{40}H_{81}OSO_3Na$	3279.95	78,719	60.0	https://www.bulkapothecary.com/raw-ingredients/other-ingredients-and-chemicals/sodium-laureth-sulfate-sles/
$C_{40}H_{82}$	1263.67	30,328	3.01	Table F10: Lubricants consumption, price, and expenditure estimates, 2018: https://www.eia.gov/state/seds/data.php?incfile=/state/seds/sep_fuel/html/fuel_lu.html&sid=US
Asphalt	5455.22	130,925	0.13	https://sciencing.com/how-6558396-calculate-asphalt-prices.html
$AlCl_3$	658.42	15,802	1.5	https://www.alibaba.com/showroom/alcl3-price.html
C_4-C_6	1776.45	42,635	0.5	https://tradingeconomics.com/commodity/naphtha
Energy generated	**kW**	**kWh/day**		
Electricity	–5684.11	136,419		

[a] The process water price is $2.4/kgal and the cooling water price is $0.1/kgal according to the H2A model (reference: H2A Hydrogen Production Model: Version 3.2018 User Guide)

Table S2. Installed capital cost of the designed plastic conversion process.

Indirect depreciable capital cost		
A1: Area 100: Feedstock and catalyst handing	$7,661,803	9.18%
A2: Area 200: Plastic conversion and product separation	$11,034,583	13.22%
A3: Area 300: Catalyst recovery and recycle	$513,127	0.61%
A4: Combustion and cooling tower system	$15,481,195	18.55%
Total direct capital cost	$34,690,709	41.58%
Indirect depreciable capital cost		
Site preparation	$690,558	0.83%
Engineering & design	$3,452,790	4.14%
Project contingency	$5,179,185	6.21%
Catalyst first fill fee	$33,860,098	40.58%
Up-front permitting costs	$5,179,185	6.21%
Total depreciable capital costs	$82,889,715	99.34%
Non-depreciable capital cost		
Land cost	$550,362	0.66%
Total Capital Costs	**$83,440,077**	**100.00%**

Table S3. Fixed cost and variable cost of the designed plastic conversion process.

Fixed operating costs		
Labor cost	$2,401,993	42.89%
G&A	$480,399	8.58%
Property taxes and insurance	$1,668,802	29.80%
Material costs for maintenance and repairs	$1,049,006	18.73%
Total Fixed Operating Costs	**$5,600,199**	100.00%
Variable operating costs		
Feedstock costs	$22,523,215	35.73%
Energy utilities costs (H_2 and electricity)	$0	0.00%
Energy by-product credits (electricity)	(3,136,079)	-4.97%
None energy material and utilities costs (catalyst, tri-isobutyl aluminum, cooling water, process water)	$87,103,408	138.17%
None energy by-product credits (lubricant, asphalt, $AlCl_3$)	(43,450,113)	-68.92%
Other variable operating costs	0	0.00%
Total Variable operating costs	**$63,040,431**	100.00%

Table S4. Retail prices of some long chain fatty alcohols.

Fatty alcohol carbon chain length	Price ($/kg)	Reference
C_{20}	$20-200/kg	https://www.alibaba.com/product-detail/1-Eicosanol-CAS-NO-629-96_60783118280.html
C_{22}	~$60 / Kg	https://www.alibaba.com/product-detail/Top-quality-Docosanol-Behenyl-Alcohol-98_141789808.html
C_{24}	~$100/ Kg	https://www.alibaba.com/product-detail/506-51-4-TETRACOSANOL_1600089028013.html

Bulk prices of C_{20} alcohol (1-icosanol) from Alibaba range from $20-200 per kg.

Supplemental References

1. Davis, R., Grundl, N., Tao, L., Biddy, M.J., Tan, E.C.D., Beckham, G.T., Humbird, D., Thompson, D.N., and Roni, M.S. (2018). Process Design and Economics for the Conversion of Lignocellulosic Biomass to Hydrocarbon Fuels and Coproducts: 2018 Biochemical Design Case Update Biochemical Deconstruction and Conversion of Biomass to Fuels and Products via Integrated Biorefinery Pathways. In Technical Report NREL (NREL/TP-5100-71949).
2. Davidson, P.J., Lappert, M.F., and Pearce, R. (1973). Silylmethyl and Related Complexes II. Preparation, Spectra, and Thermolysis of the Tetraneopentyls of Titanium, Zirconium, and Hafnium. J. Organomet. Chem. *57*, 269-277.
3. Downs, A.J., Greene, T.M., Collin, S.E., Whitehurst, L.A., Brain, P.T., Morrison, C.A., Pulham, C.R., Smart, B.A., Rankin, D.W.H., Keys, A.*, et al.* (2000). Dimethylalane, [Me2AlH]n, in the Vapor Phase and in Hydrocarbon Solution: Gas-Phase Electron Diffraction, Spectroscopic, Colligative, and ab Initio Studies. Organometallics *19*, 527-538.
4. Lehmkuhl, H., and Ziegler, K. (1970). IX Aryl- und Benzyl-aluminium-Verbindungen. In Metallorganische Verbindungen: Al, Ga, In, Tl, G. Bähr, P. Burba, H. Lehmkuhl, and K. Ziegler, eds. (Stuttgart: Georg Thieme Verlag).
5. Finholt, A.E., Bond, A.C., and Schlesinger, H.I. (1947). Lithium Aluminum Hydride, Aluminum Hydride and Lithium Gallium Hydride, and Some of their Applications in Organic and Inorganic Chemistry1. J. Am. Chem. Soc. *69*, 1199-1203.
6. Yao, N., Xiong, G., He, M., Sheng, S., Yang, W., and Bao, X. (2002). A Novel Method To Synthesize Amorphous Silica−Alumina Materials with Mesoporous Distribution without Using Templates and Pore-Regulating Agents. Chem. Mater. *14*, 122-129.
7. Wang, X.-X., Veyre, L., Lefebvre, F., Patarin, J., and Basset, J.-M. (2003). Preparation and Characterization of Zirconium Containing Mesoporous Silicas. II. Grafting Reaction of Tetraneopentyl Zirconium on MCM-41 and Characterization of the Grafted Species and of the Resulting Materials. Microporous Mesoporous Mater. *66*, 169-179.
8. Quignard, F., Lécuyer, C., Bougault, C., Lefebvre, F., Choplin, A., Olivier, D., and Basset, J.M. (1992). Surface Organometallic Chemistry: Synthesis and Characterization of a Tris(neopentyl)zirconium(IV) Complex Grafted to the Surface of a Partially Dehydroxylated Silica. Inorg. Chem. *31*, 928-930.
9. Rataboul, F., Baudouin, A., Thieuleux, C., Veyre, L., Copéret, C., Thivolle-Cazat, J., Basset, J.-M., Lesage, A., and Emsley, L. (2004). Molecular Understanding of the Formation of Surface Zirconium Hydrides upon Thermal Treatment under Hydrogen of $[(\equiv SiO)Zr(CH_2tBu)_3]$ by Using Advanced Solid-State NMR Techniques. J. Am. Chem. Soc. *126*, 12541-12550.

10. Zagdoun, A., Casano, G., Ouari, O., Schwarzwälder, M., Rossini, A.J., Aussenac, F., Yulikov, M., Jeschke, G., Copéret, C., Lesage, A., *et al.* (2013). Large Molecular Weight Nitroxide Biradicals Providing Efficient Dynamic Nuclear Polarization at Temperatures up to 200 K. J. Am. Chem. Soc. *135*, 12790-12797.
11. Siegel, R., Nakashima, T.T., and Wasylishen, R.E. (2007). Sensitivity enhancement of NMR spectra of half-integer spin quadrupolar nuclei in solids using hyperbolic secant pulses. J. Magn. Reson. *184*, 85-100.
12. Joubert, J., Delbecq, F., Thieuleux, C., Taoufik, M., Blanc, F., Copéret, C., Thivolle-Cazat, J., Basset, J.-M., and Sautet, P. (2007). Synthesis, Characterization, and Catalytic Properties of **γ**-Al_2O_3-Supported Zirconium Hydrides through a Combined Use of Surface Organometallic Chemistry and Periodic Calculations. Organometallics *26*, 3329-3335.
13. Höfer, R., and Selig, M. (2012). 10.02 - Green Chemistry and Green Polymer Chemistry. In Polymer Science: A Comprehensive Reference, K. Matyjaszewski, and M. Möller, eds. (Amsterdam: Elsevier), pp. 5-14.
14. Celik, G., Kennedy, R.M., Hackler, R.A., Ferrandon, M., Tennakoon, A., Patnaik, S., LaPointe, A.M., Ammal, S.C., Heyden, A., Perras, F.A., *et al.* (2019). Upcycling Single-Use Polyethylene into High-Quality Liquid Products. ACS Cent. Sci. *5*, 1795-1803.

Supplemental Data

1. HDPE + $Zr(CH_2CMe_3)_2$@$SiAlO_x$ + Al*i*Bu_3 (150 °C).

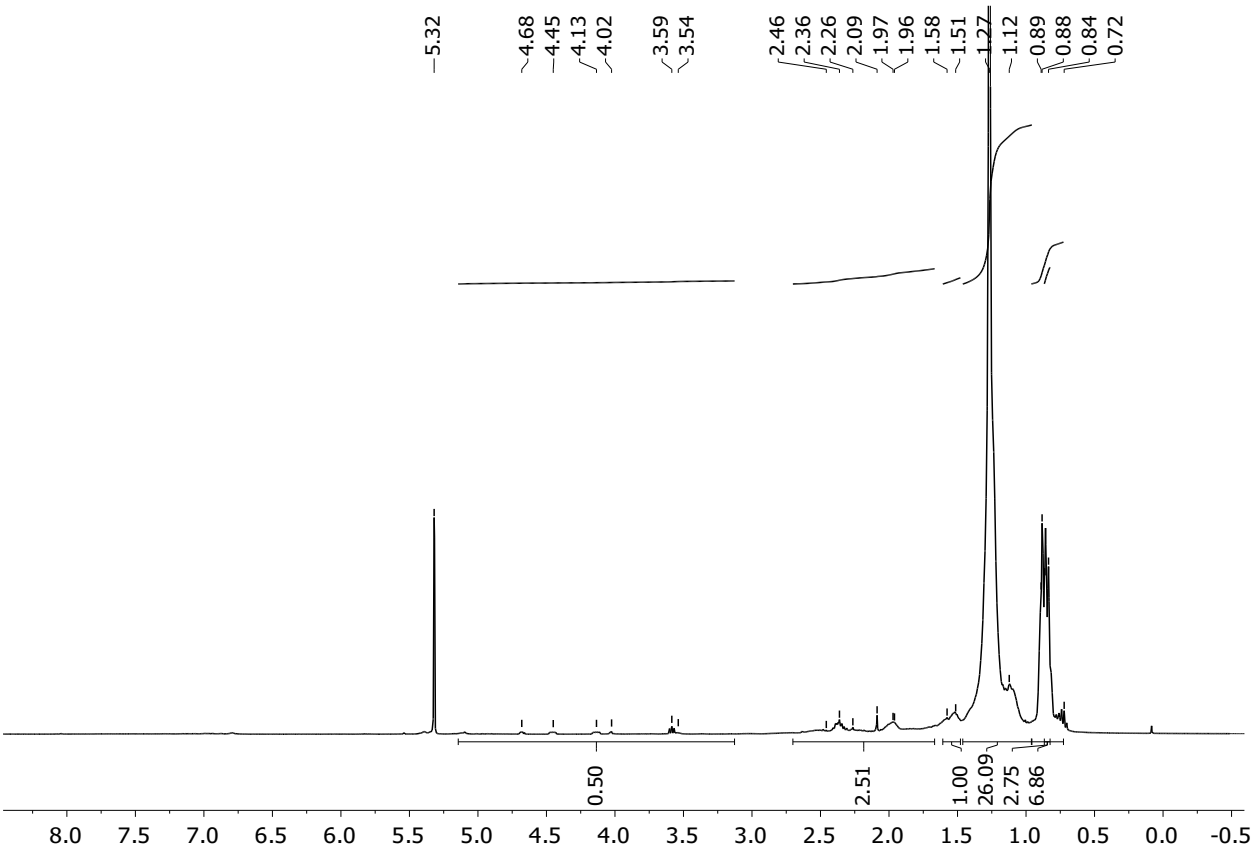

Figure S1. ^{1}H NMR spectrum of the oil isolated after reaction of HDPE and Al*i*Bu_3 in the presence of $Zr(CH_2CMe_3)_2$@$SiAlO_x$ at 150 °C for 12 h, quenched with O_2, and extracted with methylene chloride. The spectrum was acquired at room temperature in methylene chloride-d_2 and assigned based on COSY and HSQC experiments in Figures S2 and S3. Signals at 0.7-0.9 ppm correspond to methyl groups, 1.0-2.7 ppm correspond to methylene groups, and the peak at 1.5 ppm to the methine group. Peaks at 3.5-5.0 ppm have been assigned as C*H*$_2$-OH species. The data corresponds to the experiment reported in Table 1, Entry 1.

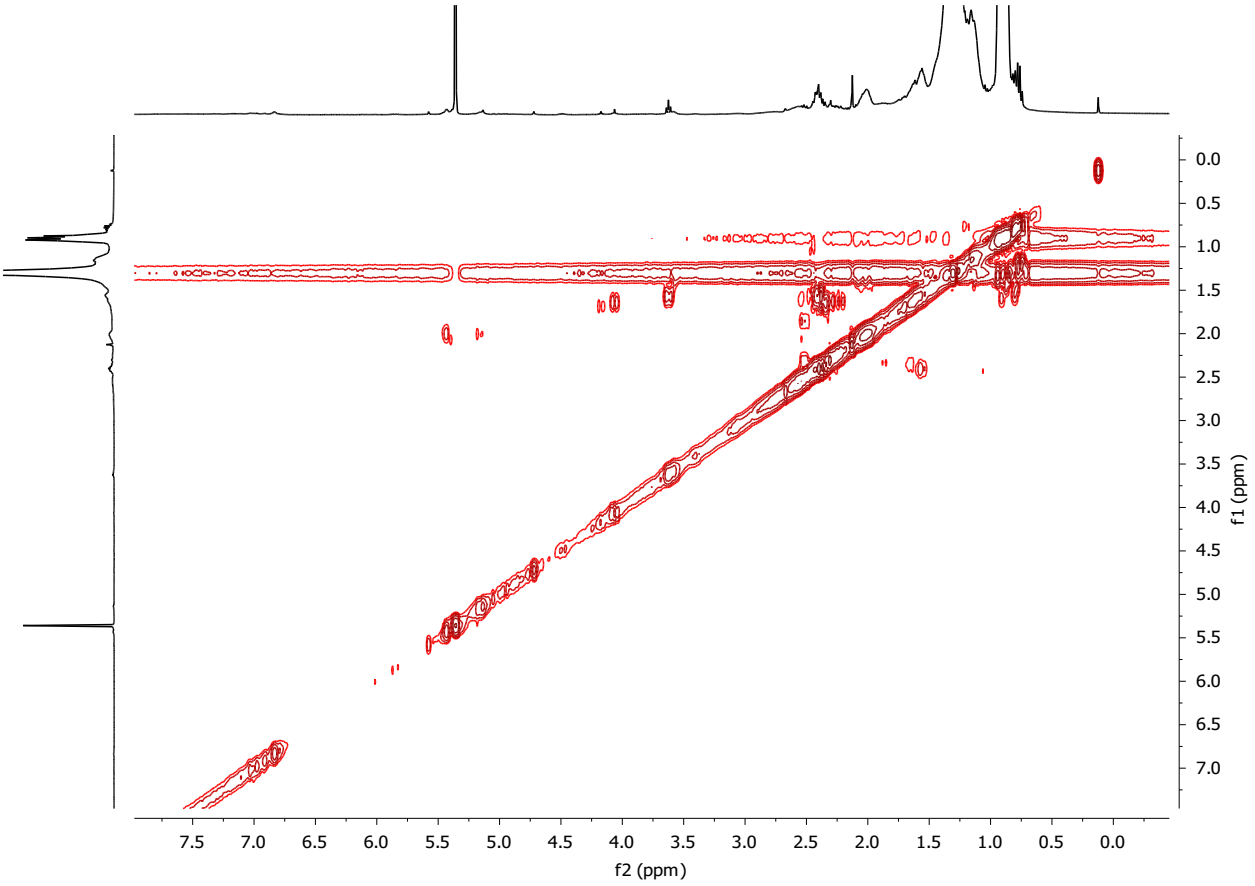

Figure S2. COSY spectrum of the oil isolated after reaction of HDPE and Al*i*Bu$_3$ in the presence of Zr(CH$_2$CMe$_3$)$_2$@SiAlO$_x$ at 150 °C for 12 h, quenched with O$_2$, and extracted with methylene chloride. The spectrum was acquired at room temperature in methylene chloride-d_2. Cross-peaks at 3.5-5.5 ppm correlate with methylene signals at 1.6-2.2 ppm indicative of -CH$_2$-CH$_2$-OH species. The data corresponds to the experiment reported in Table 1, Entry 1.

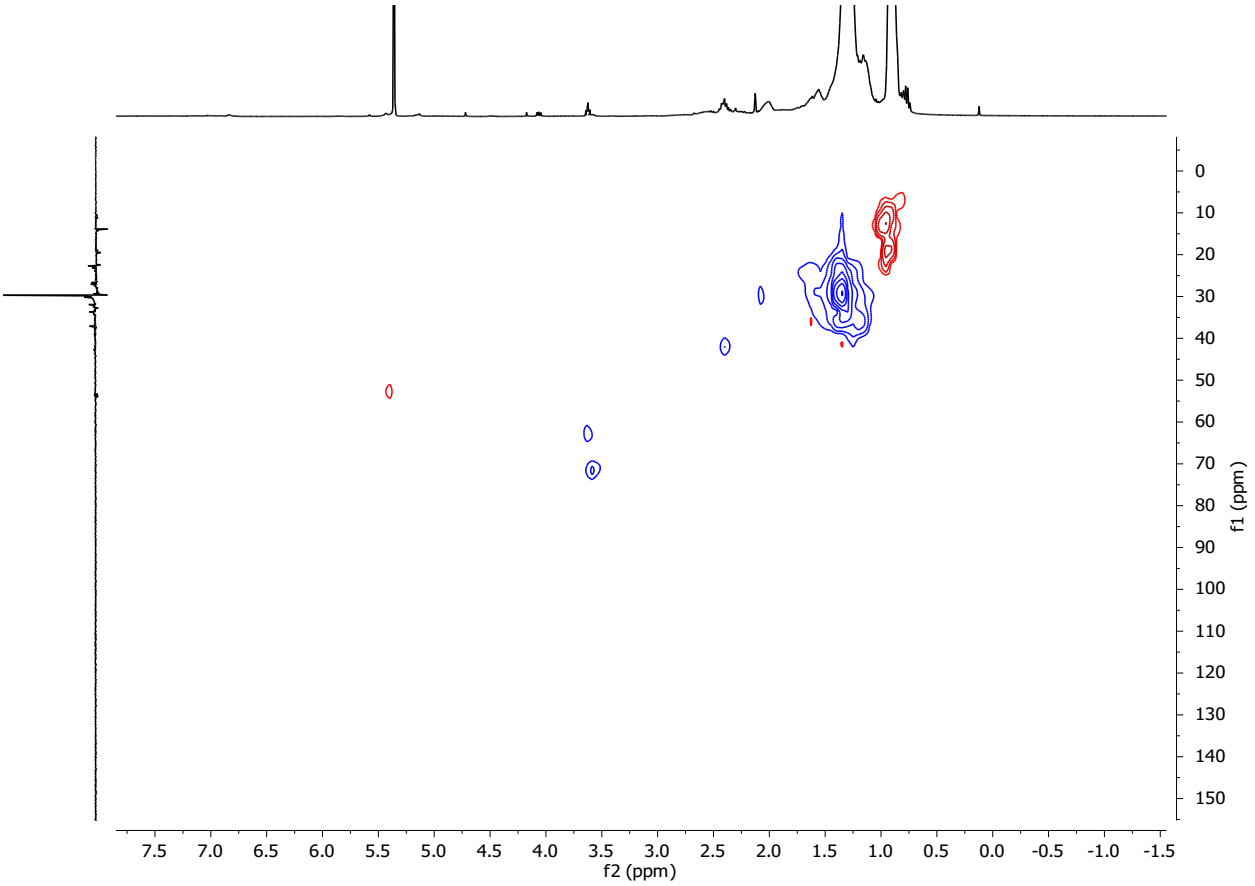

Figure S3. Phase sensitive ^{1}H-^{13}C HSQC spectrum of the oil isolated after reaction of HDPE and Al*i*Bu$_3$ in the presence of Zr(CH$_2$CMe$_3$)$_2$@SiAlO$_x$ at 150 °C for 12 h, quenched with O_2, and extracted with methylene chloride. The spectrum was acquired at room temperature in methylene chloride-d_2. The large polymer chain methylene peaks (in blue) at ^{13}C 30 ppm have the same phase as cross-peaks at ^{13}C 60-70 ppm (also blue), allowing assignment of the latter to primary alcohols -*C*H$_2$-OH. The data corresponds to the experiment reported in Table 1, Entry 1.

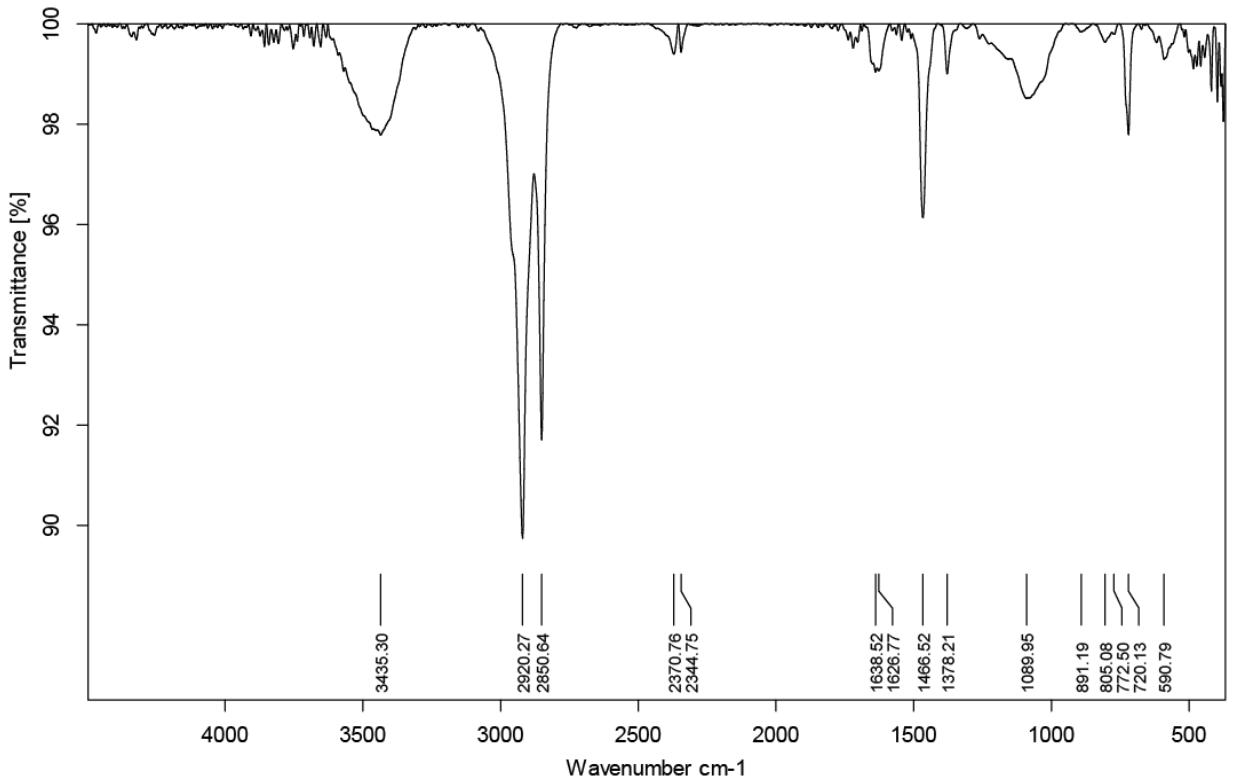

Figure S4. FT-IR spectrum (KBr) of the oil isolated after reaction of HDPE and Al*i*Bu$_3$ in the presence of Zr(CH$_2$CMe$_3$)$_2$@SiAlO$_x$ at 150 °C for 12 h, quenched with O$_2$, and extracted with methylene chloride. The broad signal at 3435 cm^{-1} corresponds to an O-H stretch. The data corresponds to the experiment reported in Table 1, Entry 1.

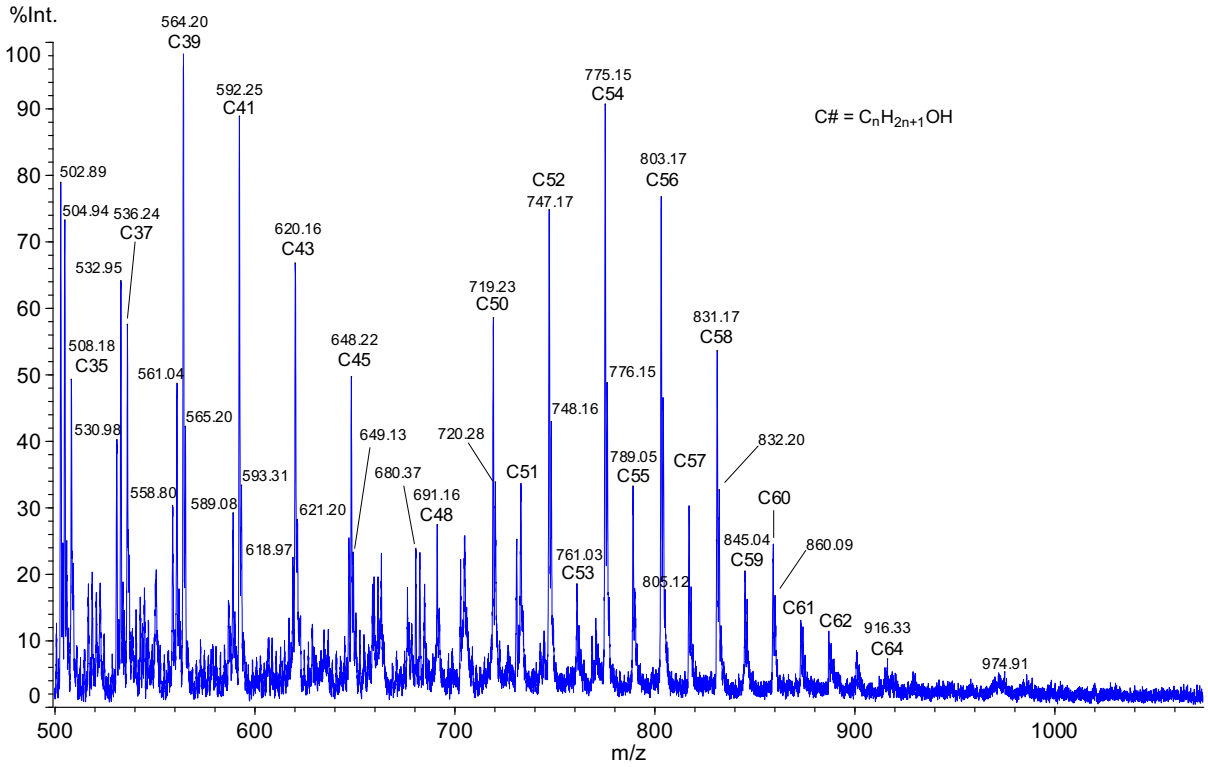

Figure S5. MALDI-TOF-MS of the oil isolated after reaction of HDPE and Al*i*Bu$_3$ in the presence of Zr(CH$_2$CMe$_3$)$_2$@SiAlO$_x$ at 150 °C for 12 h, quenched with O$_2$, and extracted with methylene chloride, acquired in linear, positive mode with AgNO$_3$ (salt) and DHB (matrix). The data corresponds to the experiment reported in Table 1, Entry 1.

2. HDPE + $Zr(CH_2CMe_3)_2$@$SiAlO_x$ + Al*i*Bu_3 (200 °C).

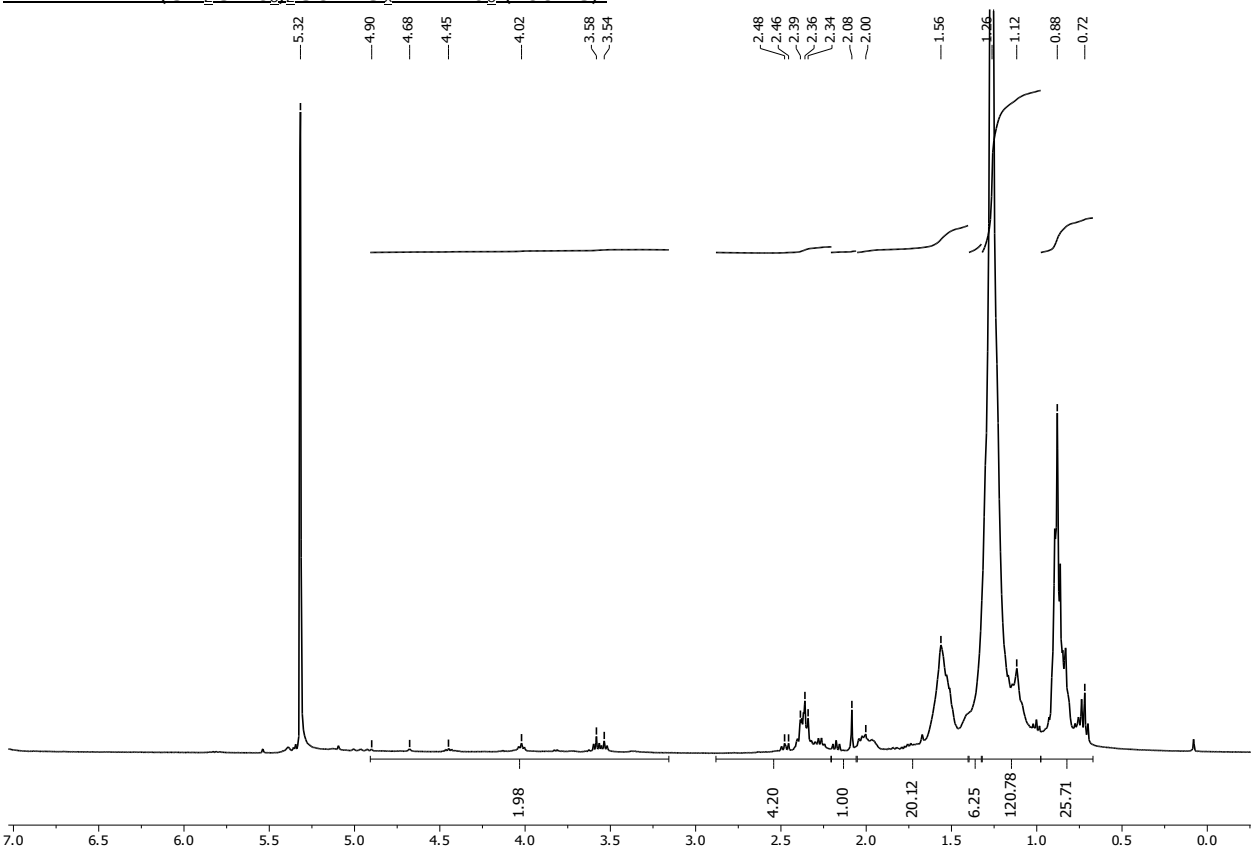

Figure S6. ^{1}H NMR spectrum of the oil isolated after reaction of HDPE and Al*i*Bu_3 in the presence of $Zr(CH_2CMe_3)_2$@$SiAlO_x$ at 200 °C for 12 h, quenched with O_2, and extracted with methylene chloride. The spectrum was acquired at room temperature in methylene chloride-d_2 and assigned based on COSY and HSQC experiments in Figures S7 and S8. Signals at 0.7-0.9 ppm correspond to methyl sgroups, peaks at 1.0-2.5 ppm are assigned to methylenes, and those at 1.4 and 2.1 ppm are attributed to methine groups. Peaks at 3.5-5.0 ppm are assigned to -CH_2-OH groups. The data corresponds to the experiment reported in Table 1, Entry 2.

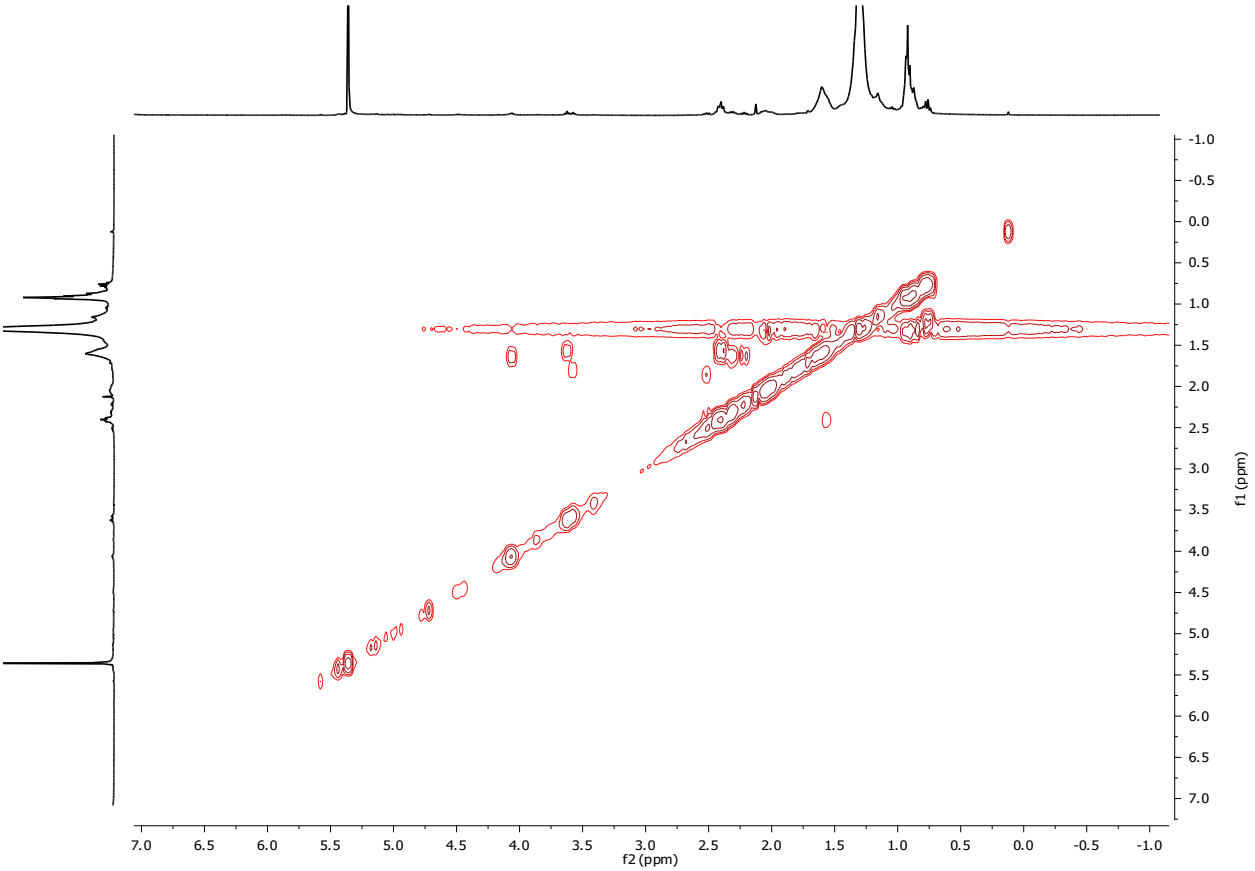

Figure S7. COSY spectrum of the oil isolated after reaction of HDPE and Al*i*Bu$_3$ in the presence of Zr(CH$_2$CMe$_3$)$_2$@SiAlO$_x$ at 200 °C for 12 h, quenched with O$_2$, and extracted with methylene chloride. The spectrum was acquired at room temperature in methylene chloride-d_2. Cross-peaks at 3.5-4.5 ppm that correspond to methylene peaks at 1.5-2.0 ppm are indicative of -CH$_2$-CH$_2$-OH species. The data corresponds to the experiment reported in Table 1, Entry 2.

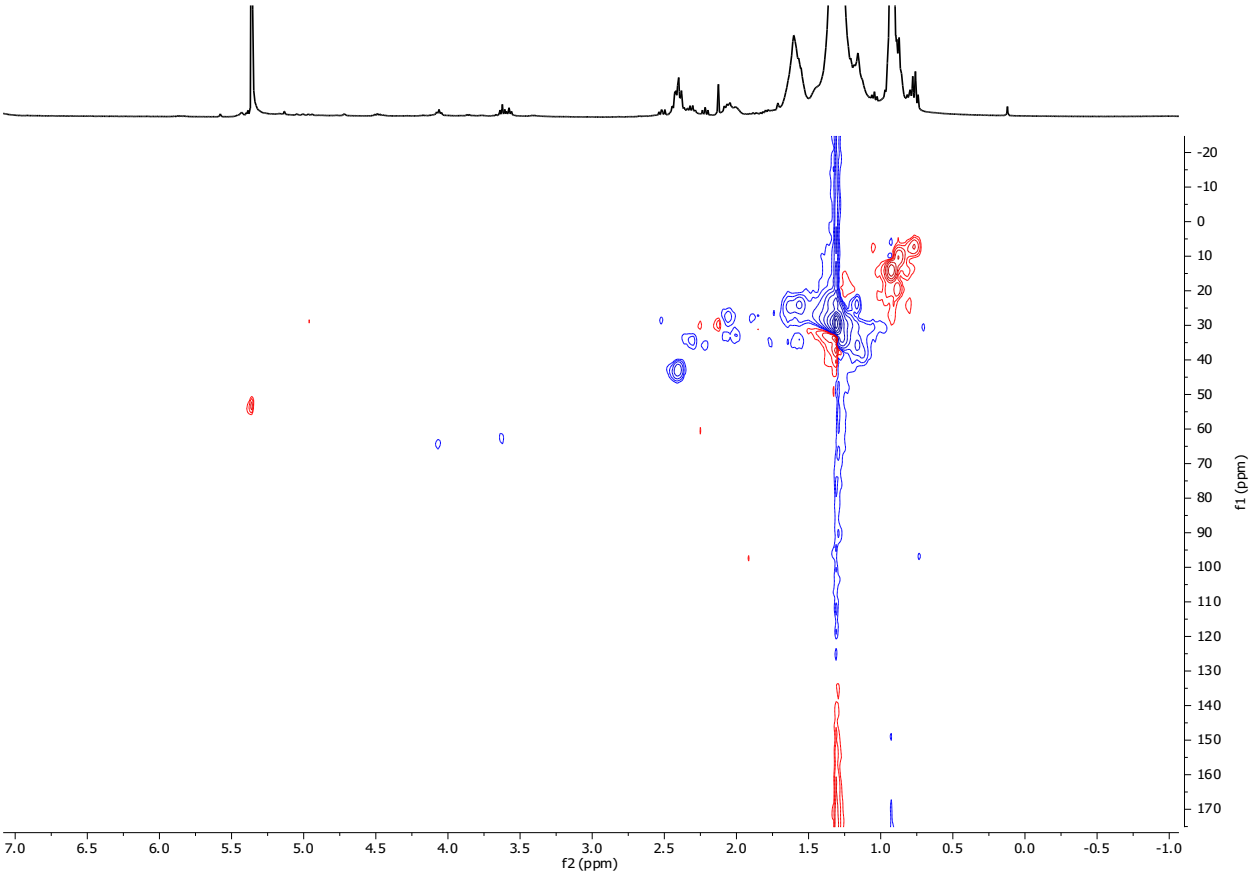

Figure S8. Phase sensitive ^{1}H-^{13}C HSQC spectrum of the oil isolated after reaction of HDPE and Al*i*Bu$_3$ in the presence of Zr(CH_2CMe_3)$_2$@SiAlO$_x$ at 200 °C for 12 h, quenched with O_2, and extracted with methylene chloride. The spectrum was acquired at room temperature in methylene chloride-d_2. The large peak assigned to polymer methylene CH_2 (in blue) at ^{13}C 30 ppm has the same phase as cross-peaks at ^{13}C 60-70 ppm (also blue), allowing assignment of the latter to primary alcohols -*C*H_2-OH. The data corresponds to the experiment reported in Table 1, Entry 2.

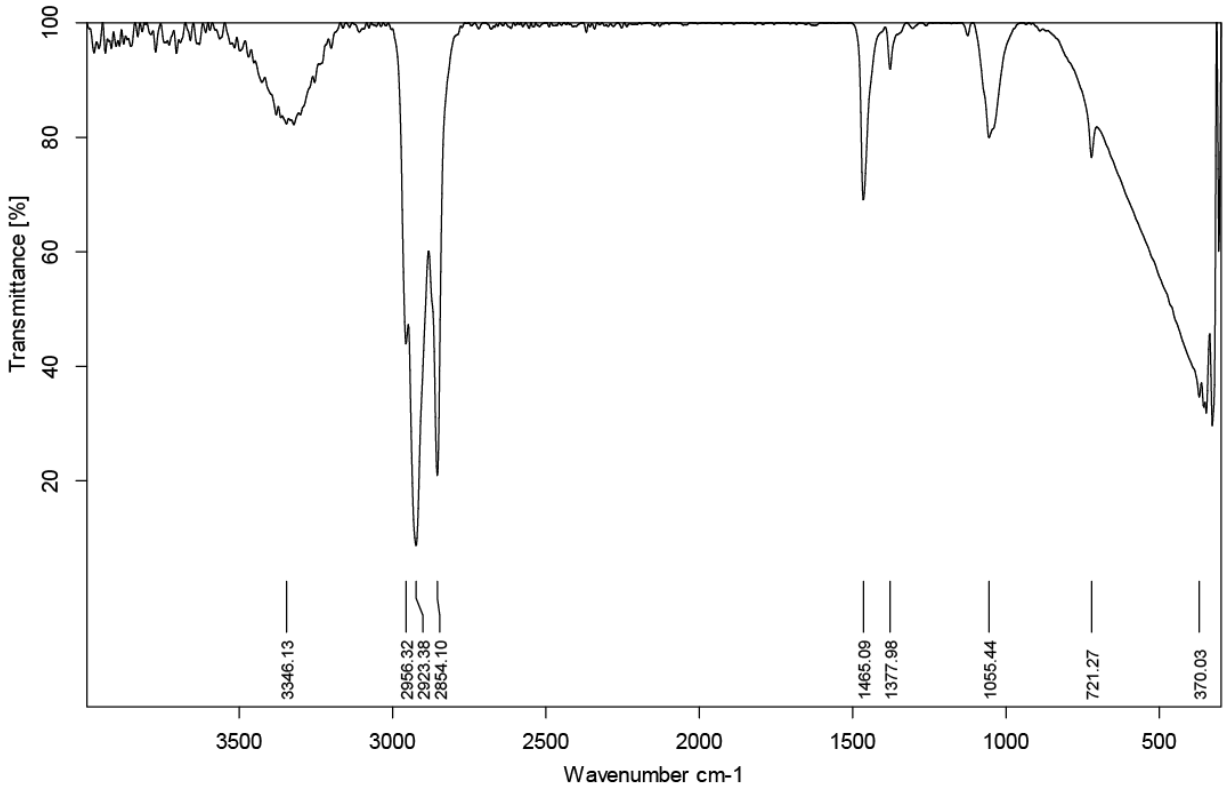

Figure S9. FT-IR spectrum (KBr) of the oil isolated after reaction of HDPE and Al*i*Bu$_3$ in the presence of Zr(CH$_2$CMe$_3$)$_2$@SiAlO$_x$ at 200 °C for 12 h, quenched with O$_2$, and extracted with methylene chloride. The broad signal at 3446 cm^{-1} corresponds to the O-H stretching mode. The data corresponds to the experiment reported in Table 1, Entry 2.

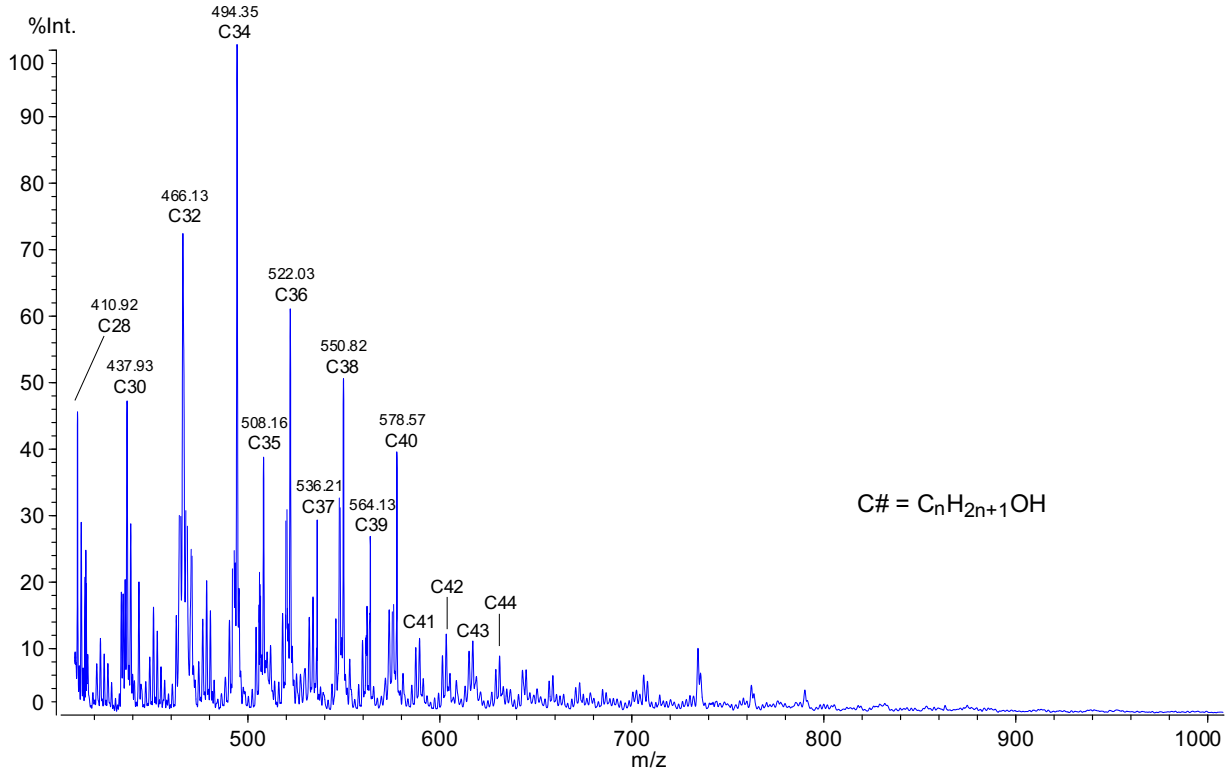

Figure S10. MALDI-TOF-MS of the oil isolated after reaction of HDPE and Al*i*Bu$_3$ in the presence of Zr(CH$_2$CMe$_3$)$_2$@SiAlO$_x$ at 200 °C for 12 h, quenched with O$_2$, and extracted with methylene chloride, acquired in linear, positive mode with AgNO$_3$ (salt) and DHB (matrix). The data corresponds to the experiment reported in Table 1, Entry 2.

3. HDPE + $Zr(CH_2CMe_3)_2$@$SiAlO_x$ + Al*i*Bu_3 (200 °C; portions of catalyst and Al*i*Bu_3 are added at 0, 12, and 24 h).

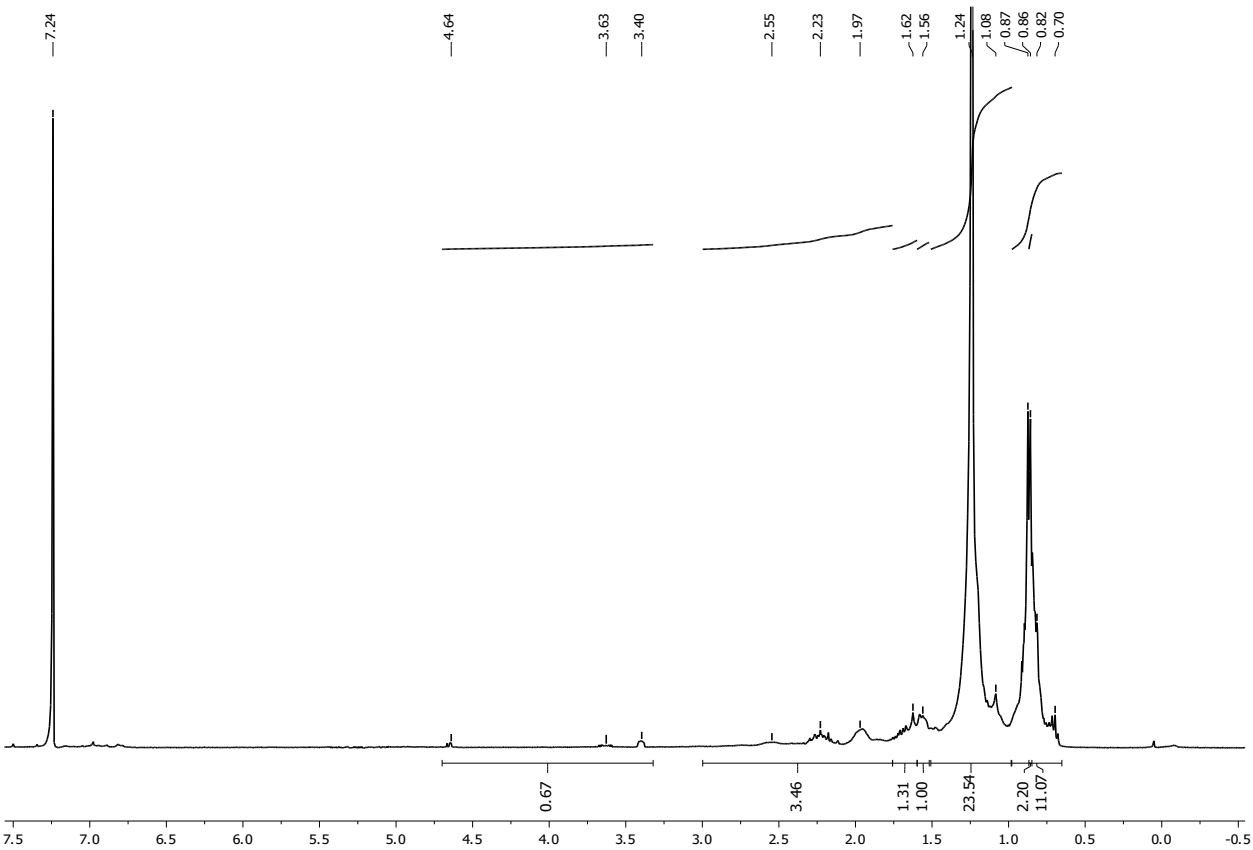

Figure S11. ^1H NMR spectrum of the oil isolated after reaction of HDPE and Al*i*Bu_3 in the presence of $Zr(CH_2CMe_3)_2$@$SiAlO_x$ added at 0, 12, and 24 h, at 200 °C, quenched with O_2, and extracted with methylene chloride. The spectrum was acquired at room temperature in chloroform-*d* and assigned based on TOCSY and HSQC experiments in Figures S12 and S13. Signals at 0.7-1.0 ppm are attributed to methyl groups, signals at 1.0-1.4 and 1.8-3.0 ppm are assigned to methylene groups, and the peak at 1.8 ppm corresponds to methine species. Peaks at 3.3-4.7 ppm are assigned to -C*H*$_2$-OH groups. The data corresponds to the experiment reported in Table 1, Entry 3.

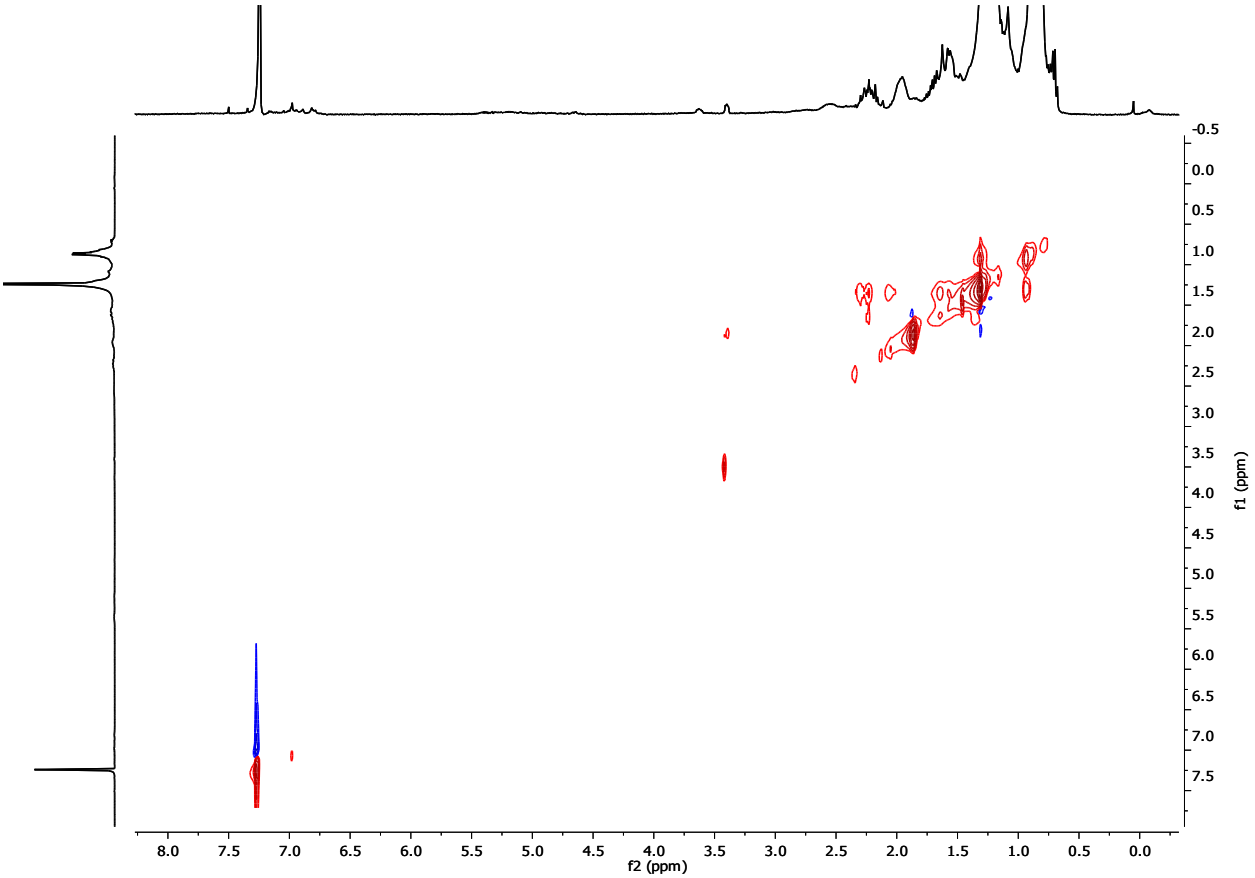

Figure S12. TOCSY spectrum of the oil isolated after reaction of HDPE and Al*i*Bu$_3$ in the presence of Zr(CH$_2$CMe$_3$)$_2$@SiAlO$_x$ added at 0, 12, and 24 h, at 200 °C, quenched with O$_2$, and extracted with methylene chloride. The spectrum was acquired at room temperature in chloroform-*d*. Cross-peaks at 3.5 ppm correlate with methylene peaks at 2.0 ppm, which is indicative of -CH$_2$-CH$_2$-OH species. The data corresponds to the experiment reported in Table 1, Entry 3.

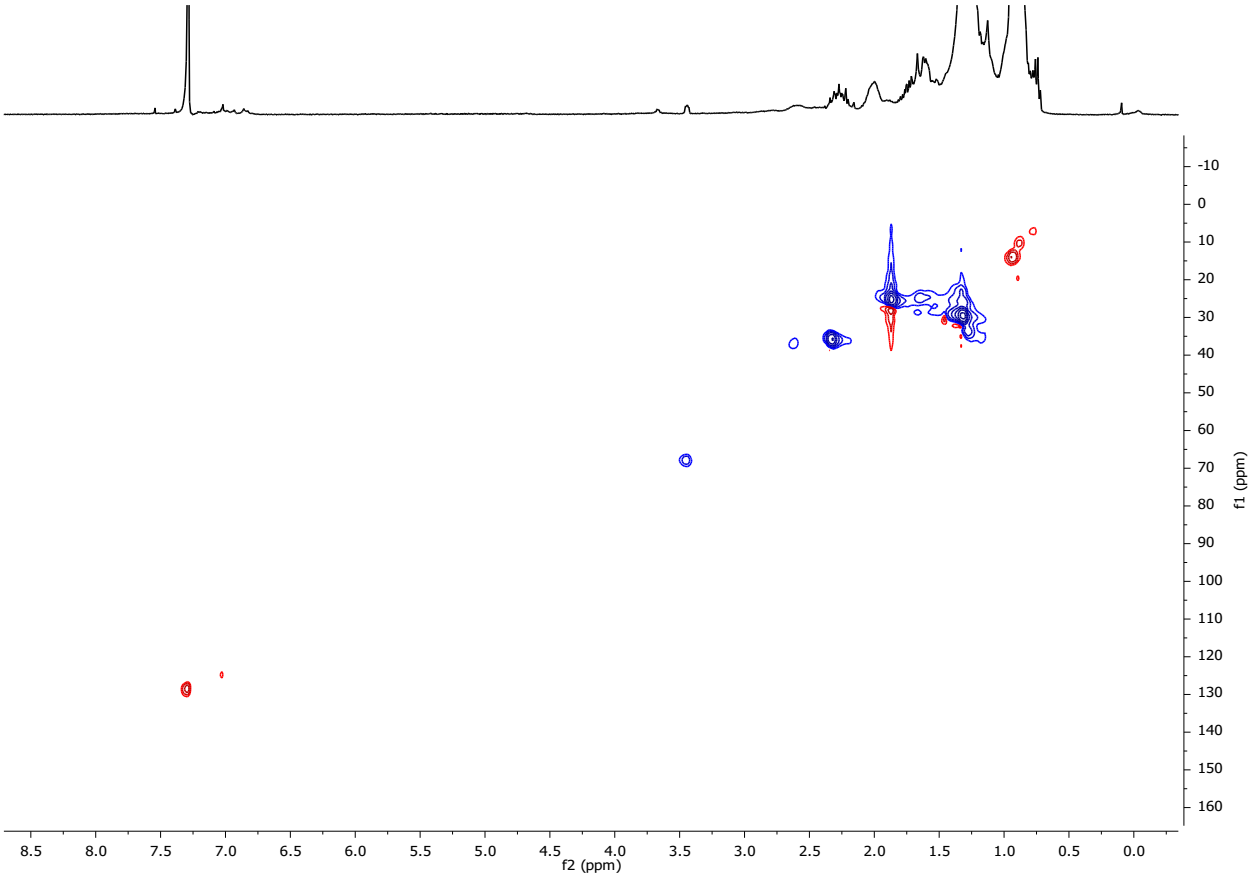

Figure S13. Phase sensitive ^{1}H-^{13}C HSQC spectrum of the oil isolated after reaction of HDPE and Al*i*Bu$_3$ in the presence of Zr(CH_2CMe_3)$_2$@SiAlO$_x$ added at 0, 12, and 24 h, at 200 °C, quenched with O_2, and extracted with methylene chloride. The spectrum was acquired at room temperature in chloroform-*d*. The large peak assigned to polymer methylene CH_2 (in blue) at ^{13}C 30 ppm have the same phase as cross-peaks at ^{13}C 60-70 ppm (also blue), allowing assignment of the latter to primary alcohols -*C*H_2-OH. The data corresponds to the experiment reported in Table 1, Entry 3.

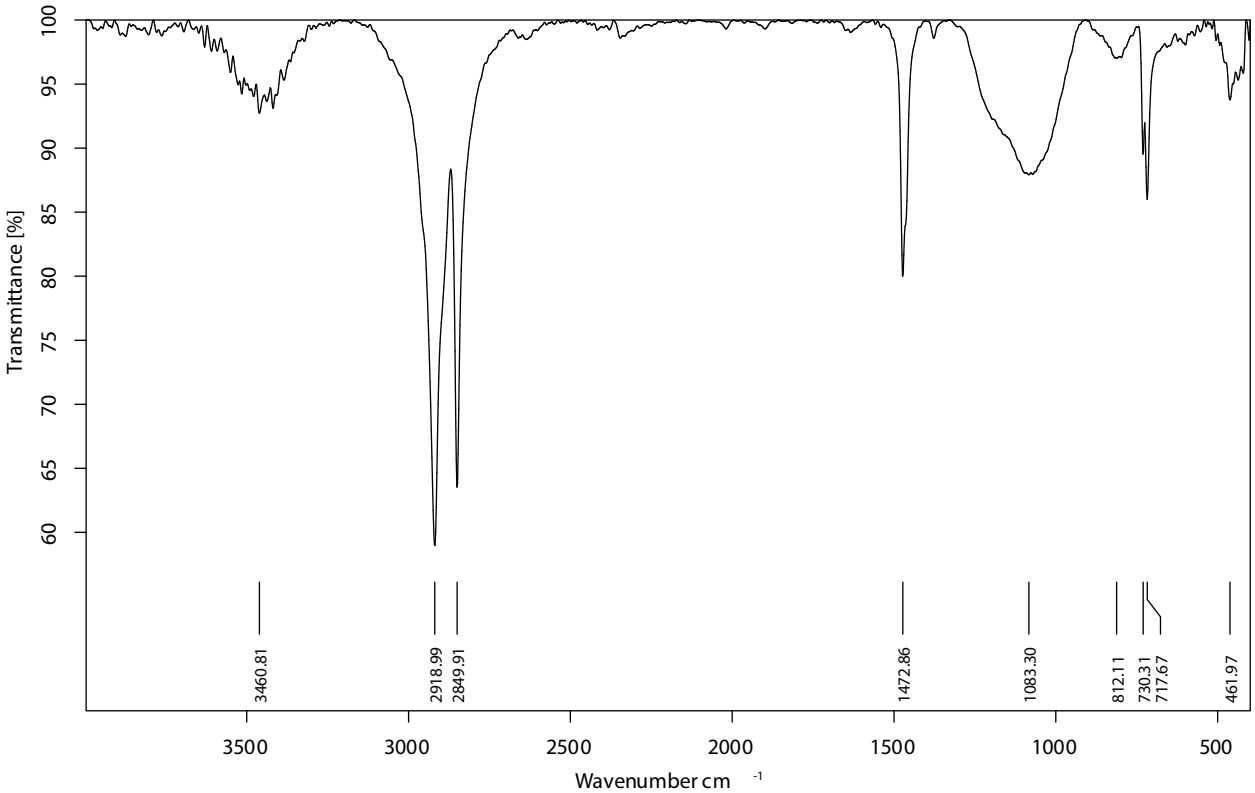

Figure S14. FT-IR spectrum (KBr) of oil isolated after reaction of HDPE and Al*i*Bu$_3$ in the presence of Zr(CH$_2$CMe$_3$)$_2$@SiAlO$_x$ added at 0, 12, and 24 h, at 200 °C, quenched with O$_2$ and extracted with methylene chloride. The broad signal at 3460 cm^{-1} corresponds to an O-H stretch. The data corresponds to the experiment reported in Table 1, Entry 3.

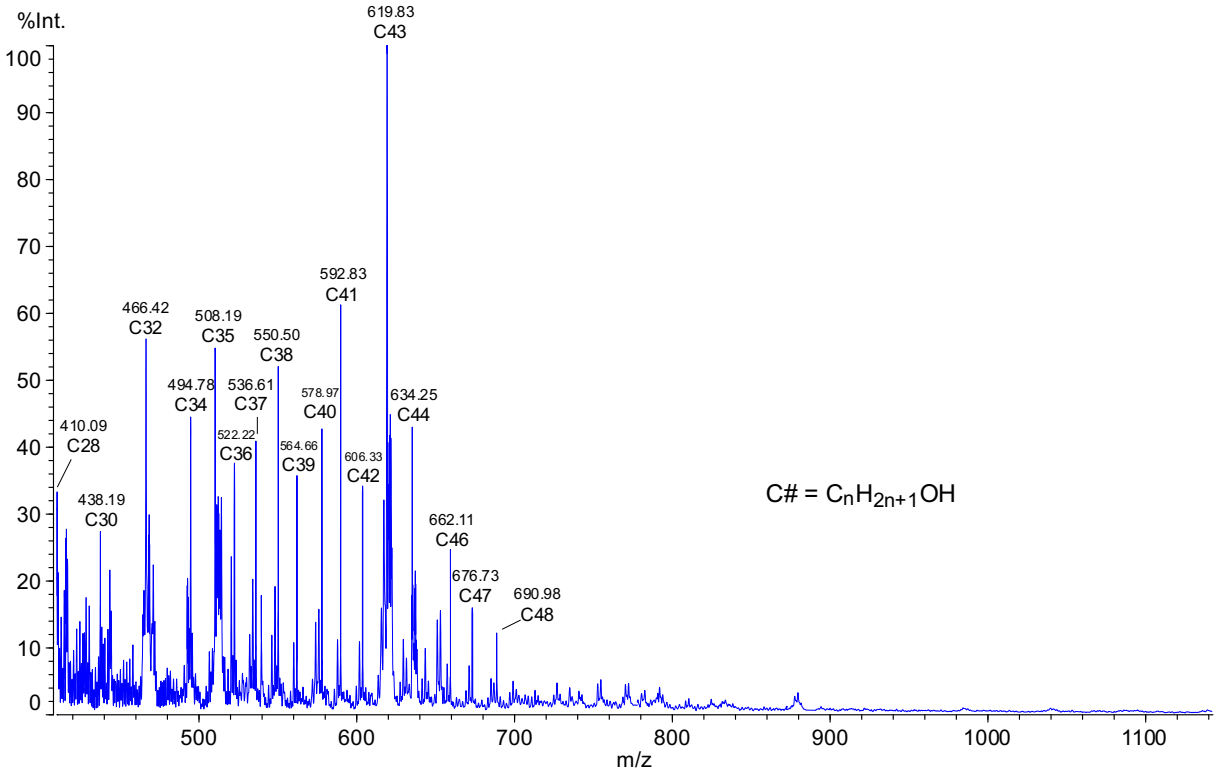

Figure S15. MALDI-TOF-MS of the oil isolated after reaction of HDPE and Al*i*Bu$_3$ in the presence of Zr(CH$_2$CMe$_3$)$_2$@SiAlO$_x$ added at 0, 12, and 24 h, at 200 °C, quenched with O$_2$, and extracted with methylene chloride. The spectrum was acquired in linear, positive mode with AgNO$_3$ (salt) and DHB (matrix), and alcohols self-ionize readily. The data corresponds to the experiment reported in Table 1, Entry 3.

4. HDPE + $Zr(CH_2CMe_3)_2$@$SiAlO_x$ + Al*i*Bu_3 (200 °C, quenched with MeOH).

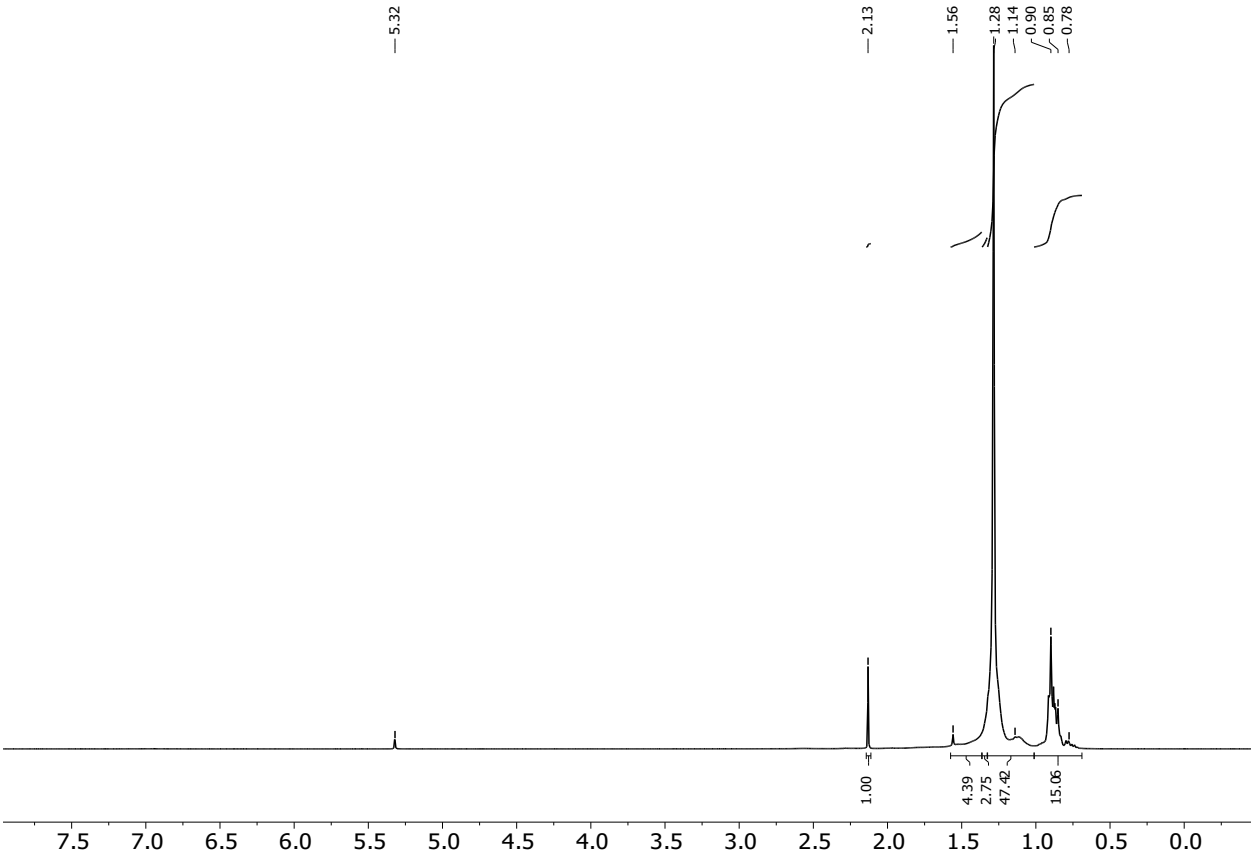

Figure S16. ^{1}H NMR spectrum of the oil isolated after reaction of HDPE and Al*i*Bu_3 in the presence of $Zr(CH_2CMe_3)_2$@$SiAlO_x$ at 200 °C for 12 h, quenched with degassed MeOH, and extracted with methylene chloride. The spectrum was acquired at room temperature in methylene chloride-d_2 and assigned based on COSY and HSQC experiments in Figures S17 and S18. Signals at 0.7-1.0 ppm correspond to methyl groups, those at 1.0-1.6 ppm correspond to methylene moieties, and those at 2.13 ppm corresponds to methine groups. Note that signals from ca 5 to 3 ppm were not detected, in contrast to spectra quenched with O_2, which contained signal in that region assigned to CH_2OH. The data corresponds to the experiment reported in Table 1, Entry 4.

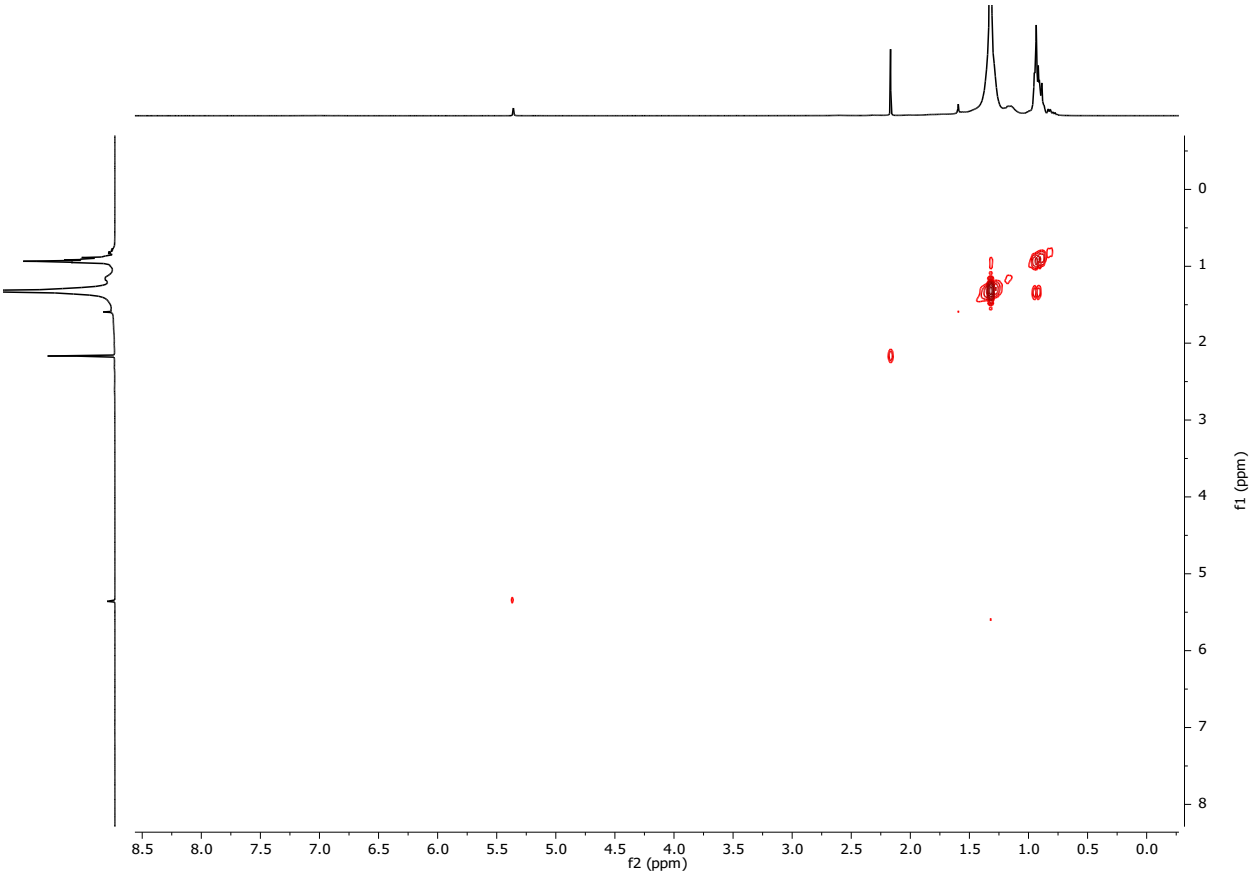

Figure S17. COSY spectrum of the oil isolated after reaction of HDPE and Al*i*Bu$_3$ in the presence of Zr(CH$_2$CMe$_3$)$_2$@SiAlO$_x$ at 200 °C for 12 h, quenched with MeOH, and extracted with methylene chloride. The spectrum was acquired at room temperature in methylene chloride-d_2. The data corresponds to the experiment reported in Table 1, Entry 4.

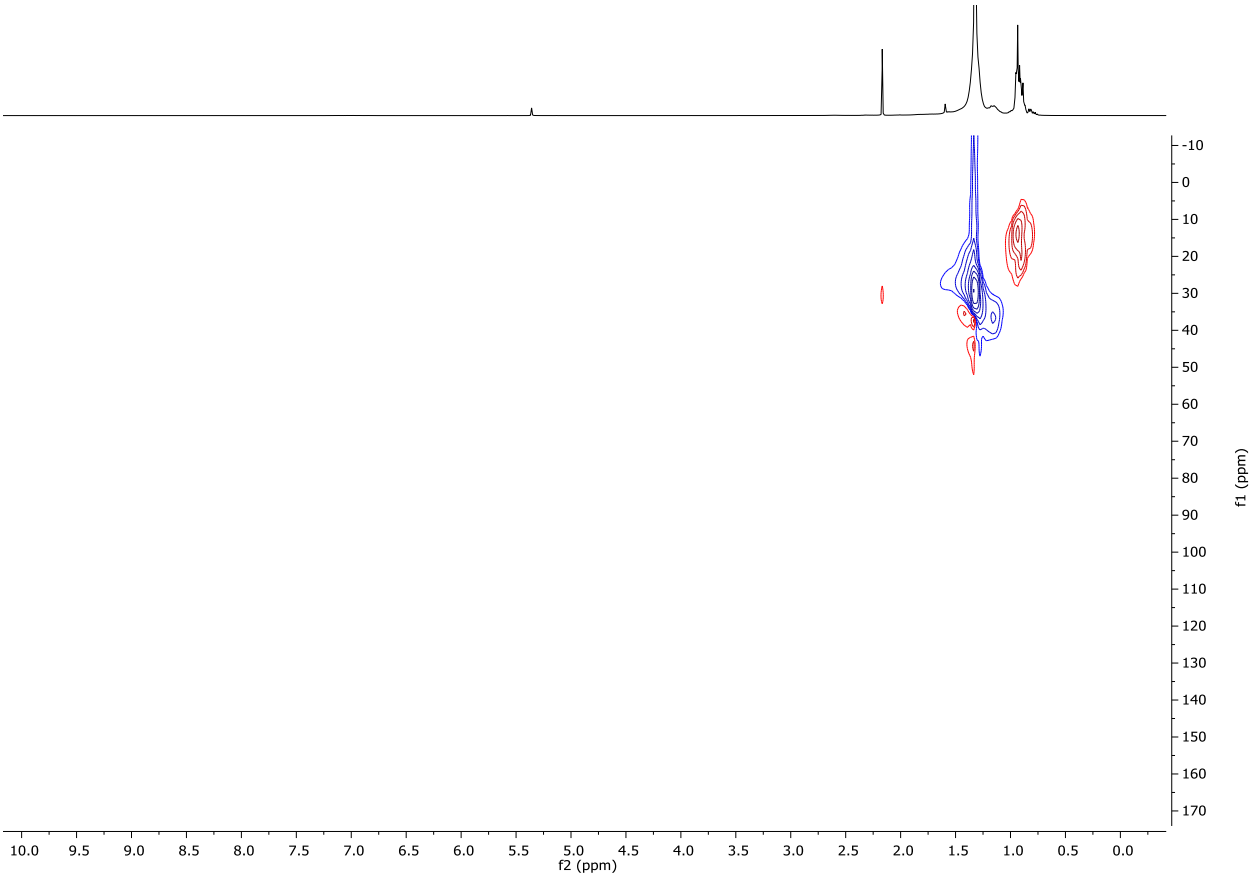

Figure S18. Phase sensitive ^{1}H-^{13}C HSQC spectrum of the oil isolated after reaction of HDPE and Al*i*Bu$_3$ in the presence of Zr(CH$_2$CMe$_3$)$_2$@SiAlO$_x$ at 200 °C for 12 h, quenched with MeOH and extracted with methylene chloride. The spectrum was acquired at room temperature in methylene chloride-d_2. The cross-peak at 32 ppm, which is opposite in phase (red) with that of the prominent methylene signal (blue), is assigned to methine groups. The data corresponds to the experiment reported in Table 1, Entry 4.

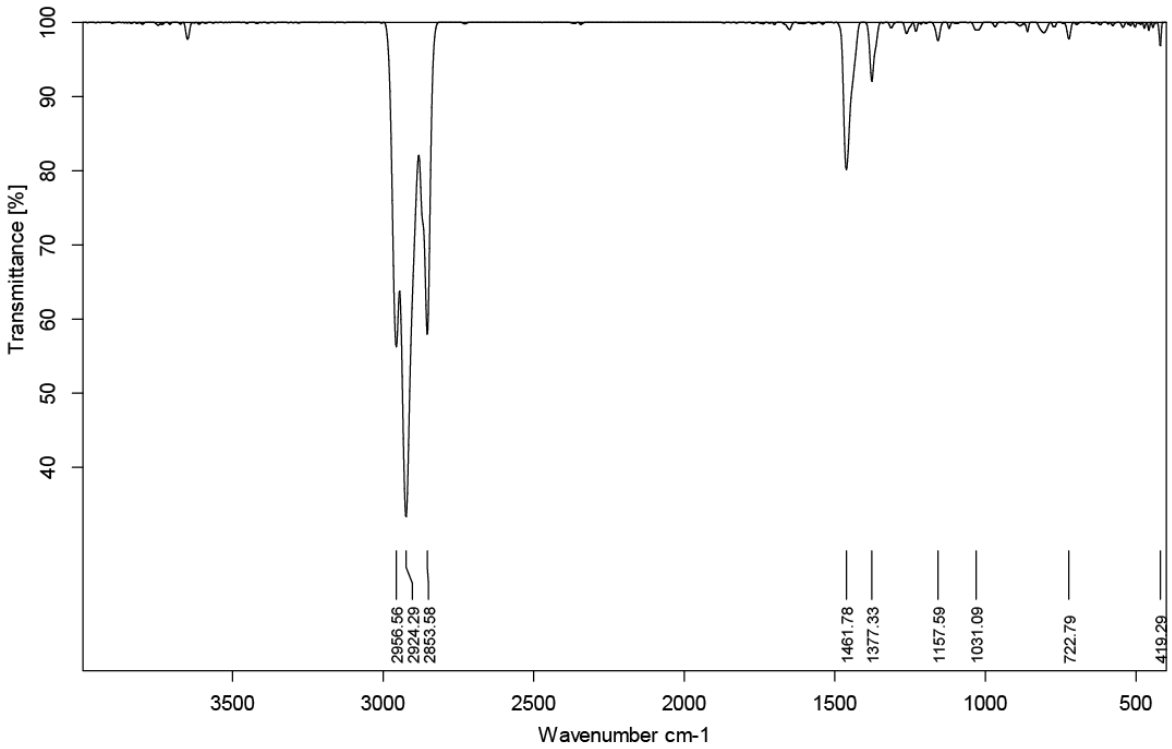

Figure S19. FT-IR spectrum (KBr) of the oil isolated after reaction of HDPE and Al*i*Bu$_3$ in the presence of Zr(CH$_2$CMe$_3$)$_2$@SiAlO$_x$ at 200 °C for 12 h, quenched with MeOH, and extracted with methylene chloride. Note that the diagnostic OH signal in O_2-quenched reactions is not detected in this material. The data corresponds to the experiment reported in Table 1, Entry 4.

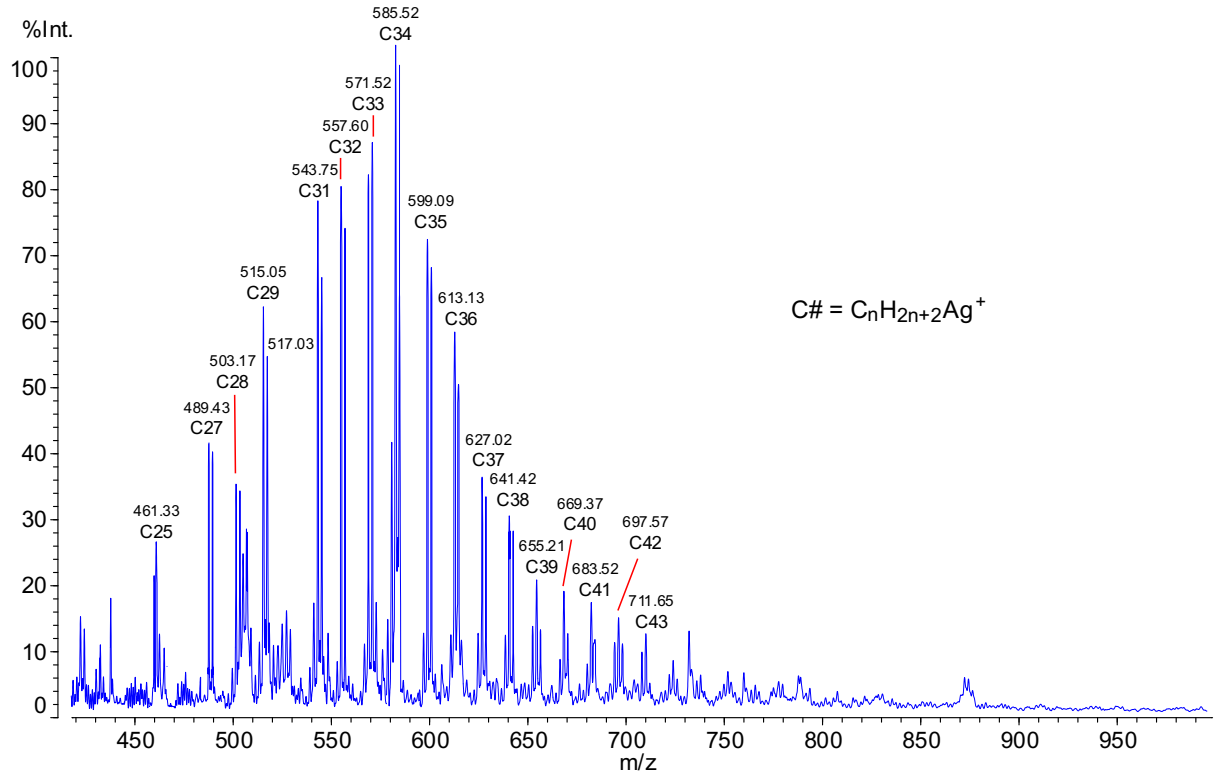

Figure S20. MALDI-TOF-MS of oil isolated after reaction of HDPE and Al*i*Bu$_3$ in the presence of Zr(CH$_2$CMe$_3$)$_2$@SiAlO$_x$ at 200 °C for 12 h, quenched with MeOH, and extracted with methylene chloride. The spectrum was acquired in linear, positive mode with AgNO$_3$ (salt) and DHB (matrix), and species appear as pairs of signals due to detection of ^{107}Ag and ^{109}Ag adducts. The data corresponds to the experiment reported in Table 1, Entry 4.

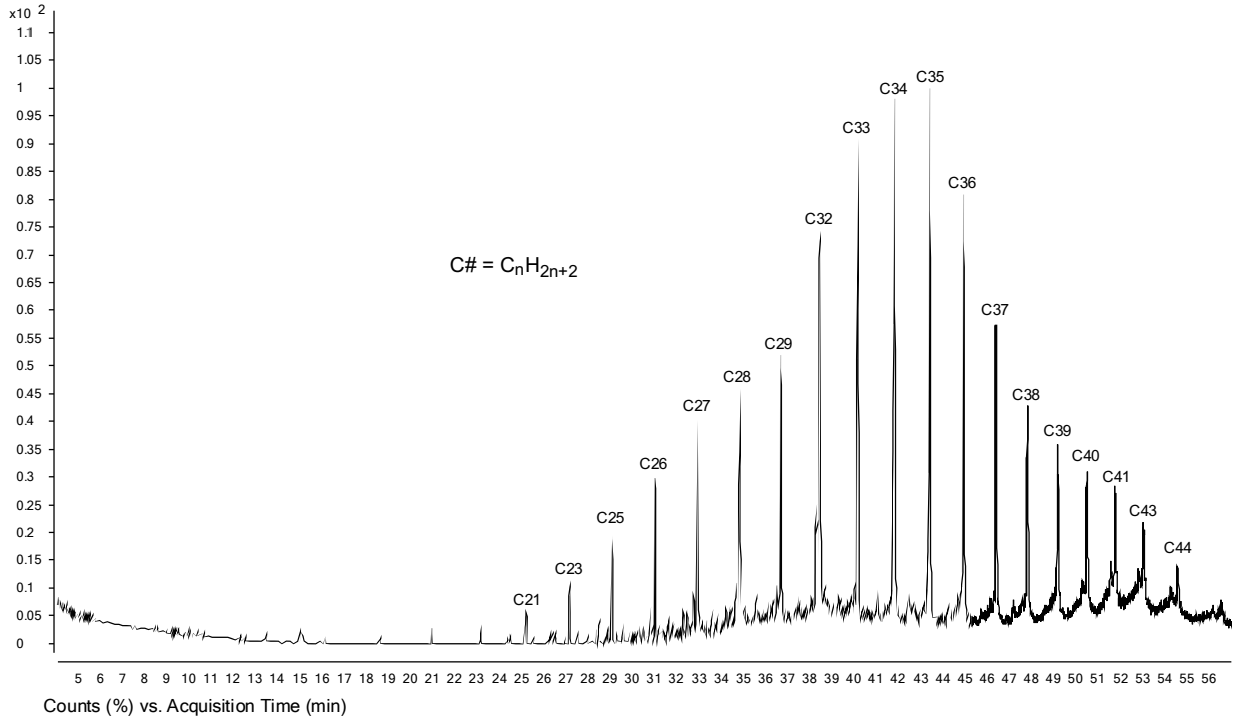

Figure S21. GC-MS of the oil isolated after reaction of HDPE and Al*i*Bu$_3$ in the presence of Zr(CH$_2$CMe$_3$)$_2$@SiAlO$_x$ at 200 °C for 12 h, quenched with MeOH, and extracted with methylene chloride. The spectrum was acquired by dissolving the sample in methylene chloride. The GC-MS spectrum corroborates the distribution of hydrocarbon species detected in the MALDI-TOF-MS spectrum (Figure S20), as well as the distributions of O_2, I_2, and CO_2-quenched reactions performed with Zr(CH$_2$CMe$_3$)$_2$@SiAlO$_x$ at 200 °C for 12 h. Hence, the MALDI-TOF-MS spectra are confirmed as representative of the samples compositions. The data corresponds to the experiment reported in Table 1, Entry 4.

5. HDPE + $Zr(CHCMe_3)_2$@$SiAlO_x$ + Al*i*Bu_3 (200 °C, quenched with I_2).

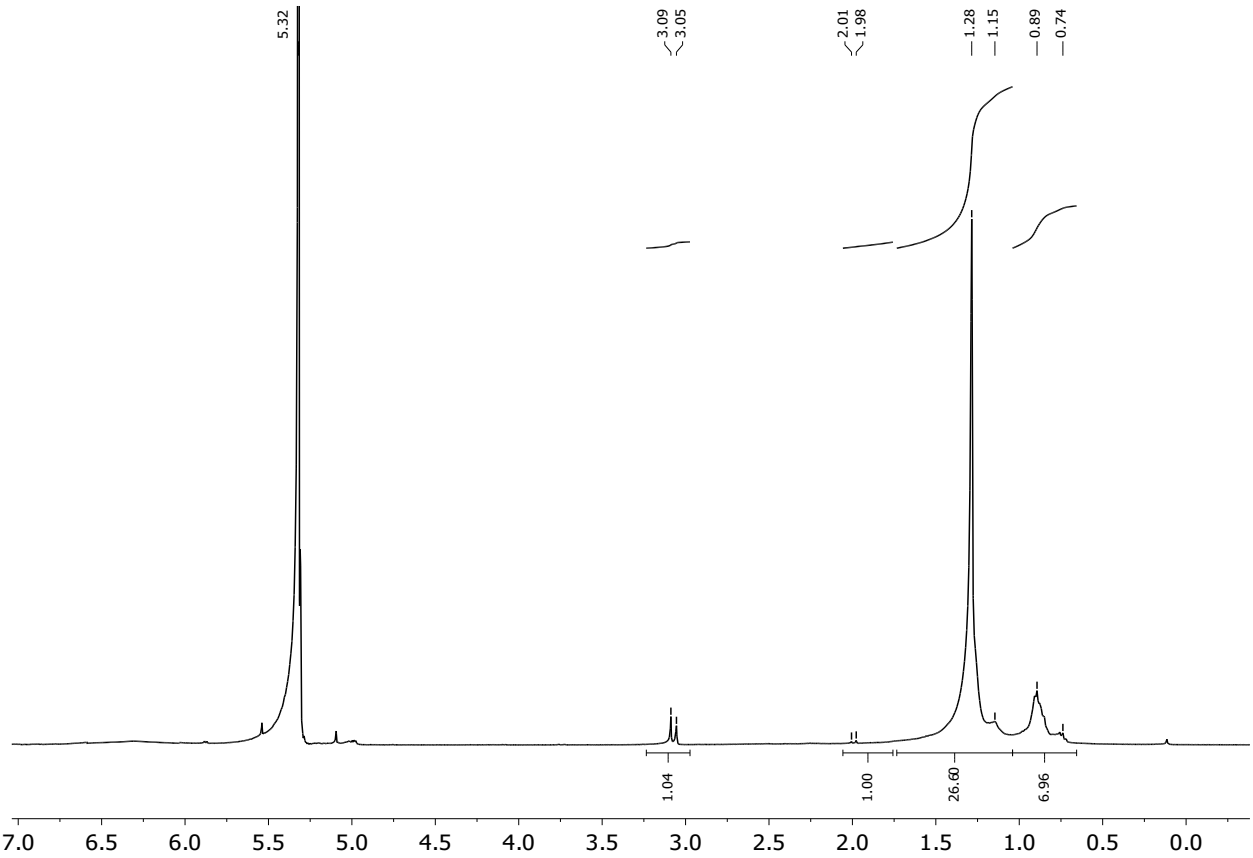

Figure S22. ^{1}H NMR spectrum of the oil isolated after reaction of HDPE and Al*i*Bu_3 in the presence of $Zr(CH_2CMe_3)_2$@$SiAlO_x$ at 200 °C for 12 h, quenched with I_2, and extracted with methylene chloride. The spectrum was acquired at room temperature in methylene chloride-d_2 and assigned based on COSY and HSQC experiments in Figures S23 and S24. Signals at 0.7-1.0 ppm are assigned to methyls, those at 1.0-1.7 ppm correspond to methylene units, and those at 1.7-2.1 ppm are attributed to methine groups. Peaks at 3.0-3.2 ppm are assigned as -C*H*$_2$-I groups. The data corresponds to the experiment reported in Table 1, Entry 5.

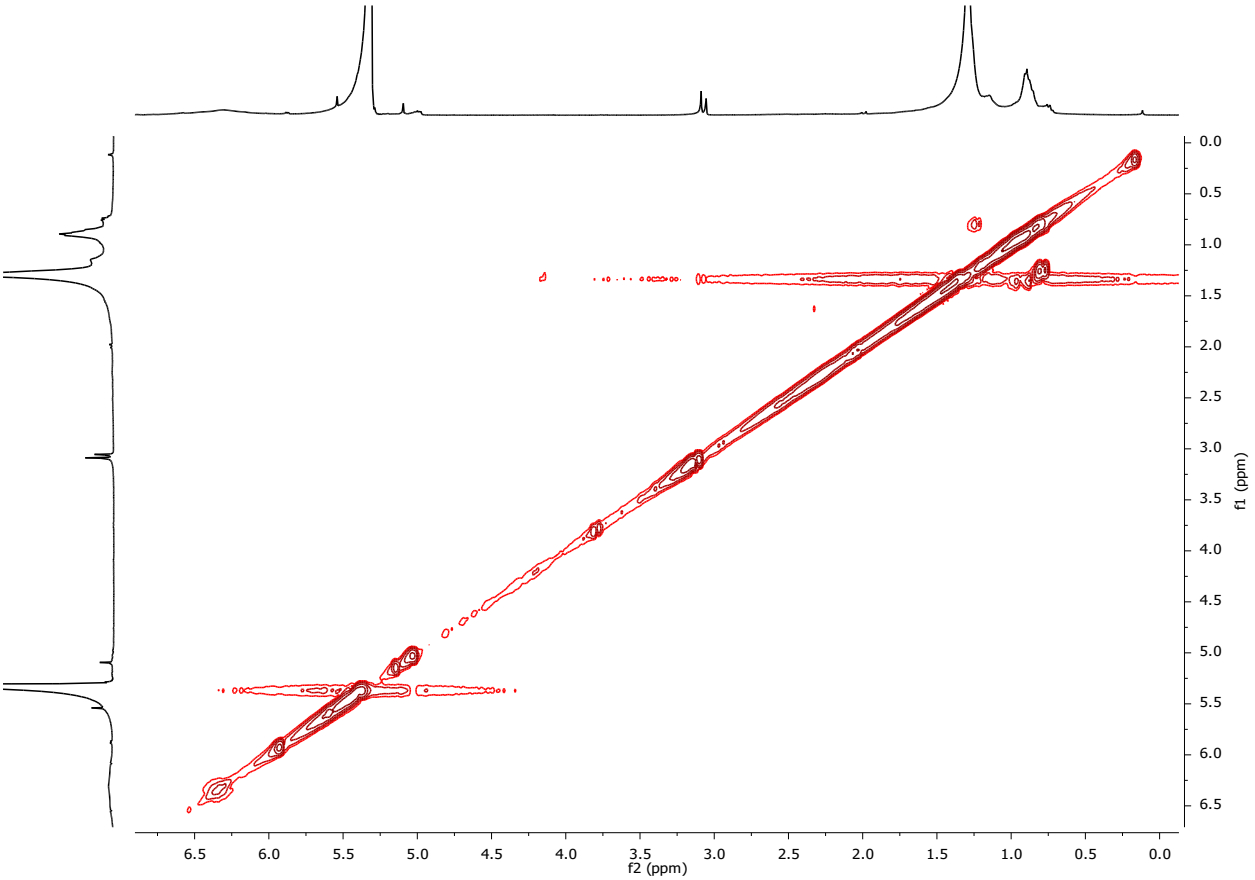

Figure S23. COSY spectrum of the oil isolated after reaction of HDPE and Al*i*Bu$_3$ in the presence of Zr(CH$_2$CMe$_3$)$_2$@SiAlO$_x$ at 200 °C for 12 h, quenched with I$_2$, and extracted with methylene chloride. The spectrum was acquired at room temperature in methylene chloride-d_2. The weak cross-peak at 3.1 ppm correlated with methylene signals at 1.3 ppm indicates -CH$_2$-CH$_2$-I species. The data corresponds to the experiment reported in Table 1, Entry 5.

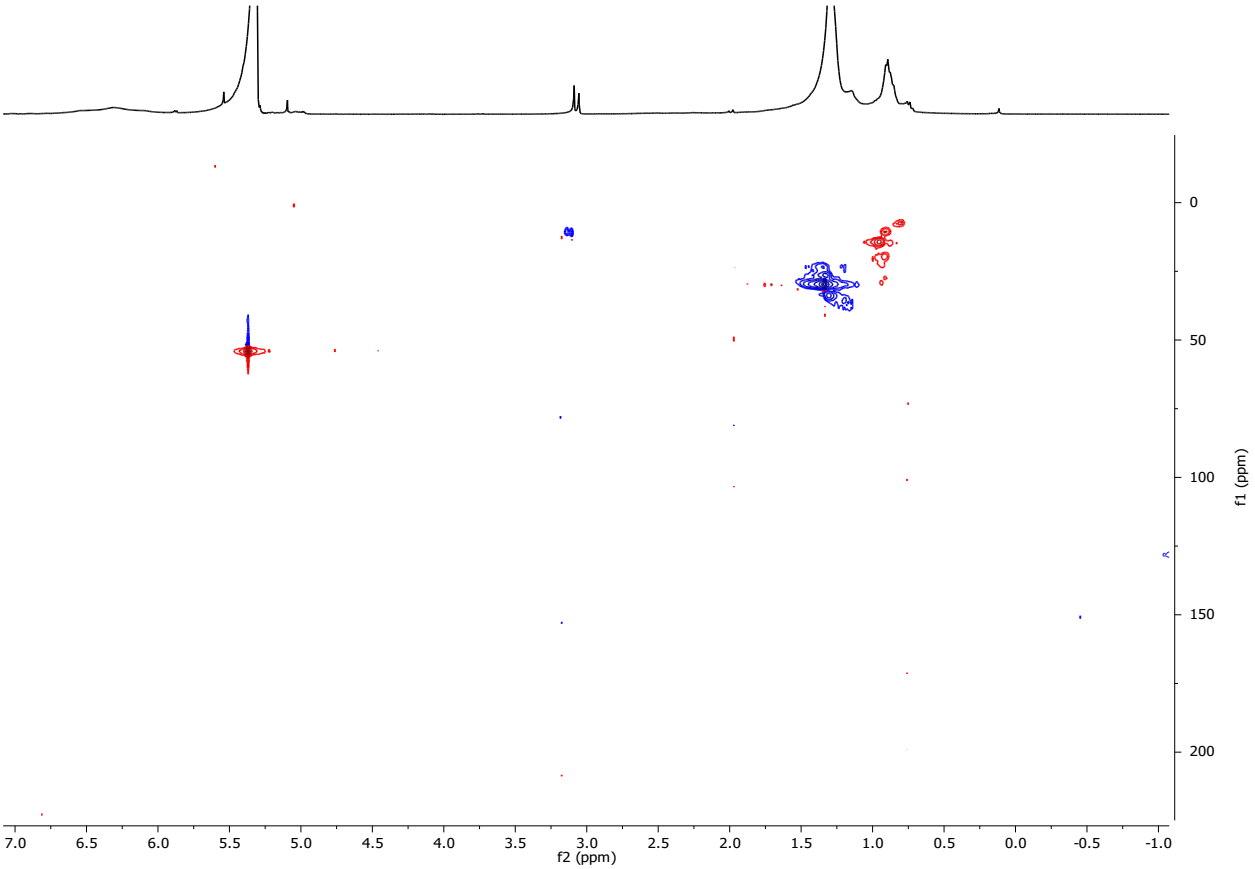

Figure S24. ^{1}H-^{13}C phase sensitive HSQC spectrum of the oil isolated after reaction of HDPE and Al*i*Bu_3 in the presence of $Zr(CH_2CMe_3)_2$@$SiAlO_x$ at 200 °C for 12 h, quenched with I_2, and extracted with methylene chloride. The spectrum was acquired at room temperature in methylene chloride-d_2. The large peak assigned to polymer methylene CH_2 (in blue) at ^{13}C 30 ppm has the same phase as cross-peaks at ^{13}C 10 ppm (also blue), allowing assignment of the latter to primary -CH_2-I. The data corresponds to the experiment reported in Table 1, Entry 5.

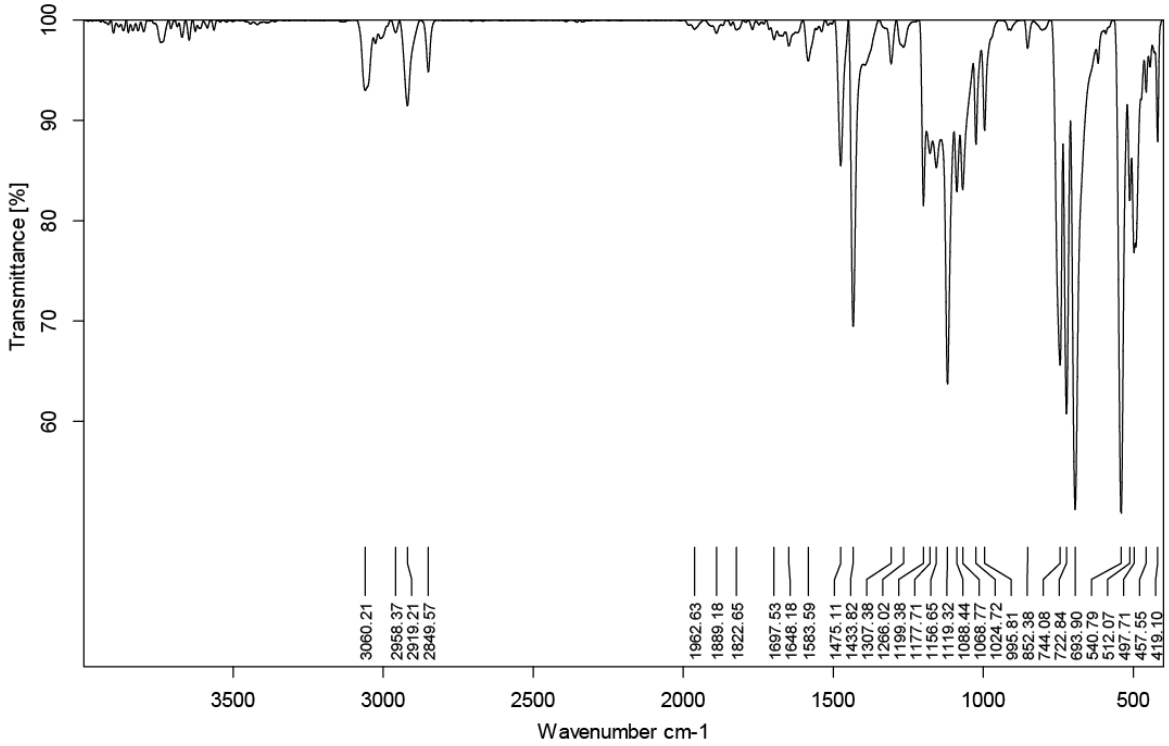

Figure S25. FT-IR spectrum (KBr) of the oil isolated after reaction of HDPE and Al*i*Bu$_3$ in the presence of Zr(CH$_2$CMe$_3$)$_2$@SiAlO$_x$ at 200 °C for 12 h, quenched with I$_2$, and extracted with methylene chloride. Signals between 490-515 cm^{-1} are assigned to C-I stretching modes. The data corresponds to the experiment reported in Table 1, Entry 5.

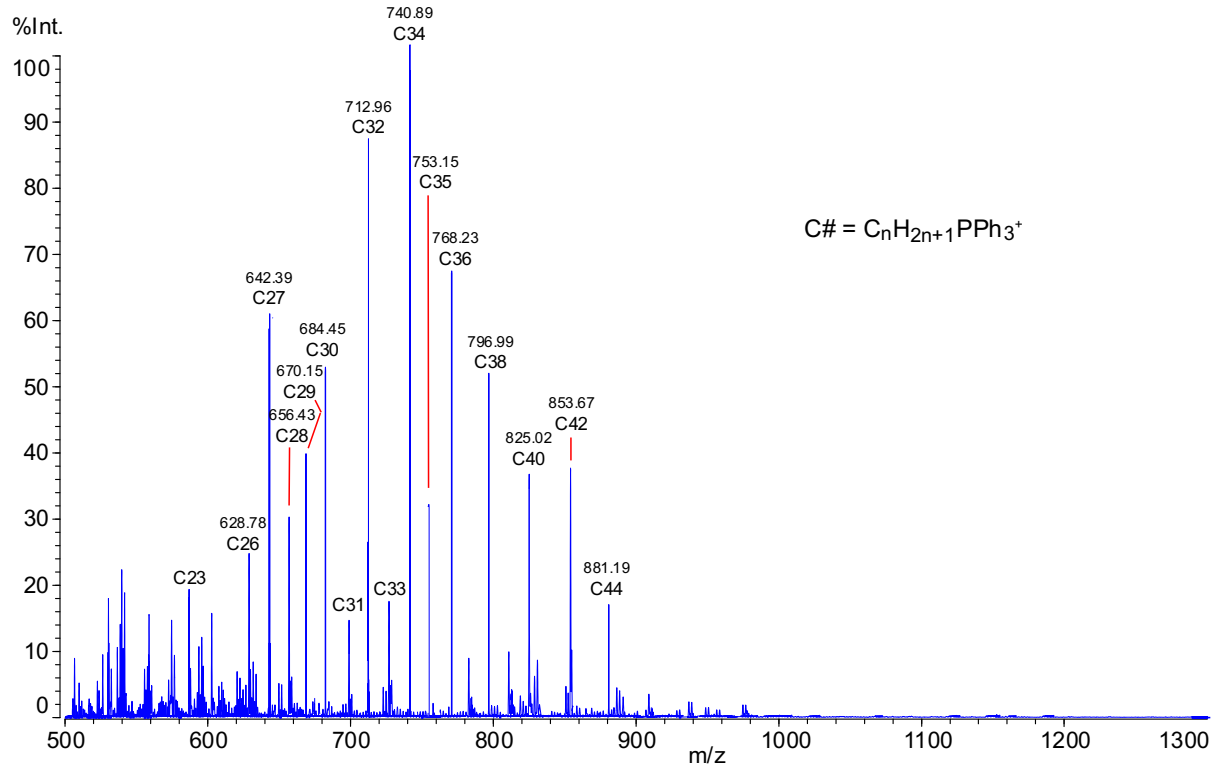

Figure S26. MALDI-TOF-MS spectrum of the oil isolated after reaction of HDPE and Al*i*Bu$_3$ in the presence of Zr(CH$_2$CMe$_3$)$_2$@SiAlO$_x$ at 200 °C for 12 h, quenched with I$_2$, and extracted with methylene chloride. The isolated sample was dissolved in methylene chloride and PPh$_3$ and heated at 50 °C for 4 h. The spectrum was acquired in linear, positive mode with DHB (matrix). Major peaks correspond to alkyl phosphonium species. The data corresponds to the experiment reported in Table 1, Entry 5.

6. HDPE + $Zr(CH_2CMe_3)_2$@$SiAlO_x$ + Al*i*Bu_3 (200 °C, quenched with CO_2).

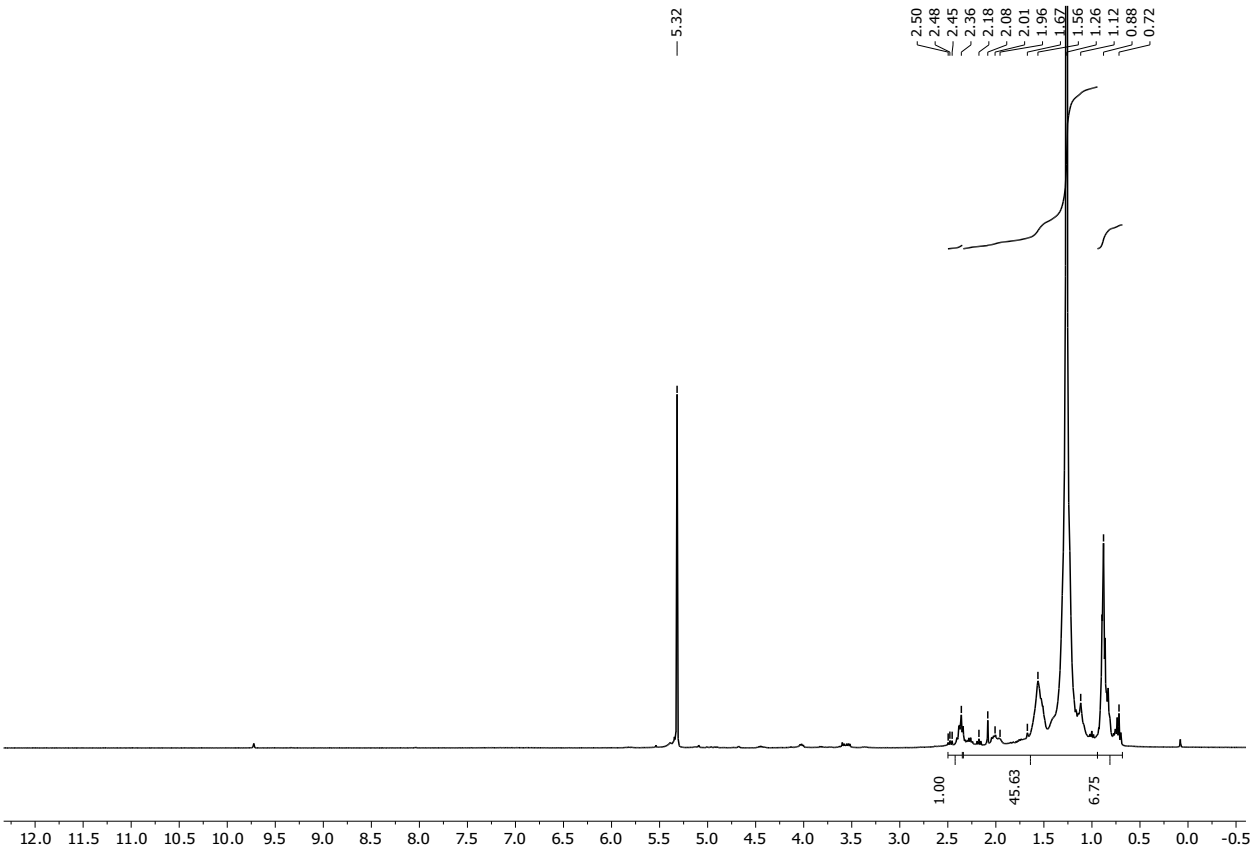

Figure S27. ^{1}H NMR spectrum of the oil isolated after reaction of HDPE and Al*i*Bu_3 in the presence of $Zr(CH_2CMe_3)_2$@$SiAlO_x$ at 200 °C for 12 h, quenched with CO_2, and extracted with methylene chloride. The spectrum was acquired at room temperature in methylene chloride-d_2 and assigned based on COSY, HSQC and HMBC experiments shown in Figures S28, S29 and S30. Signals at 0.7-0.9 ppm are assigned to methyl groups, 1.0-2.3 ppm correspond to methylene groups, and 2.3-2.5 ppm are attributed to methine groups. The data corresponds to the experiment reported in Table 1, Entry 6.

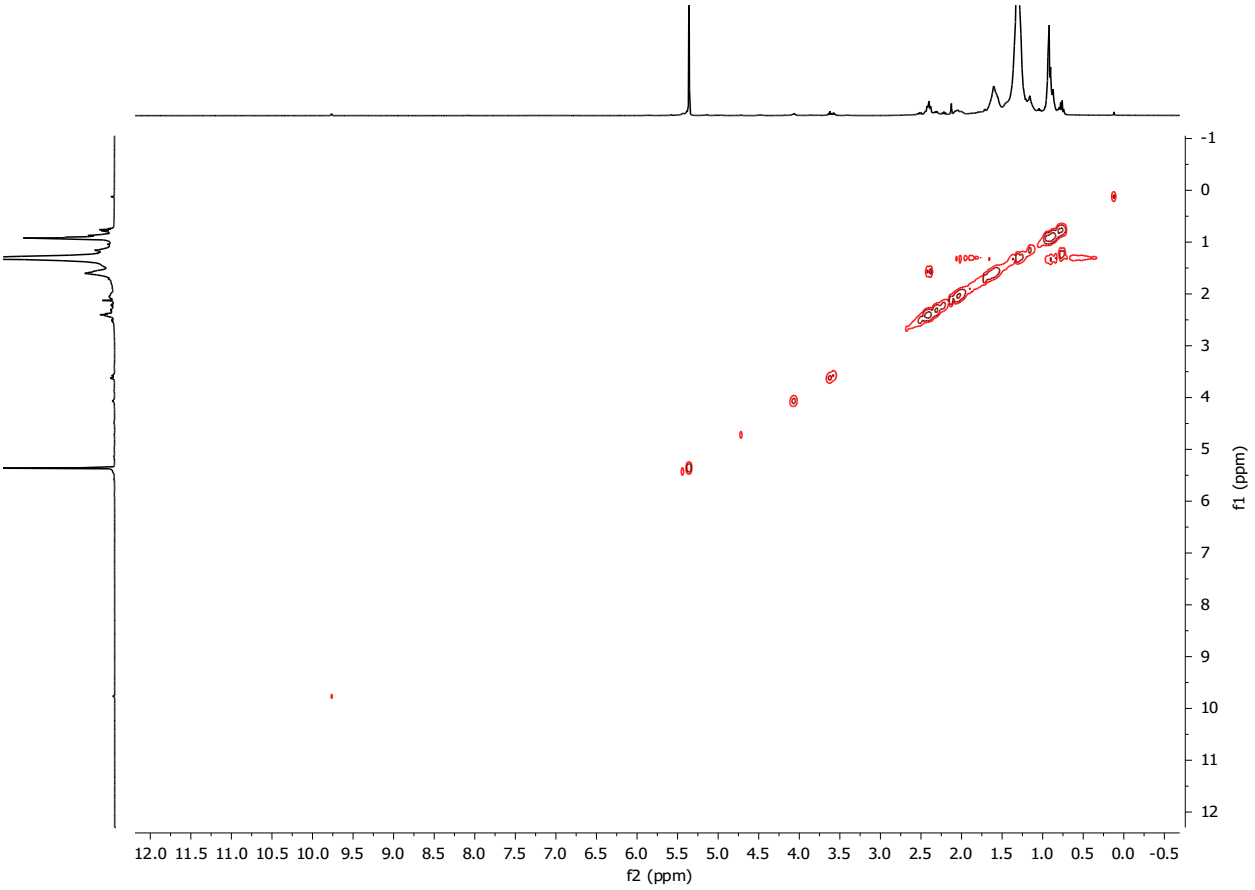

Figure S28. COSY spectrum of the oil isolated after reaction of HDPE and Al*i*Bu$_3$ in the presence of Zr(CH$_2$CMe$_3$)$_2$@SiAlO$_x$ at 200 °C for 12 h, quenched with CO_2, and extracted with methylene chloride. The spectrum was acquired at room temperature in methylene chloride-d_2. The data corresponds to the experiment reported in Table 1, Entry 6.

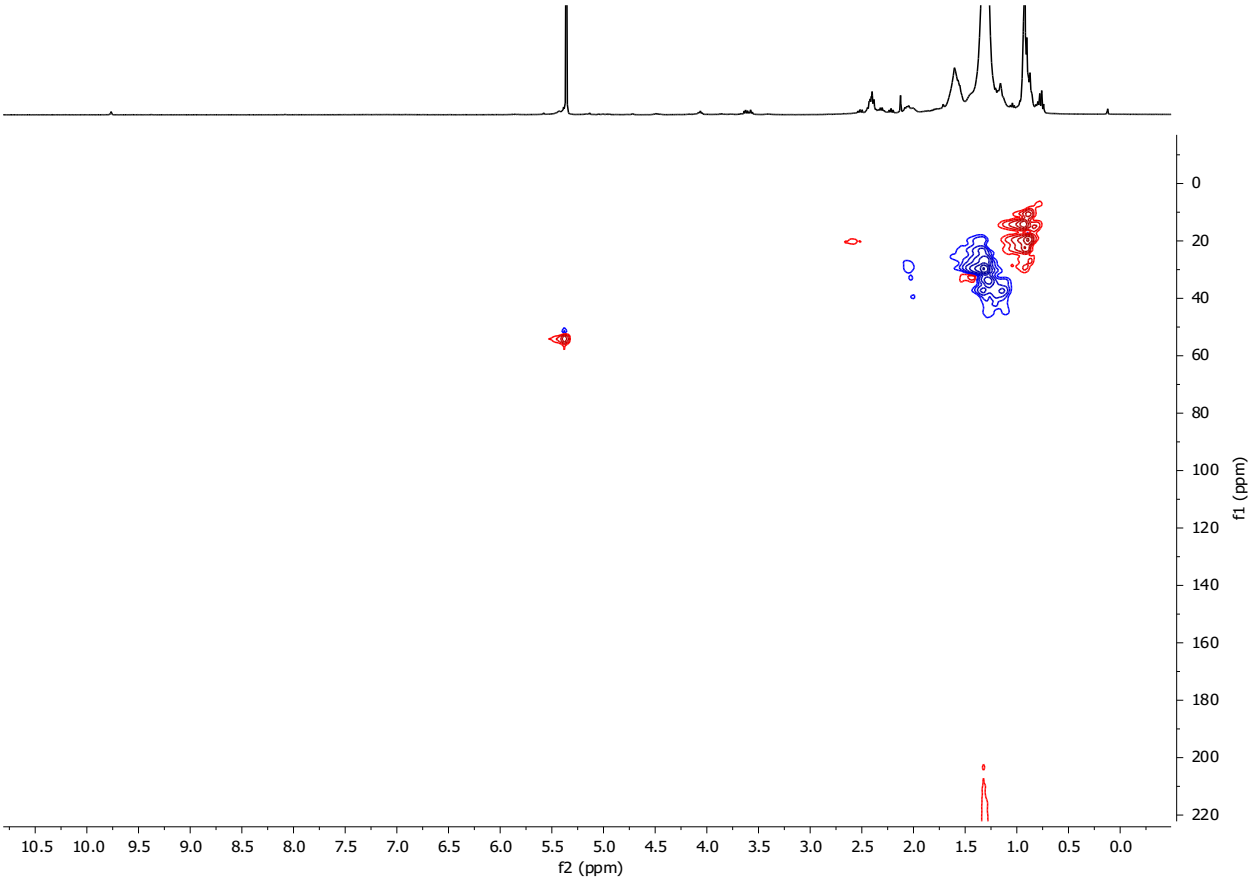

Figure S29. Phase sensitive ^{1}H-^{13}C HSQC spectrum of the oil isolated after reaction of HDPE and Al*i*Bu$_3$ in the presence of Zr(CH$_2$CMe$_3$)$_2$@SiAlO$_x$ at 200 °C for 12 h, quenched with CO_2, and extracted with methylene chloride. The spectrum was acquired at room temperature in methylene chloride-d_2. The data corresponds to the experiment reported in Table 1, Entry 6.

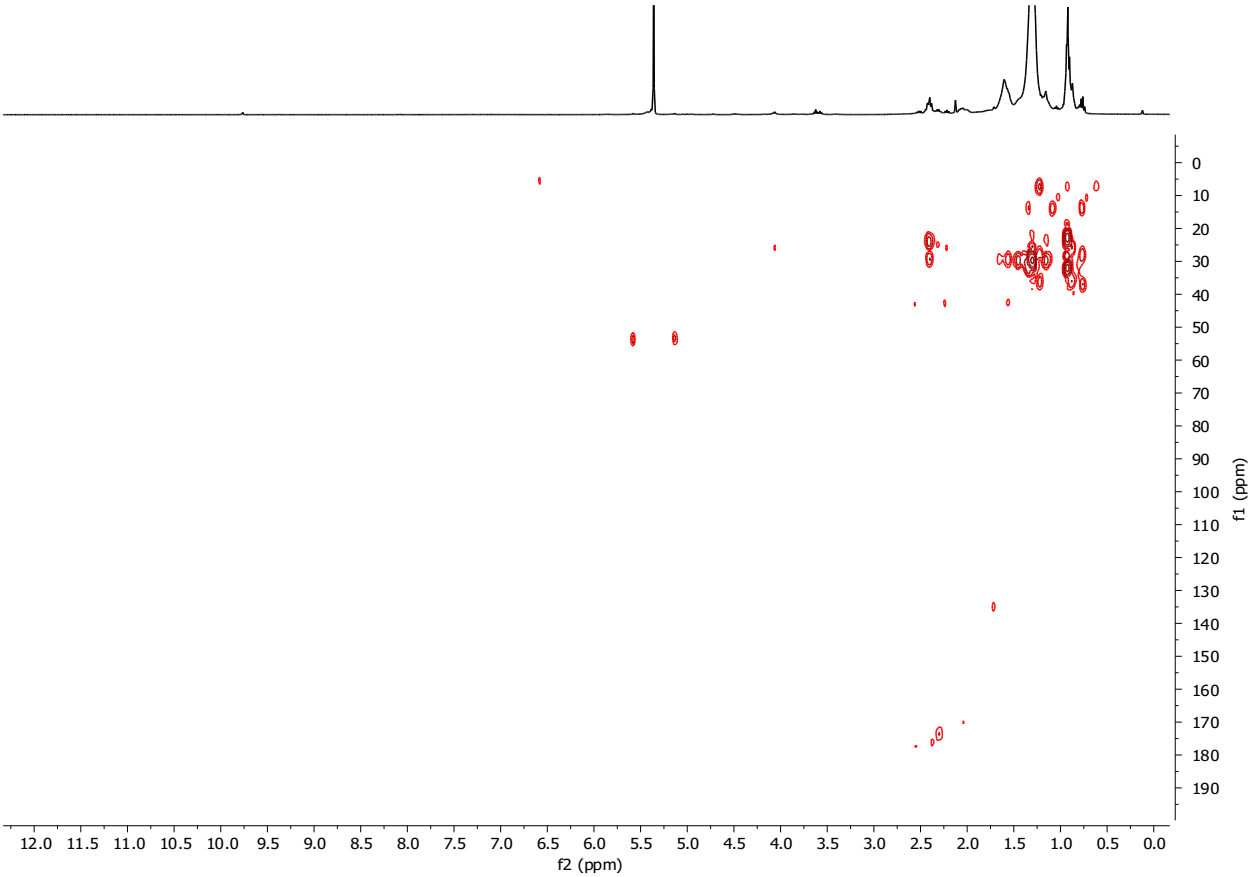

Figure S30. ^{1}H-^{13}C HMBC spectrum of the oil isolated after reaction of HDPE and Al*i*Bu$_3$ in the presence of Zr(CH$_2$CMe$_3$)$_2$@SiAlO$_x$ at 200 °C for 12 h, quenched with CO_2, and extracted with methylene chloride. The spectrum was acquired at room temperature in methylene chloride-d_2. Cross-peaks at ^{13}C 170-180 ppm reveal long-range correlations with methylene and methine signals in the ^{1}H dimension at 2.0-2.5 ppm, consistent with -CH$_2$-CH$_2$-COOH and -(R)CH-CH$_2$-COOH chain ends. The data corresponds to the experiment reported in Table 1, Entry 6.

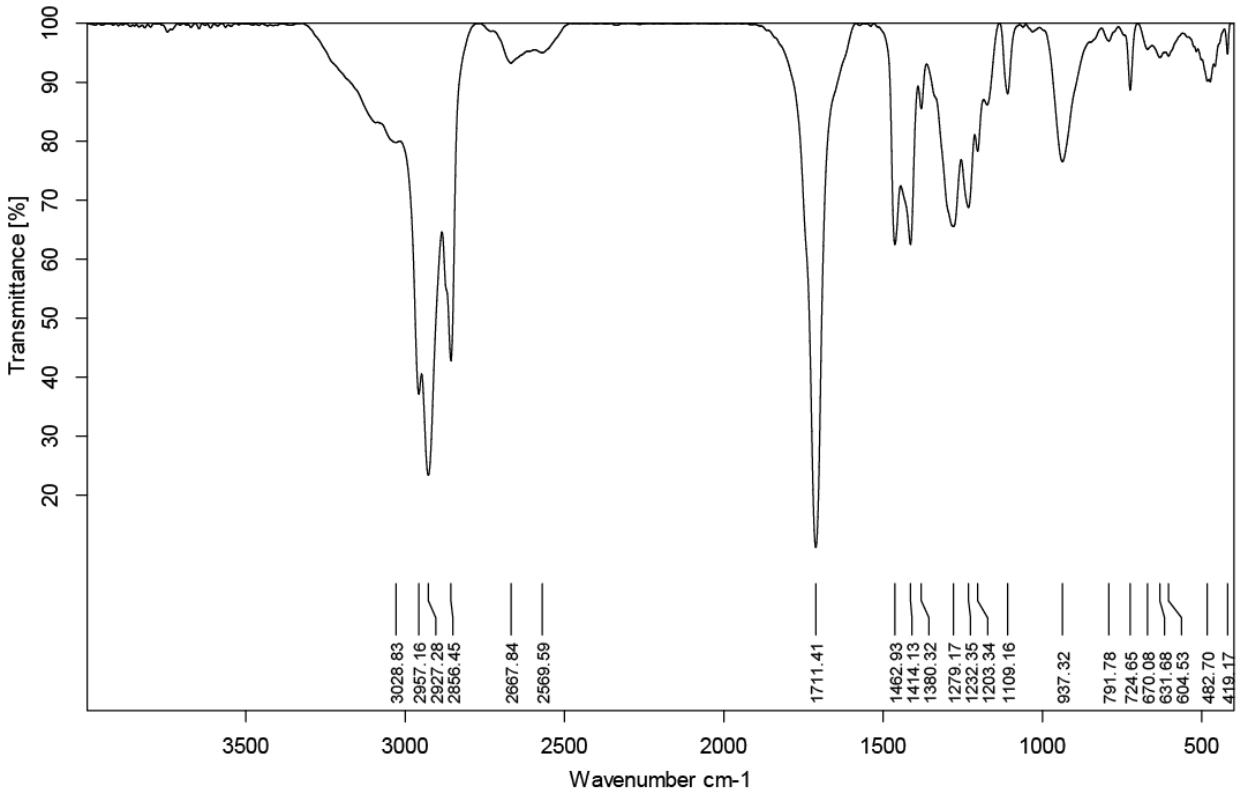

Figure S31. FT-IR spectrum (KBr) of the oil isolated after reaction of HDPE and Al*i*Bu$_3$ in the presence of Zr(CH$_2$CMe$_3$)$_2$@SiAlO$_x$ at 200 °C for 12 h, quenched with CO_2, and extracted with methylene chloride. The broad signal between 2800-3400 cm^{-1} corresponds to an O-H stretch and the intense signal at 1711 cm^{-1} corresponds to a C=O stretch typical of R-COOH species. The data corresponds to the experiment reported in Table 1, Entry 6.

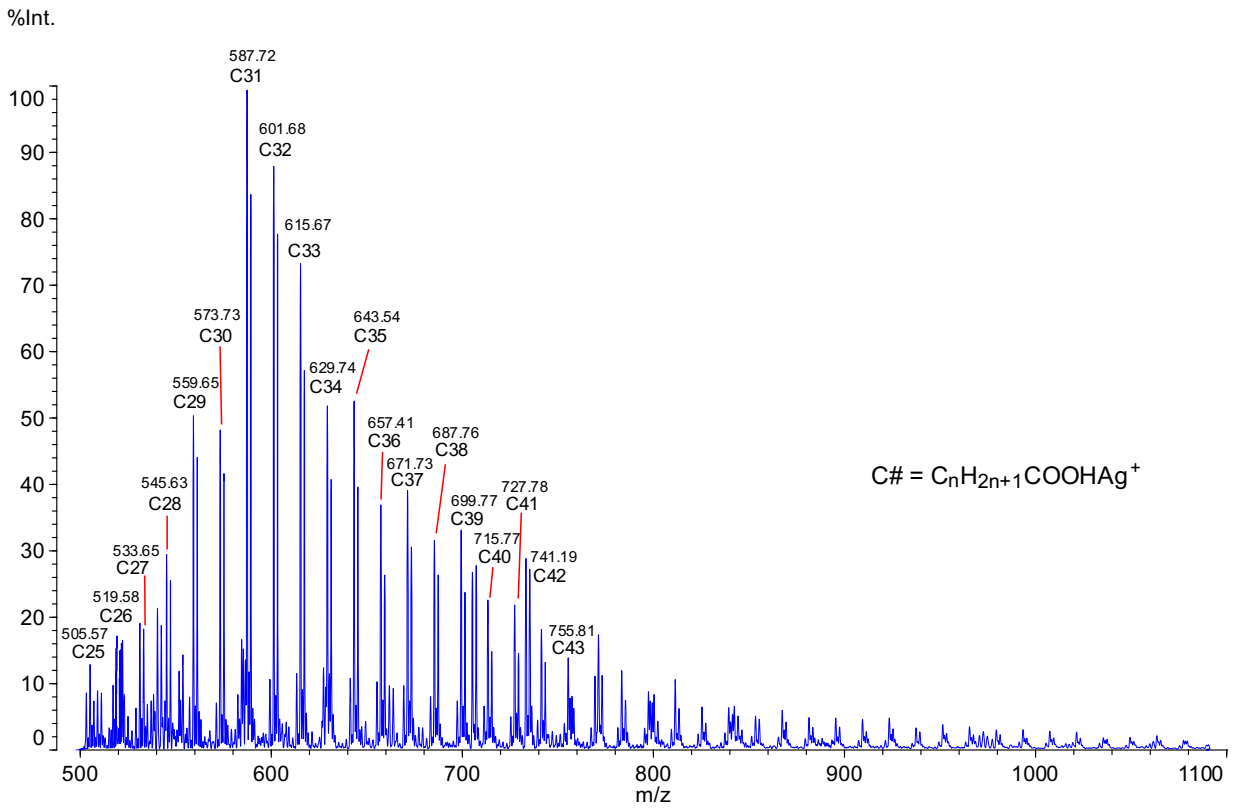

Figure S32. MALDI-TOF-MS spectrum of oil isolated after reaction of HDPE and Al*i*Bu$_3$ in the presence of Zr(CH$_2$CMe$_3$)$_2$@SiAlO$_x$ at 200 °C for 12 h, quenched with CO_2, and extracted with methylene chloride. The spectrum was acquired in linear, positive mode with $AgNO_3$ (salt) and DHB (matrix), and species appear as pairs due to ^{107}Ag and ^{109}Ag adducts. The data corresponds to the experiment reported in Table 1, Entry 6.

7. HDPE + $Zr(CH_2CMe_3)_2$@$SiAlO_x$ + $AlEt_3$ (150 °C).

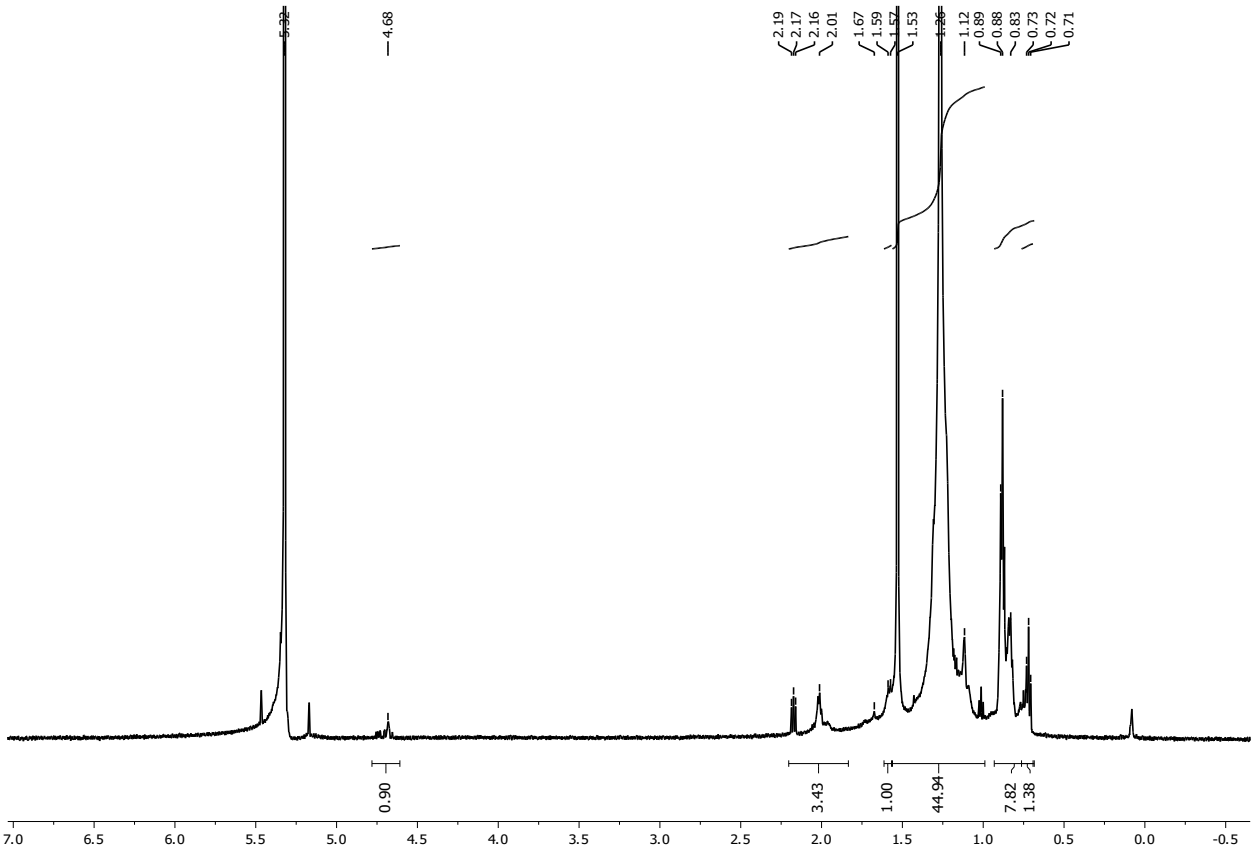

Figure S33. ^1H NMR spectrum of the oil isolated after reaction of HDPE and $AlEt_3$ in the presence of $Zr(CH_2CMe_3)_2$@$SiAlO_x$ at 150 °C for 12 h, quenched with O_2, and extracted with methylene chloride. The spectrum was acquired at room temperature in methylene chloride-d_2 and assigned based on COSY and HSQC experiments in Figures S34 and S35. Signals at 0.7-0.9 ppm correspond to methyl groups, peaks at 1.0-1.6 and 1.7-2.2 ppm are attributed to the methylene groups, and those at 1.6-1.7 ppm correspond to methine groups. Peaks at 4.6-4.8 ppm are assigned to -C*H*$_2$-OH moieties. The data corresponds to the experiment reported in Table 1, Entry 7.

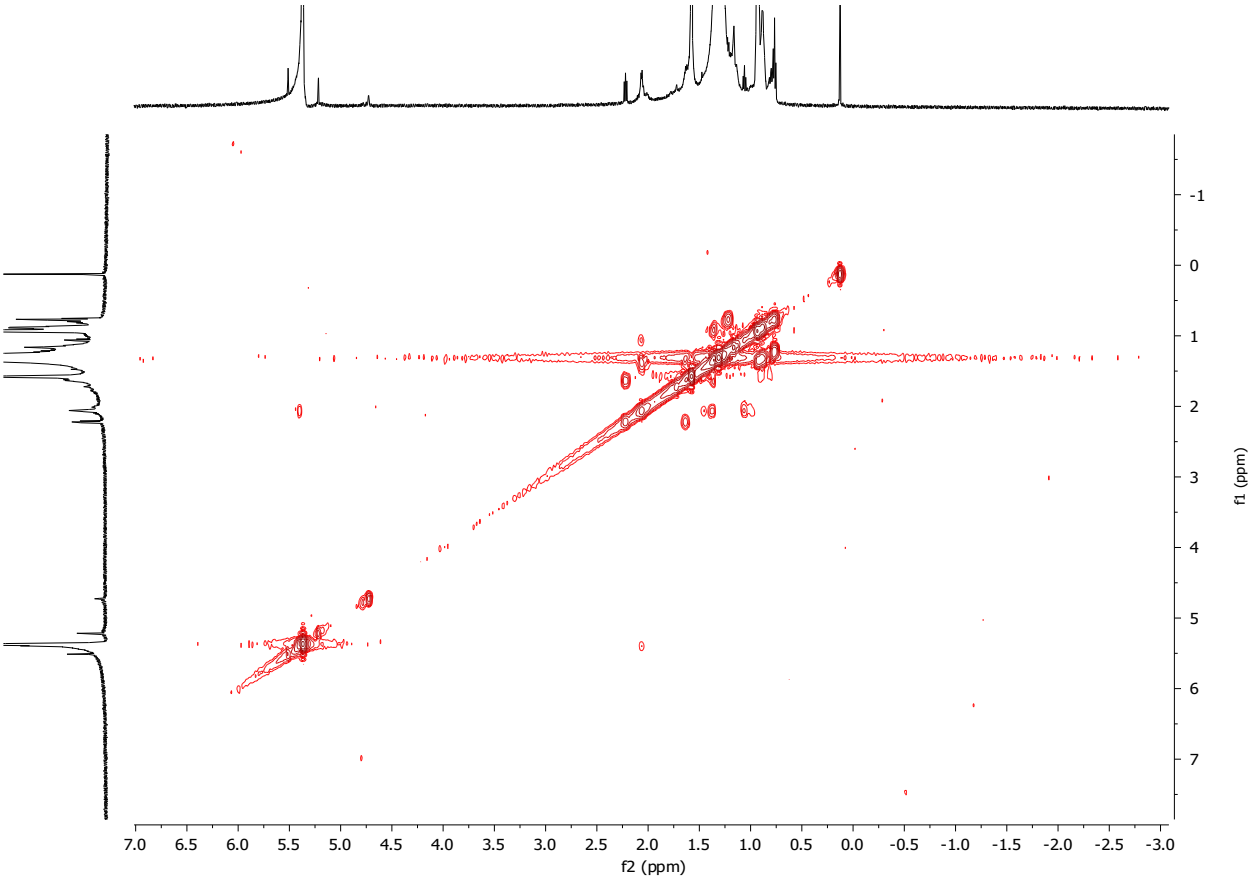

Figure S34. COSY spectrum of the oil isolated after reaction of HDPE and $AlEt_3$ in the presence of $Zr(CH_2CMe_3)_2$@$SiAlO_x$ at 150 °C for 12 h, quenched with O_2, and extracted with methylene chloride. The spectrum was acquired at room temperature in methylene chloride-d_2. The cross-peak at 4.7 ppm correlates to the methylene signal at 2.0 ppm, consistent with the -CH_2-CH_2-OH end group structure. The data corresponds to the experiment reported in Table 1, Entry 7.

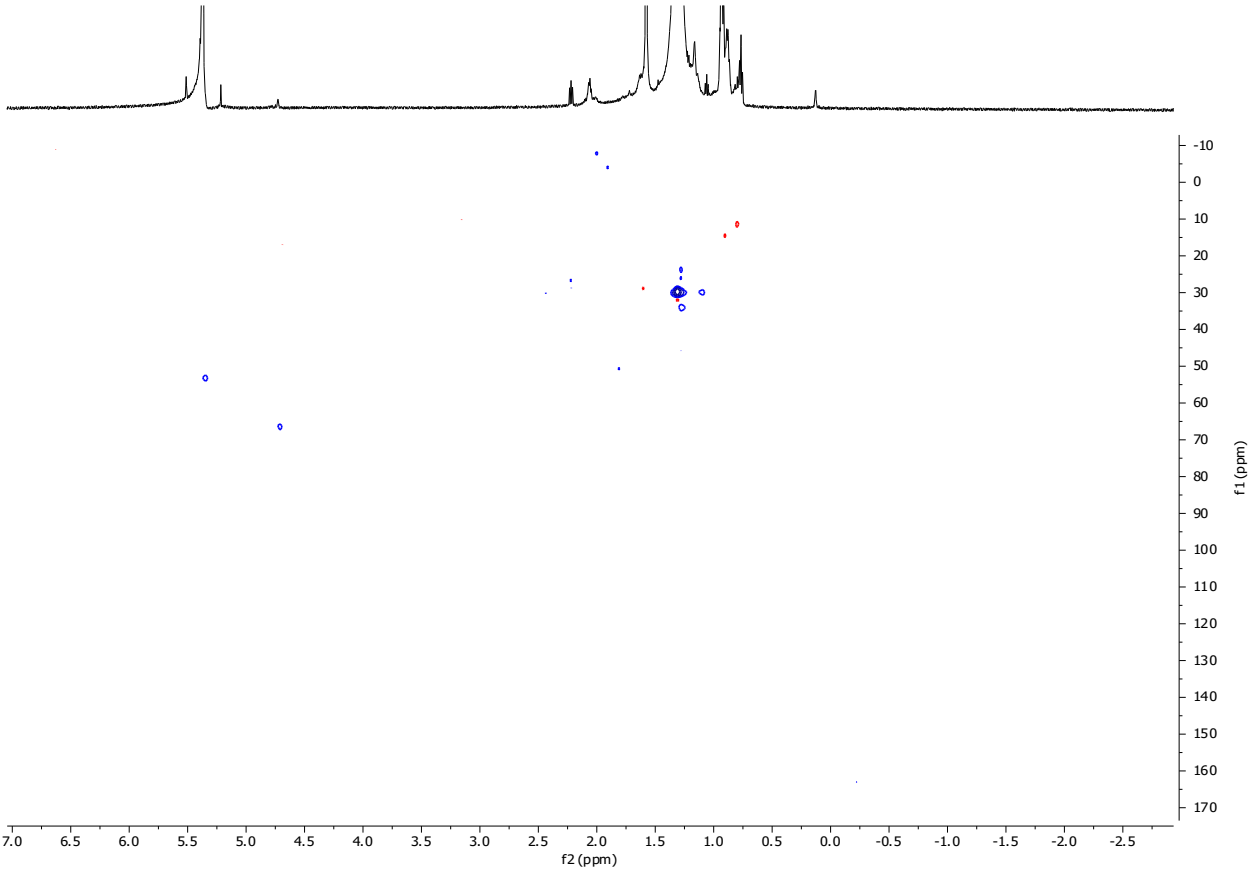

Figure S35. Phase sensitive ^{1}H-^{13}C HSQC spectrum of the oil isolated after reaction of HDPE and $AlEt_3$ in the presence of $Zr(CH_2CMe_3)_2$@$SiAlO_x$ at 150 °C for 12 h, quenched with O_2, and extracted with methylene chloride. The spectrum was acquired at room temperature in methylene chloride-d_2. Cross-peaks at ^{13}C 60-70 ppm have the same phase (blue) as the methylene peaks at 30 ppm, which is indicative of -CH_2-OH species (i.e., the alcohols are primary). The data corresponds to the experiment reported in Table 1, Entry 7.

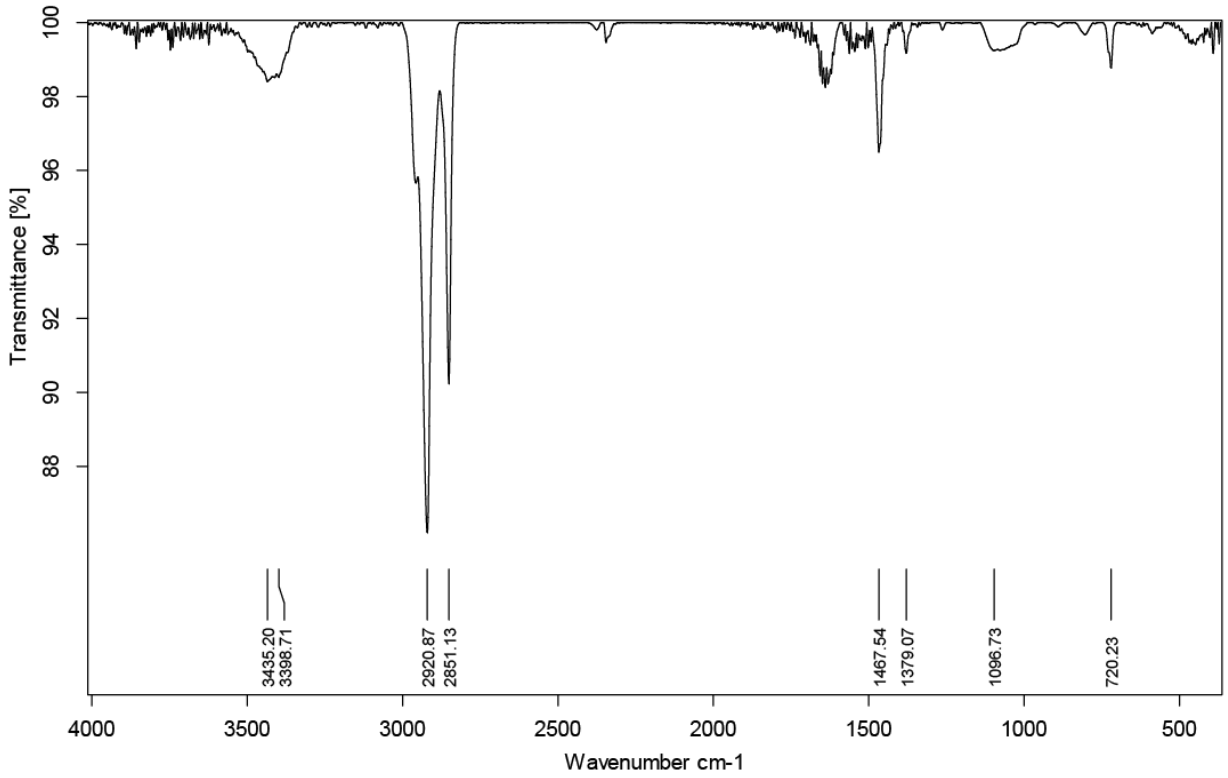

Figure S36. FT-IR spectrum (KBr) of the oil isolated after reaction of HDPE and $AlEt_3$ in the presence of $Zr(CH_2CMe_3)_2$@$SiAlO_x$ at 150 °C for 12 h, quenched with O_2, and extracted with methylene chloride. The broad signal at 3435 cm^{-1} corresponds to an O-H stretching mode. The data corresponds to the experiment reported in Table 1, Entry 7.

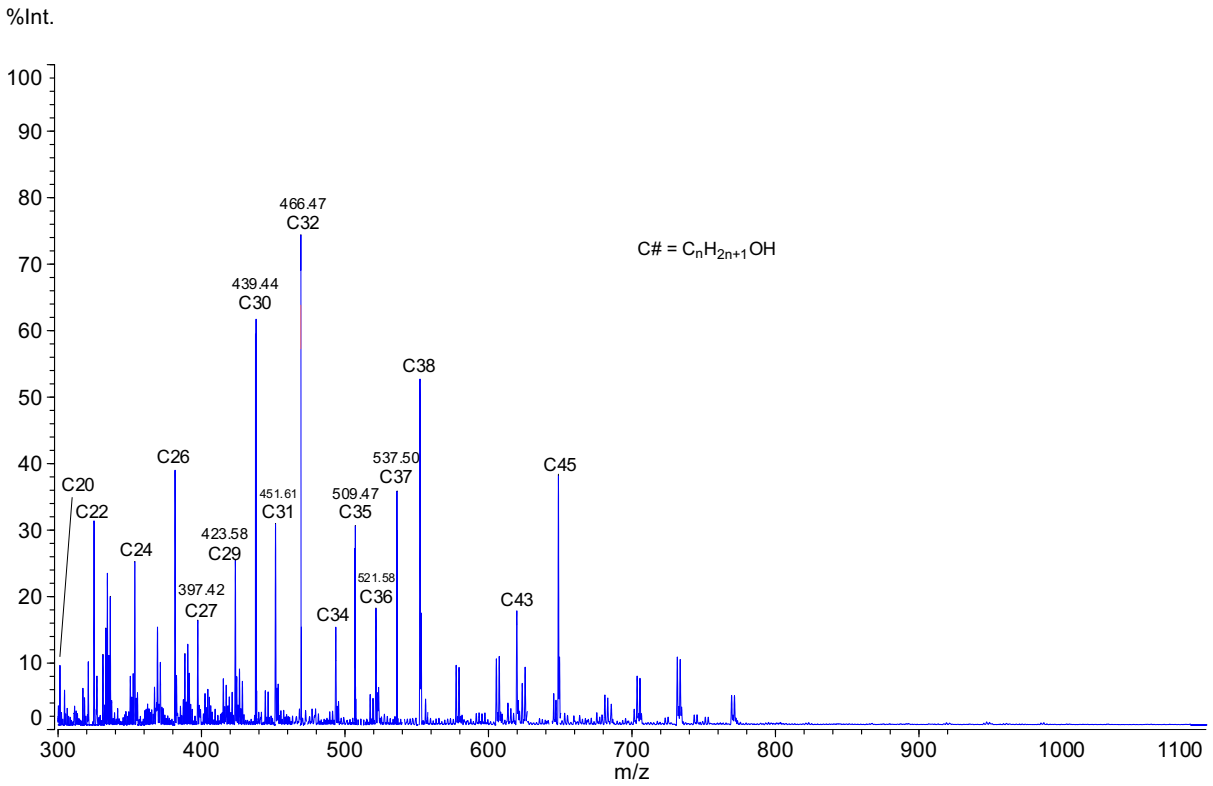

Figure S37. MALDI-TOF-MS spectrum of the oil isolated after reaction of HDPE and $AlEt_3$ in the presence of $Zr(CH_2CMe_3)_2$@$SiAlO_x$ at 150 °C for 12 h, quenched with O_2, and extracted with methylene chloride. The spectrum was acquired in linear, positive mode with $AgNO_3$ (salt) and DHB (matrix). The data corresponds to the experiment reported in Table 1, Entry 7.

8. HDPE + $Zr(CH_2CMe_3)_2$@$SiAlO_x$ + $AlEt_3$ (200 °C).

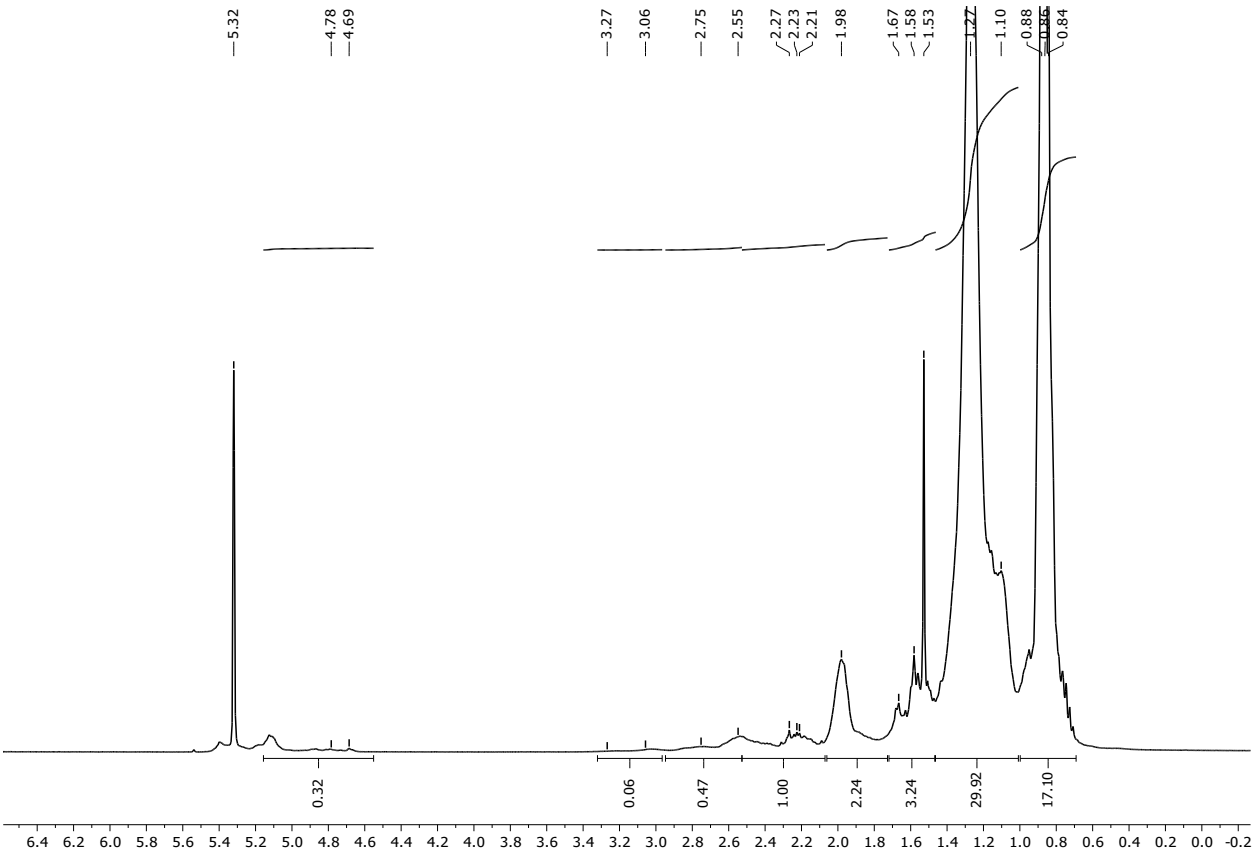

Figure S38. ^1H NMR spectrum of the oil isolated after reaction of HDPE and $AlEt_3$ in the presence of $Zr(CH_2CMe_3)_2$@$SiAlO_x$ at 200 °C for 12 h, quenched with O_2, and extracted with methylene chloride. The spectrum was acquired at room temperature in methylene chloride-d_2 and assigned based on TOCSY and HSQC experiments in Figures S39 and S40. Signals at 0.7-0.9 ppm correspond to methyl peaks at 1.0-1.5, 1.7-2.1, and 2.6-3.3 ppm are attributed to methylene moieties, and those at 1.5-1.7, 2.1-2.6 ppm correspond to methine groups. Peaks at 4.6-5.2 ppm are assigned to -CH_2-OH groups. The data corresponds to the experiment reported in Table 1, Entry 8.

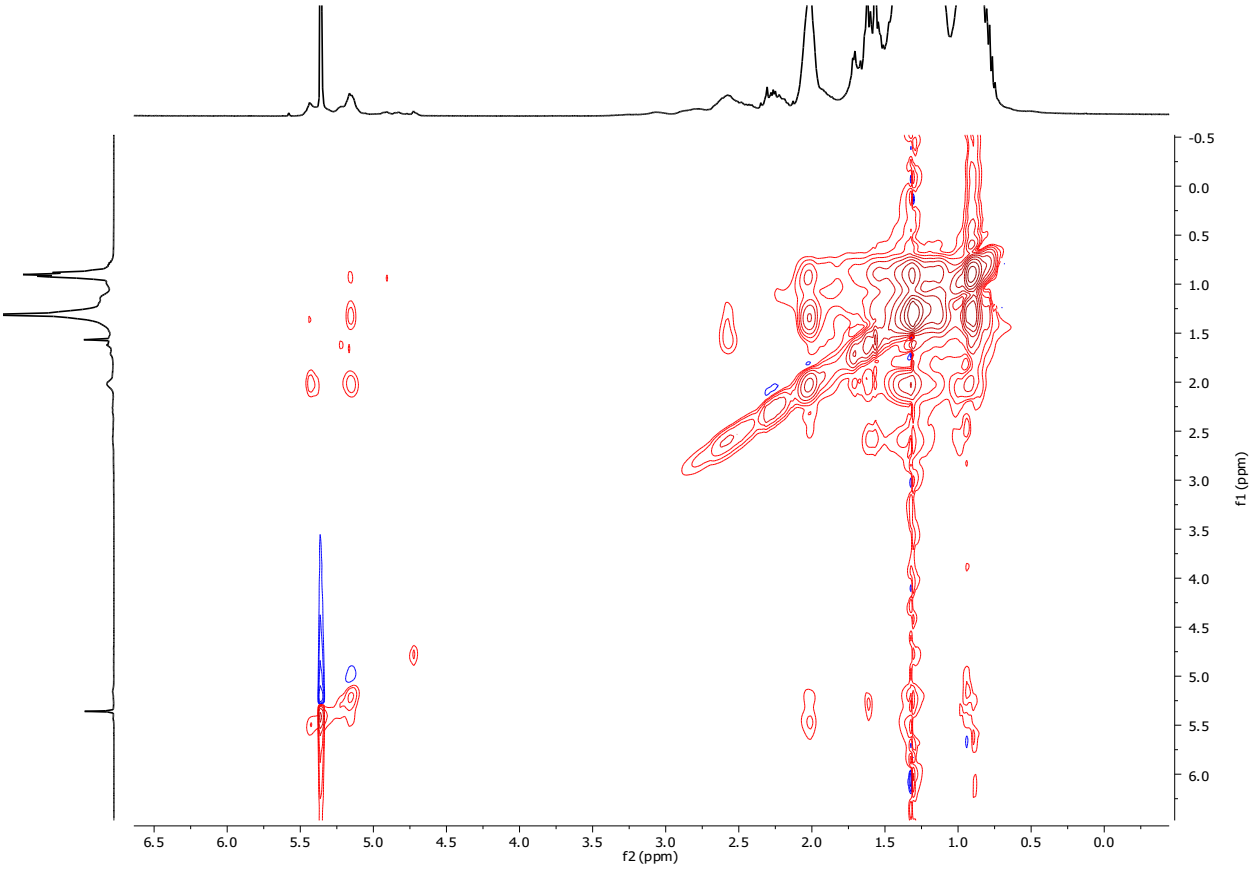

Figure S39. TOCSY spectrum of the oil isolated after reaction of HDPE and $AlEt_3$ in the presence of $Zr(CH_2CMe_3)_2$@$SiAlO_x$ at 200 °C for 12 h, quenched with O_2, and extracted with methylene chloride. The spectrum was acquired at room temperature in methylene chloride-d_2. Cross-peaks at 4.7-5.3 ppm correlating to methylene signals at 1.3 and 2.1 ppm are indicative of -CH_2-CH_2-OH structures. The data corresponds to the experiment reported in Table 1, Entry 8.

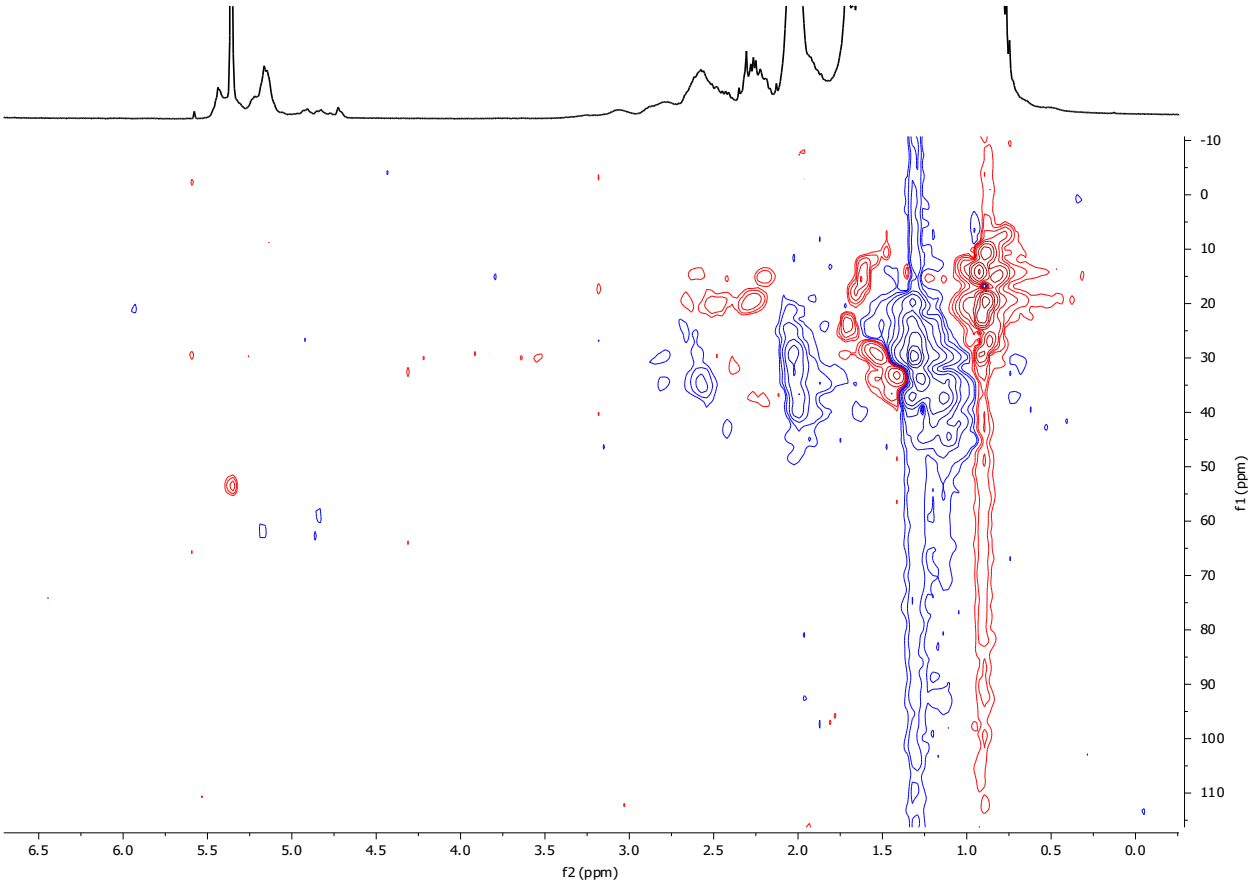

Figure S40. Phase sensitive ^{1}H-^{13}C HSQC spectrum of the oil isolated after reaction of HDPE and $AlEt_3$ in the presence of $Zr(CH_2CMe_3)_2$@$SiAlO_x$ at 200 °C for 12 h, quenched with O_2, and extracted with methylene chloride. The spectrum was acquired at room temperature in methylene chloride-d_2. Cross-peaks at ^{13}C 60-65 ppm have the same phase (blue) as methylene peaks at 30 ppm, indicative of -CH_2-OH end groups (i.e., alcohols are primary). The data corresponds to the experiment reported in Table 1, Entry 8.

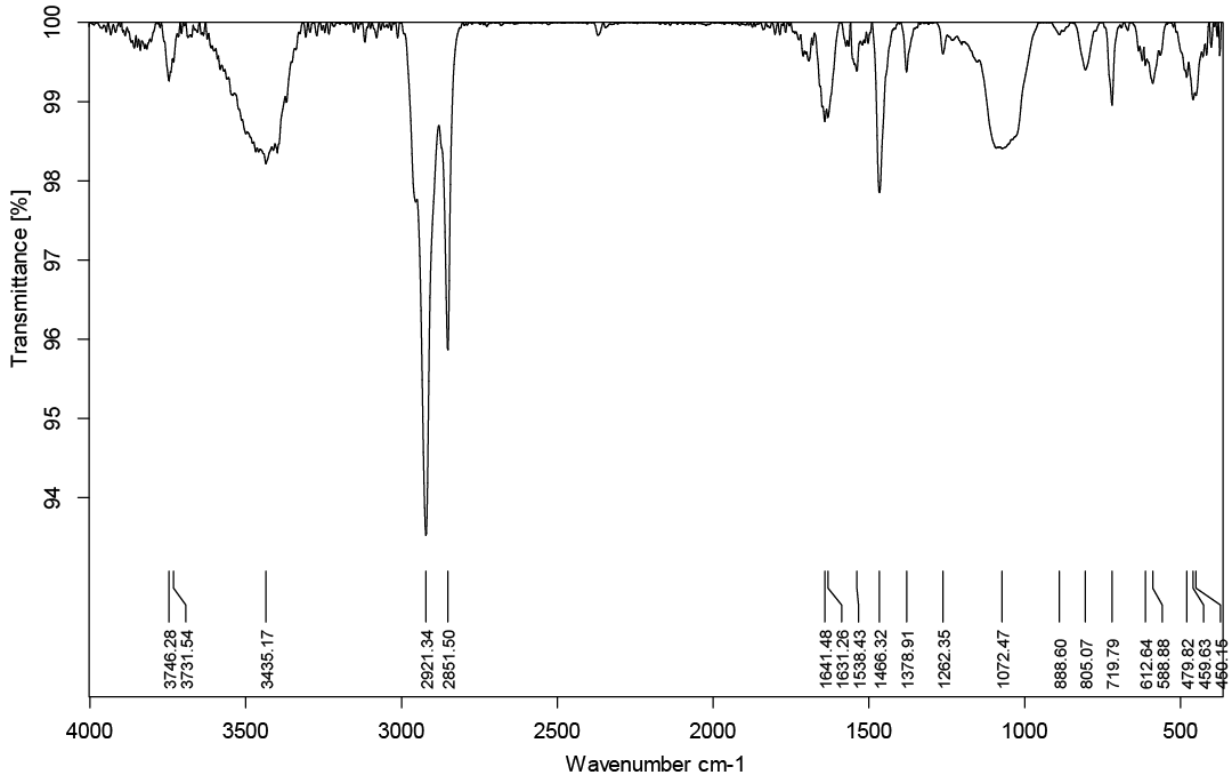

Figure S41. FT-IR spectrum (KBr) of the oil isolated after reaction of HDPE and $AlEt_3$ in the presence of $Zr(CH_2CMe_3)_2$@$SiAlO_x$ at 200 °C for 12 h, quenched with O_2, and extracted with methylene chloride. The broad signal at 3435 cm^{-1} corresponds to an O-H stretch. The data corresponds to the experiment reported in Table 1, Entry 8.

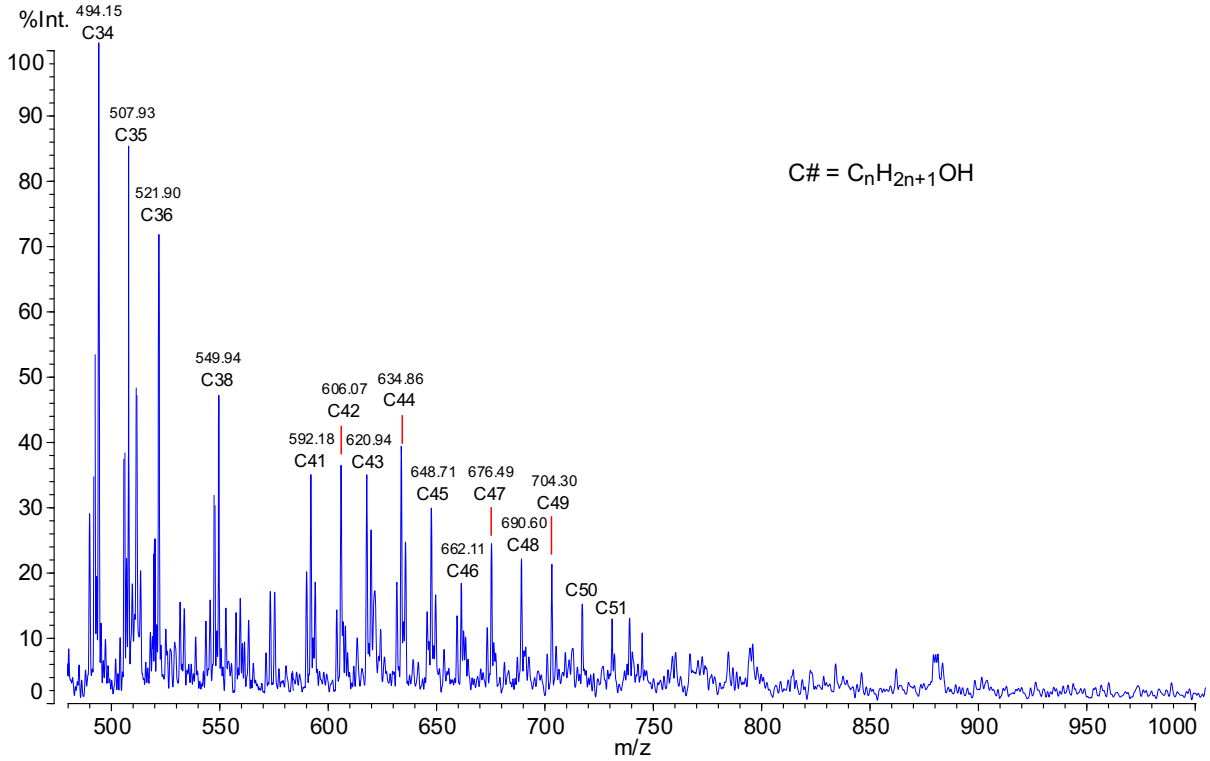

Figure S42. MALDI-TOF-MS spectrum of the oil isolated after reaction of HDPE and $AlEt_3$ in the presence of $Zr(CH_2CMe_3)_2$@$SiAlO_x$ at 200 °C for 12 h, quenched with O_2, and extracted with methylene chloride. The spectrum was acquired in linear, positive mode with $AgNO_3$ (salt) and DHB (matrix). The data corresponds to the experiment reported in Table 1, Entry 8.

9. HDPE + $Zr(CH_2CMe_3)_2$@$SiAlO_x$ + $AlPh_3$ (200 °C).

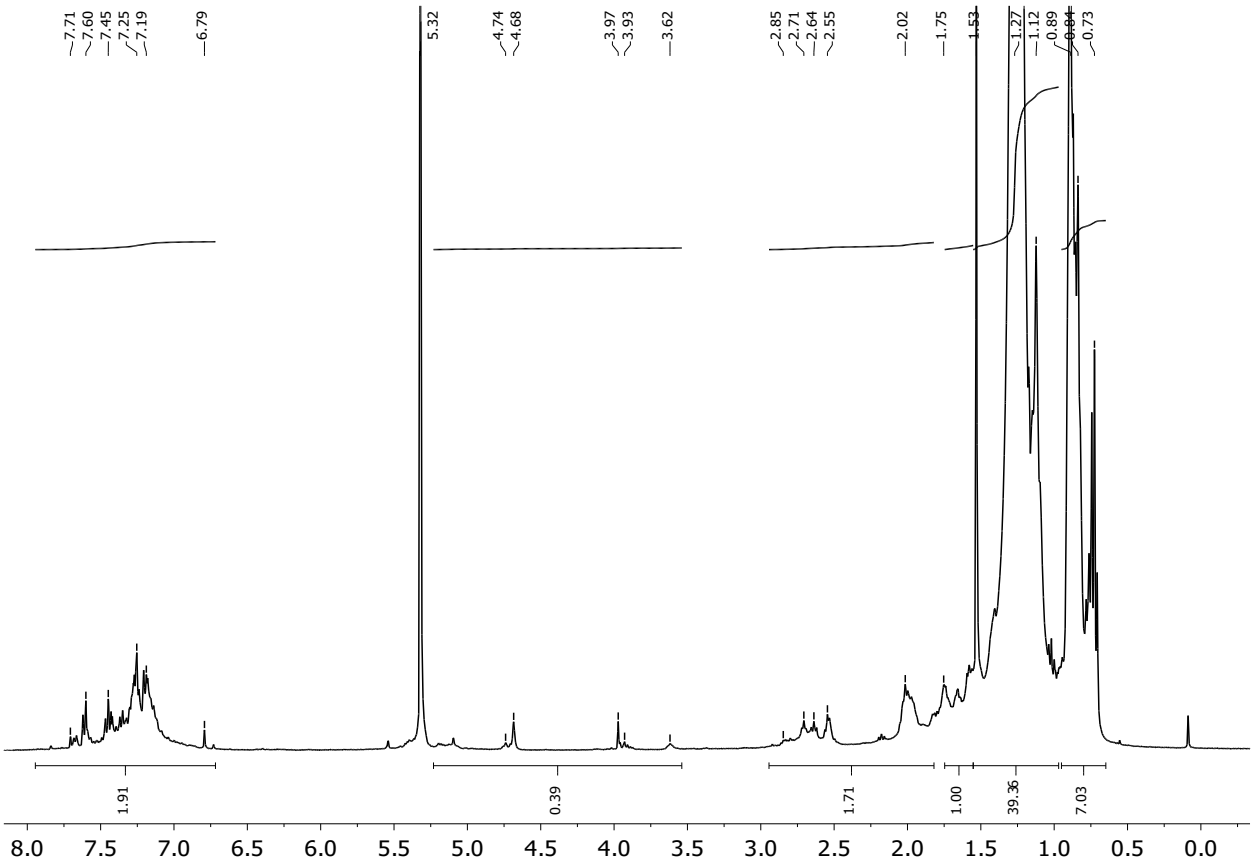

Figure S43. ^1H NMR spectrum of the oil isolated after reaction of HDPE and $AlPh_3$ in the presence of $Zr(CH_2CMe_3)_2$@$SiAlO_x$ at 200 °C for 12 h, quenched with O_2, and extracted with methylene chloride. The spectrum was acquired at room temperature in methylene chloride-d_2 and assigned based on COSY and HSQC experiments in Figures S44 and S45. Signals at 0.7-0.9 ppm correspond to methyl groups, peaks at 1.0-1.6 and 1.8-3.0 ppm are attributed to methylene, and those at 1.6-1.8 ppm are assigned to methine groups. Incorporation of phenyl groups in the product is evident from the aromatic signals between 6.8-8.0 ppm. Signals at 3.5-4.8 ppm are assigned to -CH_2-OH groups. The data corresponds to the experiment reported in Table 1, Entry 9.

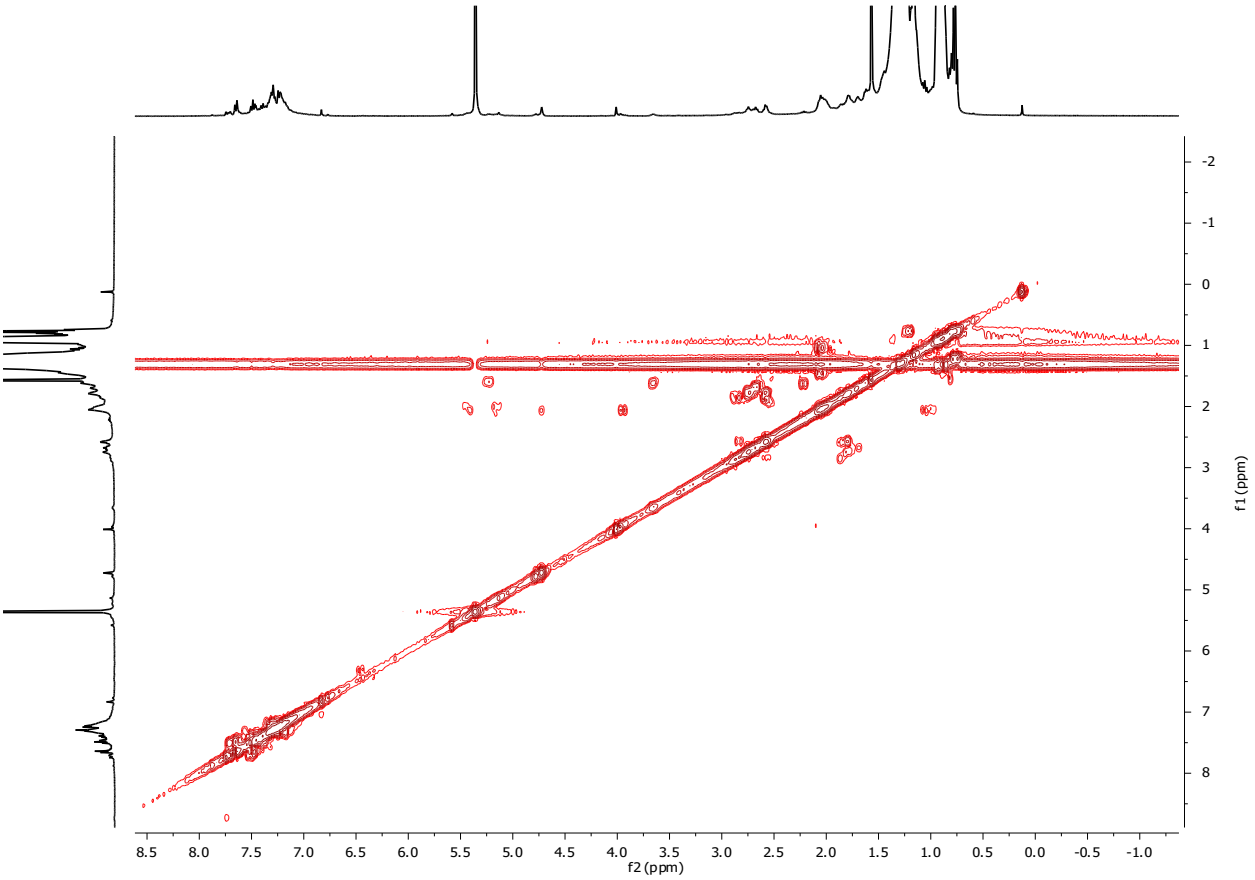

Figure S44. COSY spectrum of the oil isolated after reaction of HDPE and $AlPh_3$ in the presence of $Zr(CH_2CMe_3)_2$@$SiAlO_x$ at 200 °C for 12 h, quenched with O_2, and extracted with methylene chloride. The spectrum was acquired at room temperature in methylene chloride-d_2. Cross-peaks at 4.0, 4.7, and 5.1 ppm correlate with the methylene signals at 2.1 ppm, and cross-peaks at 3.6 and 5.2 ppm correlate with methine signals at 1.6 ppm, indicative of both -CH_2-CH_2-OH and -(R)CH-CH_2-OH structures (R = phenyl or alkyl, as shown in the HMBC below). The data corresponds to the experiment reported in Table 1, Entry 9.

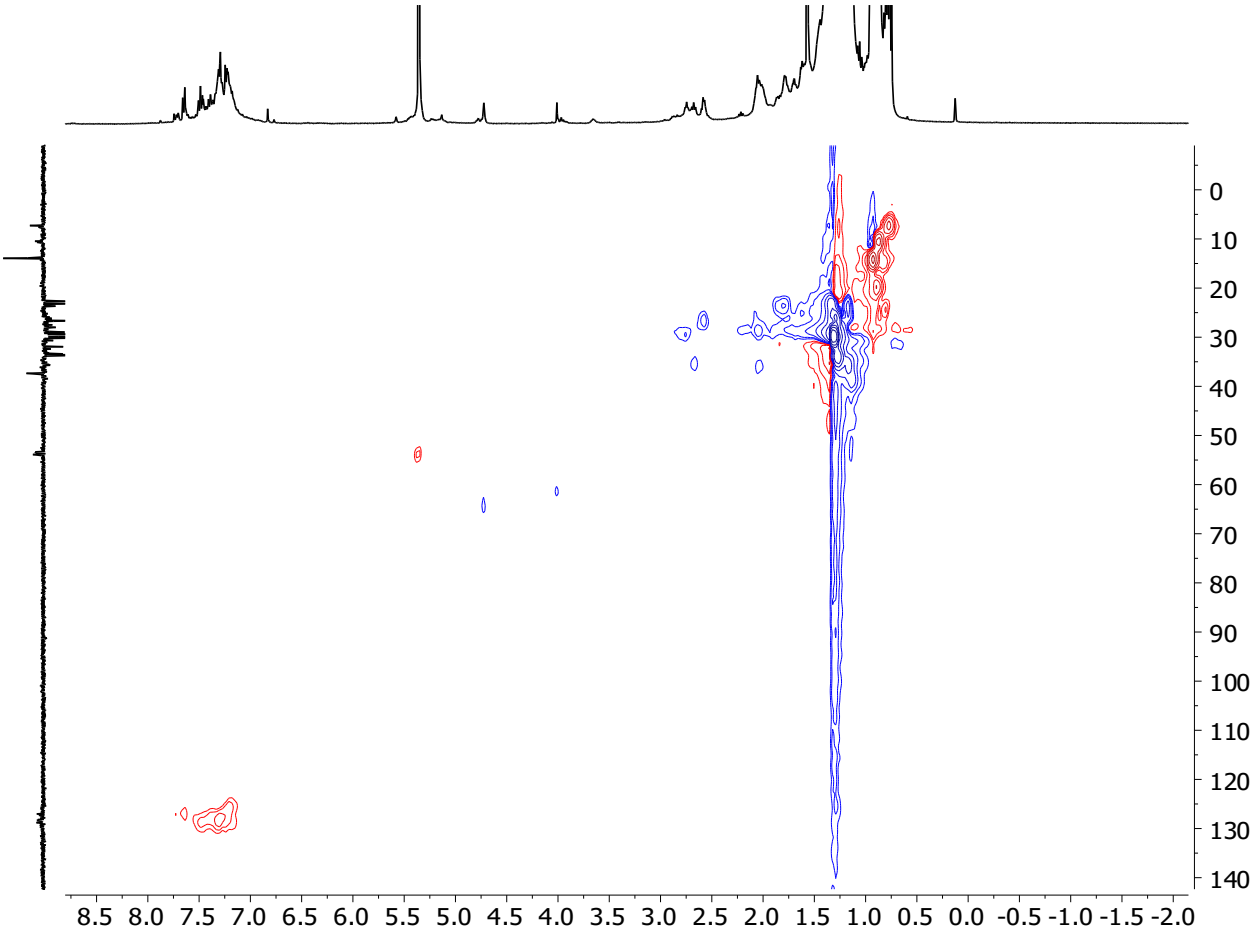

Figure S45. Phase sensitive ^{1}H-^{13}C HSQC spectrum of the oil isolated after reaction of HDPE and $AlPh_3$ in the presence of $Zr(CH_2CMe_3)_2$@$SiAlO_x$ at 200 °C for 12 h, quenched with O_2, and extracted with methylene chloride. The spectrum was acquired at room temperature in methylene chloride-d_2. Cross-peaks at ^{13}C 60-70 ppm have the same phase (blue) as methylene peaks at 30 ppm, revealing the -CH_2-OH structure. Cross-peaks at ^{13}C 125-135 ppm correspond to aromatic C-H groups and have the opposite phase (red) as methylene peaks at 30 ppm. The data corresponds to the experiment reported in Table 1, Entry 9.

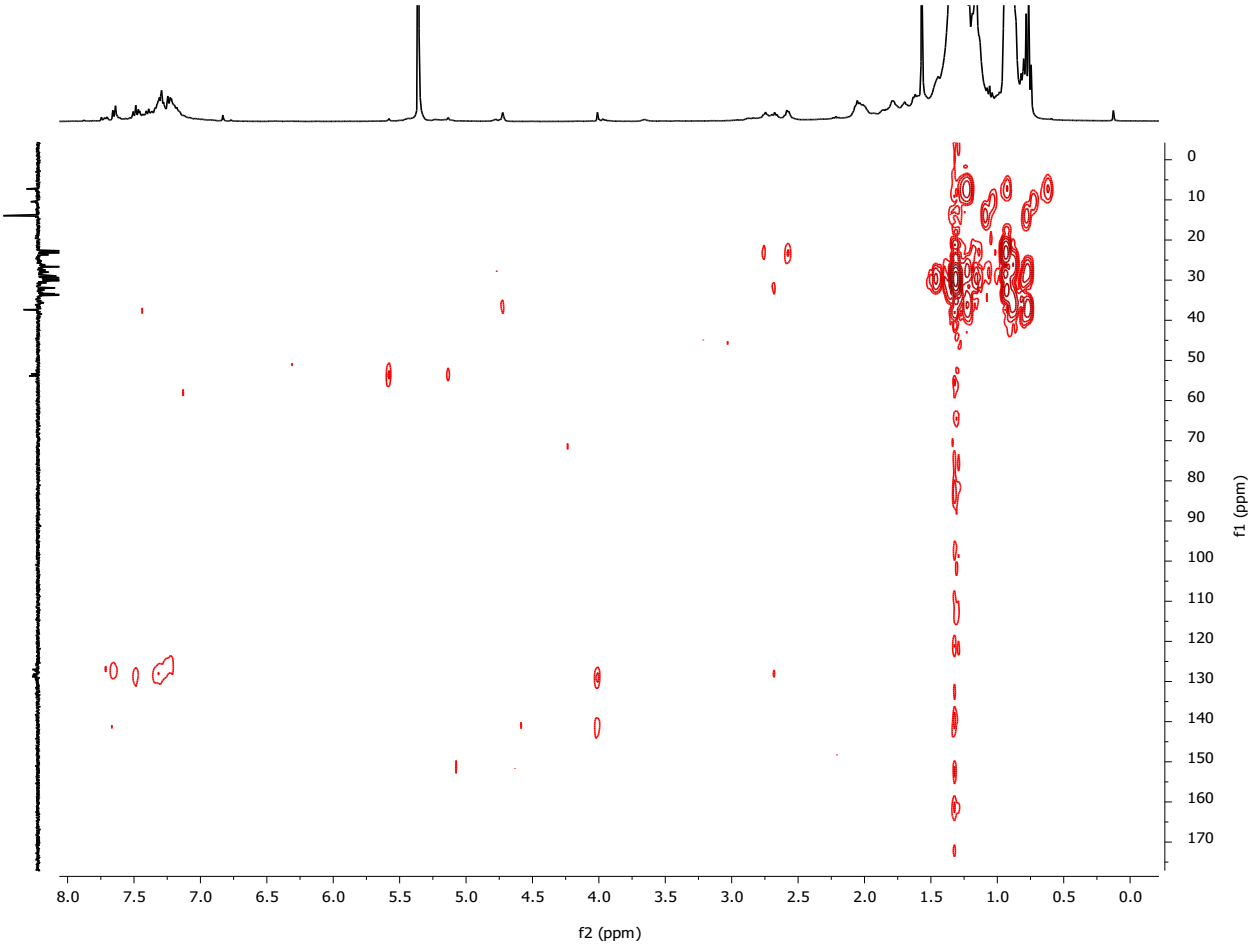

Figure S46. ^{1}H-^{13}C HMBC spectrum of the oil isolated after reaction of HDPE and $AlPh_3$ in the presence of $Zr(CH_2CMe_3)_2$@$SiAlO_x$ at 200 °C for 12 h, quenched with O_2, and extracted with methylene chloride. The spectrum was acquired at room temperature in methylene chloride-d_2. Cross-peaks at ^{13}C 130-140 ppm correlate with ^{1}H NMR signals at 4.1 ppm assigned to CH_2OH, and ^{1}H NMR signals at 7.5 ppm assigned to aromatic protons correlate with ^{13}C signals at 40 ppm assigned to methines. These observations indicate that -Ph(CH)-CH_2-OH species are formed, which would arise from phenylalumination of in-situ generated olefins (e.g., by β-alkyl or hydrogen elimination), followed by quenching with O_2. Note that the MALDI-TOF-MS shown below indicates aromatic-containing alkylalcohols are also formed during deconstruction. The data corresponds to the experiment reported in Table 1, Entry 9.

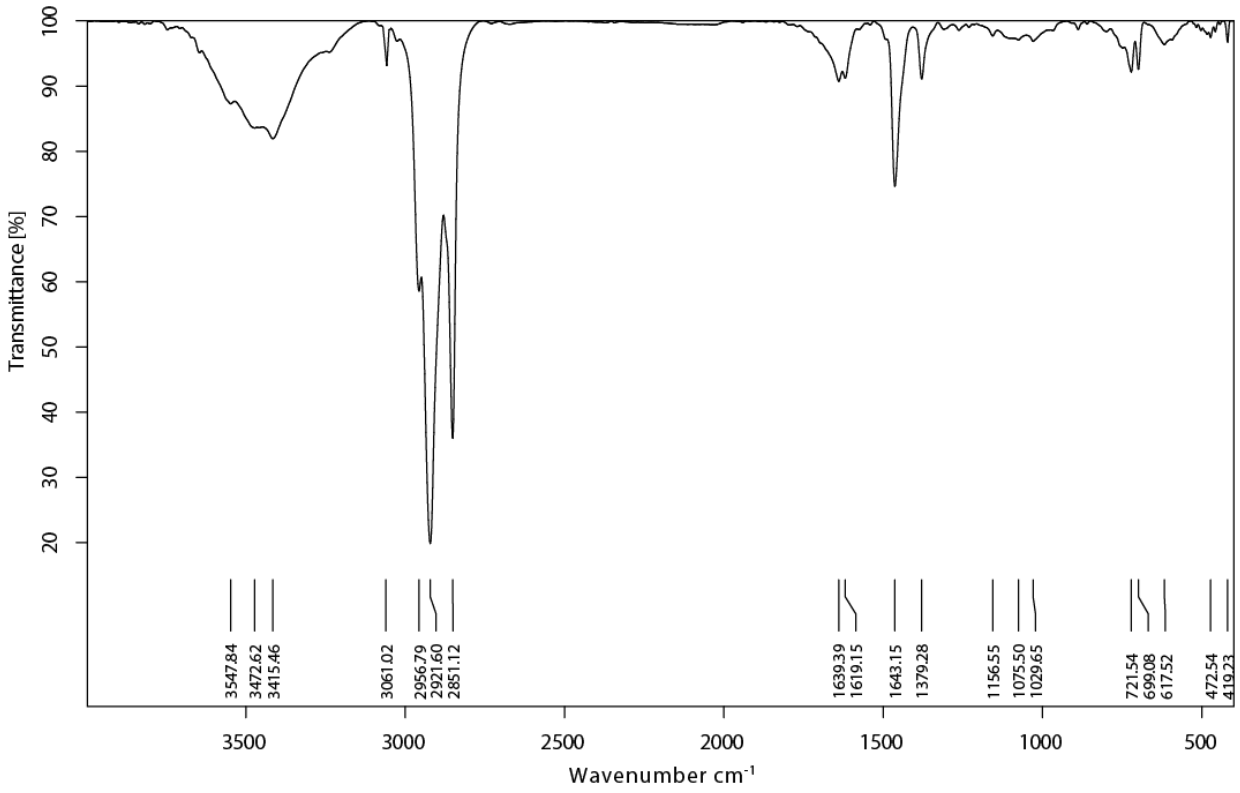

Figure S47. FT-IR spectrum (KBr) of the oil isolated after reaction of HDPE and $AlPh_3$ in the presence of $Zr(CH_2CMe_3)_2$@$SiAlO_x$ at 200 °C for 12 h, quenched with O_2, and extracted with methylene chloride. Broad signals between 3100-3700 cm^{-1} correspond to an O-H stretching modes. Signals at 3061 cm^{-1} and 1619-1639 cm^{-1} correspond to C-H and C=C stretching modes of aromatic groups. The data corresponds to the experiment reported in Table 1, Entry 9.

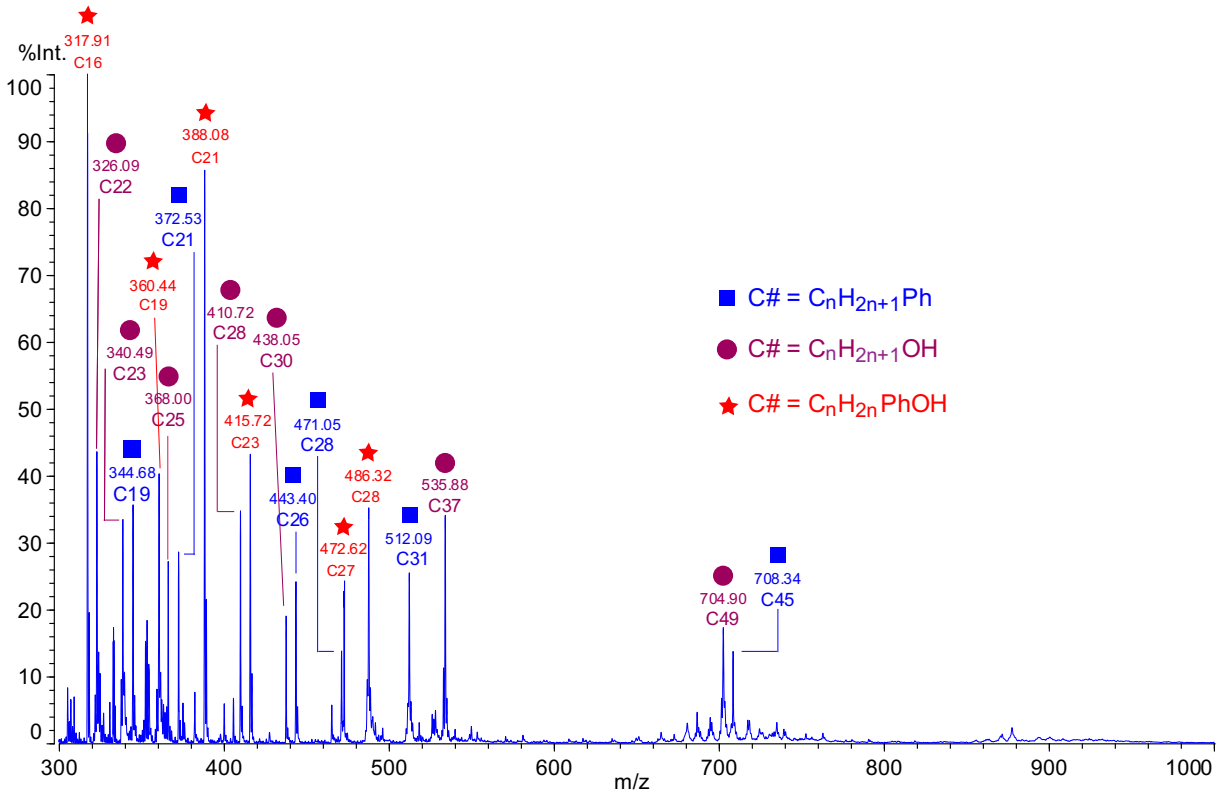

Figure S48. MALDI-TOF-MS spectrum of oil isolated after reaction of HDPE and $AlPh_3$ in the presence of $Zr(CH_2CMe_3)_2$@$SiAlO_x$ at 200 °C for 12 h, quenched with O_2, and extracted with methylene chloride. The spectrum was acquired in linear, positive mode with DHB (matrix). Three distinct types of species were identified, namely (1) alkyl benzenes (blue), (2) fatty alcohols (pink) and (3) fatty alcohols containing a single phenyl group as a result of phenylalumination (red). The data corresponds to the experiment reported in Table 1, Entry 9.

10. HDPE + $Zr(CH_2CMe_3)_2$@$SiAlO_x$ + AlH_3 (200 °C).

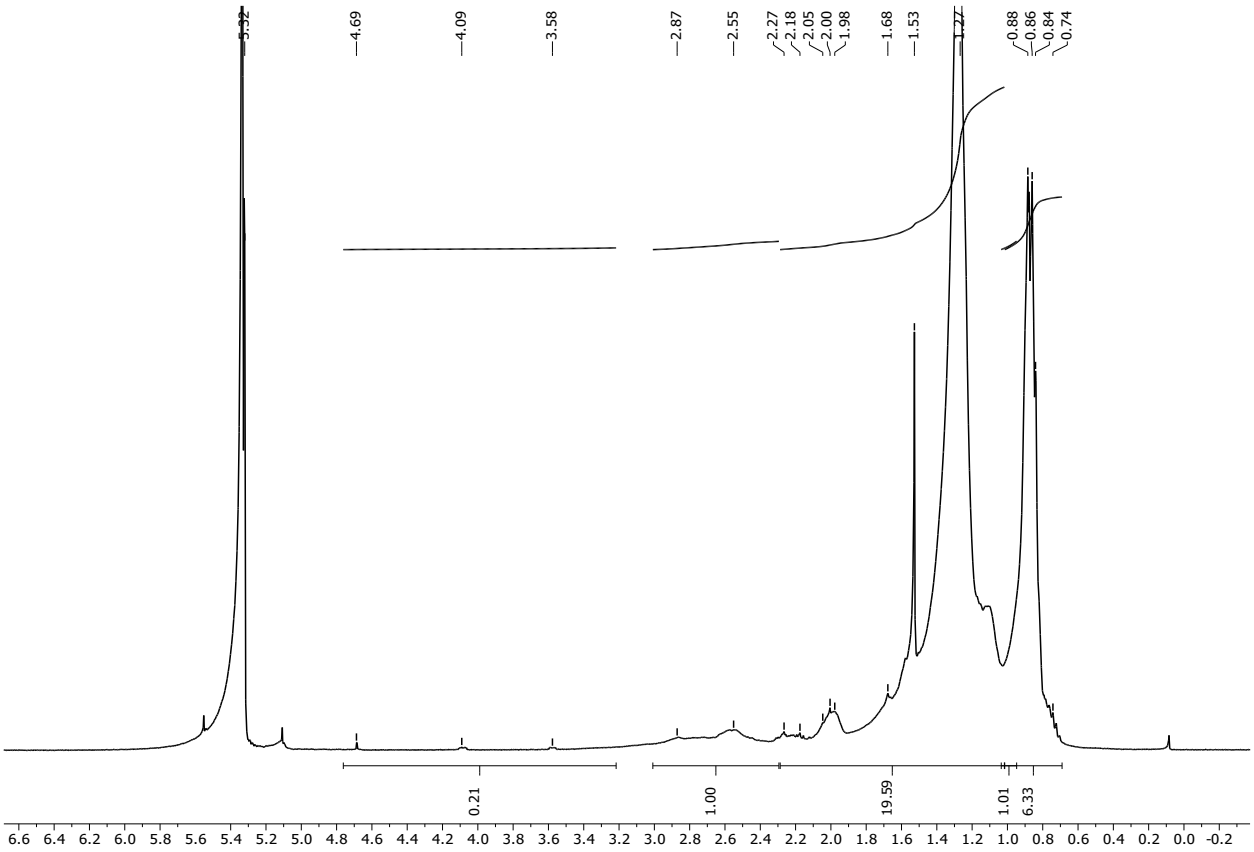

Figure S49. ^1H NMR spectrum of the oil isolated after reaction of HDPE and AlH_3 in the presence of $Zr(CH_2CMe_3)_2$@$SiAlO_x$ at 200 °C for 12 h, quenched with O_2, and extracted with methylene chloride. The spectrum was acquired at room temperature in methylene chloride-d_2 and assigned based on COSY and HSQC experiments in Figures S50 and S51. Signals at 0.7-1.0 ppm are assigned to methyls, those at 1.0-2.3 ppm correspond to methylene, and those at 2.3-3.0 ppm are attributed to methine groups. Peaks at 3.6-4.8 ppm are assigned to -CH_2-OH groups. The data corresponds to the experiment reported in Table 1, Entry 10.

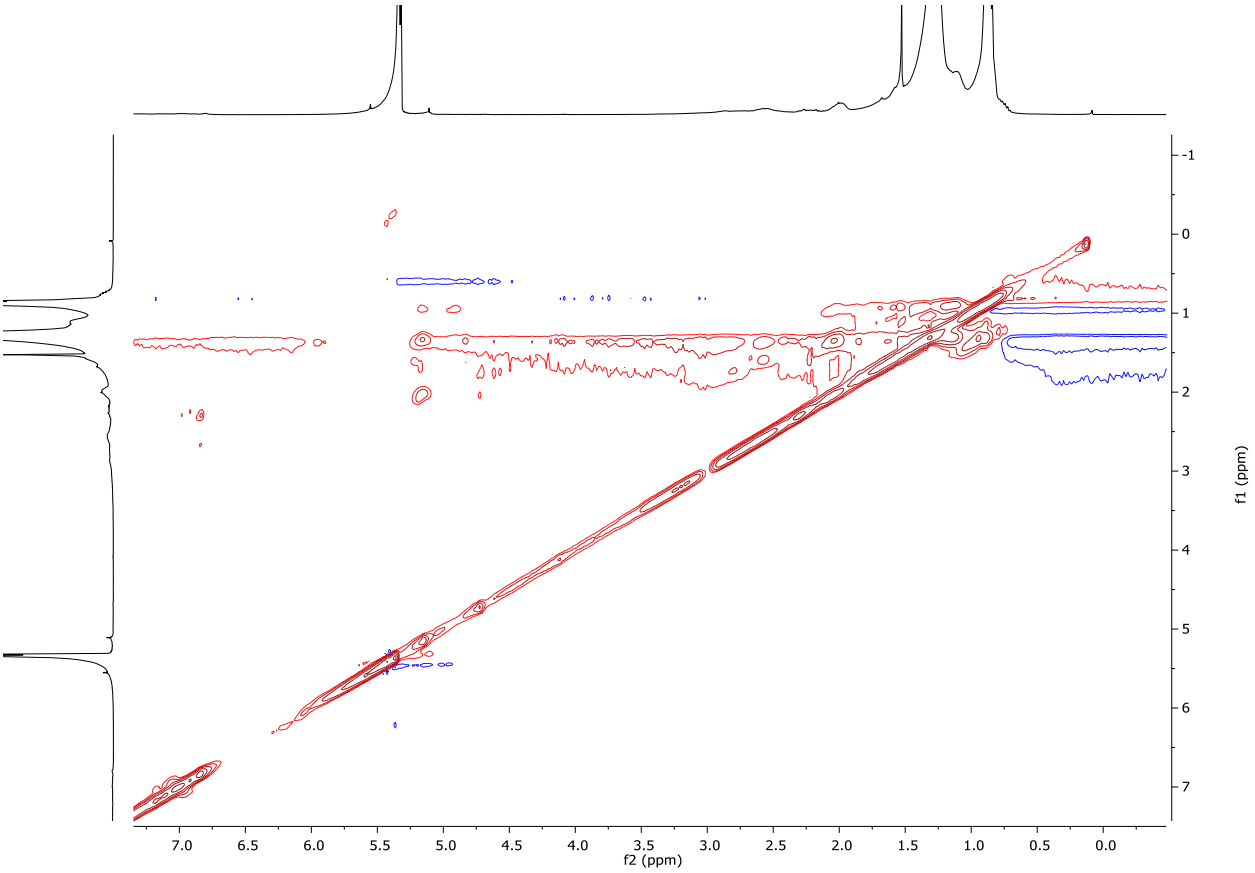

Figure S50. TOCSY spectrum of the oil isolated after reaction of HDPE and AlH_3 in the presence of $Zr(CH_2CMe_3)_2$@$SiAlO_x$ at 200 °C for 12 h, quenched with O_2, and extracted with methylene chloride. The spectrum was acquired at room temperature in methylene chloride-d_2. Cross-peaks at 4.5-4.7 ppm correlate with methylene signals at 1.6 ppm, indicative of -CH_2CH_2-OH species. The data corresponds to the experiment reported in Table 1, Entry 10.

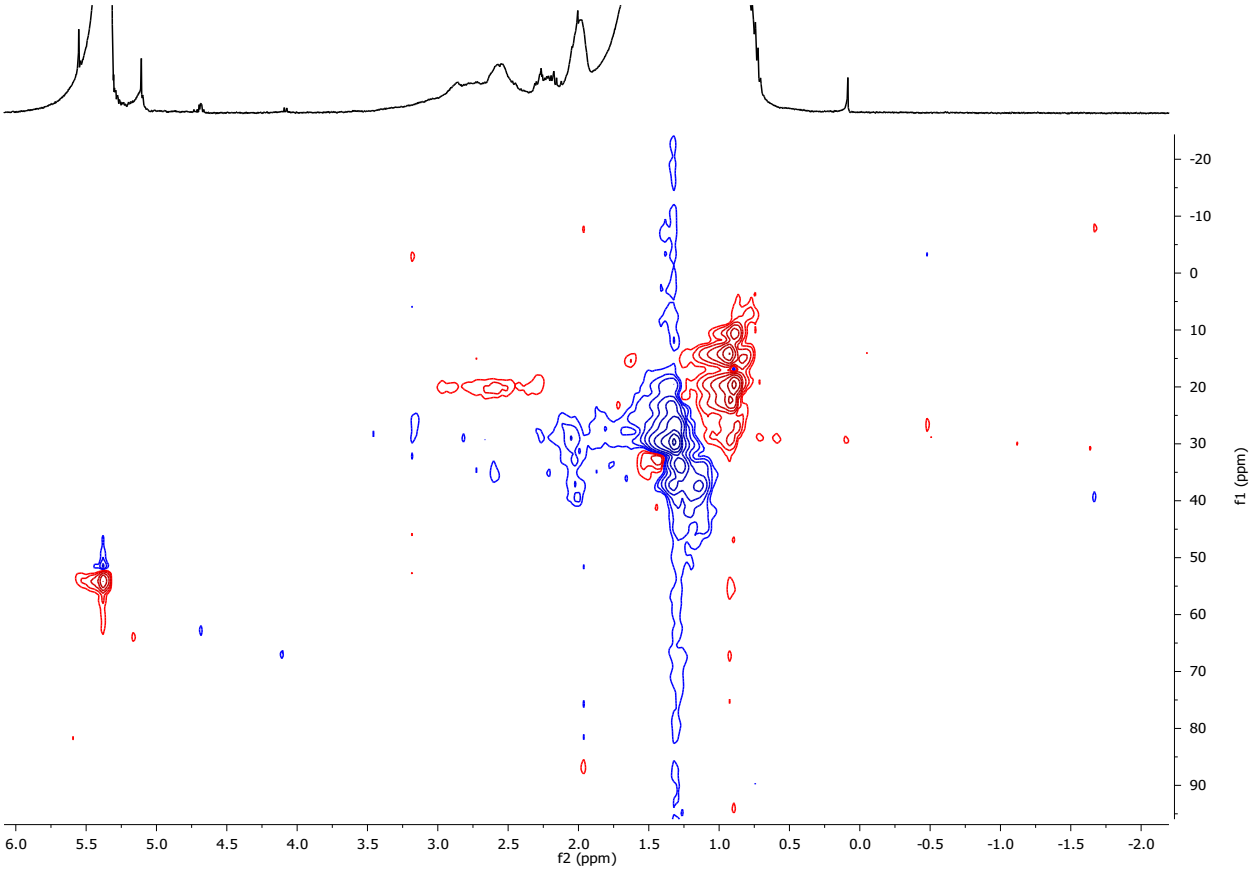

Figure S51. Phase sensitive ^{1}H-^{13}C HSQC spectrum of the oil isolated after reaction of HDPE and AlH_3 in the presence of $Zr(CH_2CMe_3)_2$@$SiAlO_x$ at 200 °C for 12 h, quenched with O_2, and extracted with methylene chloride. The spectrum was acquired at room temperature in methylene chloride-d_2. Cross-peaks at ^{13}C 60-70 ppm have the same phase (blue) as methylene peaks at 30 ppm, revealing the former are -CH_2-OH moieties (primary alcohols). The data corresponds to the experiment reported in Table 1, Entry 10.

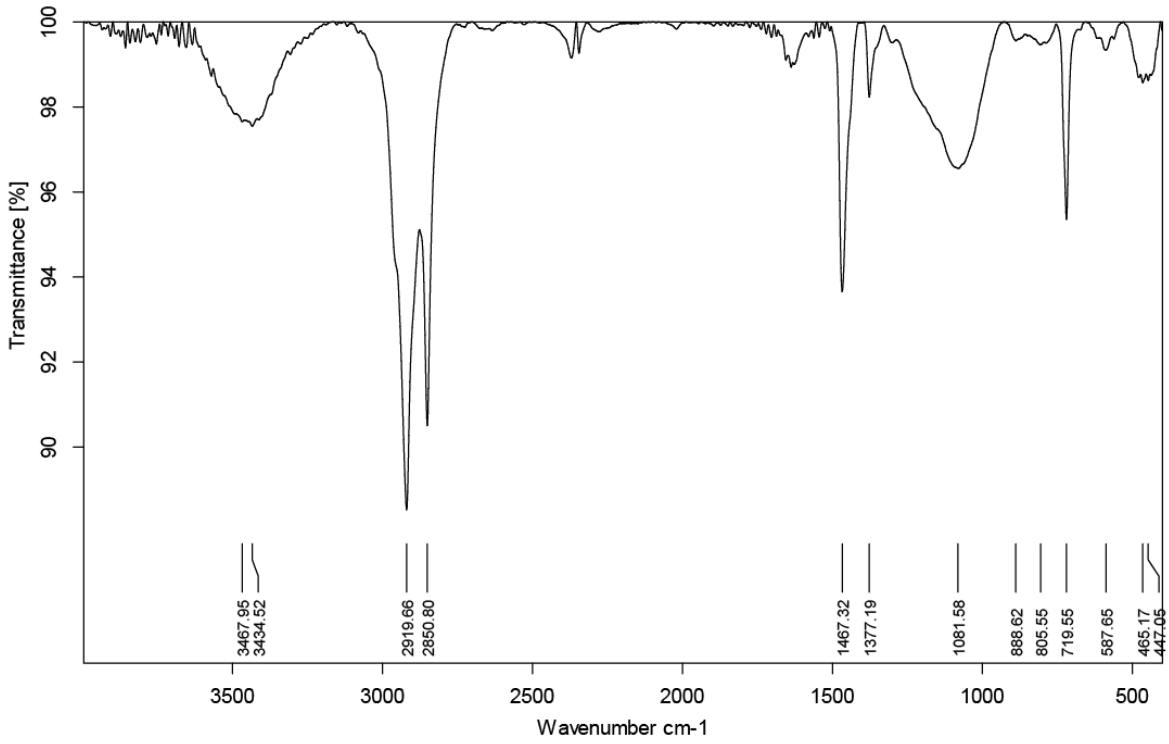

Figure S52. FT-IR spectrum (KBr) of oil isolated after reaction of HDPE and AlH_3 in the presence of $Zr(CH_2CMe_3)_2$@$SiAlO_x$ at 200 °C for 12 h, quenched with O_2, and extracted with methylene chloride. The broad signal at 3435 cm^{-1} corresponds to an O-H stretch. The data corresponds to the experiment reported in Table 1, Entry 10.

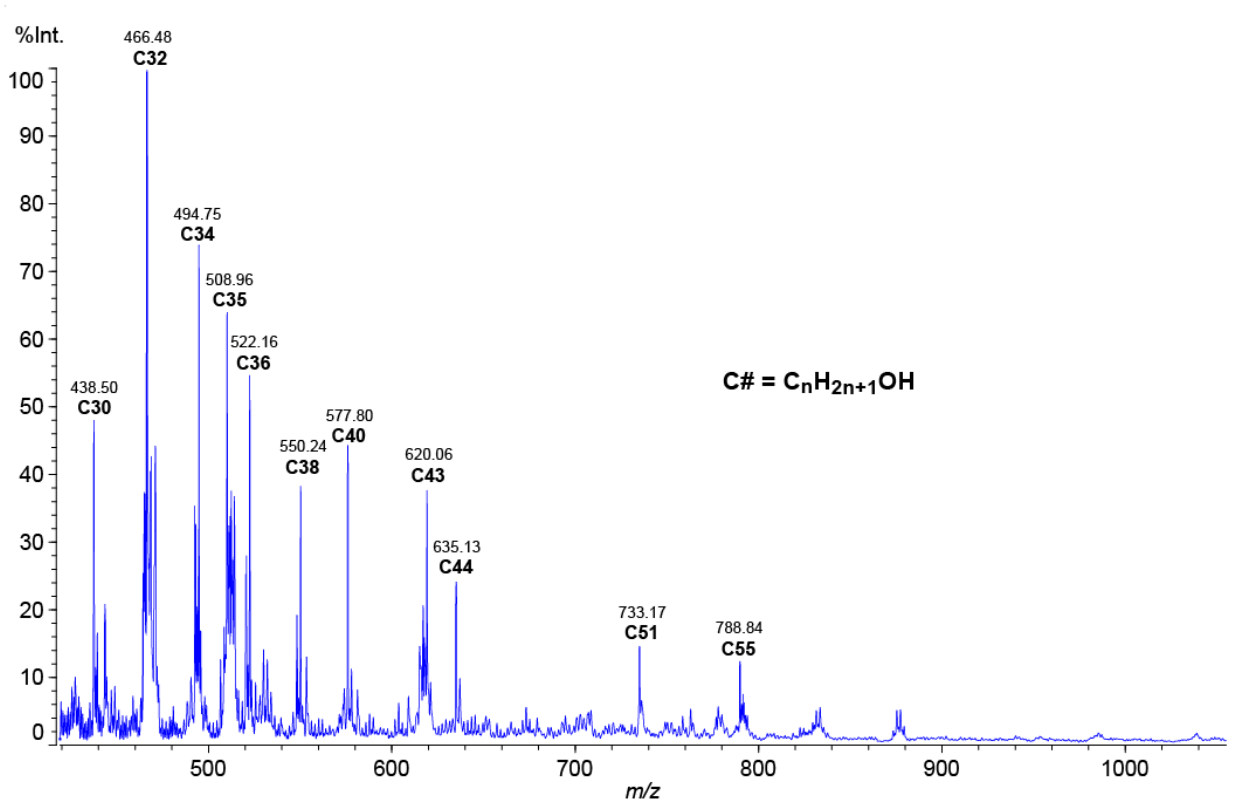

Figure S53. MALDI-TOF-MS spectrum of oil isolated after reaction of HDPE and AlH_3 in the presence of $Zr(CH_2CMe_3)_2$@$SiAlO_x$ at 200 °C for 12 h, quenched with O_2, and extracted with methylene chloride. The spectrum was acquired in linear, positive mode with $AgNO_3$ (salt) and DHB (matrix). The data corresponds to the experiment reported in Table 1, Entry 10.

11. Post-consumer HDPE plastic grocery bag + $Zr(CH_2CMe_3)_2$@$SiAlO_x$ + Al*i*Bu_3 (200 °C).

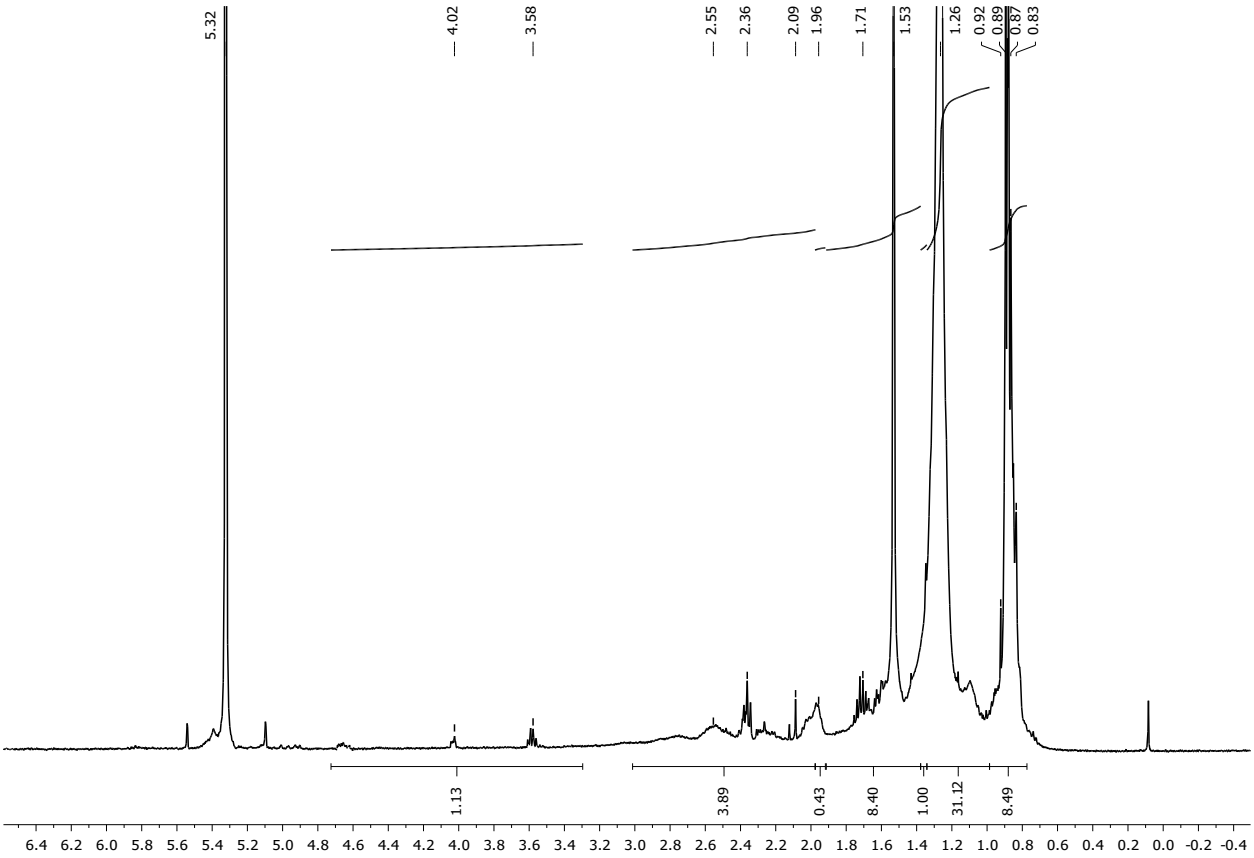

Figure S54. ^{1}H NMR spectrum of the oil isolated after reaction of a post-consumer HDPE plastic grocery bag and Al*i*Bu_3 in the presence of $Zr(CH_2CMe_3)_2$@$SiAlO_x$ at 200 °C for 12 h, quenched with O_2, and extracted with methylene chloride. The spectrum was acquired at room temperature in methylene chloride-d_2 and assigned based on TOCSY and HSQC experiments in Figures S55 and S56. Signals at 0.7-1.0 ppm correspond to methyl groups, peaks at 1.0-1.3, 1.4-1.9, and 2.0-3.0 ppm are assigned to methylene groups, and those at 1.3-1.4 and 1.9-2.0 ppm correspond to methine groups. Peaks at 3.5-4.8 ppm are assigned to -CH_2-OH groups. The data corresponds to the experiment reported in Table 1, Entry 11.

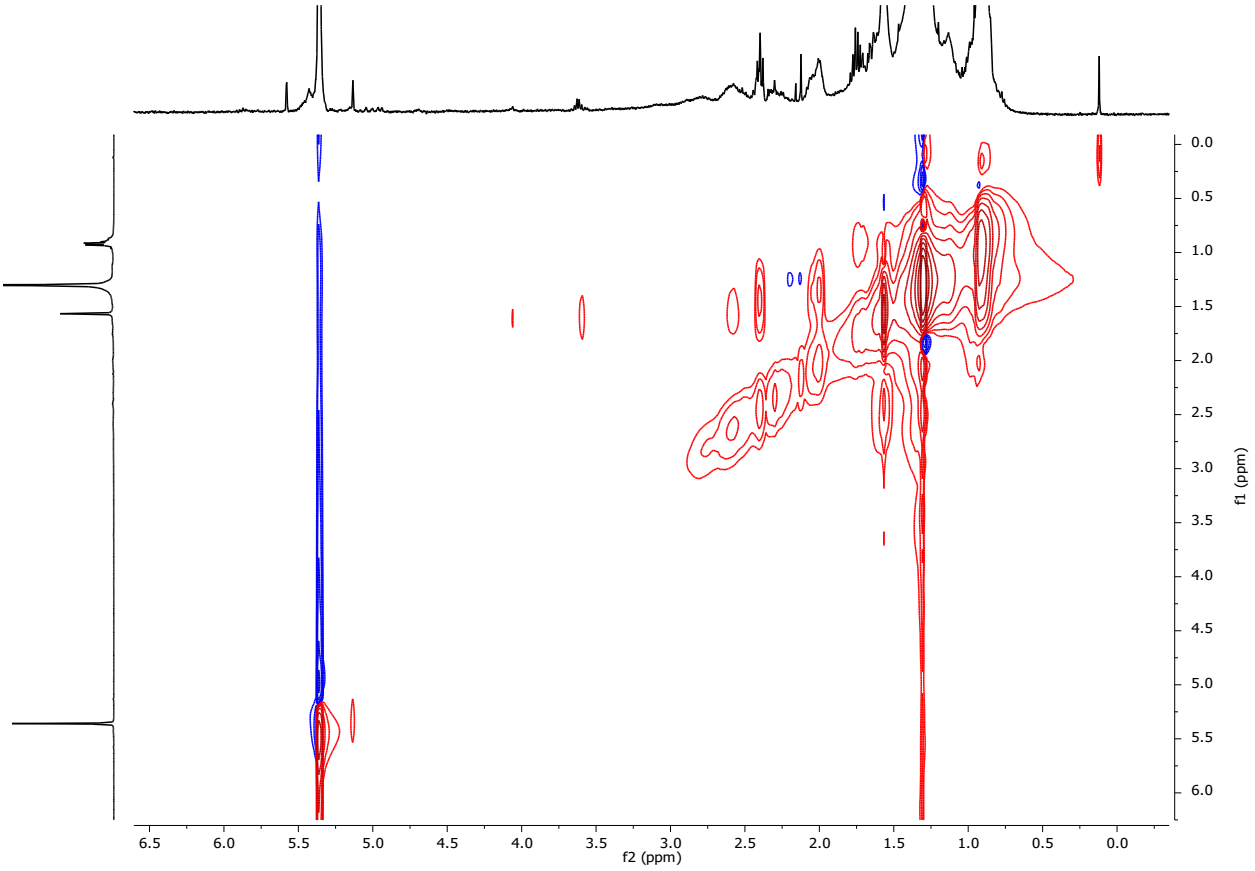

Figure S55. TOCSY spectrum of the oil isolated after reaction of a post-consumer HDPE plastic grocery bag and Al*i*Bu$_3$ in the presence of Zr(CH$_2$CMe$_3$)$_2$@SiAlO$_x$ at 200 °C for 12 h, quenched with O$_2$, and extracted with methylene chloride. The spectrum was acquired at room temperature in methylene chloride-*d*$_2$. Cross-peaks at 3.6-4.0 ppm correlate with methylene signals at 1.6 ppm, which is indicative of -CH$_2$-CH$_2$-OH species. The data corresponds to the experiment reported in Table 1, Entry 11.

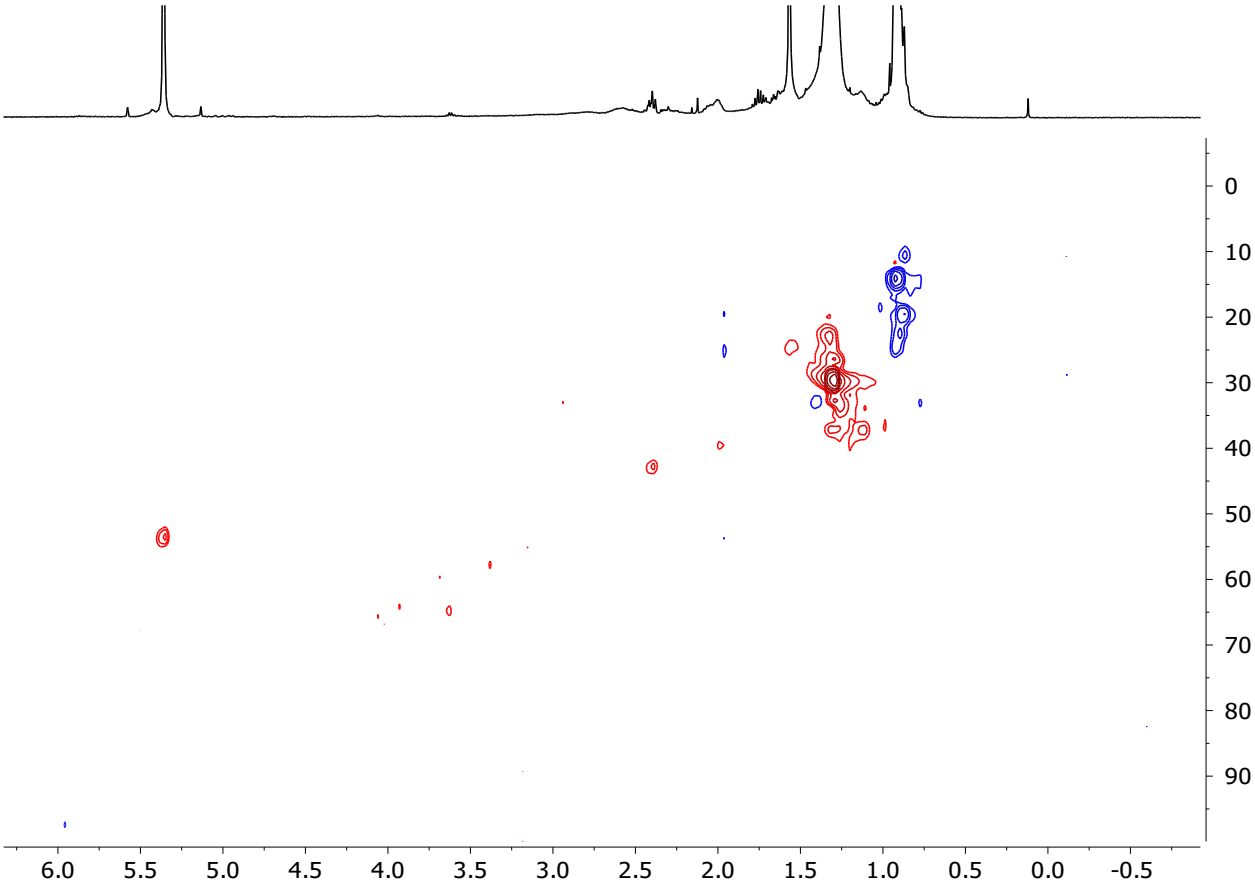

Figure S56. Phase sensitive ^{1}H-^{13}C HSQC spectrum of the oil isolated after reaction of a post-consumer HDPE plastic grocery bag and Al*i*Bu$_3$ in the presence of Zr(CH$_2$CMe$_3$)$_2$@SiAlO$_x$ at 200 °C for 12 h, quenched with O_2, and extracted with methylene chloride. The spectrum was acquired at room temperature in methylene chloride-d_2. Cross-peaks at ^{13}C 55-70 ppm have the same phase (red) as methylene peaks at 30 ppm, revealing the former are -*CH$_2$*-OH moieties. The data corresponds to the experiment reported in Table 1, Entry 11.

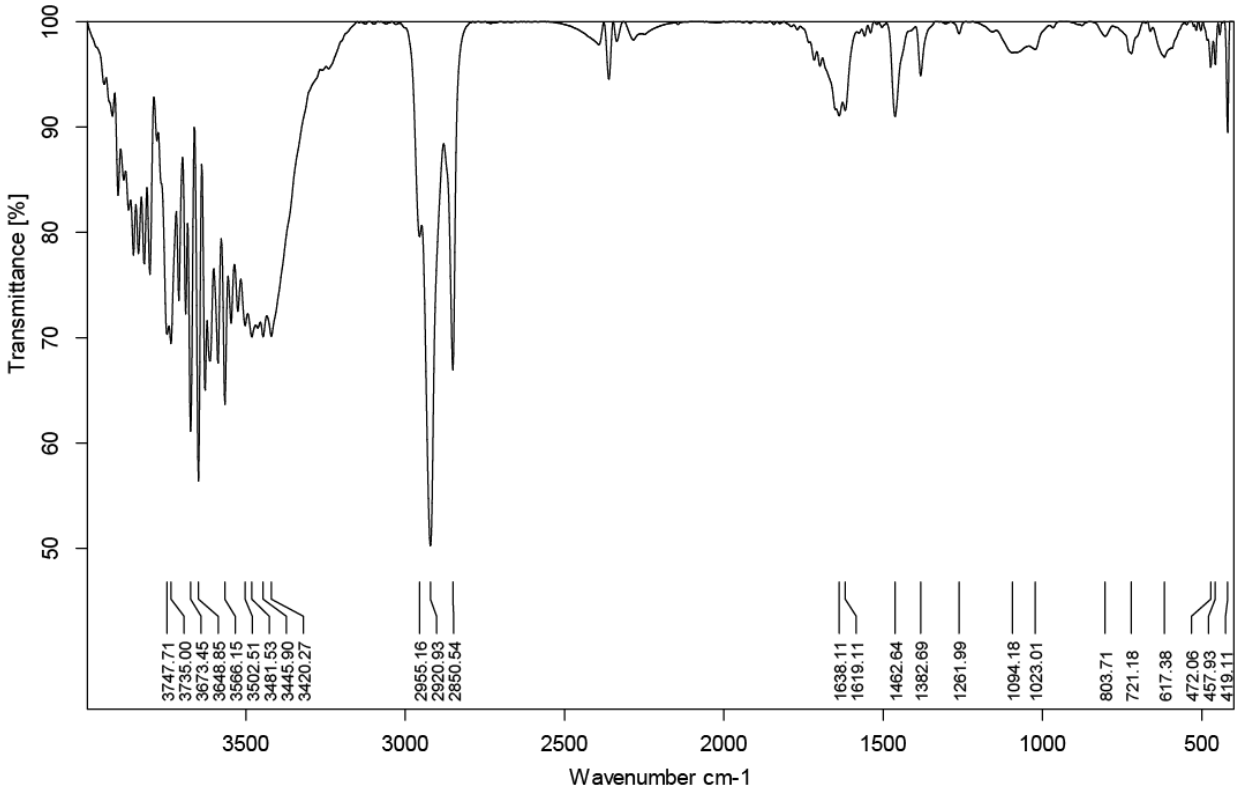

Figure S57. FT-IR spectrum (KBr) of the oil isolated after reaction of a post-consumer HDPE plastic grocery bag and Al*i*Bu$_3$ in the presence of Zr(CH$_2$CMe$_3$)$_2$@SiAlO$_x$ at 200 °C for 12 h, quenched with O$_2$, and extracted with methylene chloride. Broad signals between 3200-3600 cm^{-1} correspond to O-H stretches. The data corresponds to the experiment reported in Table 1, Entry 11.

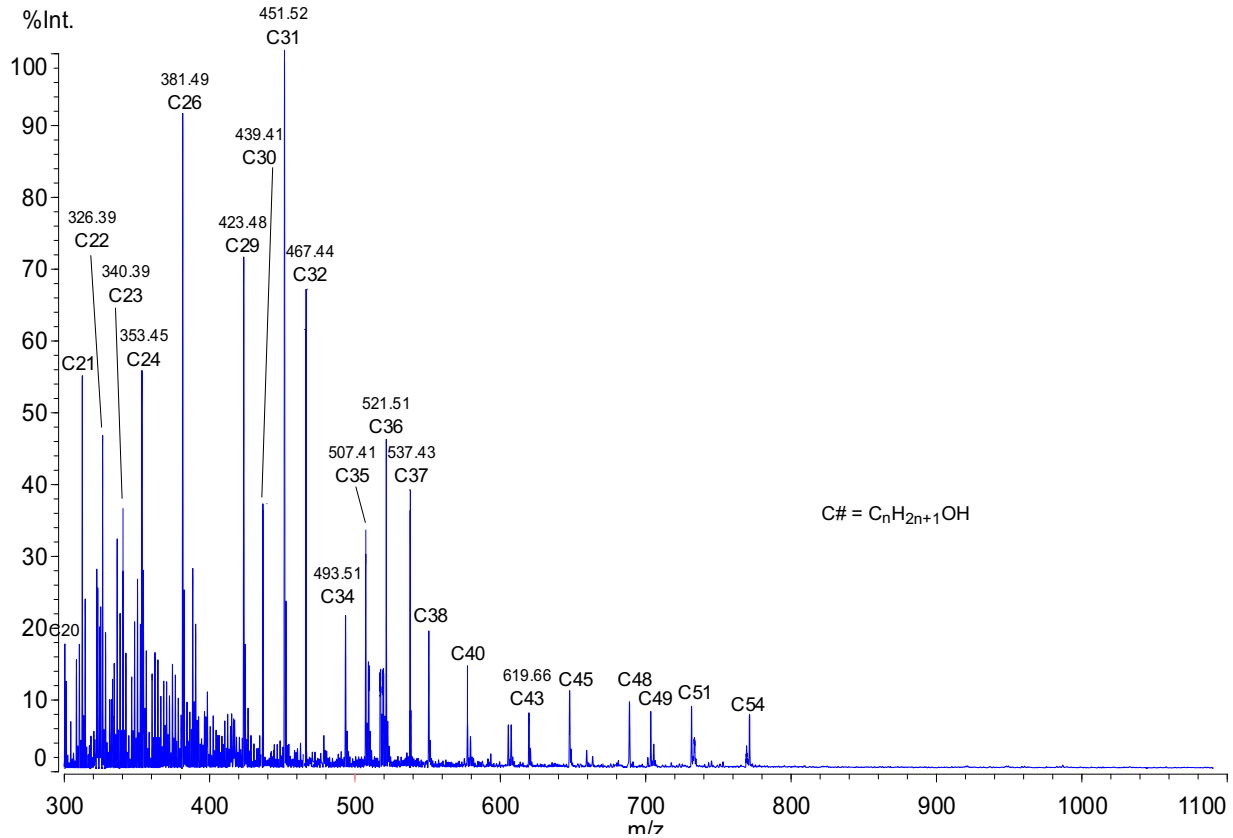

Figure S58. MALDI-TOF-MS spectrum of the oil isolated after reaction of a post-consumer HDPE plastic grocery bag and Al*i*Bu$_3$ in the presence of Zr(CH$_2$CMe$_3$)$_2$@SiAlO$_x$ at 200 °C for 12 h, quenched with O$_2$, and extracted with methylene chloride. The spectrum was acquired in linear, positive mode with AgNO$_3$ (salt) and DHB (matrix). The data corresponds to the experiment reported in Table 1, Entry 11.

12. *i*PP + $Zr(CH_2CMe_3)_2$@$SiAlO_x$ + Al*i*Bu_3 (200 °C).

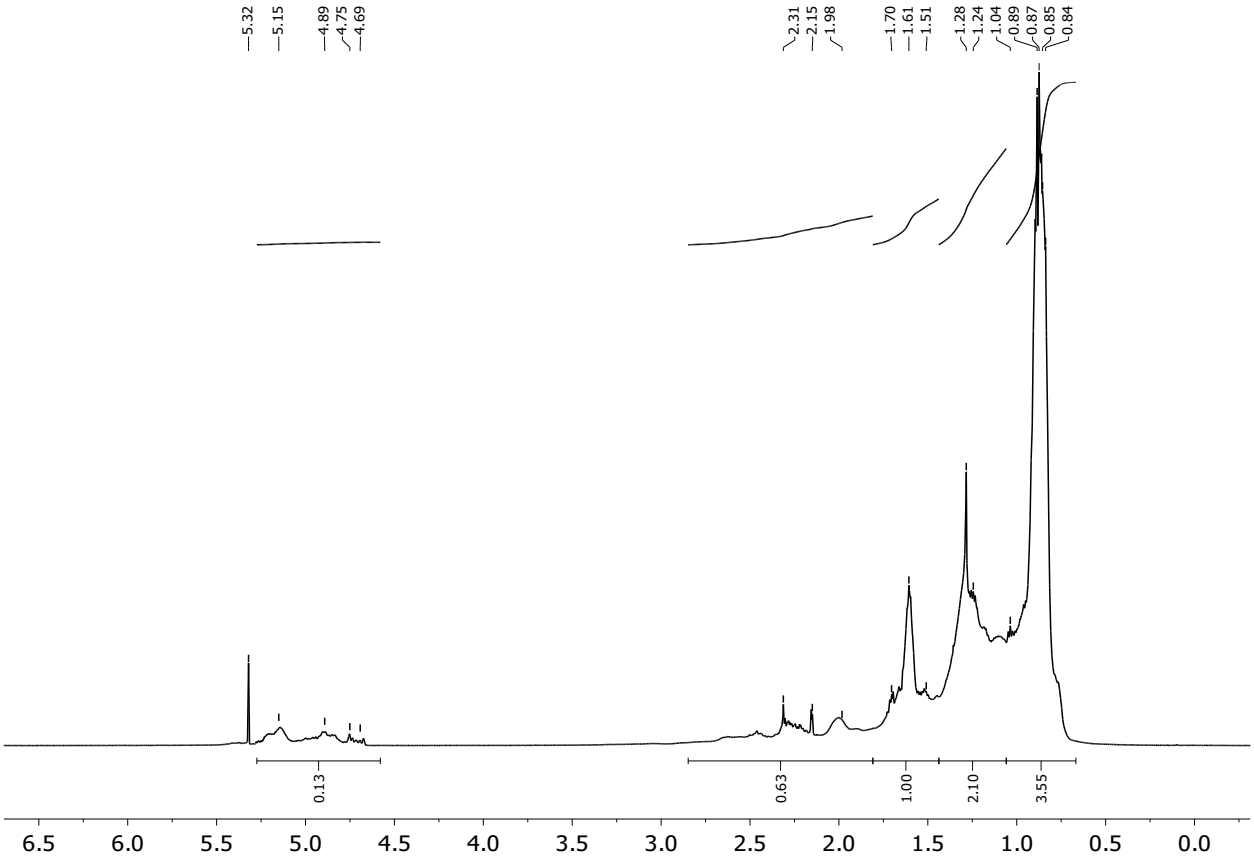

Figure S59. ^{1}H NMR spectrum of the oil isolated after reaction of isotactic polypropylene and Al*i*Bu_3 in the presence of $Zr(CH_2CMe_3)_2$@$SiAlO_x$ at 200 °C for 12 h, quenched with O_2, and extracted with methylene chloride. The spectrum was acquired at room temperature in methylene chloride-d_2 and assigned based on COSY and HSQC experiments in Figures S60 and S61. Signals at 0.7-1.0 ppm are assigned to methyl groups, peaks at 1.0-1.5 ppm correspond to methylene groups, and those at 1.5-3.0 ppm are attributed to methine groups. Peaks at 4.6-5.2 ppm are assigned to -CH_2-OH groups. The data corresponds to the experiment reported in Table 1, Entry 12.

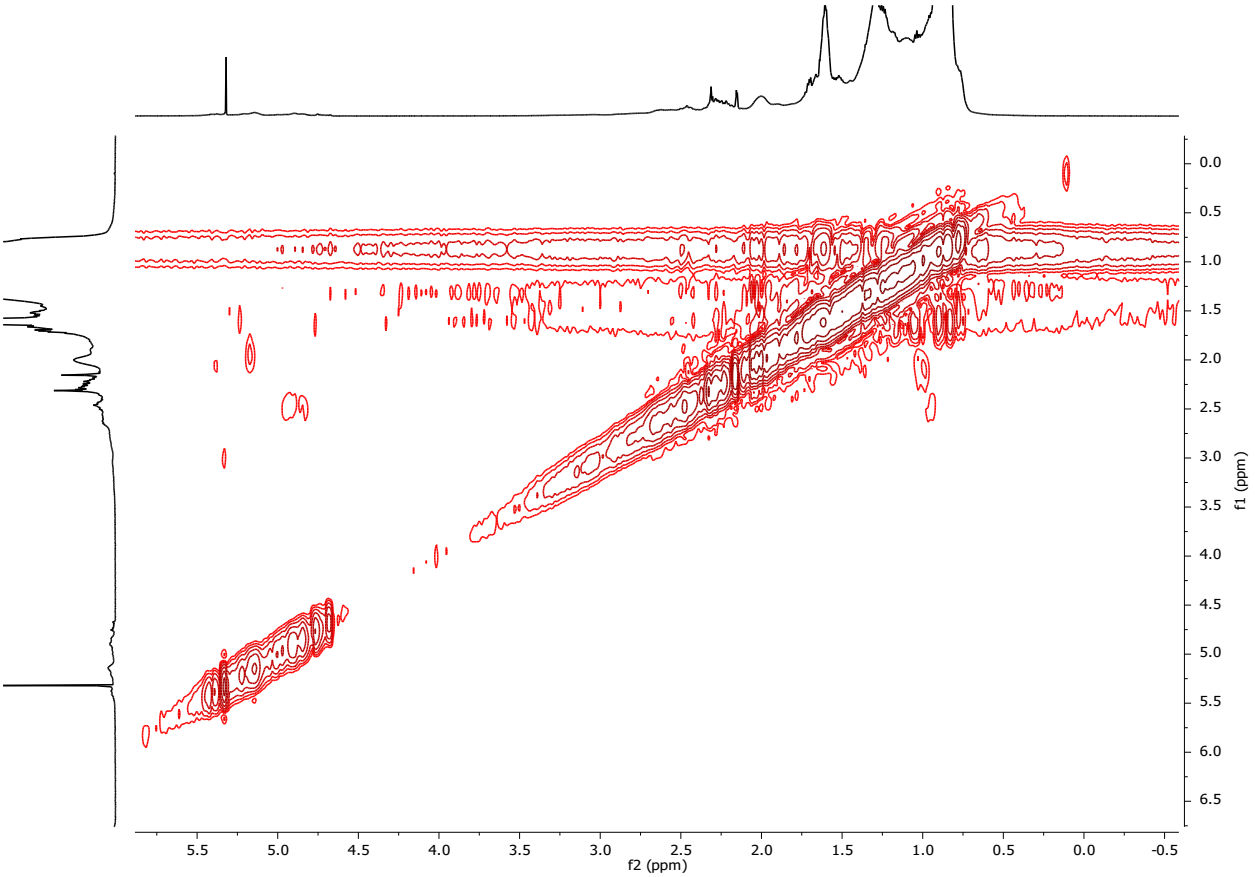

Figure S60. COSY spectrum of the oil isolated after reaction of polypropylene and Al*i*Bu$_3$ in the presence of Zr(CH$_2$CMe$_3$)$_2$@SiAlO$_x$ at 200 °C for 12 h, quenched with O$_2$, and extracted with methylene chloride. The spectrum was acquired at room temperature in methylene chloride-d_2. Cross-peaks at 4.7-5.2 ppm correlate with methine signals at 1.6-2.5 ppm, which is indicative of –(R)CH-CH$_2$-OH species. The data corresponds to the experiment reported in Table 1, Entry 12.

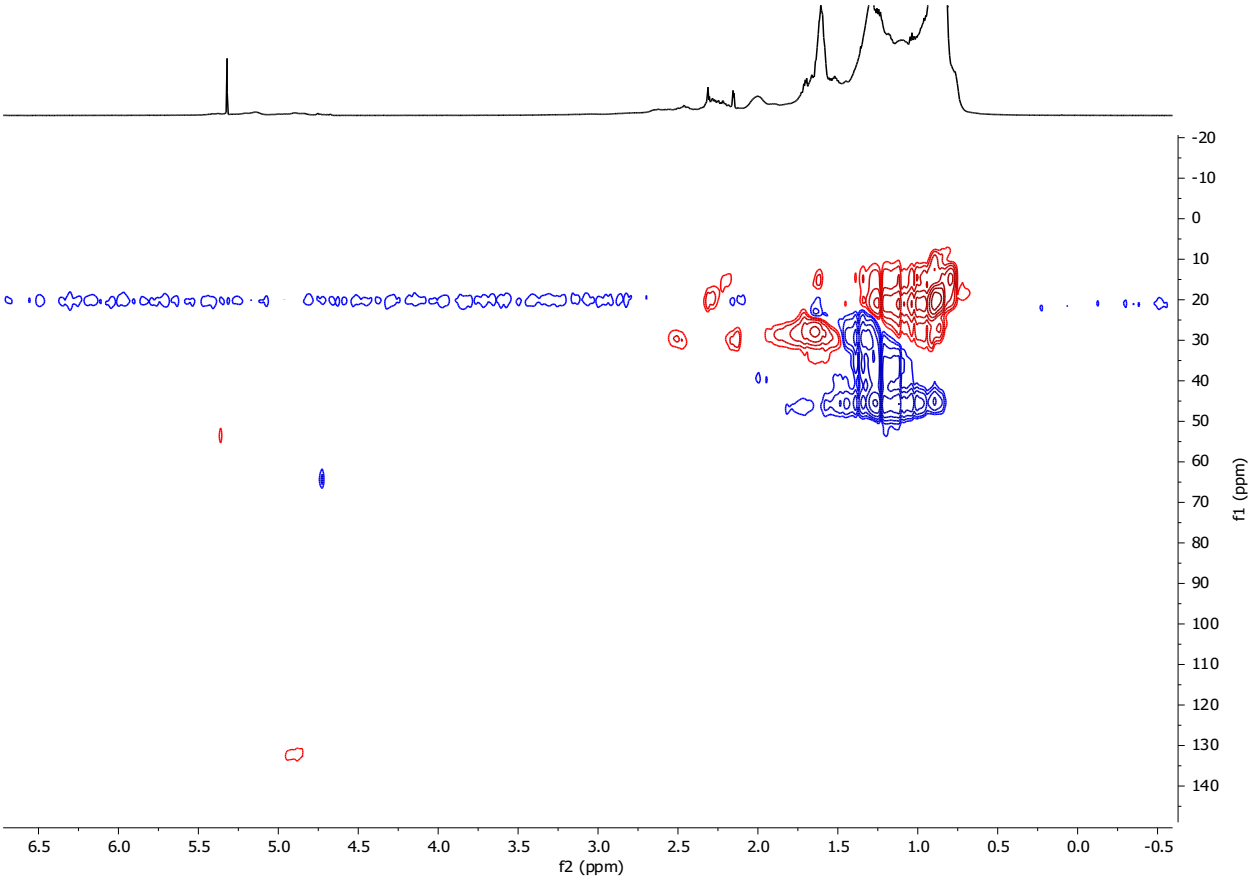

Figure S61. Phase sensitive ^{1}H-^{13}C HSQC spectrum of the oil isolated after reaction of polypropylene and Al*i*Bu$_3$ in the presence of Zr(CH$_2$CMe$_3$)$_2$@SiAlO$_x$ at 200 °C for 12 h, quenched with O_2, and extracted with methylene chloride. The spectrum was acquired at room temperature in methylene chloride-d_2. Cross-peaks at ^{13}C 60-70 ppm have the same phase (blue) as methylene peaks at 30 ppm, revealing the former are -*C*H$_2$-OH moieties. The data corresponds to the experiment reported in Table 1, Entry 12.

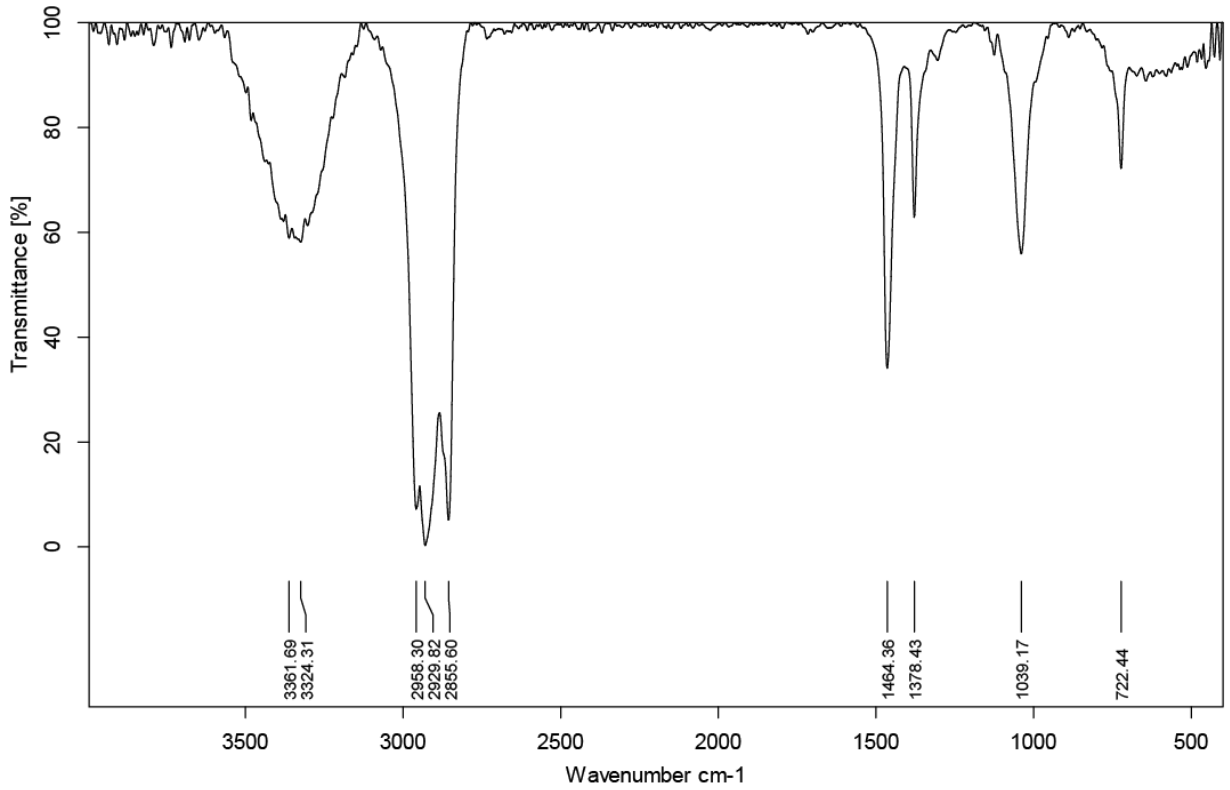

Figure S62. FT-IR spectrum (KBr) of the oil isolated after reaction of polypropylene and Al*i*Bu$_3$ in the presence of Zr(CH$_2$CMe$_3$)$_2$@SiAlO$_x$ at 200 °C for 12 h, quenched with O$_2$, and extracted with methylene chloride. Broad signals between 3200-3600 cm^{-1} correspond to O-H stretching modes. The data corresponds to the experiment reported in Table 1, Entry 12.

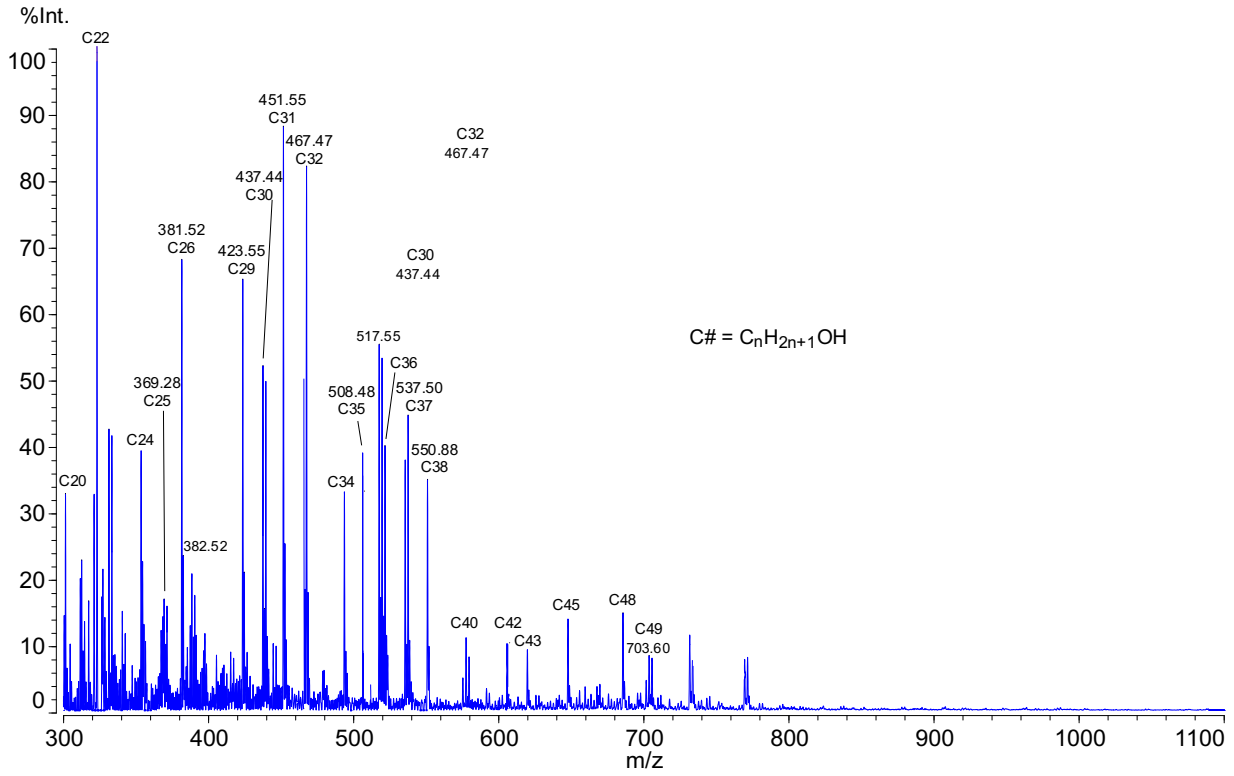

Figure S63. MALDI-TOF-MS spectrum of the oil isolated after reaction of polypropylene and Al*i*Bu$_3$ in the presence of Zr(CH$_2$CMe$_3$)$_2$@SiAlO$_x$ at 200 °C for 12 h, quenched with O$_2$, and extracted with methylene chloride. The spectrum was acquired in linear, positive mode with AgNO$_3$ (salt) and DHB (matrix). The data corresponds to the experiment reported in Table 1, Entry 12.

13. HDPE + $Zr(OCH_2CMe_3)_2$@$SiAlO_x$ + Al*i*Bu_3 (200 °C).

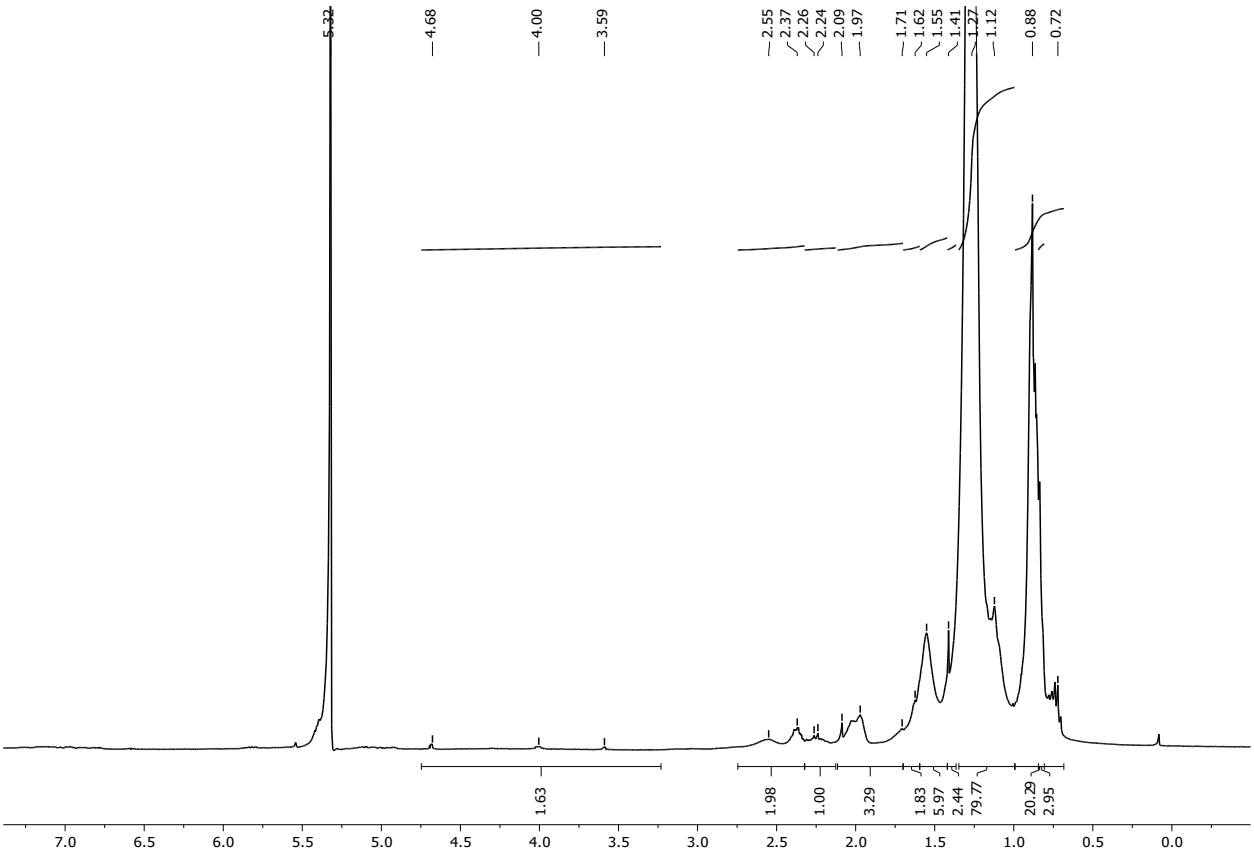

Figure S64. ^{1}H NMR spectrum of the oil isolated after reaction of HDPE and Al*i*Bu_3 in the presence of $Zr(OCH_2CMe_3)_2$@$SiAlO_x$ at 200 °C for 12 h, quenched with O_2, and extracted with methylene chloride. The spectrum was acquired at room temperature in methylene chloride-d_2 and assigned based on COSY and HSQC experiments in Figures S65 and S66. Signals at 0.7-1.0 ppm are assigned to methyls, the peaks at 1.0-1.3, 1.4-1.6, 1.7-2.1, and 2.3-2.7 ppm correspond to methylene groups, and those at 1.3-1.4, 1.6-1.7, and 2.1-2.3 ppm are attributed to methine groups. Peaks at 3.5-4.7 ppm are assigned to CH_2-OH groups. The data corresponds to the experiment reported in Table 1, Entry 13.

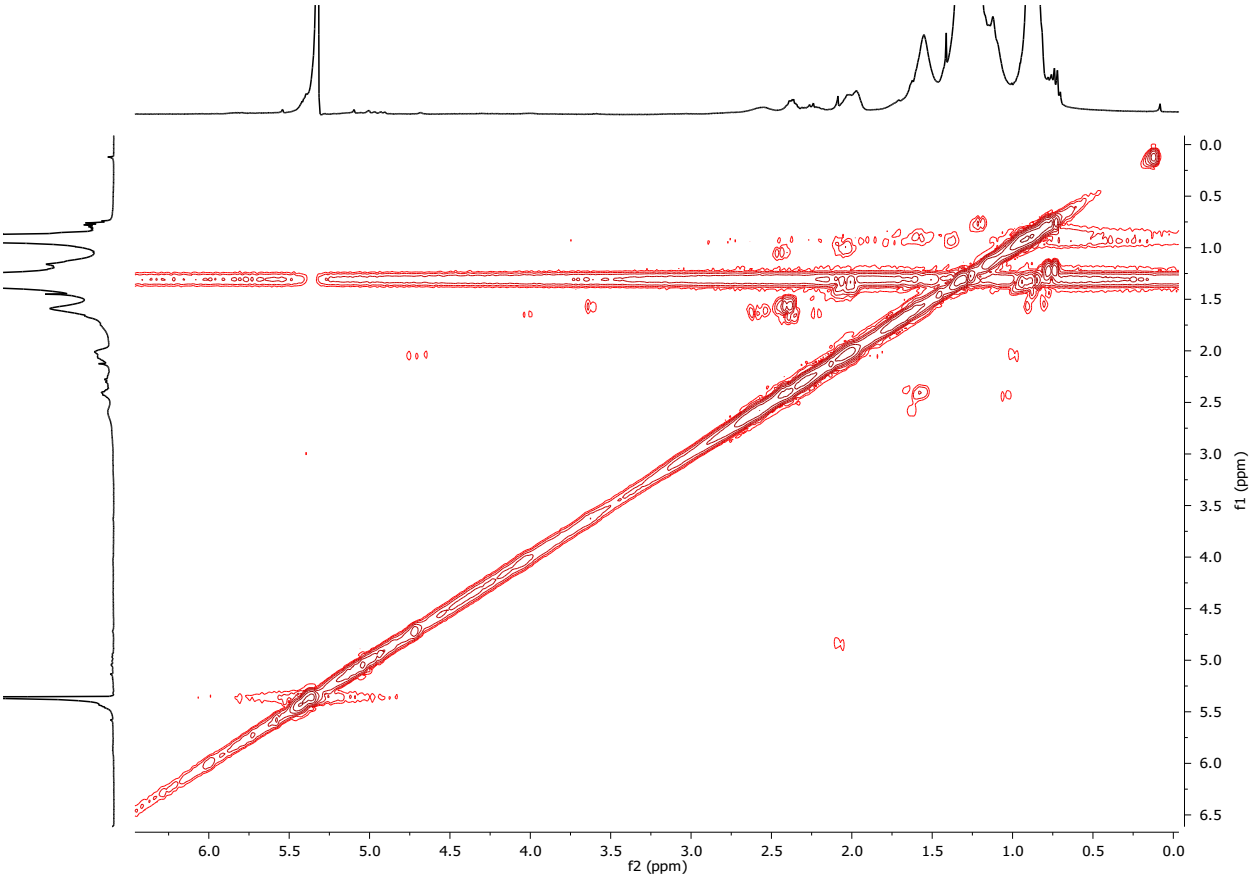

Figure S65. COSY spectrum of the oil isolated after reaction of HDPE and Al*i*Bu$_3$ in the presence of Zr(OCH$_2$CMe$_3$)$_2$@SiAlO$_x$ at 200 °C for 12 h, quenched with O$_2$, and extracted with methylene chloride. The spectrum was acquired at room temperature in methylene chloride-d_2. Cross-peaks at 3.6-4.8 ppm correlate with methylene signals at 1.5-2.0 ppm, which is indicative of CH$_2$-CH$_2$-OH moieties. The data corresponds to the experiment reported in Table 1, Entry 13.

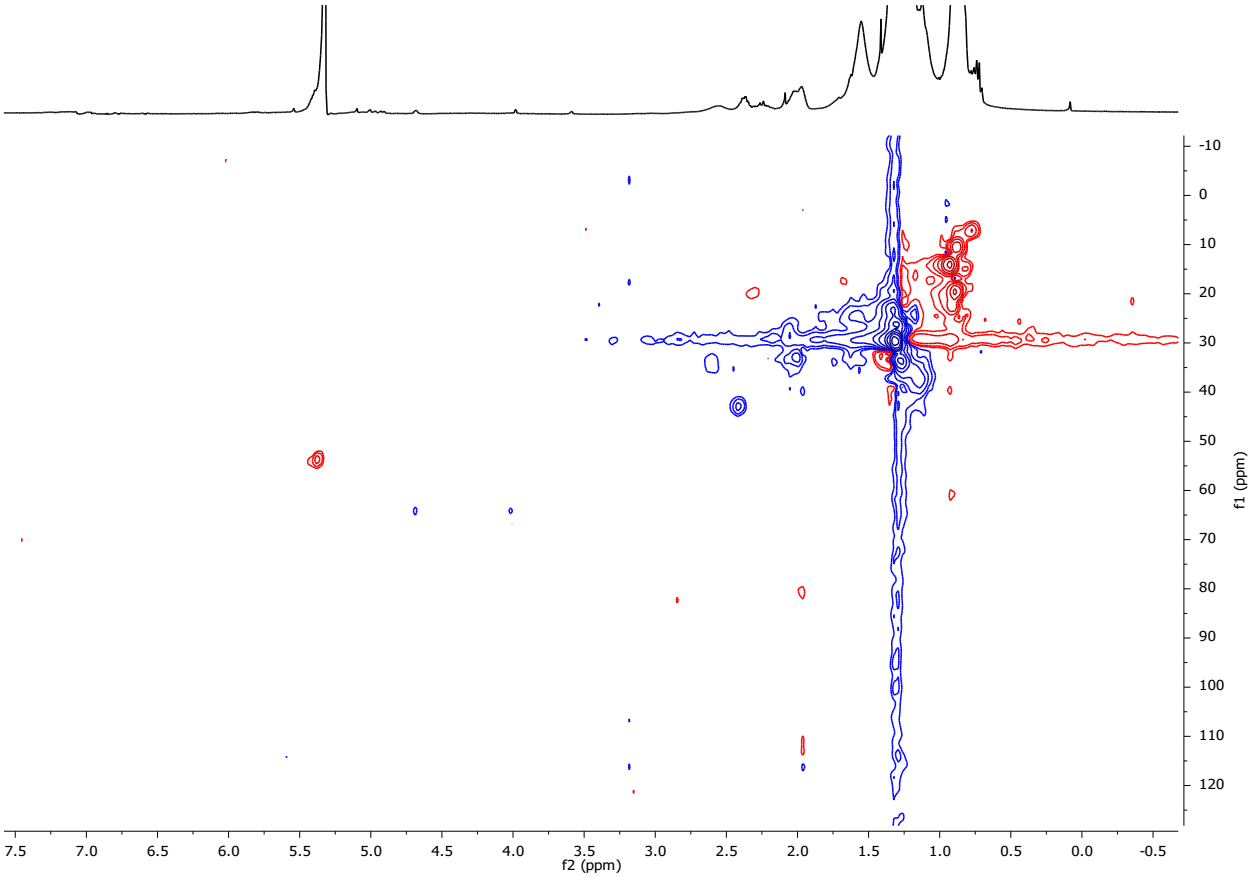

Figure S66. Phase sensitive ^{1}H-^{13}C HSQC spectrum of the oil isolated after reaction of HDPE and Al*i*Bu$_3$ in the presence of Zr(OCH$_2$CMe$_3$)$_2$@SiAlO$_x$ at 200 °C for 12 h, quenched with O_2, and extracted with methylene chloride. The spectrum was acquired at room temperature in methylene chloride-d_2. Cross-peaks at ^{13}C 60-70 ppm that have the same phase (blue) as methylene peaks at 30 ppm revealing the former are -*CH$_2$*-OH moieties. The data corresponds to the experiment reported in Table 1, Entry 13.

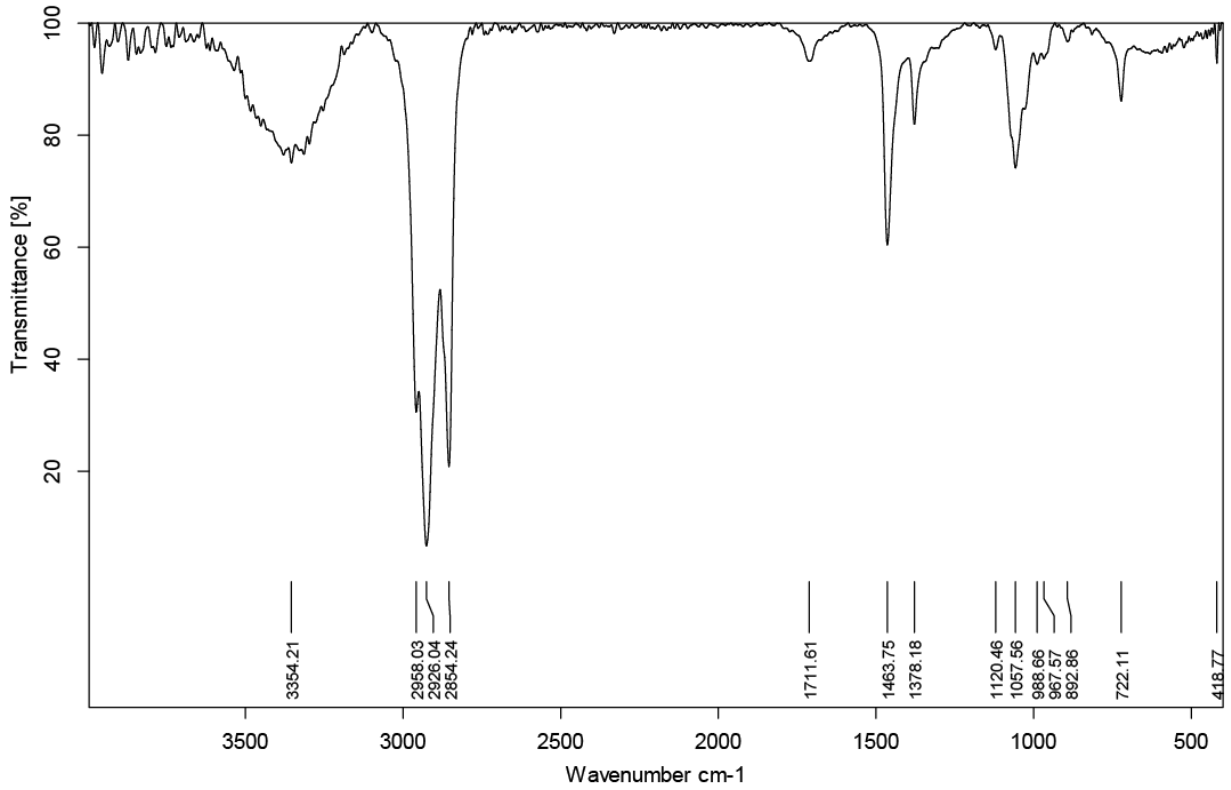

Figure S67. FT-IR spectrum (KBr) of the oil isolated after reaction of HDPE and Al*i*Bu$_3$ in the presence of Zr(OCH$_2$CMe$_3$)$_2$@SiAlO$_x$ at 200 °C for 12 h, quenched with O$_2$, and extracted with methylene chloride. The broad signal at 3354 cm^{-1} corresponds to an O-H stretch. The data corresponds to the experiment reported in Table 1, Entry 13.

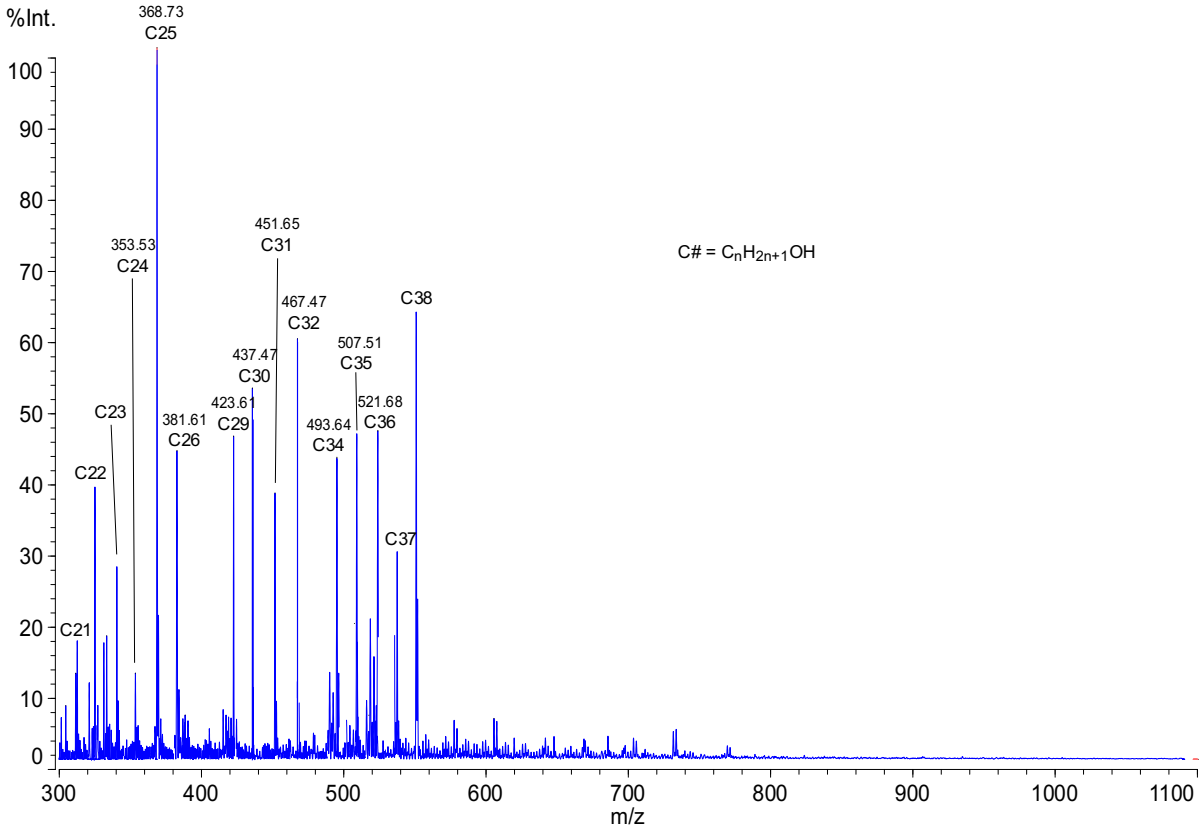

Figure S68. MALDI-TOF-MS spectrum of the oil isolated after reaction of HDPE and Al*i*Bu$_3$ in the presence of Zr(OCH$_2$CMe$_3$)$_2$@SiAlO$_x$ at 200 °C for 12 h, quenched with O$_2$, and extracted with methylene chloride. The spectrum was acquired in linear, positive mode with AgNO$_3$ (salt) and DHB (matrix). The data corresponds to the experiment reported in Table 1, Entry 13.

14. HDPE + $Zr(OCH_2CMe_3)_2$@$SiAlO_x$ + AlH_3 (200 °C).

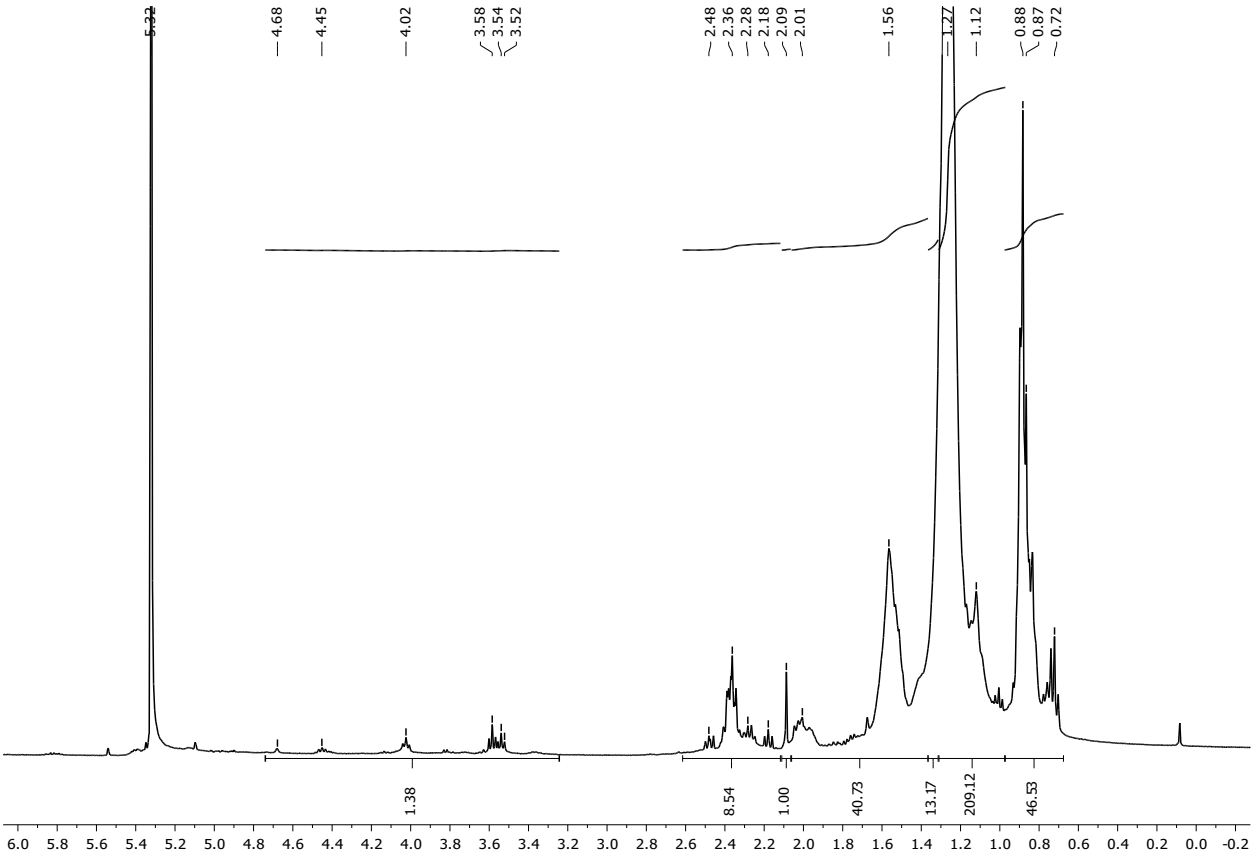

Figure S69. ^1H NMR spectrum of the oil isolated after reaction of HDPE and AlH_3 in the presence of $Zr(OCH_2CMe_3)_2$@$SiAlO_x$ at 200 °C for 12 h, quenched with O_2, and extracted with methylene chloride. The spectrum was acquired at room temperature in methylene chloride-d_2 and assigned based on COSY and HSQC experiments in Figures S70 and S71. Signals at 0.7-1.0 ppm are assigned to methyl groups, peaks at 1.0-1.3, 1.4-2.1, and 2.2-2.7 ppm correspond to methylene groups, and those at 1.3-1.4 and 2.1-2.2 ppm are attributed to methine groups. Peaks at 3.3-4.8 ppm are assigned to -CH_2-OH groups. The data corresponds to the experiment reported in Table 1, Entry 14.

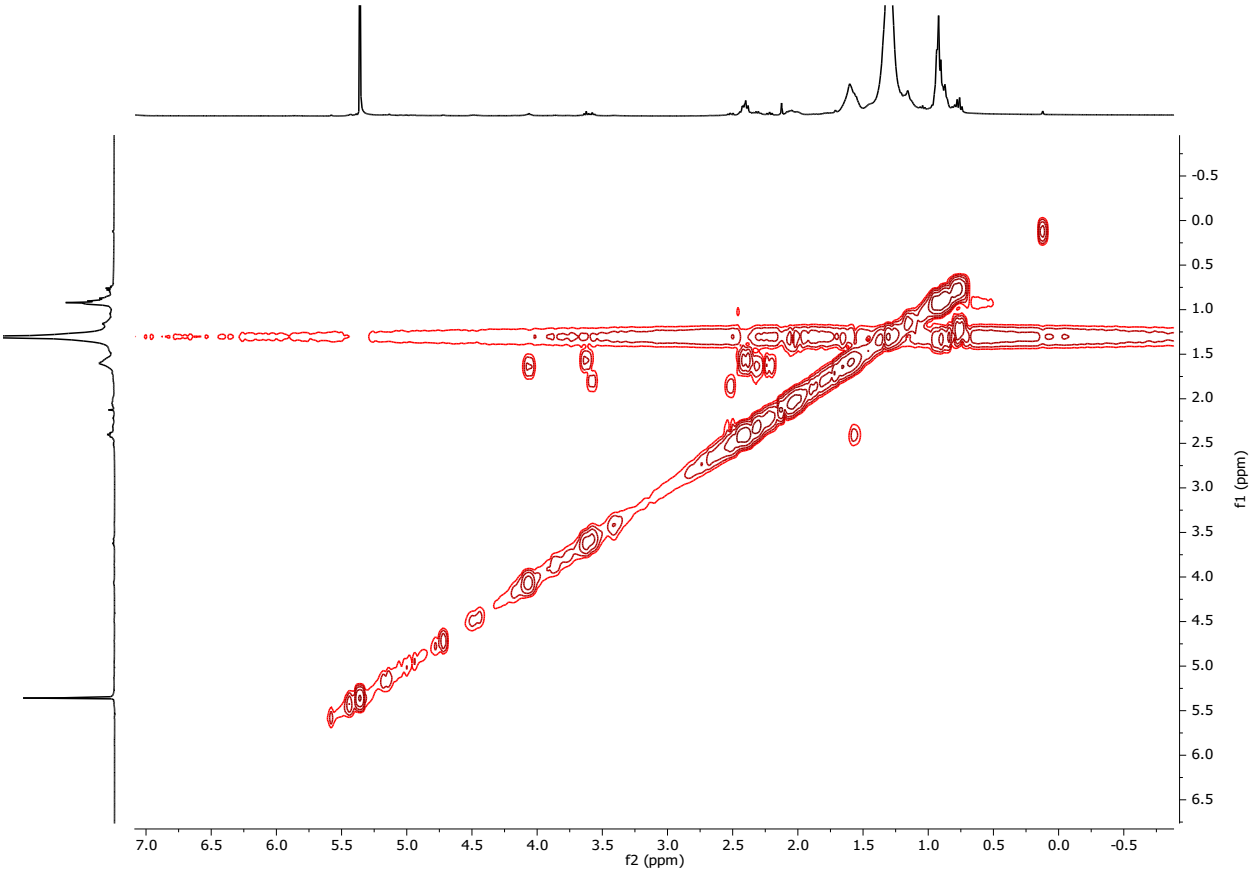

Figure S70. COSY spectrum of the oil isolated after reaction of HDPE and AlH_3 in the presence of $Zr(OCH_2CMe_3)_2$@$SiAlO_x$ at 200 °C for 12 h, quenched with O_2, and extracted with methylene chloride. The spectrum was acquired at room temperature in methylene chloride-d_2. Cross-peaks at 3.5-4.1 ppm correlate with methylene signals at 1.5-1.8 ppm, indicative of -CH_2-CH_2-OH moieties. The data corresponds to the experiment reported in Table 1, Entry 14.

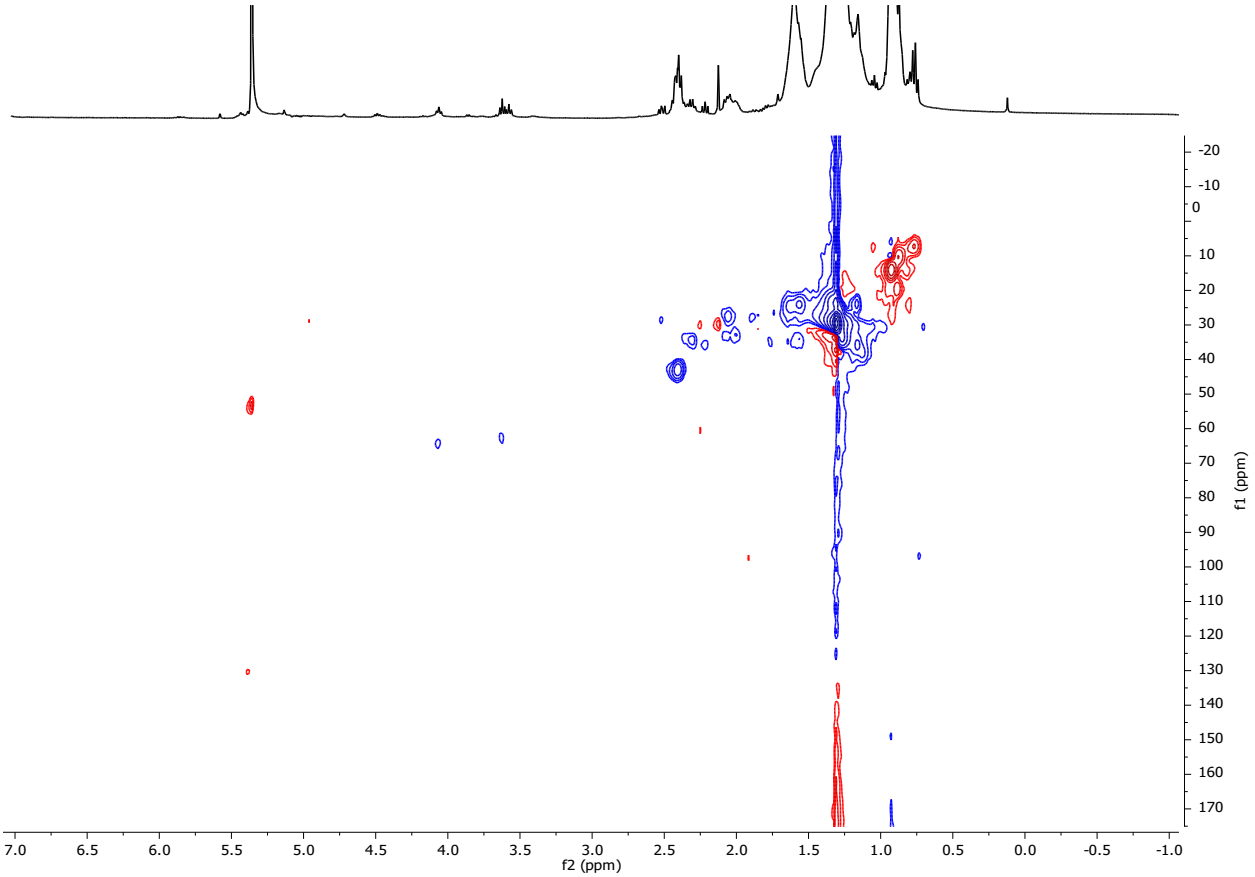

Figure S71. Phase sensitive ^{1}H-^{13}C HSQC spectrum of the oil isolated after reaction of HDPE and AlH_3 in the presence of $Zr(OCH_2CMe_3)_2$@$SiAlO_x$ at 200 °C for 12 h, quenched with O_2, and extracted with methylene chloride. The spectrum was acquired at room temperature in methylene chloride-d_2. Cross-peaks at ^{13}C 60-70 ppm have the same phase (blue) as methylene peaks at 30 ppm, revealing the former are -CH_2-OH moieties. The data corresponds to the experiment reported in Table 1, Entry 14.

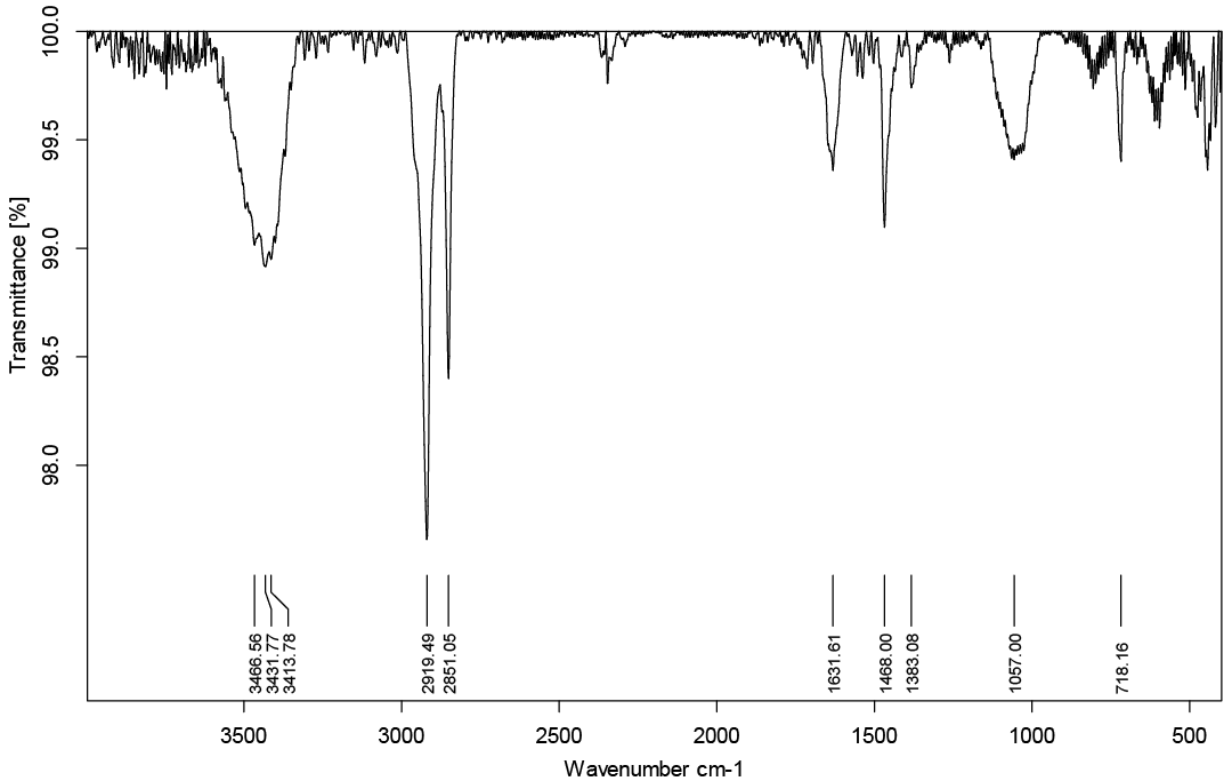

Figure S72. FT-IR spectrum (KBr) of the oil isolated after reaction of HDPE and AlH_3 in the presence of $Zr(OCH_2CMe_3)_2$@$SiAlO_x$ at 200 °C for 12 h, quenched with O_2, and extracted with methylene chloride. Broad signals between 3300-3600 cm^{-1} correspond to O-H stretches. The data corresponds to the experiment reported in Table 1, Entry 14.

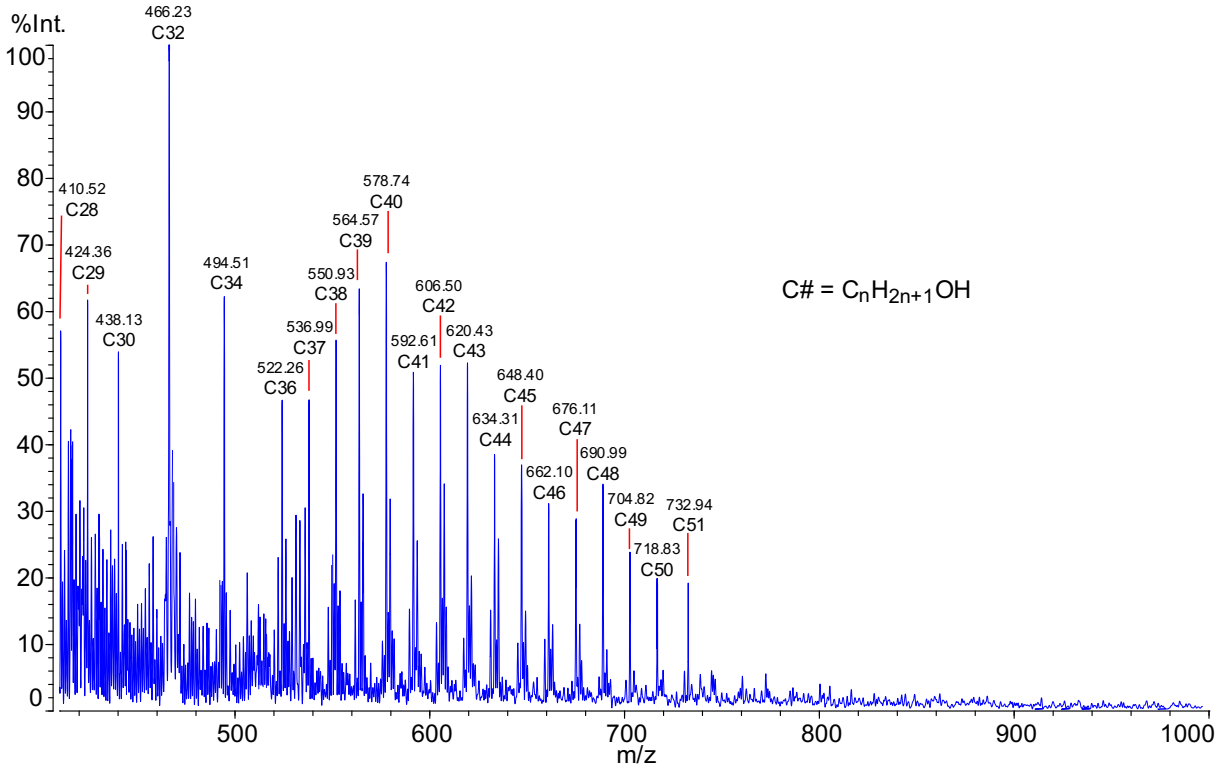

Figure S73. MALDI-TOF-MS spectrum of the oil isolated after reaction of HDPE and AlH_3 in the presence of $Zr(OCH_2CMe_3)_2$@$SiAlO_x$ at 200 °C for 12 h, quenched with O_2, and extracted with methylene chloride. The spectrum was acquired in linear, positive mode with $AgNO_3$ (salt) and DHB (matrix). The data corresponds to the experiment reported in Table 1, Entry 14.

15. HDPE + $Zr(OCH_2CMe_3)_2$@$SiAlO_x$ + AlH_3 (200 °C, Dynamic Vacuum).

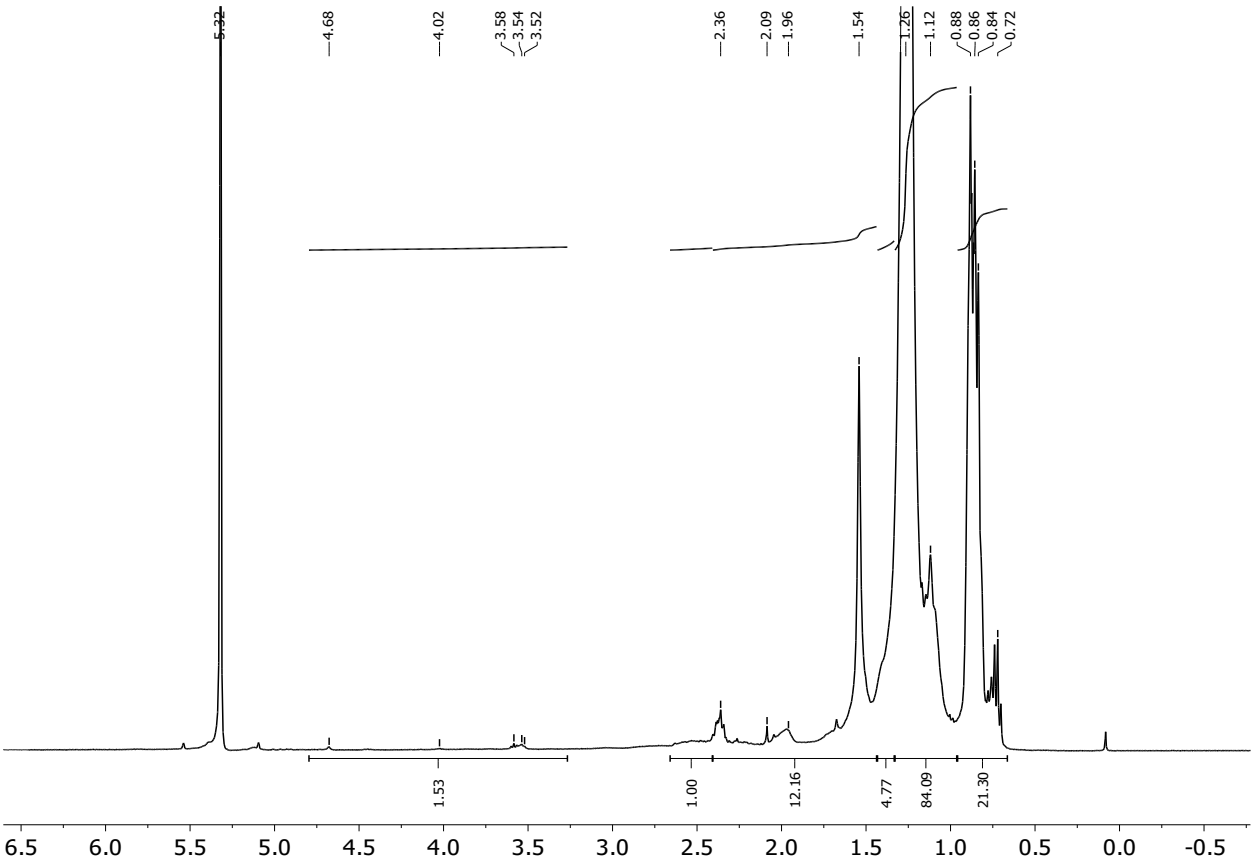

Figure S74. ^1H NMR spectrum of the oil isolated after reaction of HDPE and AlH_3 in the presence of $Zr(OCH_2CMe_3)_2$@$SiAlO_x$ at 200 °C for 12 h under dynamic vacuum, quenched with O_2, and extracted with methylene chloride. The spectrum was acquired at room temperature in methylene chloride-d_2 and assigned based on TOCSY and HSQC experiments in Figures S75 and S76. Signals at 0.7-1.0 ppm correspond to methyl groups, peaks at 1.0-1.3 and 1.5-2.4 ppm are attributed to methylene groups, and those at 1.3-1.5 and 2.4-2.7 ppm correspond to methine groups. Peaks at 3.5-4.7 ppm are assigned to -CH_2-OH groups. The data corresponds to the experiment reported in Table 1, Entry 15.

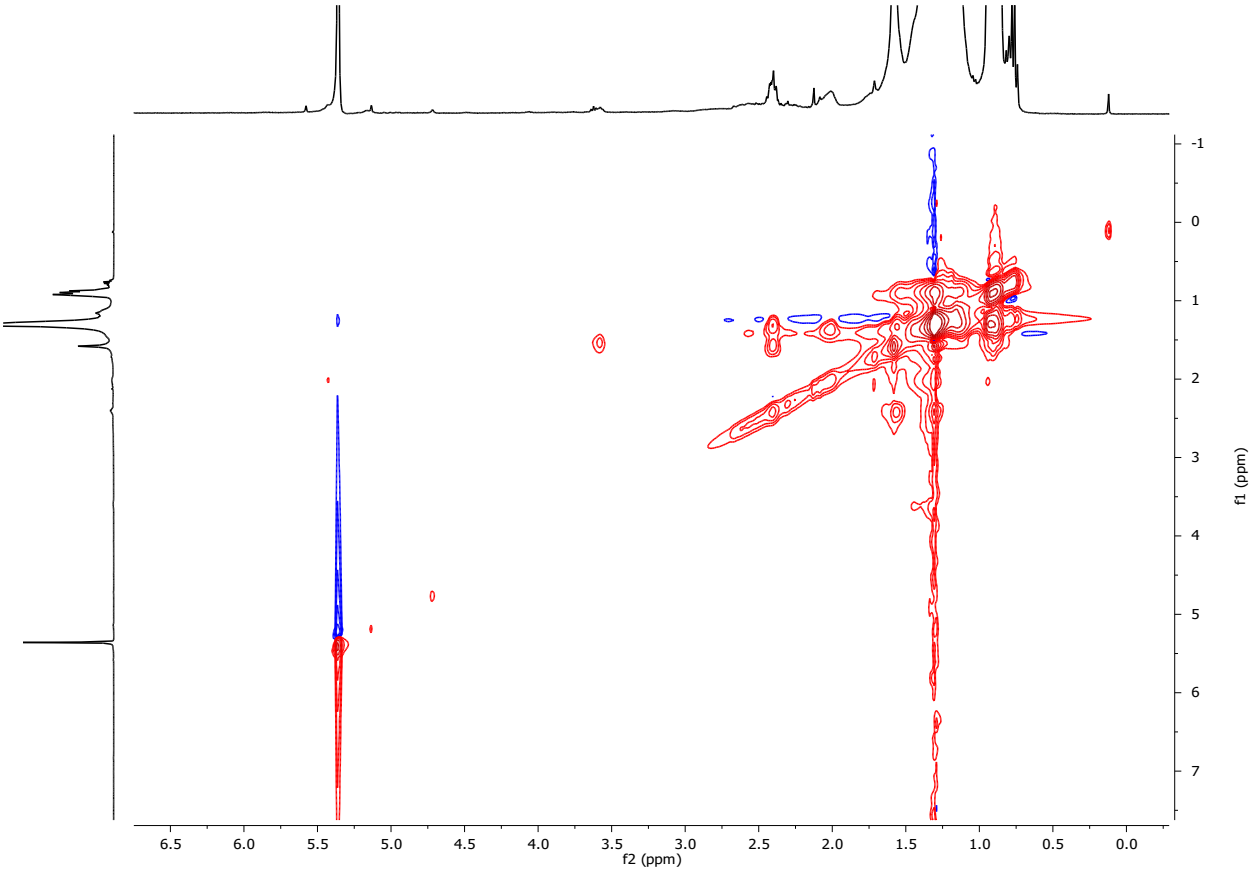

Figure S75. TOCSY spectrum of the oil isolated after reaction of HDPE and AlH_3 in the presence of $Zr(CH_2CMe_3)_2$@$SiAlO_x$ at 200 °C for 12 h under dynamic vacuum, quenched with O_2, and extracted with methylene chloride. The spectrum was acquired at room temperature in methylene chloride-d_2. The cross-peak at 3.6 ppm correlates with methylene signals at 1.6 ppm, indicative of -CH_2-CH_2-OH species. The data corresponds to the experiment reported in Table 1, Entry 15.

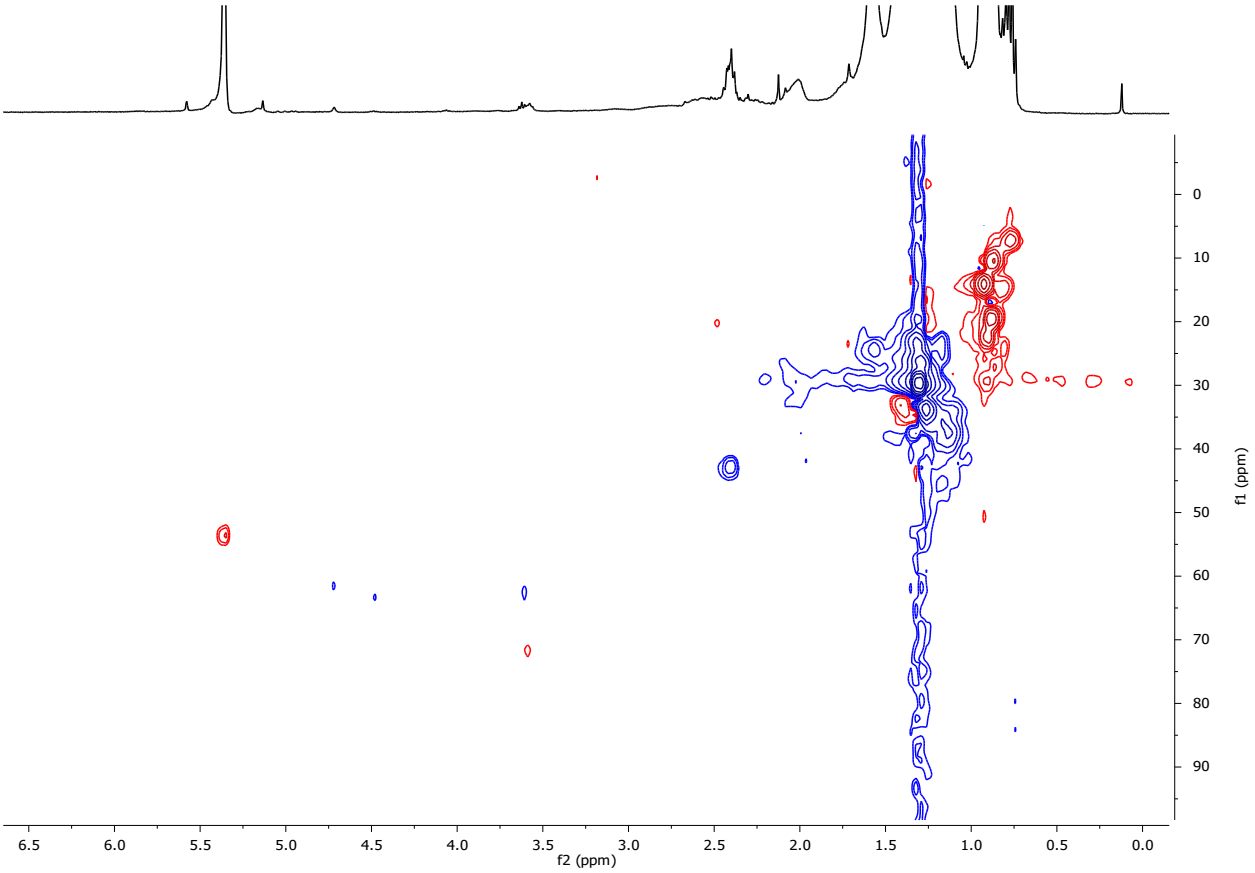

Figure S76. Phase sensitive ^{1}H-^{13}C HSQC spectrum of the oil isolated after reaction of HDPE and AlH_3 in the presence of $Zr(CH_2CMe_3)_2$@$SiAlO_x$ at 200 °C for 12 h under dynamic vacuum, quenched with O_2 and extracted with methylene chloride. The spectrum was acquired at room temperature in methylene chloride-d_2. Cross-peaks at ^{13}C 60-70 ppm have the same phase (blue) as methylene peaks at ^{13}C 30 ppm, revealing the former are -*CH*$_2$-OH moieties (primary alcohols), whereas the cross-peak at ^{13}C 72 ppm (red) is attributed to an –(R)*CH*-OH species (i.e. a secondary alcohol). The data corresponds to the experiment reported in Table 1, Entry 15.

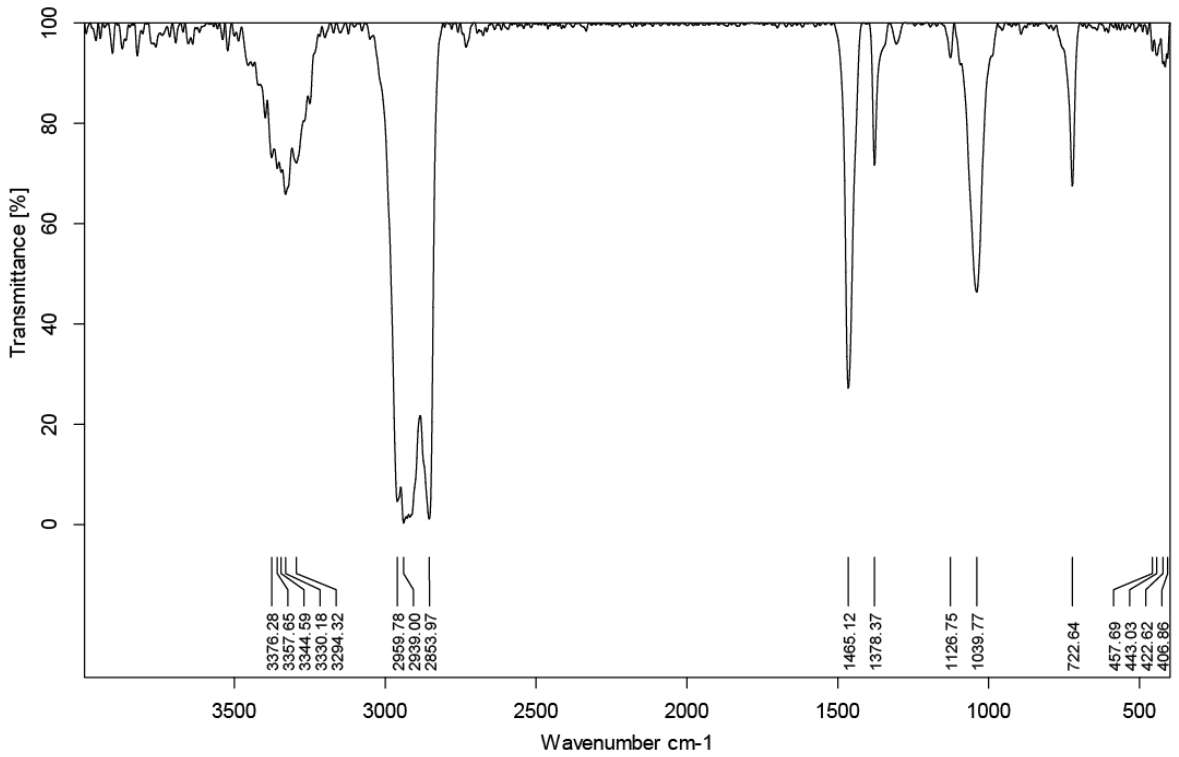

Figure S77. FT-IR spectrum (KBr) of the oil isolated after reaction of HDPE and AlH_3 in the presence of $Zr(CH_2CMe_3)_2$@$SiAlO_x$ at 200 °C for 12 h under dynamic vacuum, quenched with O_2, and extracted with methylene chloride. Broad signals between 3200-3500 cm^{-1} correspond to O-H stretches. The data corresponds to the experiment reported in Table 1, Entry 15.

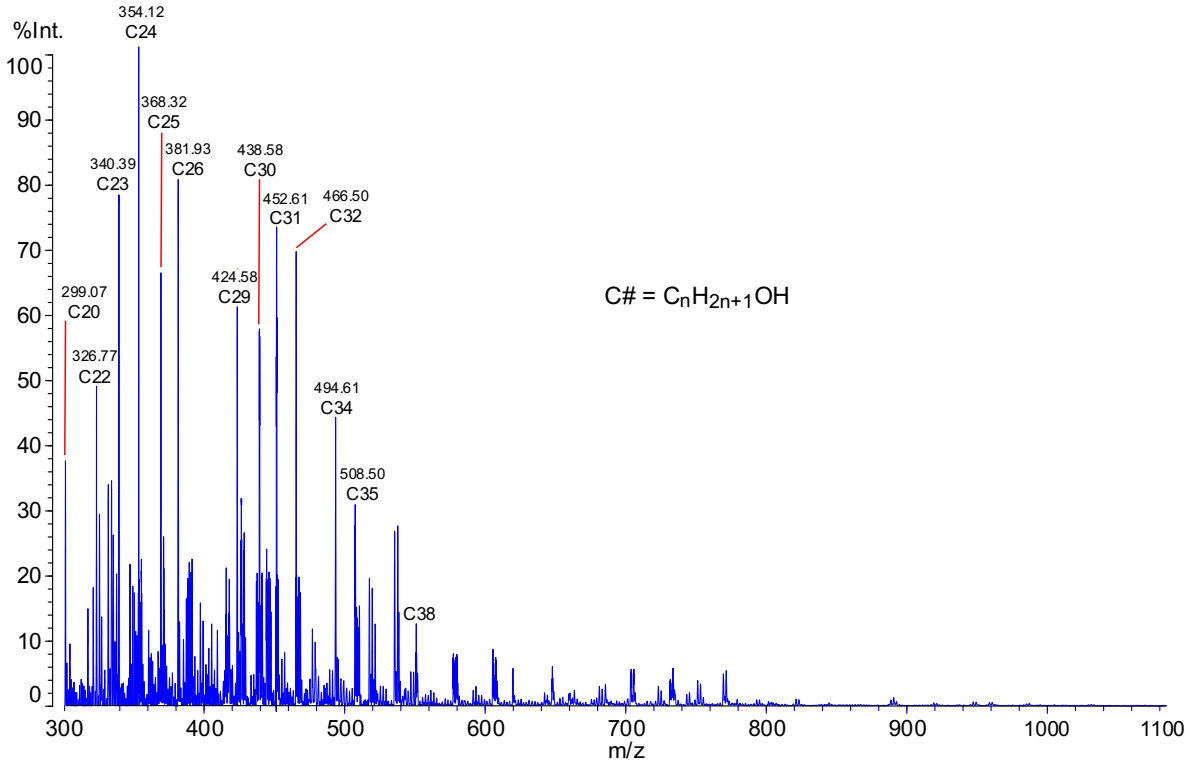

Figure S78. MALDI-TOF-MS spectrum of the oil isolated after reaction of HDPE and AlH_3 in the presence of $Zr(CH_2CMe_3)_2$@$SiAlO_x$ at 200 °C for 12 h under dynamic vacuum, quenched with O_2, and extracted with methylene chloride. The spectrum was acquired in linear, positive mode with $AgNO_3$ (salt) and DHB (matrix). The data corresponds to the experiment reported in Table 1, Entry 15.

16. HDPE + $Zr(CH_2CMe_3)_2@SiO_2$ + Al*i*Bu_3 (200 °C).

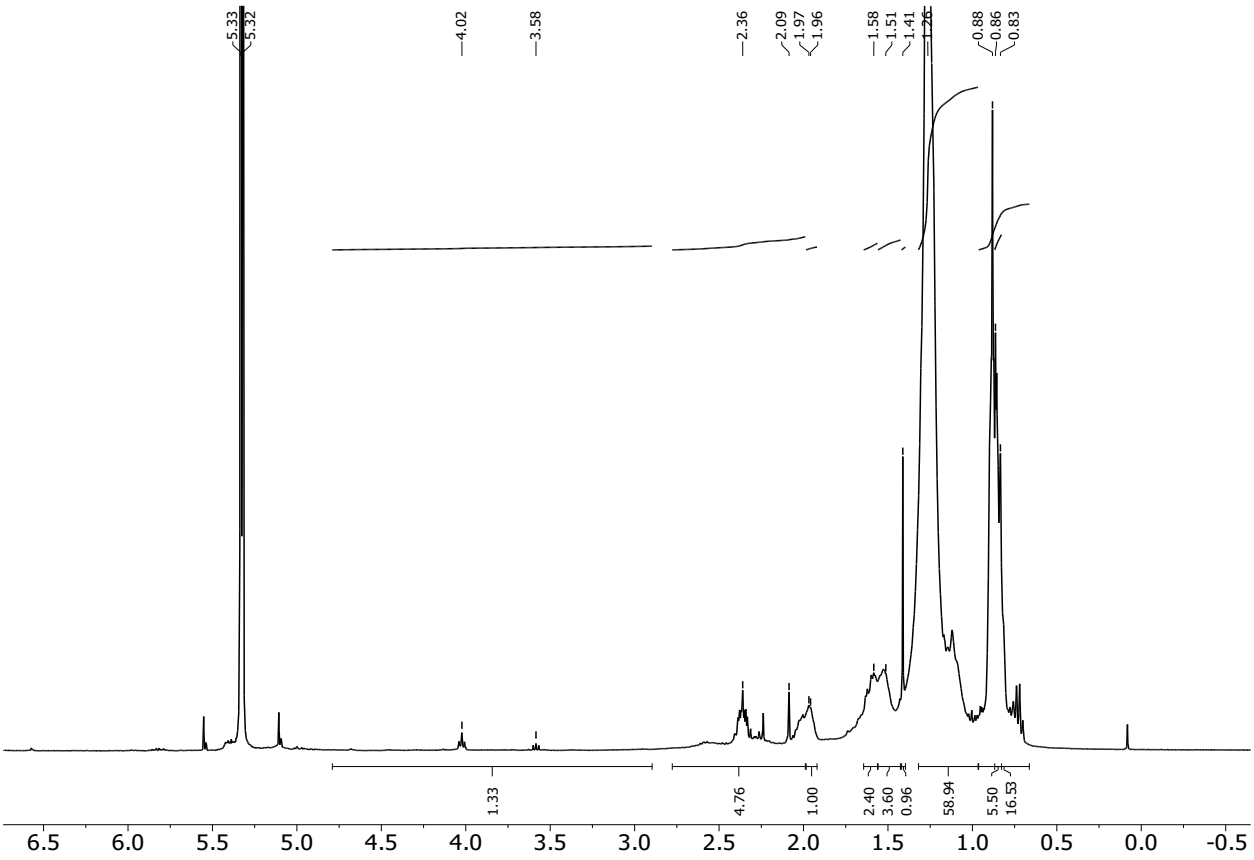

Figure S79. ^{1}H NMR spectrum of the oil isolated after reaction of HDPE and Al*i*Bu_3 in the presence of $Zr(CH_2CMe_3)_2@SiO_2$ at 200 °C for 12 h, quenched with O_2, and extracted with methylene chloride. The spectrum was acquired at room temperature in methylene chloride-d_2 and assigned based on COSY and HSQC experiments in Figures S80 and S81. Signals at 0.7-1.0 ppm are assigned to methyl groups, peaks at 1.0-1.3, 1.4-1.6, and 2.0-2.7 ppm correspond to methylene groups, and those at 1.3-1.4, 1.6-1.7, and 1.8-2.0 ppm are attributed to methine groups. Peaks at 3.3-4.7 ppm are assigned to -CH_2-OH groups. The data corresponds to the experiment reported in Table 1, Entry 16.

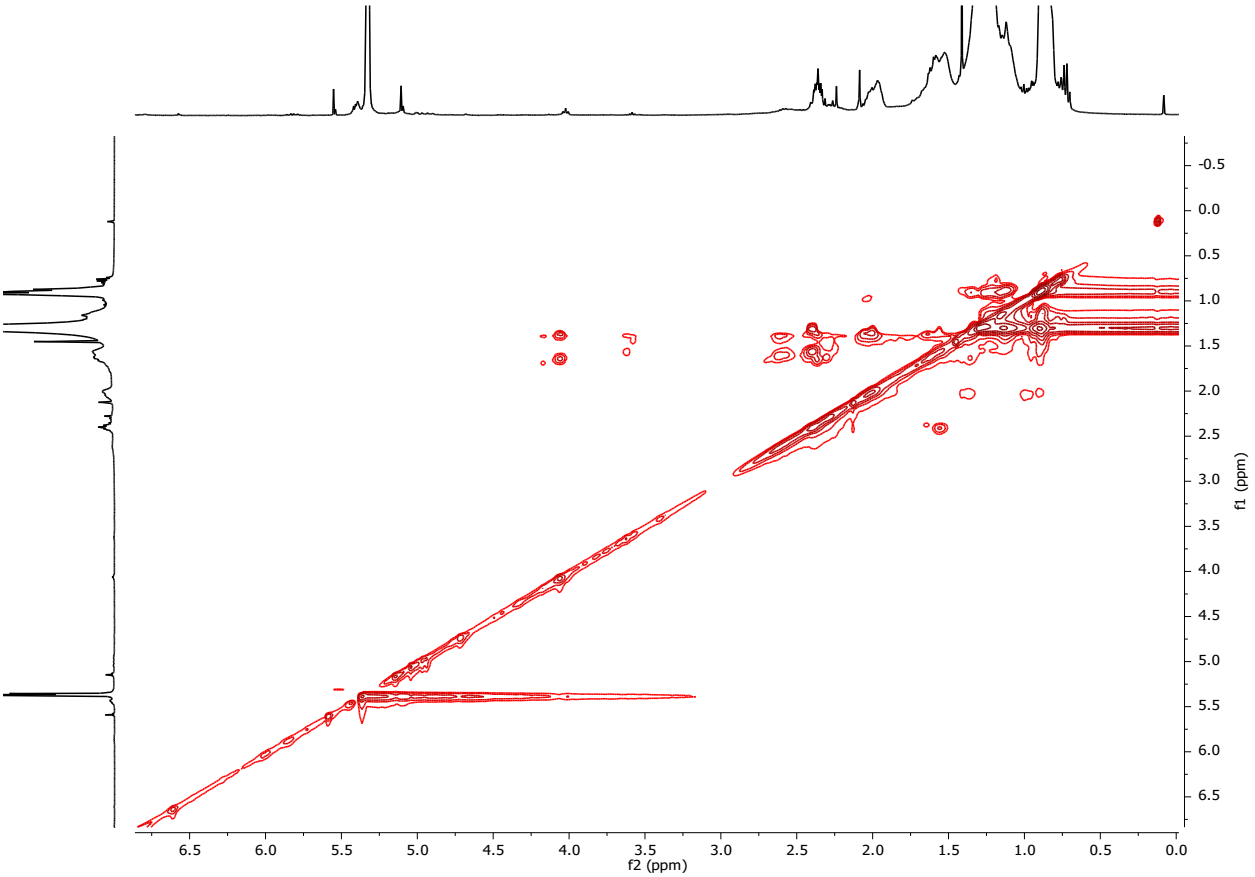

Figure S80. COSY spectrum of the oil isolated after reaction of HDPE and Al*i*Bu$_3$ in the presence of Zr(CH$_2$CMe$_3$)$_2$@SiO$_2$ at 200 °C for 12 h, quenched with O$_2$, and extracted with methylene chloride. The spectrum was acquired at room temperature in methylene chloride-d_2. Cross-peaks at 3.6-4.0 ppm correlate with methylene signals at 1.4-1.6 ppm, indicative of -CH$_2$-CH$_2$-OH species. The data corresponds to the experiment reported in Table 1, Entry 16.

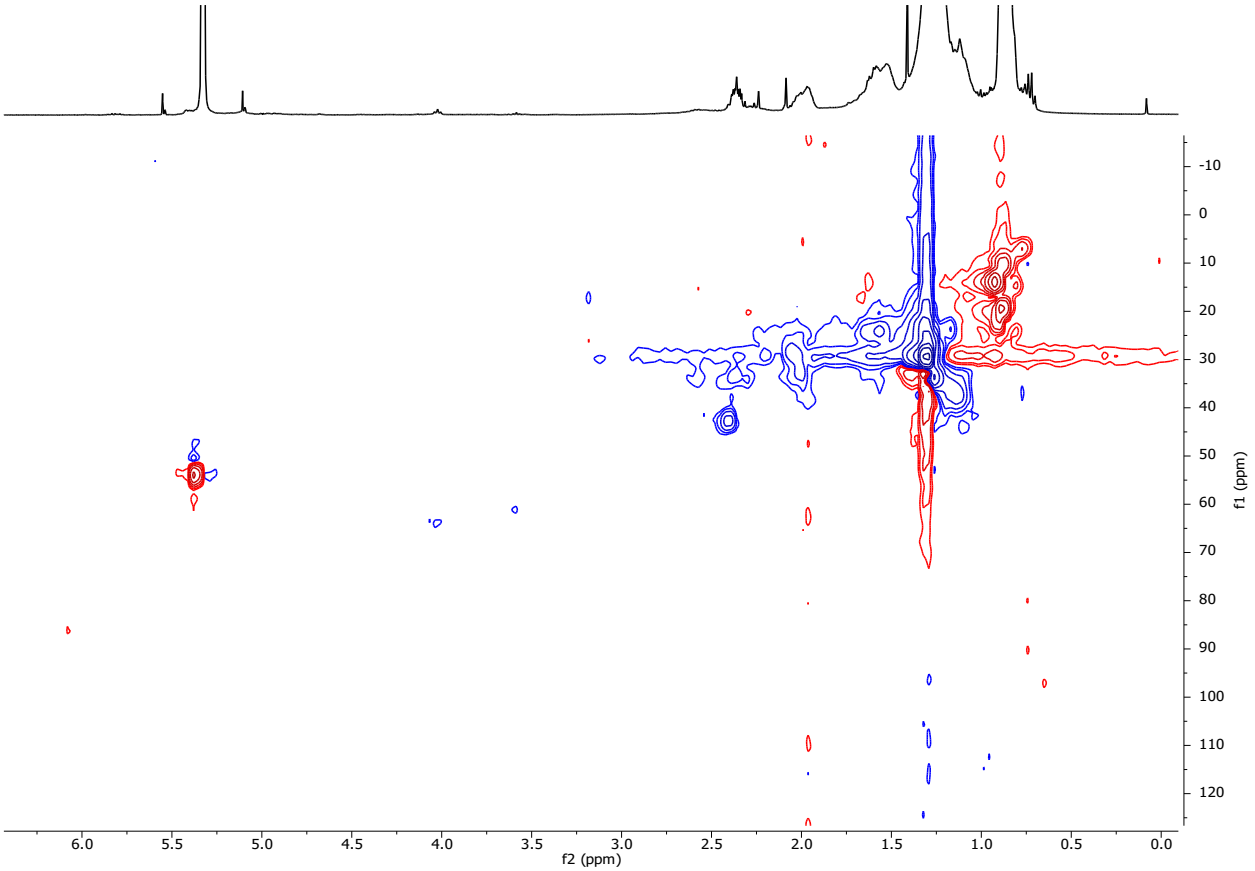

Figure S81. Phase sensitive ^{1}H-^{13}C HSQC spectrum of the oil isolated after reaction of HDPE and Al*i*Bu$_3$ in the presence of Zr(CH$_2$CMe$_3$)$_2$@SiO$_2$ at 200 °C for 12 h, quenched with O$_2$, and extracted with methylene chloride. The spectrum was acquired at room temperature in methylene chloride-d_2. Cross-peaks at ^{13}C 60-70 ppm have the same phase (blue) as methylene peaks at 30 ppm, revealing the former are -*CH$_2$*-OH moieties. The data corresponds to the experiment reported in Table 1, Entry 16.

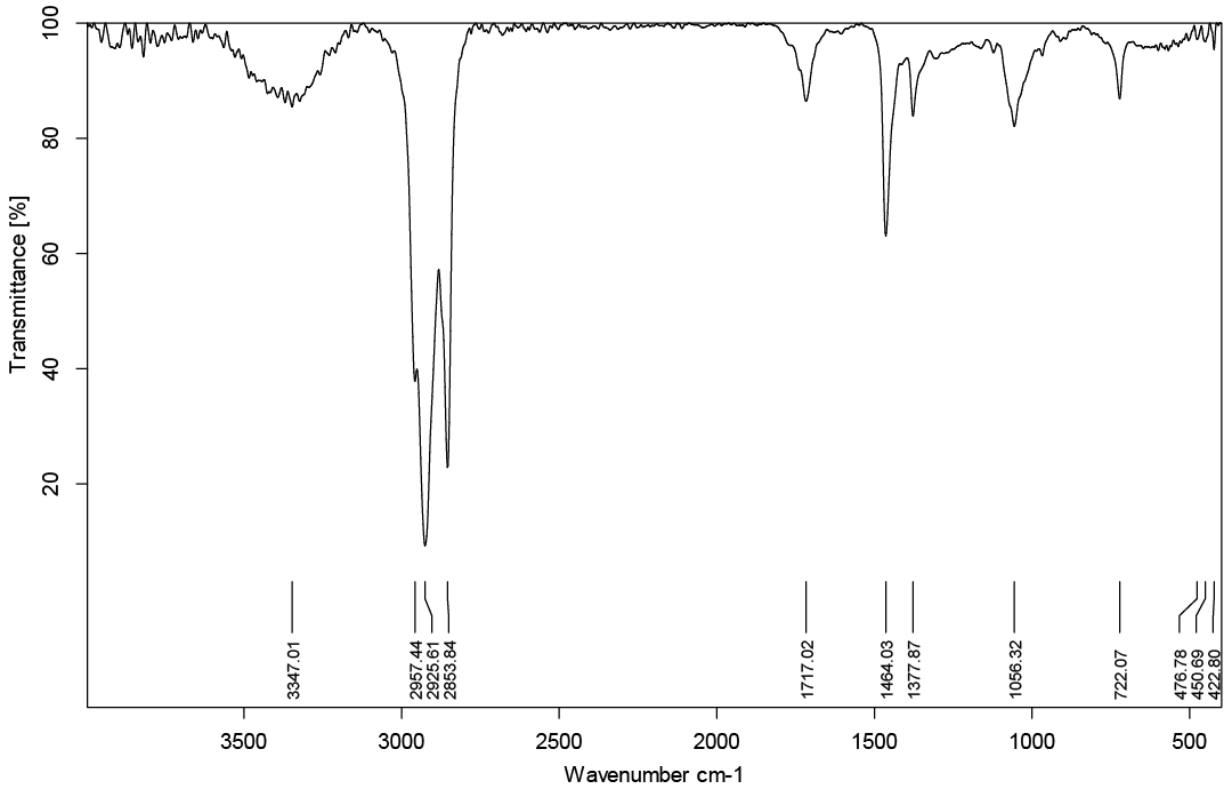

Figure S82. FT-IR spectrum (KBr) of the oil isolated after reaction of HDPE and Al*i*Bu$_3$ in the presence of Zr(CH$_2$CMe$_3$)$_2$@SiO$_2$ at 200 °C for 12 h, quenched with O$_2$, and extracted with methylene chloride. The broad signal at 3347 cm^{-1} corresponds to an O-H stretch. The data corresponds to the experiment reported in Table 1, Entry 16.

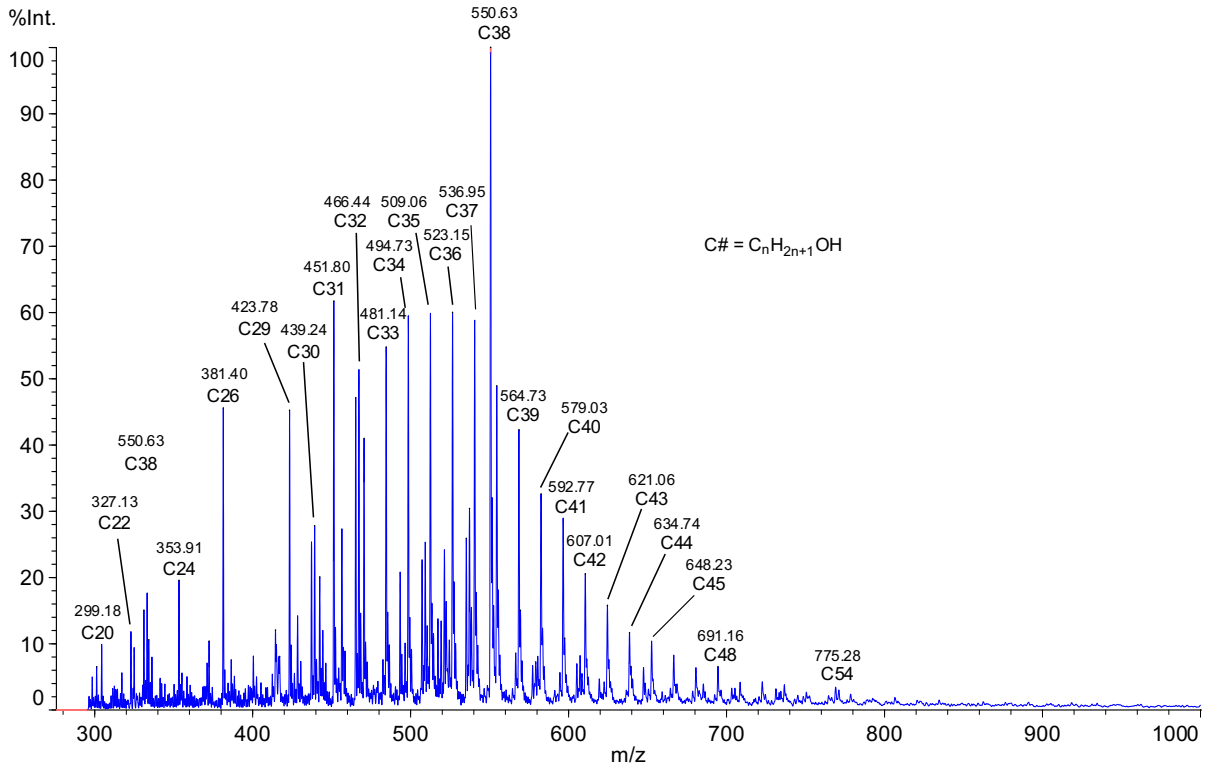

Figure S83. MALDI-TOF-MS spectrum of the oil isolated after reaction of HDPE and Al*i*Bu$_3$ in the presence of Zr(CH$_2$CMe$_3$)$_2$@SiO$_2$ at 200 °C for 12 h, quenched with O$_2$, and extracted with methylene chloride. The spectrum was acquired in linear, positive mode with AgNO$_3$ (salt) and DHB (matrix). The data corresponds to the experiment reported in Table 1, Entry 16.

17. HDPE + $Zr(CH_2CMe_3)_2@SiO_2$ + $AlEt_3$ (200 °C).

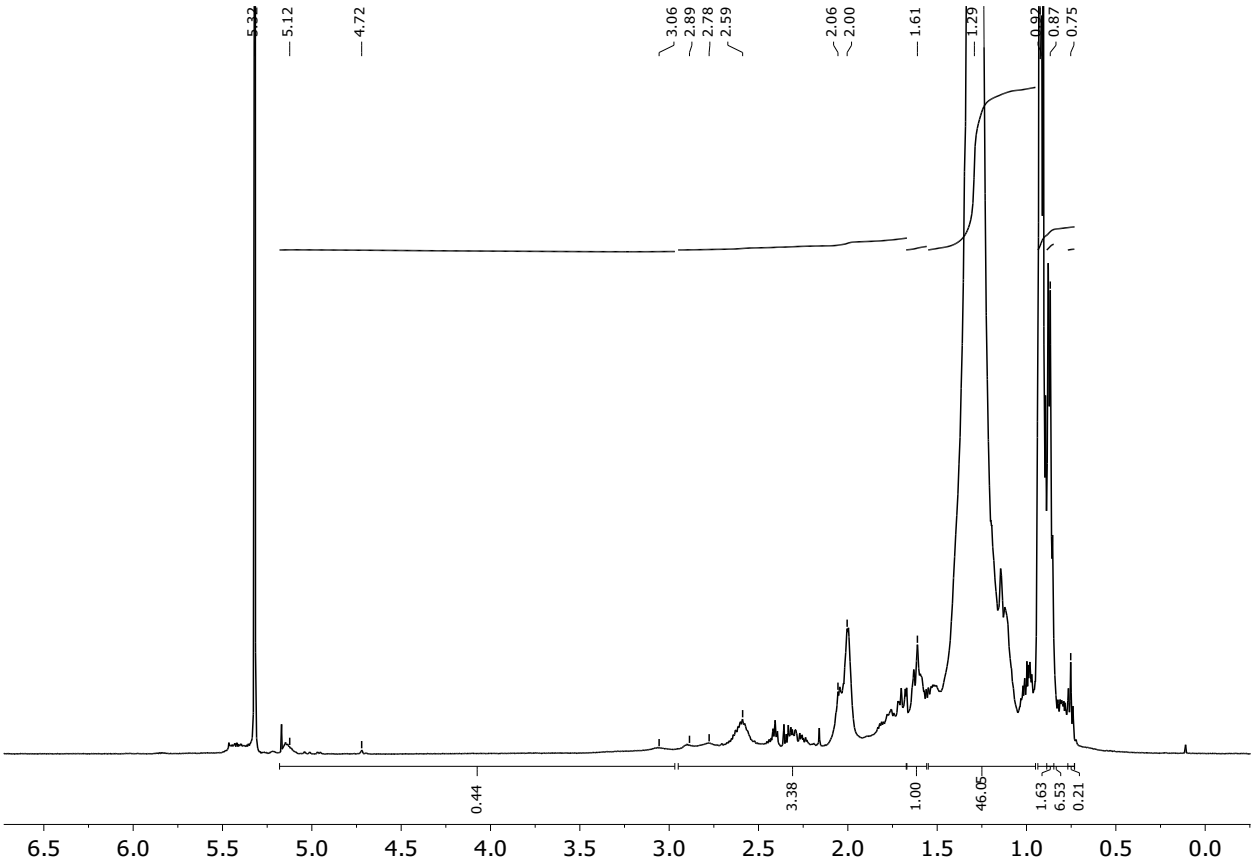

Figure S84. ^1H NMR spectrum of the oil isolated after reaction of HDPE and $AlEt_3$ in the presence of $Zr(CH_2CMe_3)_2@SiO_2$ at 200 °C for 12 h, quenched with O_2, and extracted with methylene chloride. The spectrum was acquired at room temperature in methylene chloride-d_2 and assigned based on COSY and HSQC experiments in Figures S85 and S86. Signals at 0.7-1.0 ppm are assigned to methyl groups, peaks at 1.0-1.6 and 1.7-3.0 ppm correspond to methylene groups, and those at 1.6-1.7 ppm are attributed to methine groups. Peaks at 3.0-5.2 ppm are assigned to -CH_2-OH groups. The data corresponds to the experiment reported in Table 1, Entry 17.

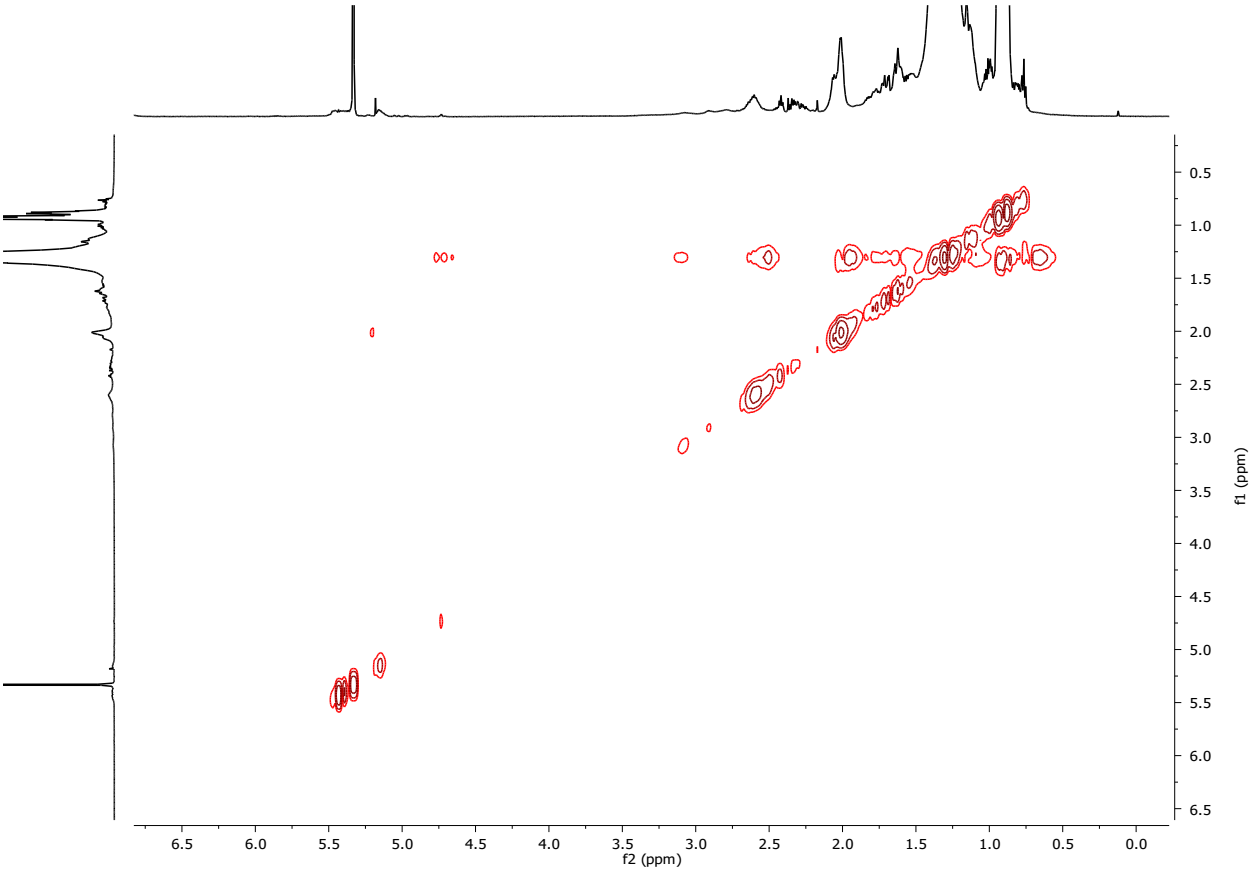

Figure S85. COSY spectrum of the oil isolated after reaction of HDPE and $AlEt_3$ in the presence of $Zr(CH_2CMe_3)_2$@SiO_2 at 200 °C for 12 h, quenched with O_2, and extracted with methylene chloride. The spectrum was acquired at room temperature in methylene chloride-d_2. Cross-peaks at 4.7-5.2 ppm correlate with methylene signals at 1.3-2.0 ppm, indicative of -CH_2-CH_2-OH moieties. The data corresponds to the experiment reported in Table 1, Entry 17.

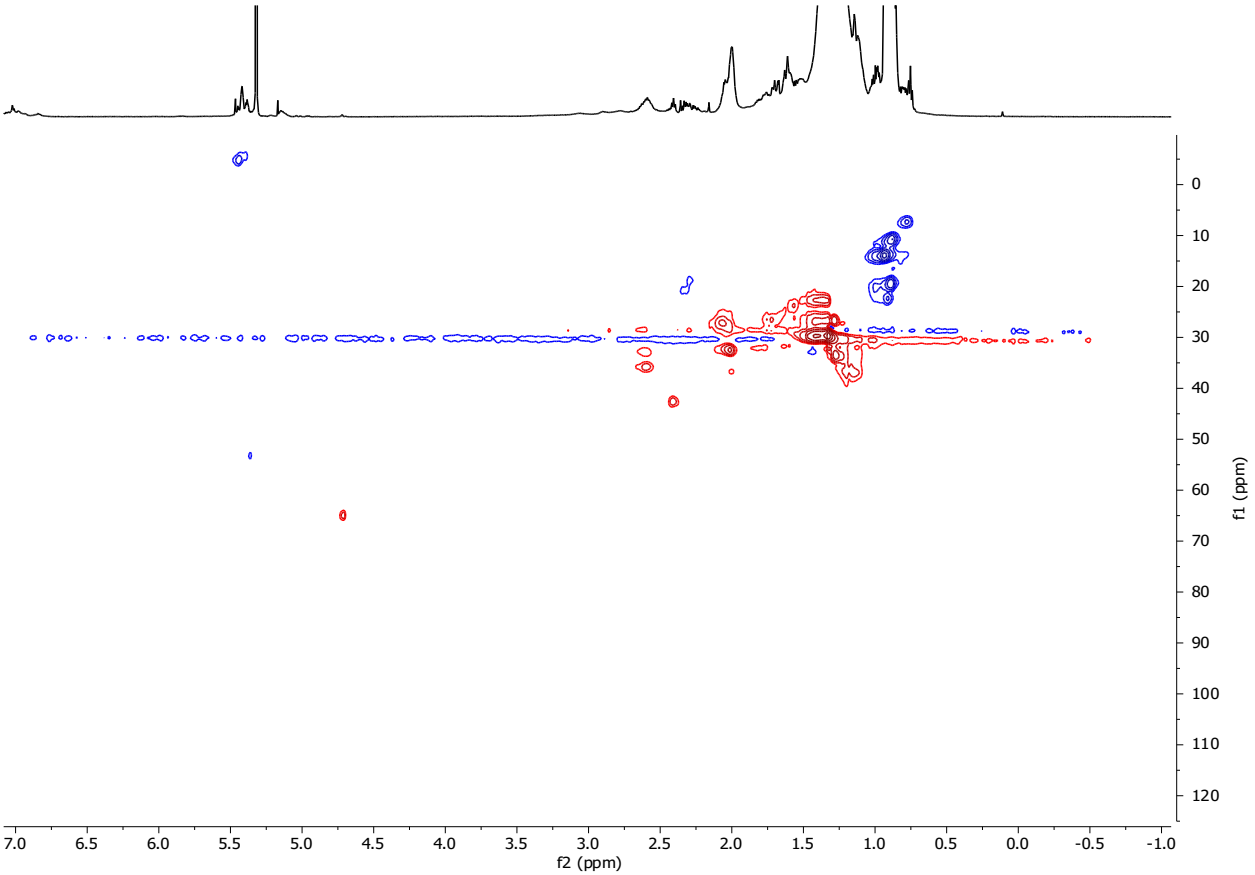

Figure S86. Phase sensitive ^{1}H-^{13}C HSQC spectrum of the oil isolated after reaction of HDPE and $AlEt_3$ in the presence of $Zr(CH_2CMe_3)_2$@SiO_2 at 200 °C for 12 h, quenched with O_2, and extracted with methylene chloride. The spectrum was acquired at room temperature in methylene chloride-d_2. Cross-peaks at ^{13}C 60-70 ppm have the same phase (red) as methylene peaks at 30 ppm revealing the former are -CH_2-OH moieties. The data corresponds to the experiment reported in Table 1, Entry 17.

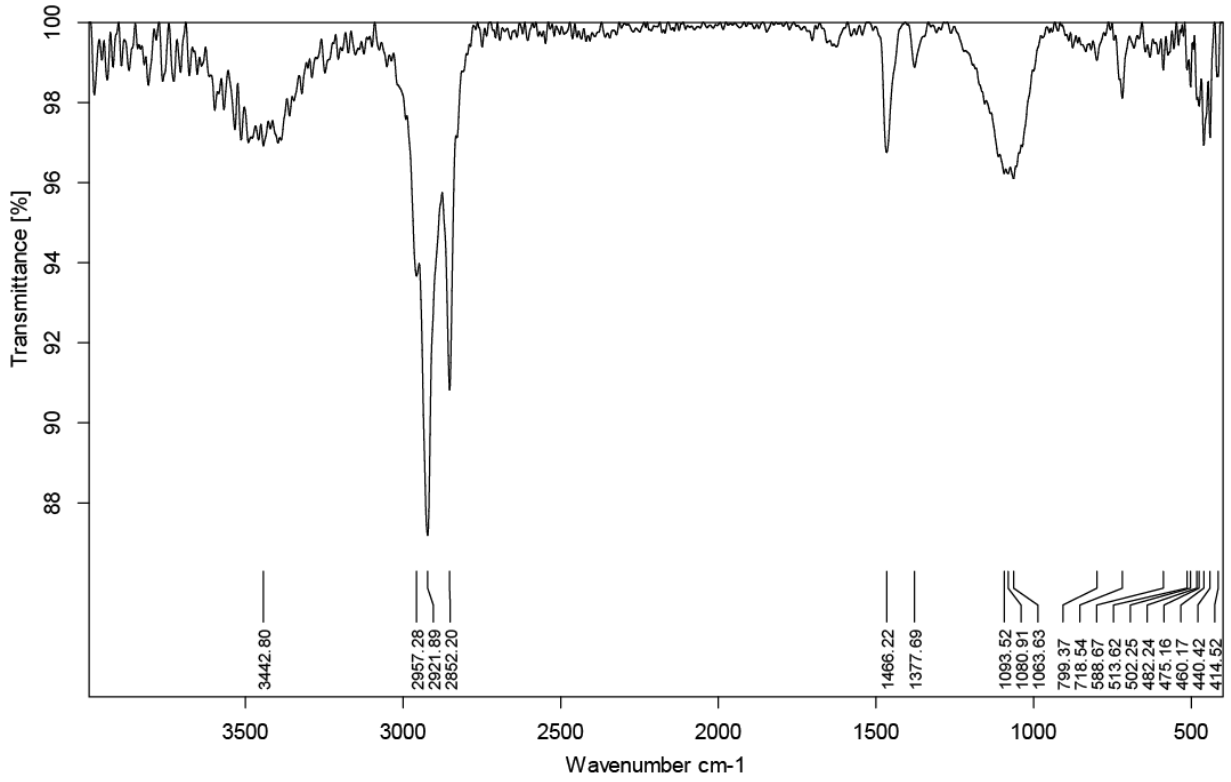

Figure S87. FT-IR spectrum (KBr) of the oil isolated after reaction of HDPE and $AlEt_3$ in the presence of $Zr(CH_2CMe_3)_2@SiO_2$ at 200 °C for 12 h, quenched with O_2, and extracted with methylene chloride. The broad signal at 3442 cm^{-1} corresponds to an O-H stretch. The data corresponds to the experiment reported in Table 1, Entry 17.

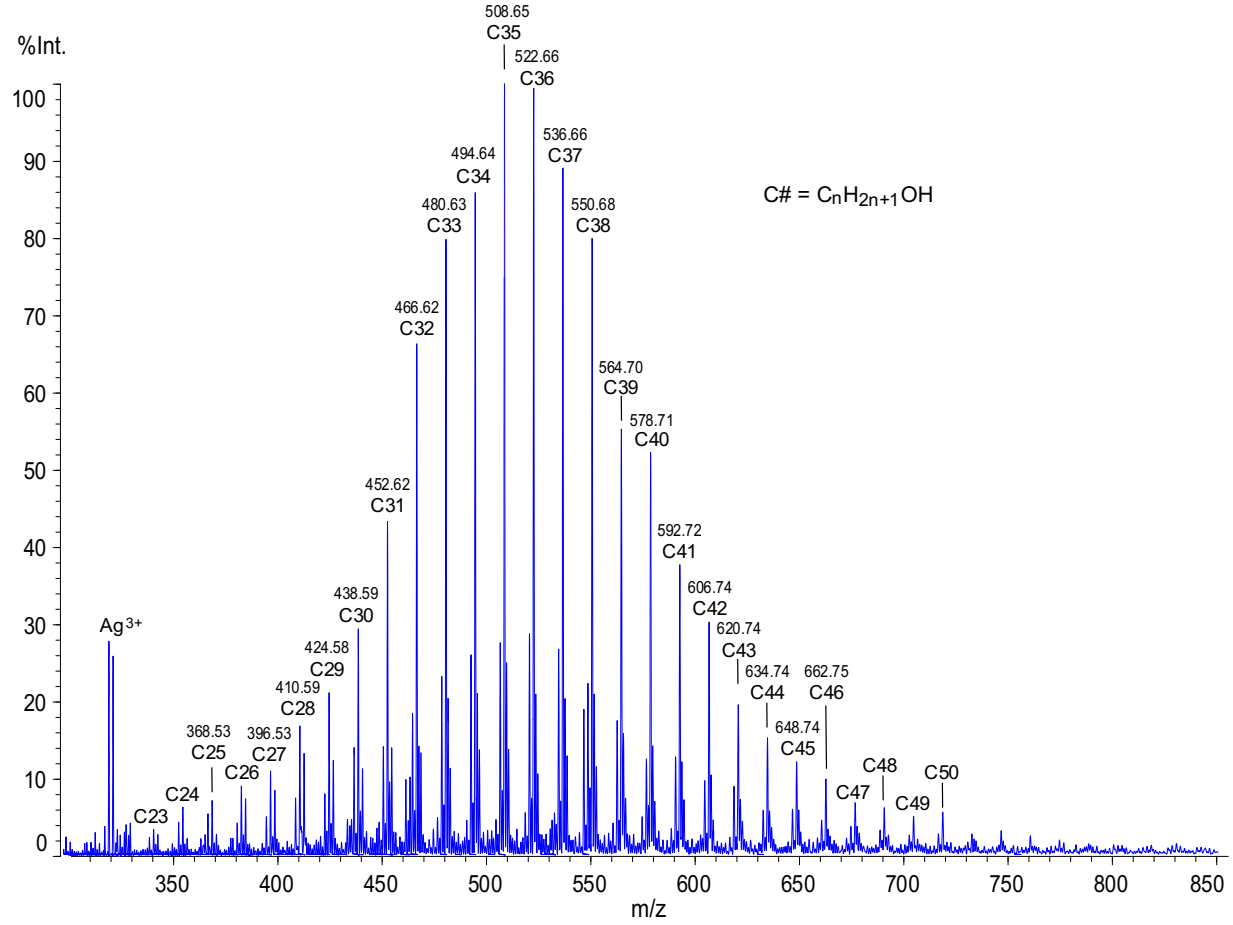

Figure S88. MALDI-TOF-MS spectrum of the oil isolated after reaction of HDPE and $AlEt_3$ in the presence of $Zr(CH_2CMe_3)_2$@SiO_2 at 200 °C for 12 h, quenched with O_2, and extracted with methylene chloride. The spectrum was acquired in linear, positive mode with $AgNO_3$ (salt) and DHB (matrix). The data corresponds to the experiment reported in Table 1, Entry 17.

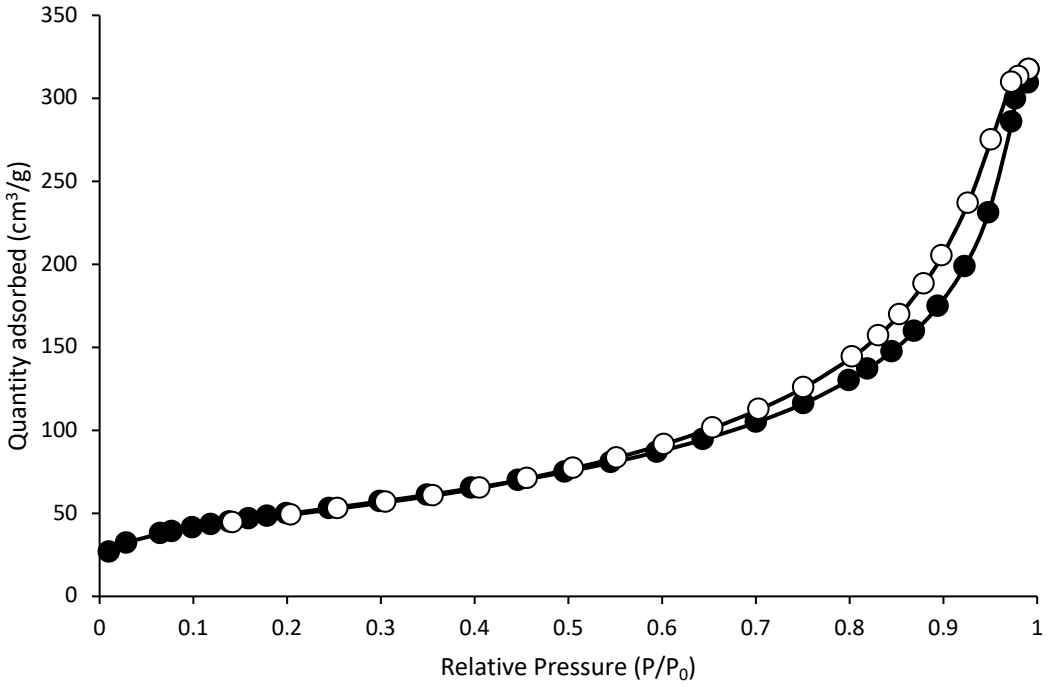

Figure S89. Nitrogen adsorption/desorption isotherm of $SiAlO_x$, to determine surface area of 182 m^2/g prior to grafting $Zr(CH_2CMe_3)_4$.

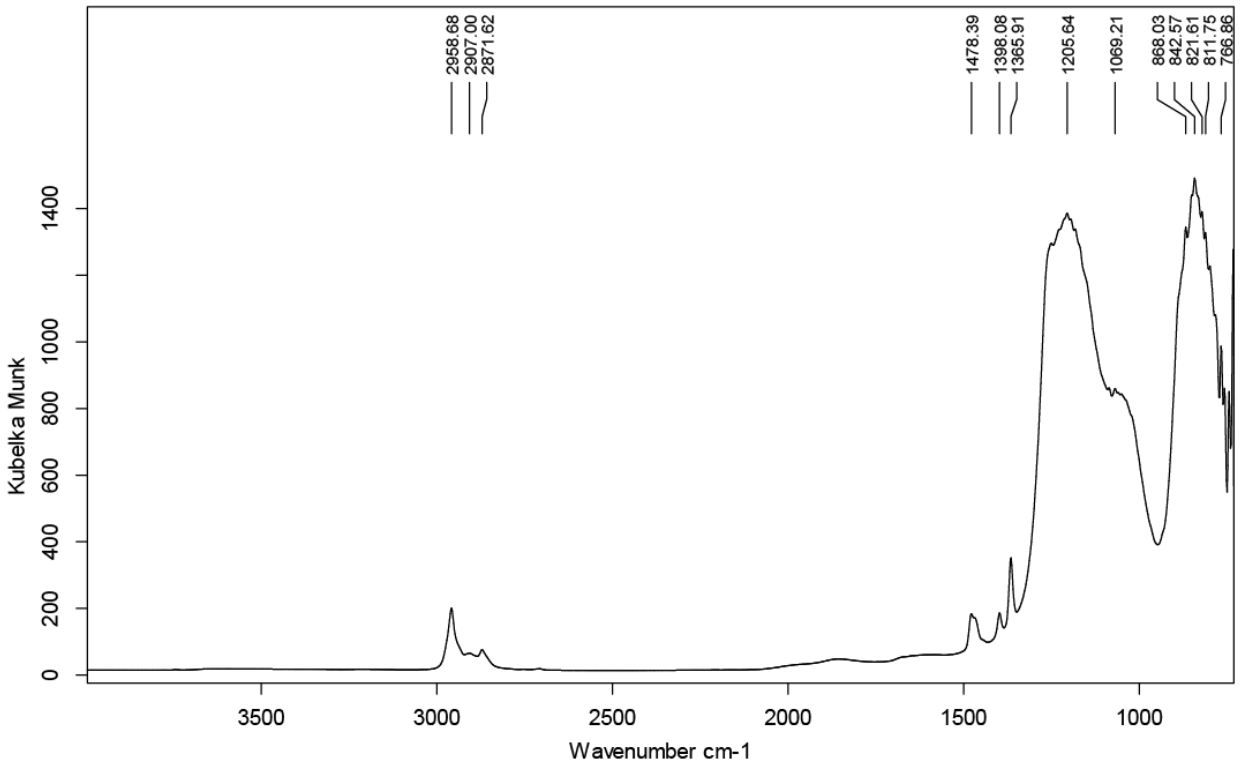

Figure S90. DRIFT spectrum of $Zr(CH_2CMe_3)_2$@$SiAlO_x$ acquired at room temperature. Compare with DRIFT spectra after treatment with Al*i*Bu_3, shown in Figure 3.

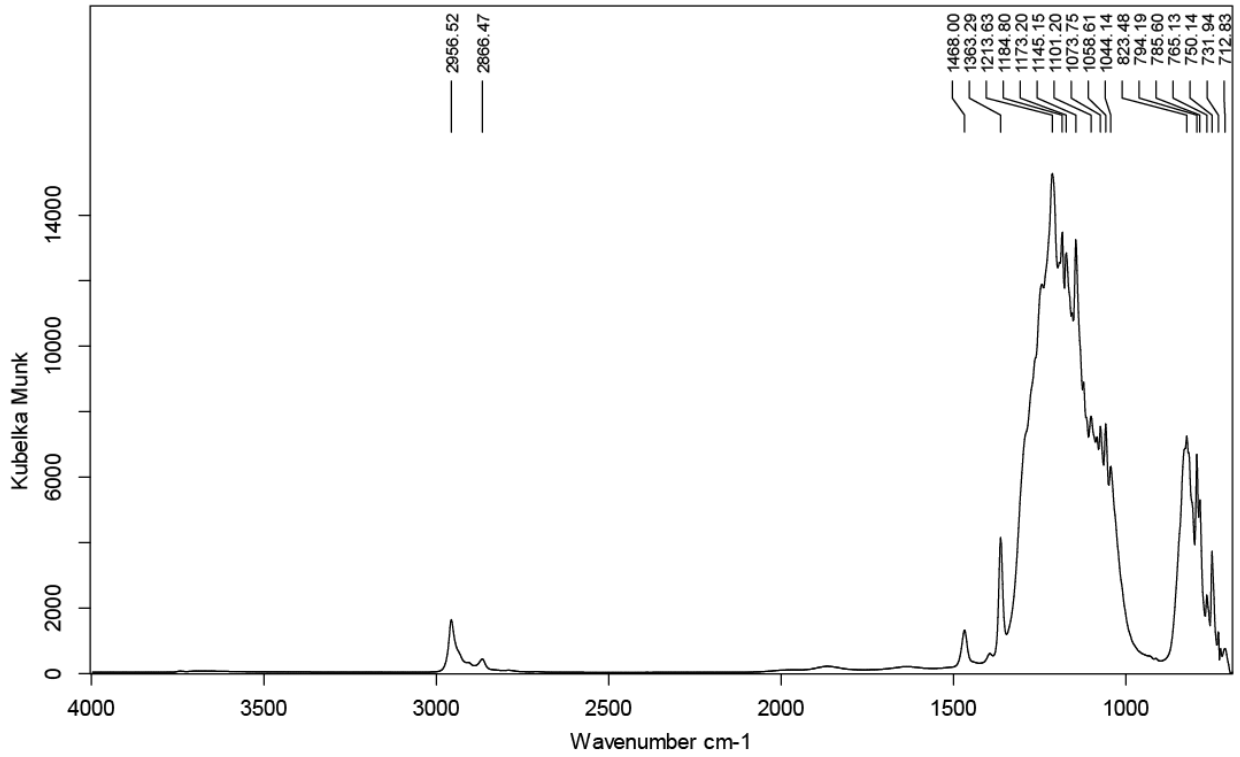

Figure S91. DRIFT spectrum of $Zr(CH_2CMe_3)_2@SiO_2$ acquired at room temperature is similar to that of $Zr(CH_2CMe_3)_2@SiAlO_x$ in Figure S90.

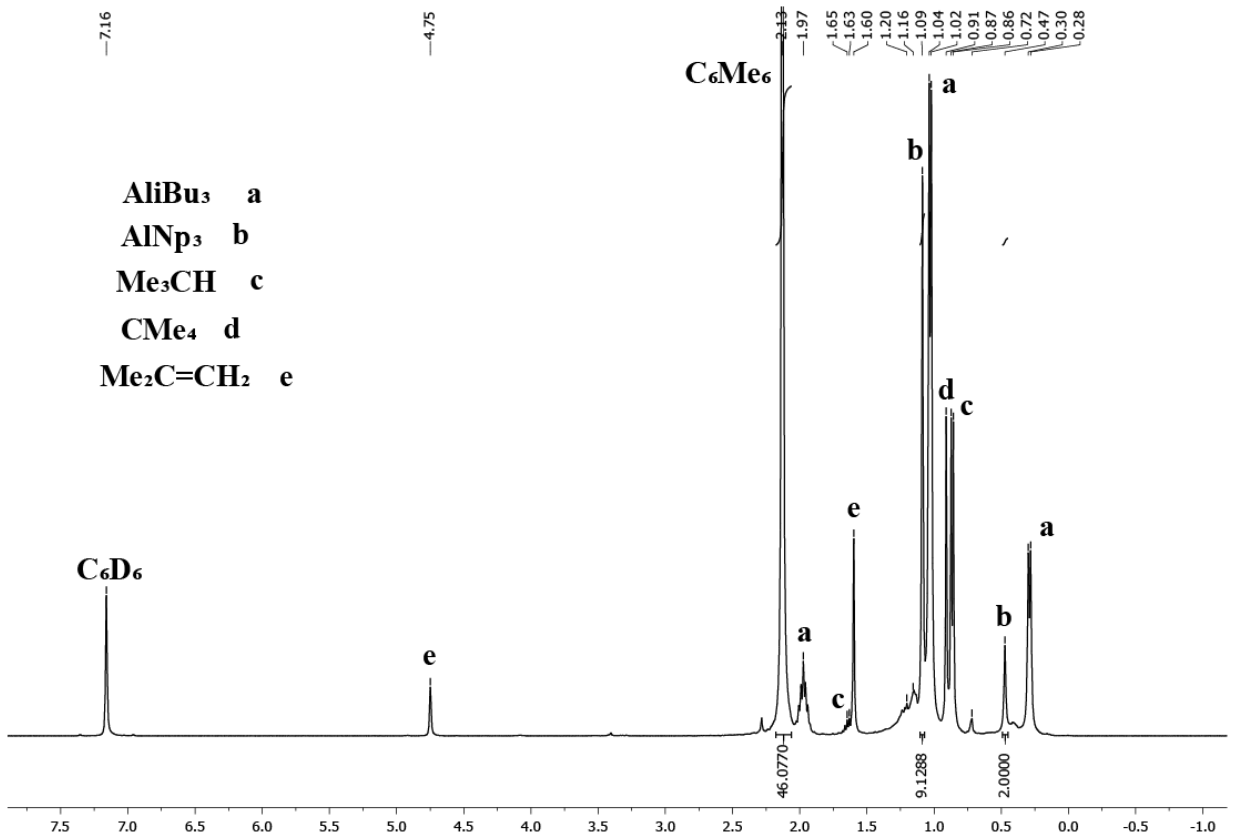

Figure S92. ^{1}H NMR spectrum of $Zr(CH_2CMe_3)_2$@$SiAlO_x$ + Al*i*Bu$_3$ (3 equiv.) at room temperature in benzene-d_6. The presence of $Al(CH_2CMe_3)_3$ (b) is consistent with an alkyl exchange reaction between surface Zr-CH_2CMe_3 groups and Al-CH_2CHMe_2. About 33% of the total neopentyl groups are transferred to aluminum from zirconium. The presence of isobutylene (e) is consistent with the presence of Zr-H surface species, presumably arising due to alkyl exchange of surface Zr sites with Al*i*Bu$_3$ followed by **β**-hydride eliminations of in-situ formed Zr-CH_2-$CHMe_2$ groups. Note that Al*i*Bu$_3$ by itself is stable in C_6D_6 at room temperature and no isobutylene is observed. The alkanes isobutane and neopentane are likely formed from the reaction of Al*i*Bu$_3$ and $Al(CH_2CMe_3)_3$ with uncapped surface Si-OH groups (~0.08 mmol/g).

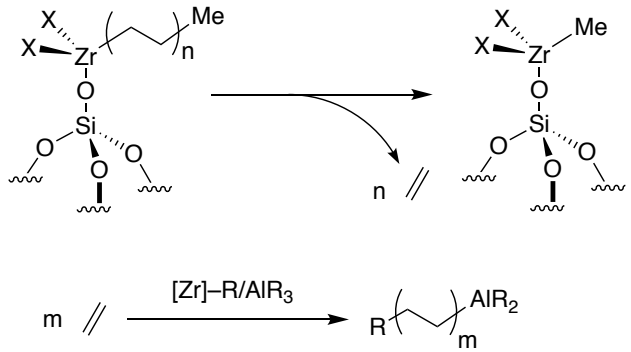

Figure S93. Depolymerization and re-oligomerization sequence to generate long chain alkylaluminum products is ruled out by attempted ethylene oligomerization under reaction conditions.

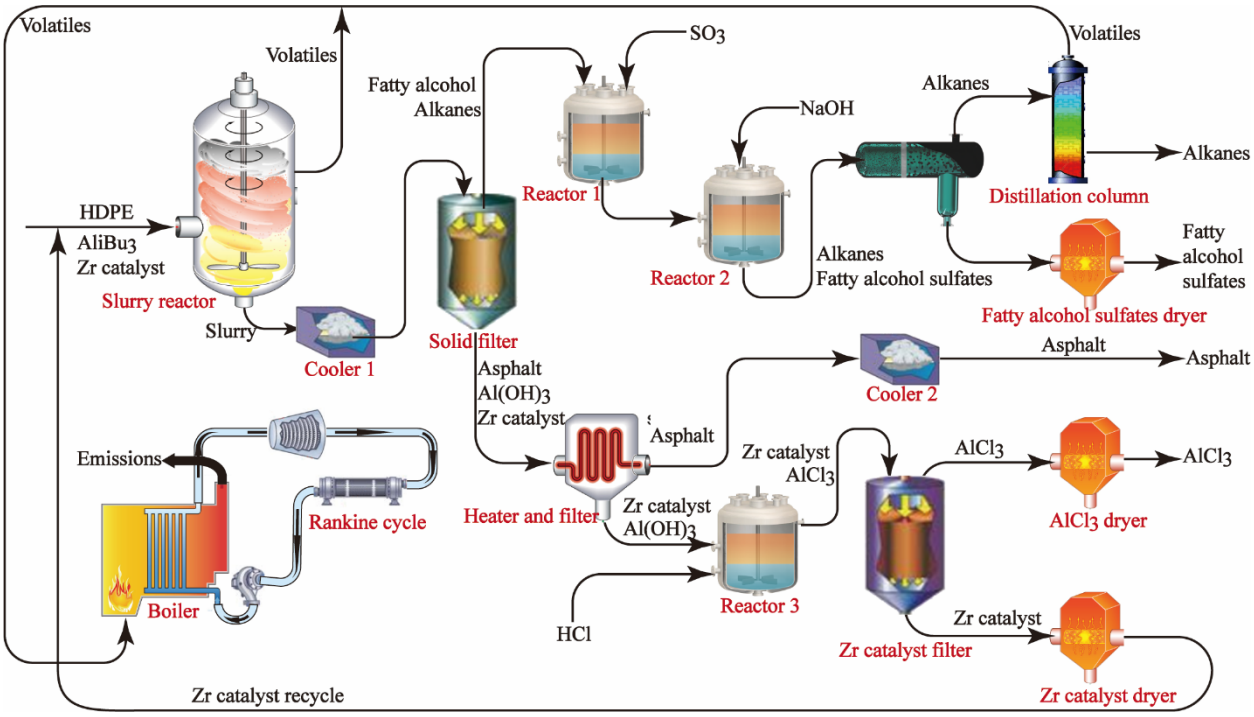

Figure S94. The process of polymer conversion to fatty alcohols and other products.

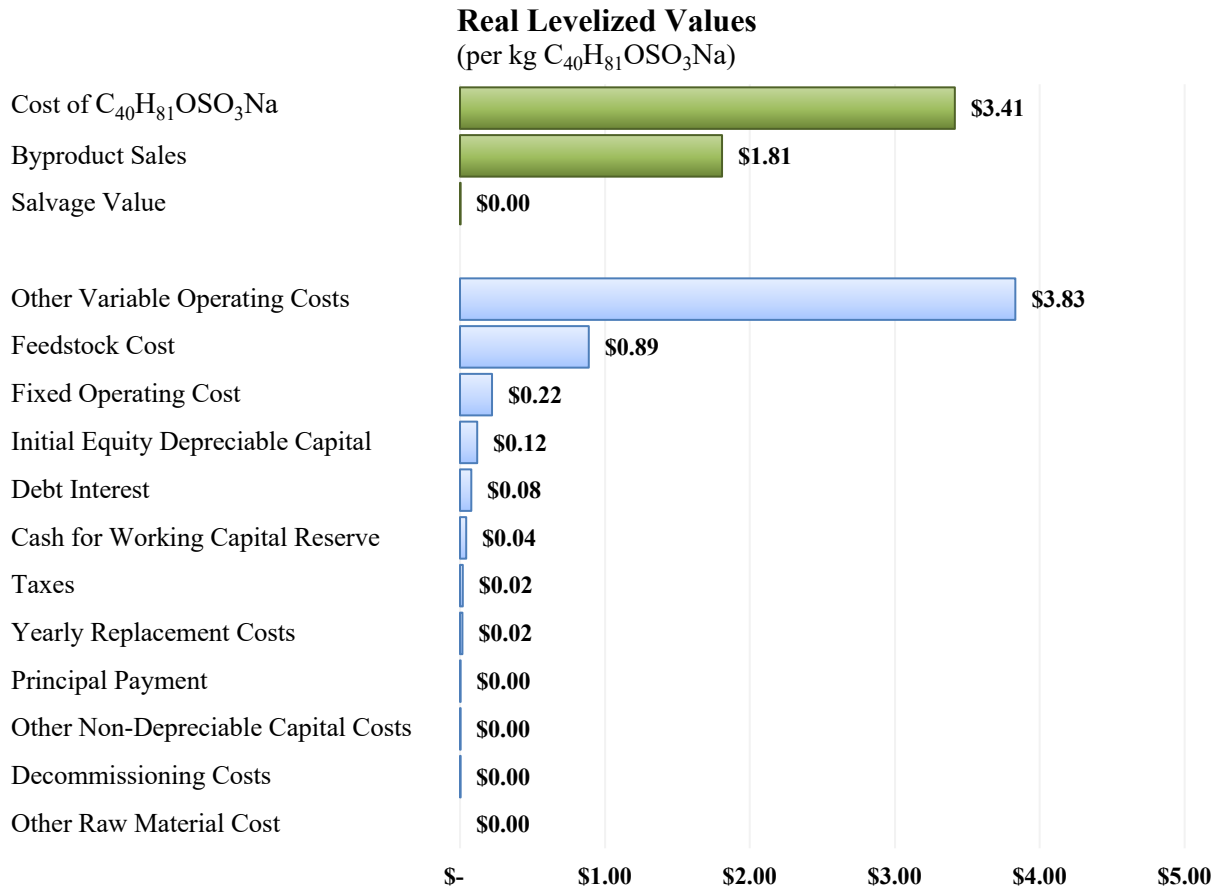

Figure S95. The cost breakdown of C_{40} sodium fatty alcohol sulfate product.

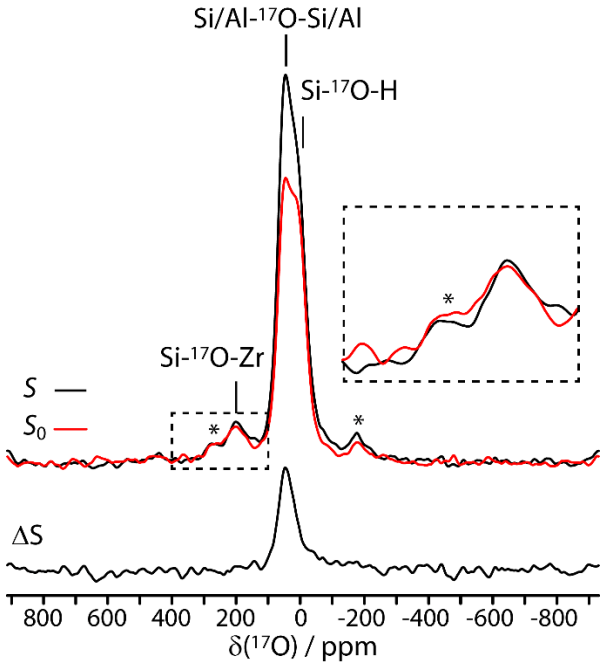

Figure S96. $^{17}O\{^{27}Al\}$ TRAPDOR spectra for the $SiAl^{17}O_x$-supported $Zr(OCH_2CMe_3)_4$ pre-catalyst. Three resonances can be identified belonging to the Zr-bound oxygens, the framework oxygens, and hydroxyl species. As can be seen only the framework oxygen is dephased by the ^{27}Al pulse, indicating that the vast majority of Zr sites are bound to a silanol and are not in an immediate proximity of an Al site.